**T.C.**

**SINOP UNIVERSITY**

**INSTITUTE OF GRADUATE STUDIES**

**DEPARTMENT OF NUCLEAR ENGINEERING**

# RESEARCH AND DEVELOPMENT OF ABS FILAMENT'S CAPABILITY FOR GAMMA AND NEUTRON RADIATION SHIELDING

**BATUHAN GÜLTEKİN**

**MASTER'S THESIS**

**THESIS ADVISOR**
**Assoc. Prof. Dr. HASAN OĞUL**

**SINOP- 2023**

**THESIS ACCEPTANCE**

As a result of the defense exam held on **25.07.2023**, the thesis entitled as "**RESEARCH AND DEVELOPMENT OF ABS FILAMENT'S CAPABILITY FOR GAMMA AND NEUTRON RADIATION SHIELDING**" prepared by **BATUHAN GÜLTEKİN** has been found successful, and the thesis has been **ACCEPTED** as a **MASTER'S THESIS** by our jury.

| | | |
|---|---|---|
| **Advisor** | Assoc. Prof. Dr. Hasan OĞUL<br>Sinop University / Faculty of Engineering and Architecture | Signature |
| **Committee Member** | Asst. Prof. Dr. Hakan US<br>Sinop University / Faculty of Engineering and Architecture | Signature |
| **Committee Member** | Assoc. Prof. Dr. Kamuran DİLSİZ<br>Bingöl University / Faculty of Science and Literature | Signature |

**Institute Manager** Prof. Dr. Fadime DİRİK .....

## ETHICAL DECLARATION

I hereby declare that in this thesis study, which I have prepared in accordance with the rules of thesis writing, I have obtained the data, information, and documents presented within the thesis in compliance with academic and ethical standards. I affirm that I have presented all the information, documents, evaluations, and results in a manner consistent with scientific ethics and moral principles. I declare that I have provided appropriate citations and references, adhering to proper attribution for all the works I have utilized in this thesis. I assure that no alterations have been made to the used data. I state that the research presented in this thesis is original. In the event of any contrary circumstances, I accept all potential rights losses that may arise against me.

**Batuhan GÜLTEKİN**

## ABSTRACT

### M.S.C THESIS

### RESEARCH AND DEVELOPMENT OF ABS FILAMENT'S CAPABILITY FOR GAMMA AND NEUTRON RADIATION SHIELDING

**BATUHAN GÜLTEKİN**

**SINOP UNIVERSITY INSTITUTE OF GRADUATE STUDIES**

**DEPARTMENT OF NUCLEAR ENGINEERING**

**SUPERVISOR: Assoc. Prof. Dr. HASAN OĞUL**

Radiation is a fundamental safety concern for nearly all nuclear applications, requiring careful control to protect living organisms and surrounding materials. In this context, radiation shielding materials have been researched and utilized in nuclear technologies. Material selection must be based on the radiation's application, type, and energy. Polymer materials are preferred for radiation protection applications due to their superior properties such as chemical inertness, durability, flexibility, strength, and cost-effectiveness. In this thesis, the gamma and neutron shielding properties of ABS (Acrylonitrile Butadiene Styrene) thermoplastics commonly used in 3D printing have been comprehensively investigated through enrichment with Er2O3 and Gd2O3 additives. Employing a versatile approach encompassing experimental, theoretical, and simulation methods, the efficacy of these modified thermoplastics in attenuating gamma and neutron radiation has been studied across different material thicknesses and radiation energies. Furthermore, the microstructures of the produced materials have been examined to ensure structural integrity. The research includes a comparative analysis of two different production methods: casting and 3D printing. The manufactured samples were systematically labeled based on the production technique and the nano-oxide compounds they contained. Various radioactive point sources were utilized to measure gamma radiation attenuation, and the HPGe detector system, along with theoretical tools like XCOM and EpiXS, as well as simulations such as FLUKA and GEANT4, were employed. Simultaneously, neutron attenuation properties were evaluated through theoretical calculations and FLUUKA and GEANT4 simulations. SEM/EDS analysis was conducted to examine microstructures, and TGA analysis was performed for thermal characterization, ultimately determining the optimal shielding material for each sample. Through rigorous analysis and evaluations, this thesis contributes to the development and optimization of radiation shielding materials, particularly for applications requiring customization and complex structures, such as those produced using 3D printing technology.



**KEYWORDS:** Gamma Shielding, Neutron Shielding, 3D Printer, ABS, XCOM, EpiXS, FLUKA, GEANT4

July 2023, 266 pages

# ÖZET

## YÜKSEK LİSANS TEZİ

## ABS FİLAMENTİNİN GAMA VE NÖTRON RADYASYONU ZIRHLAMA KABİLİYETİNİN ARAŞTIRILMASI VE GELİŞTİRİLMESİ

**BATUHAN GÜLTEKİN**

**SİNOP ÜNİVERSİTESİ LİSANSÜSTÜ EĞİTİM ENSTİTÜSÜ**
**NÜKLEER ENERJİ MÜHENDİSLİĞİ ANABİLİM DALI**
**DANIŞMAN: Doç. Dr. HASAN OĞUL**

Radyasyon, neredeyse tüm nükleer uygulamalar için ana güvenlik sorunudur ve canlıları ve uygulamaların çevresindeki malzemeleri korumak için kontrol altında tutulmalıdır. Bu bağlamda, radyasyon koruma malzemeleri araştırılmış ve nükleer teknolojilerde kullanılmıştır. Radyasyon kullanım alanına, türüne ve enerjisine bağlı olarak malzeme seçimi yapılmalıdır. Polimer malzemeler, kimyasal inertlik, direnç, esneklik, mukavemet ve düşük maliyet gibi üstün özelliklerinden dolayı radyasyon koruma uygulamalarında tercih edilmektedir. Bu tezde, 3D baskıda yaygın olarak kullanılan ABS (Akrilonitril Bütadien Stiren) termoplastiklerin $Er_2O_3$ ve $Gd_2O_3$ katkı maddeleri ile zenginleştirilmesi sonucu elde edilen gama ve nötron koruma özellikleri kapsamlı bir şekilde incelenmiştir. Değişik malzeme kalınlıkları ve radyasyon enerjileri üzerinde, deneysel, teorik ve simülasyon yöntemlerini kapsayan çok yönlü bir yaklaşım kullanarak, bu modifiye termoplastiklerin gama ve nötron radyasyonunu zayıflatma etkinliği araştırılmıştır. Ayrıca, üretilen malzemelerin mikroyapıları, yapısal bütünlüğü sağlamak amacıyla incelenmiştir. Araştırma, döküm ve 3D baskı olmak üzere iki farklı üretim yönteminin karşılaştırmalı bir analizini içermektedir. Üretilen örnekler, üretim tekniğine ve içerdiği nano oksit bileşiklerine göre sistematik olarak kodlandı. Gama radyasyonu zayıflatmasını ölçmek için çeşitli radyoaktif nokta kaynakları kullanıldı ve HPGe dedektör sistemi, XCOM, EpiXS gibi teorik ve FLUKA ve GEANT4 gibi araçlar ile birlikte çalışıldı. Eş zamanlı olarak, nötron zayıflatma özellikleri teorik ve FLUKA ve GEANT4 simülasyon hesaplamaları ile değerlendirildi. Mikroyapıları incelemek için SEM / EDS ve Termal inceleme için TGA analizi yapıldı ve her örnek için en uygun koruma malzemesi belirlendi. Titiz analizler ve değerlendirmelerle, bu tez, özellikle 3D baskı teknolojisi ile üretilen özelleştirilebilir ve karmaşık yapılar gerektiren uygulamalar için radyasyon koruma malzemelerinin geliştirilmesi ve optimizasyonuna katkıda bulunmaktadır.

**ANAHTAR KELİMER:** Gama Zırhlama, Nötron Zırhlama, 3D Yazıcı, ABS, XCOM, EpiXS, FLUKA, GEANT4

Temmuz 2023, 266 sayfa

## ACKNOWLEDGMENTS

I am indebted and grateful to my advisor, Assoc. Prof. Dr. Hasan OĞUL, who has been instrumental in selecting the topic of this study, sharing valuable knowledge with me, and generously dedicating his time and expertise to assist and support me whenever needed. I would also like to express my gratitude to my esteemed mentors, Dr. Fatih BULUT and Asst. Prof. Dr. Hakan US, for their continuous support and sharing their knowledge with me. Additionally, during my undergraduate and graduate studies, I received the support and guidance of esteemed professors such as Prof. Dr. Meryem SEFERİNOĞLU, Prof. Dr. Turgay KORKUT, Assoc. Prof. Dr. Hatun KORKUT, Asst. Prof. Dr. Hüseyin ŞAHİNER, Asst. Prof. Dr. Ali TİFTİKÇİ. The generosity with which these distinguished professors shared their wealth of knowledge and experience has been invaluable to the development of my thesis. I would like to express my gratitude to them and offer my sincerest thanks.

Furthermore, I owe a great debt of gratitude to my mother Zeynep GÜLTEKİN, my father Ali GÜLTEKİN, my sister Tuğçe GÜLTEKİN, and my entire family for their unwavering support throughout this challenging research journey and throughout my entire educational life. Their financial and emotional support, as well as their constant presence, mean the world to me. I sincerely thank our esteemed family elder Mehmet ÇAVUŞOĞLU for being with me both financially and morally throughout my graduate education. Lastly, I would like to thank my dear friends Berat BOZDEMİR and Emre TEKBIYIK, who have never hesitated to support me, always stood by my side, and made countless sacrifices for me. Their unwavering support and encouragement have been invaluable.

This thesis study was supported by two separate grants from TUBITAK-ARDEB's 1002-A Rapid Support Program (Project No: 122M736), and TUBITAK-BIDEB's 2210-C Domestic Priority Areas Master's Scholarship Program.

The numerical calculations reported in this thesis were partially conducted at TUBITAK ULAKBIM, High Performance and Grid Computing Center (TRUBA resources).

**Batuhan GÜLTEKİN**

**TABLE OF CONTENTS**

**THESIS ACCEPTANCE** ..... **ii**
**ETHICAL DECLARATION** ..... **iii**
**ABSTRACT** ..... **iv**
**ÖZET** ..... **v**
**ACKNOWLEDGMENTS** ..... **vi**
**LIST OF TABLES** ..... **xii**
**LIST OF FIGURES** ..... **xvii**
**LIST OF SYMBOLS AND ABBREVIATIONS** ..... **xxii**
**1. INTRODUCTION** ..... **1**
**2. THEORETICAL FRAMEWORK** ..... **6**
2.1. Radiation ..... 6
2.1.1. Ionizing radiation ..... 7
2.1.2. Non-ionizing radiation ..... 8
2.2. Radiation Sources ..... 9
2.2.1. Natural sources of radiation ..... 10
2.2.2. Artificial sources of radiation ..... 11
2.3. Types of Radioactive Decay ..... 12
2.3.1. Alpha decay ..... 13
2.3.2. Beta decay ..... 13
2.3.3. Positron emission ..... 14
2.3.4. Electron capture ..... 14
2.3.5. Gamma emission ..... 15
2.3.6. Spontaneous fission ..... 16
2.4. The Discovery and Characteristics of Gamma Rays ..... 16
2.4.1. Gamma sources ..... 17
2.5. The Discovery and Characteristics of Neutron Particles ..... 20
2.5.1.Neutron sources ..... 22
2.5.1.1.Alpha-neutron sources ..... 22
2.5.1.2.Photon-neutron sources ..... 23
2.5.1.3. Activation neutrons sources ..... 24
2.5.1.4. Spontaneous fission neutron sources ..... 24
2.5.1.5. Nuclear reactions ..... 25
2.5.1.6. Nuclear reactors ..... 26
2.6. The Interaction of Radiation with Matter ..... 27

2.6.1. Interaction mechanisms of photons with matter ..... 28
2.6.1.1. Photoelectric effect ..... 28
2.6.1.2. Rayleigh scattering ..... 29
2.6.1.3. Compton scattering ..... 30
2.6.1.4. Pair production ..... 31
2.6.2. Interaction mechanisms of neutrons with matter ..... 32
2.6.2.1. Scattering ..... 33
2.6.2.1.1. Elastic scattering ..... 33
2.6.2.1.2. Inelastic scattering ..... 34
2.6.2.2. Absorption interaction ..... 35
2.6.2.2.1. Radiative capture ..... 35
2.6.2.2.2. Fission ..... 36
2.6.2.3. Transfer interaction ..... 36
2.6.2.3.1. Charged particle reactions ..... 36
2.7. Radiation Units ..... 37
2.7.1. Activity unit ..... 37
2.7.2. Irradiation dose unit ..... 38
2.7.3. Absorbed dose unit ..... 38
2.7.4. Equivalent dose unit ..... 39
2.7.5. Effective dose unit ..... 39
2.8. Methods of Protection Against Radiation ..... 40
2.8.1. Time rule ..... 41
2.8.2. Distance rule ..... 42
2.8.3. Shielding rule ..... 42
2.9. Radiation Shielding ..... 43
2.9.1. Passive shields ..... 44
2.9.1.1. Passive radiation shielding categories ..... 44
2.9.2. Active shields ..... 45
2.9.3. Radiation shielding types based on their purposes ..... 45
2.9.4. Slowing down and absorption of gamma rays ..... 46
2.9.5. Slowing down and absorption of neutron particles ..... 50
2.9.6. Commonly used materials in radiation shielding ..... 52
2.9.6.1. Lead (Pb) ..... 52
2.9.6.2. Concrete ..... 53
2.9.6.3. Steel ..... 54

2.9.6.4. Boron (B) ..... 55
2.9.6.5. Paraffin ..... 56
2.9.6.6. Polymethylmethacrylate (PMMA) ..... 57
2.9.6.7. Polyethylene (PE) ..... 58
2.9.6.8. Bismuth (Bi) ..... 59
2.9.6.9. Tungsten (W) ..... 60
2.9.6.10. Cadmium (Cd) ..... 62
2.9.6.11. Barium (Ba) ..... 63
2.9.6.12. Gadolinium (Gd) ..... 64
2.9.6.13. Erbium (Er) ..... 65
2.9.6.14. Antimony (Sb) ..... 66
2.9.6.15. Tin (Sn) ..... 67
2.10. Polymers ..... 68
2.10.1. Fibers ..... 69
2.10.2. Elastomers ..... 70
2.10.3. Plastics ..... 71
2.10.4. Termosets ..... 72
2.10.5. Thermoplastics ..... 73
2.11. 3D Printers and Filaments ..... 74
2.11.1. 3D printers ..... 74
2.11.2. 3D printer filaments ..... 76
2.11.2.1. Acrylonitrile butadiene styrene (ABS) filament ..... 77
2.11.2.2. Polylactic acid (PLA) filament ..... 78
2.11.2.3.Thermoplastic polyurethane (TPU) filament ..... 78
2.11.2.4. Polyethylene terephthalate glycol-modified (PETG) filament ..... 79
2.11.2.5. Polyvinyl alcohol (PVA) filament ..... 79
2.11.2.6. Nylon filament ..... 80
2.12. Nanomaterials ..... 81
2.13. Polymer Matrix Nanocomposites (PMNC) ..... 81
2.13.1. Methods for the synthesis of polymer nanocomposites ..... 82
2.13.1.1. Sol-gel method ..... 82
2.13.1.2. In-situ polymerization method ..... 83
2.13.1.3. Mechanical mixing method ..... 83
2.13.1.4. Electrostatic self-assembly method ..... 84
**3. MATERIALS AND METHODS ..... 86**

3.1. Materials ..... 87
3.1.1. Acrylonitrile butadiene styrene granules ..... 87
3.1.2. Pure Acetone ..... 89
3.1.3. Erbium oxide ($Er_2O_3$) nanopowder ..... 90
3.1.4. Gadolinium oxide ($Gd_2O_3$) nanopowder ..... 92
3.1.5. Steel casting molds ..... 93
3.1.6. Twin-screw extruder machine ..... 94
3.1.7. Thermostatic drying oven ..... 96
3.1.8. Hammer mill grinder ..... 97
3.1.9. Scanning Electron Microscope ..... 99
3.1.10. Thermogravimetric Analyzer (TGA) ..... 101
3.2. Methods ..... 101
3.2.1. Sample production ..... 101
3.2.1.1.Sample production with nano powder additive using casting type technique .. 103
3.2.1.2. Filament production with twin-screw extrusion incorporating nanoparticles . 106
3.2.1.3. Sample production from nanocomposite filament with 3D printing technique. ..... 108
3.2.2. Sample density measurement ..... 109
3.2.3. Structural analysis ..... 111
3.2.4. Thermal analysis ..... 112
3.2.5. Radiation shielding analysis ..... 113
3.2.5.1. Gamma radiation shielding analysis ..... 113
3.2.5.1.1. High-purity germanium detectors (HPGe) analysis ..... 113
3.2.5.1.2. WinXCom analysis ..... 116
3.2.5.1.3. EpiXS analysis ..... 118
3.2.5.1.3. GEANT4 (gamma) analysis ..... 119
3.2.5.1.4. FLUKA (gamma) analysis ..... 124
3.2.5.2. Neutron radiation shielding analysis ..... 128
3.2.5.2.1. GEANT4 (neutron) analysis ..... 129
3.2.5.2.2. FLUKA (neutron) analysis ..... 131
3.2.5.2.3. Effective neutron removal cross section analysis using analytical calculation method ..... 131
**4. RESULTS ..... 132**
4.1. Gamma Radiation Shielding Analysis Results ..... 132
4.1.1. M-series (molded samples) gamma shielding results ..... 132

4.1.1.1. Linear attenuation coefficient (LAC) results for the M-series ..... 132
4.1.1.2. Mass attenuation coefficient (MAC) results for the M-series ..... 134
4.1.1.3. Half value layer (HVL) results for the M-series ..... 137
4.1.1.4. Tenth value layer (TVL) results for the M-series ..... 140
4.1.1.5. Mean free path (MFP) results for the M-series ..... 142
4.1.1.6. Radiation protection efficiency (RPE) results for the M-series ..... 145
4.1.1.7. Buildup factor (energy absorption) results for the M-series ..... 149
4.1.1.8. Buildup factor (exposure) results for the M-series ..... 154
4.1.2. P-series (printed samples) gamma shielding results ..... 159
4.1.2.1. Linear attenuation coefficient (LAC) results for the P-series ..... 159
4.1.2.2. Mass attenuation coefficient (MAC) results for the P-series ..... 161
4.1.2.3. Half value layer (HVL) results for the P-series ..... 163
4.1.2.4. Tenth value layer (TVL) results for the P-series ..... 166
4.1.2.5. Mean free path (MFP) results for the P-series ..... 168
4.1.2.6. Radiation protection efficiency (RPE) results for the P-series ..... 172
4.1.1.7. Buildup factor (energy absorption) results for the P-series ..... 176
4.1.2.8. Buildup factor (exposure) results for the P-series ..... 182
4.1.3. Common gamma shielding results of the M and P series ..... 188
4.1.3.1. Effective atomic number ($Z_{eff}$) results for the M and P Series ..... 188
4.1.3.2. Electron density ($N_E x 10^{23}$) results for the M and P Series ..... 189
4.2. Neutron Radiation Shielding Analysis Results ..... 189
4.2.1. Effective neutron removal cross section results for the M and P series ..... 190
4.2.2. M-series (molded samples) neutron shielding results ..... 193
4.2.3. P-series (printed samples) neutron shielding results ..... 196
4.3. Structural Analysis Results ..... 199
4.3.1. SEM (scanning electron microscopy) analysis results ..... 199
4.3.1.1. M-series (molded samples) SEM analysis results ..... 199
4.3.1.2. P-series (printed samples) SEM analysis results ..... 201
4.3.1. EDS (energy dispersive x-ray spectroscopy) analysis results ..... 204
4.4. Thermal Analysis Results ..... 207
4.4.1. M-series (molded samples) thermal analysis results ..... 207
4.4.2. P-series (printed samples) thermal analysis results ..... 207
**5. CONCLUSION AND DISCUSSION ..... 209**
**REFERENCES ..... 239**
**CURRICULUM VITAE ..... 242**

## LIST OF TABLES

**Table 2.1:** Some examples of gamma sources along with their half-life and main energy values ..... 17
**Table 2.2:** The properties of neutrons ..... 20
**Table 2.3:** Applications of Neutrons. ..... 21
**Table 2.4:** Accepted neutron energy ranges encompassing the characteristics of advanced generation sources ..... 21
**Table 2.5:** Q value and neutron yield for (α,n) reactions from light nuclei ..... 23
**Table 2.6:** The types of fundamental radiation and their characteristics ..... 27
**Table 2.7:** Classification of concrete based on density ..... 54
**Table 3.1:** Chemical properties of ABS ..... 88
**Table 3.2:** Mechanical Properties of ABS ..... 88
**Table 3.3:** Thermal properties of ABS ..... 88
**Table 3.4:** Electrical Properties of ABS ..... 89
**Table 3.5:** Material properties of acetone ..... 89
**Table 3.6:** Chemical properties of erbium oxide nanopowder ..... 91
**Table 3.7:** Physical properties of erbium oxide nanopowder ..... 91
**Table 3.8:** Physical-chemical1 properties of gadolinium oxide nanopowder ..... 92
**Table 3.9:** Specifications of twin-screw extruder ..... 95
**Table 3.10:** Specifications of thermostatic drying oven ..... 97
**Table 3.11:** Specifications of hammer mill Grinder ..... 98
**Table 3.12:** Characteristics of a Scanning Electron Microscope ..... 100
**Table 3.13:** Percentage of nanoparticle additive and density table for M-Series polymer samples ..... 102
**Table 3.14**: Percentage of nanoparticle additive and density table for P-Series polymer samples ..... 102
**Table 3.15:** The experimental densities obtained for the M-Series and P-Series using the Archimedes method ..... 110
**Table 3.16:** Element Distribution Table by Weight Percentage ..... 113
**Table 3.17:** Technical specifications for HPGe ..... 115
**Table 3.18:** FLUKA Unit System ..... 126
**Table 4.1:** Linear attenuation coefficient (LAC) results for the M-ABS-0 ..... 132
**Table 4.2**: Linear attenuation coefficient (LAC) results for the M-ABS-Er5 ..... 132
**Table 4.3:** Linear attenuation coefficient (LAC) results for the M-ABS-Gd5 ..... 133
**Table 4.4:** Linear attenuation coefficient (LAC) results for the M-ABS-Er10 ..... 133
**Table 4.5:** Linear attenuation coefficient (LAC) results for the M-ABS-Gd10 ..... 133
**Table 4.6:** Linear attenuation coefficient (LAC) results for the M-ABS-Er10Gd5 ..... 133
**Table 4.7:** Linear attenuation coefficient (LAC) results for the M-ABS-Er5Gd10 ..... 134
**Table 4.8:** Linear attenuation coefficient (LAC) results for the M-ABS-Er20 ..... 134
**Table 4.9:** Linear attenuation coefficient (LAC) results for the M-ABS-Gd20 ..... 134
**Table 4.10:** Mass attenuation coefficient (MAC) results for the M-ABS-0 ..... 135
**Table 4.11:** Mass attenuation coefficient (MAC) results for the M-ABS-Er5 ..... 135
**Table 4.12:** Mass attenuation coefficient (MAC) results for the M-ABS-Gd5 ..... 135
**Table 4.13:** Mass attenuation coefficient (MAC) results for the M-ABS-Er10 ..... 136
**Table 4.14:** Mass attenuation coefficient (MAC) results for the M-ABS-Gd10 ..... 136
**Table 4.15:** Mass attenuation coefficient (MAC) results for the M-ABS-Er10Gd5 ..... 136
**Table 4.16:** Mass attenuation coefficient (MAC) results for the M-ABS-Er5Gd10 ..... 136
**Table 4.17:** Mass attenuation coefficient (MAC) results for the M-ABS-Er20 ..... 137

**Table 4.18:** Mass attenuation coefficient (MAC) results for the M-ABS-Gd20 ..... 137
**Table 4.19:** Half value layer (HVL) results for the M-ABS-0..... 137
**Table 4.20:** Half value layer (HVL) results for the M-ABS-Er5..... 138
**Table 4.21:** Half value layer (HVL) results for the M-ABS-Gd5..... 138
**Table 4.22:** Half value layer (HVL) results for the M-ABS-Er10..... 138
**Table 4.23:** Half value layer (HVL) results for the M-ABS-Gd10..... 138
**Table 4.24:** Half value layer (HVL) results for the M-ABS-Er10Gd5..... 139
**Table 4.25:** Half value layer (HVL) results for the M-ABS-Er5Gd10..... 139
**Table 4.26:** Half value layer (HVL) results for the M-ABS-Er20..... 139
**Table 4.27:** Half value layer (HVL) results for the M-ABS-Gd20..... 139
**Table 4.28:** Tenth value layer (TVL) results for the M-ABS-0..... 140
**Table 4.29:** Tenth value layer (TVL) results for the M-ABS-Er5..... 140
**Table 4.30:** Tenth value layer (TVL) results for the M-ABS-Gd5..... 140
**Table 4.31:** Tenth value layer (TVL) results for the M-ABS-Er10..... 141
**Table 4.32:** Tenth value layer (TVL) results for the M-ABS-Gd10..... 141
**Table 4.33:** Tenth value layer (TVL) results for the M-ABS-Er10Gd5..... 141
**Table 4.34:** Tenth value layer (TVL) results for the M-ABS-Er5Gd10..... 141
**Table 4.35:** Tenth value layer (TVL) results for the M-ABS-Er20..... 142
**Table 4.36:** Tenth value layer (TVL) results for the M-ABS-Gd20..... 142
**Table 4.37:** Mean free path (MFP) results for the the M-ABS-0..... 142
**Table 4.38:** Mean free path (MFP) results for the the M-ABS-Er5..... 143
**Table 4.39:** Mean free path (MFP) results for the the M-ABS-Gd5..... 143
**Table 4.40:** Mean free path (MFP) results for the the M-ABS-Er10..... 143
**Table 4.41:** Mean free path (MFP) results for the the M-ABS-Gd10..... 143
**Table 4.42:** Mean free path (MFP) results for the the M-ABS-Er10Gd5..... 144
**Table 4.43:** Mean free path (MFP) results for the the M-ABS-Er5Gd10..... 144
**Table 4.44:** Mean free path (MFP) results for the the M-ABS-Er20..... 144
**Table 4.45:** Mean free path (MFP) results for the the M-ABS-Er20..... 144
**Table 4.46:** Mean free path (MFP) results for the the M-ABS-Gd20..... 145
**Table 4.47:** Radiation Protection Efficiency (RPE) 0,50 mm = 0,05 cm (FLUKA) results for the M series..... 146
**Table 4.48:** Radiation Protection Efficiency (RPE) 0,75 mm = 0,075 cm (FLUKA) results for the M series..... 146
**Table 4.49:** Radiation Protection Efficiency (RPE) 10 mm = 1 cm (FLUKA) results for the M series..... 147
**Table 4.50:** Radiation Protection Efficiency (RPE) 20 mm = 2 cm (FLUKA) results for the M series..... 147
**Table 4.51:** Radiation Protection Efficiency (RPE) 50mm = 5 cm (FLUKA) results for the M series..... 148
**Table 4.52:** Radiation Protection Efficiency (RPE) 100 mm = 10 cm (FLUKA) results for the M series ..... 148
**Table 4.53:** Buildup Factor (Energy Absorption) - (1-MFP) results for the M series . 150
**Table 4.54:** Buildup Factor (Energy Absorption) - (5-MFP) results for the M series . 151
**Table 4.55:** Buildup Factor (Energy Absorption) - (10-MFP) results for the M series 152
**Table 4.56:** Buildup Factor (Energy Absorption) - (40-MFP) results for the M series 153
**Table 4.57:** Buildup Factor (Exposure) - (1-MFP) results for the M series ..... 155
**Table 4.58:** Buildup Factor (Exposure) - (5-MFP) results for the M series ..... 156
**Table 4.59:** Buildup Factor (Exposure) - (10-MFP) results for the M series ..... 157
**Table 4.60:** Buildup Factor (Exposure) - (40-MFP) results for the M series ..... 158
**Table 4.61:** Linear attenuation coefficient (LAC) results for the P-ABS-0..... 159

**Table 4.62:** Linear attenuation coefficient (LAC) results for the P-ABS-Er5 ..... 159
**Table 4.63:** Linear attenuation coefficient (LAC) results for the P-ABS-Gd5 ..... 159
**Table 4.64:** Linear attenuation coefficient (LAC) results for the P-ABS-Er10 ..... 159
**Table 4.65:** Linear attenuation coefficient (LAC) results for the P-ABS-Gd10 ..... 160
**Table 4.66:** Linear attenuation coefficient (LAC) results for the -ABS-Er10Gd5 ..... 160
**Table 4.67:** Linear attenuation coefficient (LAC) results for the P-ABS-Er5Gd10 .... 160
**Table 4.68:** Linear attenuation coefficient (LAC) results for the -ABS-Er20 ..... 160
**Table 4.69:** Linear attenuation coefficient (LAC) results for the P-ABS-Gd20 ..... 161
**Table 4.70:** Linear attenuation coefficient (LAC) results for the Lead (Pb) ..... 161
**Table 4.71:** Mass attenuation coefficient (MAC) results for the P-ABS-0 ..... 161
**Table 4.72:** Mass attenuation coefficient (MAC) results for the P-ABS-Er5 ..... 161
**Table 4.73:** Mass attenuation coefficient (MAC) results for the P-ABS-Gd5 ..... 162
**Table 4.74:** Mass attenuation coefficient (MAC) results for the P-ABS-Er10 ..... 162
**Table 4.75:** Mass attenuation coefficient (MAC) results for the P-ABS-Gd10 ..... 162
**Table 4.76:** Mass attenuation coefficient (MAC) results for the P-ABS-Er10Gd5 ..... 162
**Table 4.77:** Mass attenuation coefficient (MAC) results for the P-ABS-Er5Gd10 ..... 163
**Table 4.78:** Mass attenuation coefficient (MAC) results for the P-ABS-Er20 ..... 163
**Table 4.79:** Mass attenuation coefficient (MAC) results for the Lead (Pb) ..... 163
**Table 4.80:** Half value layer (HVL) results for the P-ABS-0 ..... 163
**Table 4.81:** Half value layer (HVL) results for the P-ABS-Er5 ..... 164
**Table 4.82:** Half value layer (HVL) results for the P-ABS-Gd5 ..... 164
**Table 4.83:** Half value layer (HVL) results for the P-ABS-Er10 ..... 164
**Table 4.84:** Half value layer (HVL) results for the P-ABS-Gd10 ..... 164
**Table 4.85:** Half value layer (HVL) results for the P-ABS-Er10Gd5 ..... 165
**Table 4.86:** Half value layer (HVL) results for the P-ABS-Er5Gd10 ..... 165
**Table 4.87:** Half value layer (HVL) results for the P-ABS-Er20 ..... 165
**Table 4.88:** Half value layer (HVL) results for the P-ABS-Gd20 ..... 165
**Table 4.89:** Half value layer (HVL) results for the Lead (Pb) ..... 166
**Table 4.90:** Tenth value layer (TVL) results for the P-ABS-0 ..... 166
**Table 4.91:** Tenth value layer (TVL) results for the P-ABS-Er5 ..... 166
**Table 4.92:** Tenth value layer (TVL) results for the P-ABS-Gd5 ..... 166
**Table 4.93:** Tenth value layer (TVL) results for the P-ABS-Er10 ..... 167
**Table 4.94:** Tenth value layer (TVL) results for the P-ABS-Gd10 ..... 167
**Table 4.95:** Tenth value layer (TVL) results for the P-ABS-Er10Gd5 ..... 167
**Table 4.96:** Tenth value layer (TVL) results for the P-ABS-Er5Gd10 ..... 167
**Table 4.97:** Tenth value layer (TVL) results for the P-ABS-Er20 ..... 168
**Table 4.98:** Tenth value layer (TVL) results for the P-ABS-Gd20 ..... 168
**Table 4.99:** Tenth value layer (TVL) results for the Lead (Pb) ..... 168
**Table 4.100:** Mean free path (MFP) results for the P-ABS-0 ..... 168
**Table 4.101:** Mean free path (MFP) results for the P-ABS-Er5 ..... 169
**Table 4.102:** Mean free path (MFP) results for the P-ABS-Gd5 ..... 169
**Table 4.103:** Mean free path (MFP) results for the P-ABS-Er10 ..... 169
**Table 4.104:** Mean free path (MFP) results for the P-ABS-Gd10 ..... 169
**Table 4.105:** Mean free path (MFP) results for the P-ABS-Er10Gd5 ..... 170
**Table 4.106:** Mean free path (MFP) results for the P-ABS-Er5Gd10 ..... 170
**Table 4.107:** Mean free path (MFP) results for the P-ABS-Er20 ..... 170
**Table 4.108:** Mean free path (MFP) results for the P-ABS-Gd20 ..... 170
**Table 4.109:** Mean free path (MFP) results for the Lead (Pb) ..... 171
**Table 4.110:** Radiation Protection Efficiency (RPE) 0,50 mm = 0,05 cm (FLUKA) results for the P series ..... 173

**Table 4.111:** Radiation Protection Efficiency (RPE) 0,75 mm = 0,075 cm (FLUKA) results for the P series ..... 173
**Table 4.112:** Radiation Protection Efficiency (RPE) 10 mm = 1 cm (FLUKA) results for the P series..... 174
**Table 4.113:** Radiation Protection Efficiency (RPE) 20 mm = 2 cm (FLUKA) results for the P series..... 174
**Table 4.114**: Radiation Protection Efficiency (RPE) 50 mm = 5 cm (FLUKA) results for the P series..... 175
**Table 4.115:** Radiation Protection Efficiency (RPE) 100 mm = 10 cm (FLUKA) results for the P series..... 175
**Table 4.116:** Buildup Factor (Energy Absorption) - (1-MFP) results for the P series 177
**Table 4.117:** Buildup Factor (Energy Absorption) - (5-MFP) results for the P series 178
**Table 4.118:** Buildup Factor (Energy Absorption) - (10-MFP) results for the P series ..... 179
**Table 4.119:** Buildup Factor (Energy Absorption) - (40-MFP) results for the P series ..... 180
**Table 4.120:** Buildup Factor (Energy Absorption) results for the Lead..... 181
**Table 4.121:** Buildup Factor (Exposure) - (1-MFP) results for the P series..... 183
**Table 4.122:** Buildup Factor (Exposure) - (5-MFP) results for the P series..... 184
**Table 4.123:** Buildup Factor (Exposure) - (10-MFP) results for the P series..... 185
**Table 4.124:** Buildup Factor (Exposure) - (40-MFP) results for the P series..... 186
**Table 4.125:** Buildup Factor (Exposure) results for the Lead ..... 187
**Table 4.126:** Effective Atomic Number (Zeff) results for the M and P Series..... 188
**Table 4.127:** Electron density ($N_E$ x$10^{23}$) results for the M and P series..... 189
**Table 4.128:** The effective neutron removal cross-section values for the ABS-M series ..... 191
**Table 4.129:** The effective neutron removal cross-section values for the ABS-P series ..... 191
**Table 4.130:** The effective neutron removal cross-section values for paraffin and ordinary concrete ..... 192
**Table 4.131:** The results of 4.5 MeV neutron irradiation on ABS-M series samples with a thickness of 1 cm..... 193
**Table 4.132:** The types of interactions between 4.5 MeV neutrons and ABS-M series samples with a thickness of 1 cm..... 193
**Table 4.133:** The number of neutrons that pass through ABS-M series samples at different sample thicknesses with a neutron energy of 4.5 MeV..... 194
**Table 4.134:** The number of neutrons that pass through 1 cm thickness ABS-M series samples at different neutron energies ..... 194
**Table 4.135:** The number of neutrons that pass through 5 cm thickness ABS-M series samples at different neutron energies ..... 195
**Table 4.136:** The results of 4.5 MeV neutron irradiation on ABS-P series samples with a thickness of 1 cm..... 196
**Table 4.137:** The types of interactions between 4.5 MeV neutrons and ABS-P series samples with a thickness of 1 cm..... 196
**Table 4.138:** The number of neutrons that pass through ABS-P series samples at different sample thicknesses with a neutron energy of 4.5 MeV..... 197
**Table 4.139:** The number of neutrons that pass through 1 cm thickness ABS-P series samples at different neutron energies ..... 197
**Table 4.140:** The number of neutrons that pass through 5 cm thickness ABS-P series samples at different neutron energies ..... 198

**Table 4.141:** GEANT4 simulation results for thermal and fast neutrons for 1 cm thick ABS-P series samples ..... 198
**Table 4.142:** The elemental mass percentages of the produced ABS samples can be determined through Energy Dispersive Spectroscopy (EDS) maping analysis. ..... 204
**Table 4.143:** Percentage mass loss in temperature-dependent ABS-M series samples using a thermostatic drying oven ..... 207
**Table 4.144:** Percentage mass loss in temperature-dependent ABS-M series samples using a thermostatic drying oven ..... 207

## LIST OF FIGURES

**Figure 2.1:** Classification of radiation based on its ionizing property ..... 7
**Figure 2.2:** Types of Ionizing Radiation ..... 8
**Figure 2.3:** Types of Non-Ionizing Radiation ..... 9
**Figure 2.4:** Sources of radiation exposure ..... 10
**Figure 2.5:** Natural sources of radiation ..... 11
**Figure 2.6:** Artificial sources of radiation ..... 11
**Figure 2.7:** Types of radioactive decay ..... 12
**Figure 2.8:** Alpha Decay schematic ..... 13
**Figure 2.9:** Beta Decay schematic ..... 14
**Figure 2.10:** Positron emission schematic ..... 14
**Figure 2.11:** Electron capture schematic ..... 15
**Figure 2.12:** Gamma emission schematic ..... 16
**Figure 2.13:** Spontaneous fission schematic ..... 16
**Figure 2.14:** A representative visual of some radioactive gamma sources ..... 17
**Figure 2.15:** A representative visual of gamma-ray bursts ..... 18
**Figure 2.16:** A representative visual of nuclear power plant ..... 18
**Figure 2.17:** A representative visual of nuclear weapon ..... 19
**Figure 2.18:** A representative visual of particle accelerator ..... 19
**Figure 2.19:** A representative visual of radiation therapy ..... 19
**Figure 2.20:** An example of a fission reaction observed in a reactor and the relationship graph between the mass numbers (A) of the newly formed nuclei after fission. ..... 26
**Figure 2.21:** Photoelectric effect schematic ..... 29
**Figure 2.22:** Rayleigh scattering schematic ..... 30
**Figure 2.23:** Compton scattering schematic ..... 31
**Figure 2.24:** Pair production schematic ..... 32
**Figure 2.25:** Interaction mechanisms of neutrons with matter ..... 33
**Figure 2.26:** Elastic Scattering schematic ..... 34
**Figure 2.27:** Inelastic Scattering schematic ..... 35
**Figure 2.28:** Radiative capture schematic ..... 36
**Figure 2.29:** Methods of protection against radiation ..... 41
**Figure 2.30:** Mechanisms of photon attenuation ..... 46
**Figure 2.31:** The mineral appearance of lead metal ..... 53
**Figure 2.32:** An example concrete picture ..... 54
**Figure 2.33:** An example concrete picture ..... 55
**Figure 2.34:** The mineral appearance of boron ..... 56
**Figure 2.35:** An example paraffin picture ..... 56
**Figure 2.36:** An example Polymethylmethacrylate picture ..... 58
**Figure 2.37:** An example Polymethylmethacrylate picture ..... 59
**Figure 2.38:** The mineral appearance of bismuth ..... 60
**Figure 2.39:** The mineral appearance of tungsten ..... 62
**Figure 2.40:** The mineral appearance of cadmium ..... 63
**Figure 2.41:** The mineral appearance of barium ..... 64
**Figure 2.42:** The mineral appearance of gadolinium. ..... 65
**Figure 2.43:** The mineral appearance of erbium ..... 66
**Figure 2.44:** The mineral appearance of antimony ..... 67
**Figure 2.45:** The mineral appearance of tin ..... 68
**Figure 2.46:** Polymerization schematic ..... 68

**Figure 2.47:** Classification of polymers ..... 69
**Figure 2.48:** Carbon Fiber Reinforced Polymer fabric ..... 70
**Figure 2.49:** Polybutene material ..... 71
**Figure 2.50:** Polymethyl methacrylate (PMMA) material ..... 72
**Figure 2.51:** Phenol formaldehyde resins (phenolics) material ..... 73
**Figure 2.52:** Polyvinyl chloride (PVC) pipes ..... 74
**Figure 2.53:** 3D Printing Market from 2012 to 2025 ..... 76
**Figure 2.54:** Schematic illustration of the nanocomposite sol-gel polymerization ..... 83
**Figure 2.55:** Schematic illustration of the in-situ polymerization metod ..... 83
**Figure 2.56:** A Schematic illustration of the dry (mechanical) mixing metod ..... 84
**Figure 2.57:** A Schematic illustration of the Electrostatic self-assembly method ..... 85
**Figure 3.1:** ABS granules ..... 88
**Figure 3.2:** Erbium oxide nanopowder ..... 91
**Figure 3.3:** Gadolinium oxide nanopowder ..... 92
**Figure 3.4:** The technical drawing visual of the internal components of the casting mold ..... 93
**Figure 3.5:** The technical drawing visual of the external components of the casting mold. ..... 94
**Figure 3.6:** The twin-screw extruder device's general visual from the right and left sides. ..... 95
**Figure 3.7:** Thermostatic Drying Oven owned by Sinop University's Scientific and Technological Research Application and Research Center ..... 97
**Figure 3.8:** Hammer mill grinder ..... 98
**Figure 3.9:** JEOL, JSM-5300 scanning electron microscope owned by Karadeniz Technical University ..... 100
**Figure 3.10:** Perkin-Elmer, Diamond thermogravimetric analysis system owned by Erciyes University Nanotechnology research center ..... 101
**Figure 3.11:** a-) The process involves precisely weighing a specified amount of ABS granules, b-) The weighed ABS granules are then placed in a pre-selected jar that can be tightly sealed, c-) Using a graduated liquid volume cylinder, a desired amount of pure acetone is measured, d-) The measured acetone is added to the jar containing the ABS granules and left for 24 hours to allow the ABS to dissolve completely in the acetone, e-) A magnetic stirrer is then used to increase the homogeneity and consistency of the resulting solution ..... 104
**Figure 3.12:** a-) The molds were positioned and waxed with a mold-release agent to ensure the easy removal of the samples. b-) Before initiating the casting process, the casting mold was heated until it reached the desired temperature (80°C). c-) The solution was poured into the casting mold. ..... 105
**Figure 3.13:** Samples of casting type composite specimens enhanced with nano-powder additives; 1) M-ABS-0 (0% Additive), 2) M-ABS-Er5 (5% Additive), 3) M-ABS-Er10 (10% Additive), 4) M-ABS-Er20 (20% Additive), 5) M-ABS-Er5Gd10 (5%, 10% Additive), 6) M-ABS-Gd5 (5% Additive), 7) M-ABS-Gd10 (10% Additive), 8) M-ABS-Gd20 (20% Additive), 9) M-ABS-Er10Gd5 (10%, 5% Additive) ..... 105
**Figure 3.14:** 1) Measurement of granule size, 2) Measurement of additive added to the granule, 3) Combination of granule and nanoparticles for twin-screw extrusion 4) Conversion of granule into filament form 5) Recycling of granule through a hammer mill grinder to enhance filament homogeneity 6) Extrusion of nanoparticle-enhanced granule 7) Conversion of granule back into filament form 8) Obtaining filament windings ..... 106

**Figure 3.15:** Samples of F-series filament specimens enhanced with nano-powder additives; 1) F-ABS-0 (0% Additive), 2) F-ABS-Er5 (5% Additive), 3) F-ABS-Gd5 (5% Additive), 4) F-ABS-Er10 (10% Additive), 5) F-ABS-Gd10 (10% Additive), 6) F-ABS-Er10Gd5 (10%, 5% Additive), 7) F-ABS-Er5Gd10 (5%, 10% Additive), 8) F-ABS-Er20 (20% Additive), 9) F-ABS-Gd20 (20% Additive)..... 107
**Figure 3.16**: The Creality CR-10 Smart Pro 3D Direct Drive printer ..... 108
**Figure 3.17:** Samples of casting type composite specimens enhanced with nano-powder additives; 1) P-ABS-0 (0% Additive), 2) P-ABS-Er5 (5% Additive), 3) P-ABS-Er10 (10% Additive), 4) P-ABS-Er20 (20% Additive), 5) P-ABS-Er5Gd10 (5%, 10% Additive), 6) P-ABS-Gd5 (5% Additive), 7) P-ABS-Gd10 (10% Additive), 8) P-ABS-Gd20 (20% Additive), 9) P-ABS-Er10Gd5 (10%, 5% Additive)..... 109
**Figure 3.18:** The Archimedes Density Kit..... 110
**Figure 3.19:** HPGe detector owned by Kastamonu University Scientific and Technological Research Application and Research Center..... 114
**Figure 3.20:** Cross-sectional view of the HPGe detector ..... 115
**Figure 3.21:** WinXCOM user interface page..... 117
**Figure 3.22:** WinXCOM material content identification interface..... 117
**Figure 3.23:** EpiXS user interface page..... 119
**Figure 3.24:** EpiXS material content identification interface..... 119
**Figure 3.25:** Geant4 visualization of the developed code. (a) Solid surface view, (b) wire frame view, (c) hidden edges view. ..... 122
**Figure 3.26:** Nanopowder-additive and non-additive samples defined in the GEANT4 terminal interface ..... 123
**Figure 3.27:** Command and parameters for starting the GEANT4 simulation program ..... 123
**Figure 3.28:** Flair material content identification interface for Fluka access ..... 127
**Figure 3.29:** Screenshot of flair interface for left view of simulation ..... 127
**Figure 3.28:** Screenshot of flair interface for four views of simulation ..... 128
**Figure 3.30:** Nanopowder-additive and non-additive samples defined in the GEANT4 (neutron) terminal in-terface..... 130
**Figure 3.31:** Command and parameters for starting the GEANT4 simulation program ..... 130
**Figure 4.1:** SEM image of the ABS sample produced by mold production without additives (M-ABS-0) ..... 199
**Figure 4.2:** SEM images of ABS samples with additives produced by the mold production method; a) %5Er, b) %5Gd, c) %10Er, d) %10Gd ..... 200
**Figure 4.3:** SEM images of ABS samples with additives produced by the mold production method; e) %10Er, %5Gd, f) %5Er, %10Gd, g) %20Er ve h) %20Gd..... 200
**Figure 4.4:** SEM image of the ABS sample produced with a 3D printer without additives (P-ABS-0)..... 202
**Figure 4.5:** SEM images of ABS samples with additives produced by the 3D printer method; a) %5Er, b) %5Gd, c) %10Er, d) %10Gd..... 202
**Figure 4.6**: SEM images of ABS samples with additives produced by the 3D printer method; ; e) %10Er, %5Gd, f) %5Er, %10Gd, g) %20Er ve h) %20Gd ..... 203
**Figure 4.7:** a) Er element distribution for M-ABS-Er5, b) Gd element distribution for M-ABS-Gd5, c) Er element distribution for M-ABS-Er10, d) Gd element distribution for M-ABS-Gd10, e) Er element distribution for M-ABS-Er20, f) Gd element distribution for M-ABS-Gd20 ..... 205
**Figure 4.8:** a) Er element distribution for P-ABS-Er5, b) Gd element distribution for P-ABS-Gd5, c) Er element distribution for P-ABS-Er10, d) Gd element distribution for P-

ABS-Gd10, e) Er element distribution for P-ABS-Er20, f) Gd element distribution for P-ABS-Gd20 ..... 206
**Figure 5.1:** Linear attenuation coefficient graphs for M-ABS-0, M-ABS-Er5, M-ABS-Gd5, and M-ABS-Er10 ..... 211
**Figure 5.2:** Linear attenuation coefficient graphs for M-ABS-Gd10, M-ABS-Er10Gd5, M-ABS-Er5Gd10, M-ABS-Er20, and M-ABS-Gd20 ..... 212
**Figure 5.3:** Mass attenuation coefficient graphs for P-ABS-0, P-ABS-Er5, P-ABS-Gd5, and P-ABS-Er10 ..... 213
**Figure 5.4:** Mass attenuation coefficient graphs for P-ABS-Gd10, P-ABS-Er10Gd5, P-ABS-Er5Gd10, P-ABS-Er20, and P-ABS-Gd20 ..... 214
**Figure 5.5:** Mass attenuation coefficient graphs for M-ABS-0, M-ABS-Er5, M-ABS-Gd5, and M-ABS-Er10 ..... 215
**Figure 5.6:** Mass attenuation coefficient graphs for M-ABS-Gd10, M-ABS-Er10Gd5, M-ABS-Er5Gd10, M-ABS-Er20, and M-ABS-Gd20 ..... 216
**Figure 5.7:** Mass attenuation coefficient graphs for P-ABS-0, P-ABS-Er5, P-ABS-Gd5, and P-ABS-Er10 ..... 217
**Figure 5.8:** Mass attenuation coefficient graphs for P-ABS-Gd10, P-ABS-Er10Gd5, P-ABS-Er5Gd10, P-ABS-Er20, and P-ABS-Gd20 ..... 218
**Figure 5.9:** HVL (Half-Value Layer) graphs for M-ABS-0, M-ABS-Er5, M-ABS-Gd5, and M-ABS-Er10 ..... 219
**Figure 5.10:** HVL (Half-Value Layer) graphs for M-ABS-Gd10, M-ABS-Er10Gd5, M-ABS-Er5Gd10, M-ABS-Er20, and M-ABS-Gd20 ..... 220
**Figure 5.11:** HVL (Half-Value Layer) graphs for P-ABS-0, P-ABS-Er5, P-ABS-Gd5, and P-ABS-Er10 ..... 221
**Figure 5.12:** HVL (Half-Value Layer) graphs for P-ABS-Gd10, P-ABS-Er10Gd5, P-ABS-Er5Gd10, P-ABS-Er20, and P-ABS-Gd20 ..... 222
**Figure 5.13:** RPE (Radiation Protection Efficiency) graphs dependent on sample thickness for ABS-M series ..... 223
**Figure 5.14:** RPE (Radiation Protection Efficiency) graphs dependent on sample thickness for ABS-P series ..... 223
**Figure 5.15:** Buildup factor (energy absorption) graphs: graphs dependent on Mean Free Path (MFP) and energy for ABS-M series ..... 224
**Figure 5.16:** Buildup factor (energy absorption) graphs: graphs dependent on Mean Free Path (MFP) and energy for ABS-P series ..... 224
**Figure 5.17:** Buildup factor (Exposure) graphs: graphs dependent on Mean Free Path (MFP) and energy for ABS-M series ..... 225
**Figure 5.18:** Buildup factor (Exposure) graphs: graphs dependent on Mean Free Path (MFP) and energy for ABS-M series ..... 225
**Figure 5.19:** Zeff graph of the prepared M and P series samples as a function of gamma energy ..... 226
**Figure 5.20:** NE graph of the prepared M and P series samples as a function of gamma energy ..... 227
**Figure 5.21:** The number of 10 million neutrons in the energy range of 0.1 to 14.5 MeV transmitted through the M series samples with a thickness of 1 cm ..... 227
**Figure 5.22:** The number of 10 million neutrons in the energy range of 0.1 to 14.5 MeV transmitted through the P series samples with a thickness of 1 cm. ..... 227
**Figure 5.23:** The number of 10 million neutrons with an energy of 4.5 MeV that passed through different thicknesses of M series samples ..... 228
**Figure 5.24:** The number of 10 million neutrons with an energy of 4.5 MeV that passed through different thicknesses of P series samples ..... 228

**Figure 5.25:** Radiation protection efficiency graphs obtained through FLUKA: a-) ABS-Er20 and b-) ABS-Gd20 ..... 228
**Figure 5.26:** Percentage mass loss in temperature-dependent ABS samples using a thermostatic drying oven ..... 234
**Figure 5.27:** The percentage mass loss at varying temperatures of ABS-Er20 and ABS-Gd20 samples was compared with ABS-0 samples using a thermostatic drying oven 235
**Figure 5.28:** ABS-Er20 and ABS-Gd20 samples' percentage mass change at different temperatures was compared with ABS-0 samples using a Thermogravimetric Analyzer. ..... 236

## LIST OF SYMBOLS AND ABBREVIATIONS

**Symbols**

| | | |
|---|---|---|
| **Bq** | **:** | Bequerel (Bq) is the SI unit of activity |
| **C** | **:** | Carbon |
| **Ci** | **:** | Cruie, a specialized unit of activity |
| **cm** | **:** | Centimeter |
| **$cm^2$** | **:** | Square centimeter |
| **$cm^3$** | **:** | Cubic centimeter |
| **e** | **:** | Electron |
| **$e^+$** | **:** | Positron |
| **eV** | **:** | Electron volt |
| **Er** | **:** | Erbium |
| **Gd** | **:** | Gadolinium |
| **Gy** | **:** | Gray, absorbed dose unit |
| **Γ** | **:** | Gamma-ray constant |
| **H** | **:** | Hydrogen |
| **h** | **:** | Planck constant |
| **keV** | **:** | Kiloelectron volt |
| **kg** | **:** | Kilogram |
| **mm** | **:** | Millimeter |
| **$m^2$** | **:** | Square meter |
| **MeV** | **:** | Million electron volts |
| **N** | **:** | Nitrogen |
| **n** | **:** | Neutron |
| **nm** | **:** | Nanometer |
| **O** | **:** | Oxygen |
| **$^oC$** | **:** | Celsius |
| **$^oK$** | **:** | Kelvin |
| **p** | **:** | Proton |
| **Pb** | **:** | Lead |
| **s** | **:** | Second |
| **$\alpha$** | **:** | Alfa |
| **β** | **:** | Beta |
| **$\gamma$** | **:** | Gamma |
| **X** | **:** | X-rays |
| **Å** | **:** | Wavelength of a neutron. |
| **I** | **:** | The number of gamma/neutrons passing per unit area |
| **$I_0$** | **:** | The number of gamma/neutrons sent to the material |
| **$\Sigma_R/\rho$** | **:** | Effective neutron capture cross-section |
| **μ** | **:** | Linear attenuation coefficient |
| **$\sigma_t$** | **:** | Total cross-section |
| **$t_{1/2}$** | **:** | Half-life |
| **$m_e$** | **:** | Electron mass |
| **τ** | **:** | Interaction coefficient of the photoelectric effect |
| **$\kappa$** | **:** | Pair production coefficient |
| **A** | **:** | Activity of the source |
| **B** | **:** | Correction factor |

| | | |
|---|---|---|
| **Sv** | **:** | Sievert, Equivalent Dose Unit |
| **R** | **:** | X-ray, radiation intensity unit |
| **rad** | **:** | Absorbed radiation dose |
| **Rem** | **:** | Equivalent Dose Special Unit |

**Abbreviations**

| | | |
|---|---|---|
| **ABS** | **:** | Acrylonitrile Butadiene Styrene |
| **ALARA** | **:** | As Low As Reasonably Achievable |
| **ASTM** | **:** | American Society for Testing and Materials |
| **CERN** | **:** | European Organization for Nuclear Research |
| **$CO_2$** | **:** | Carbon dioxide |
| **E** | **:** | Energy of a Photon |
| **EBM** | **:** | Electron Beam Melting |
| **ESR-EPR** | **:** | Microwaves |
| **FDA** | **:** | Food and Drug Administration |
| **FDM** | **:** | Fused Deposition Modeling |
| **FLUKA** | **:** | Fluktuierende Kaskade |
| **GEANT4** | **:** | GEometry ANd Tracking |
| **HVL** | **:** | Half Value Layer |
| **PA** | **:** | Polyamide |
| **K** | **:** | Pair Production Absorption Coefficient |
| **MFP** | **:** | Mean free path |
| **MOEJ** | **:** | Ministry of the Environment Japan |
| **PA** | **:** | Poliamid |
| **PLA** | **:** | Polylactic Acid |
| **SEM** | | Scanning Electron Microscope |
| **SI** | **:** | International System of Units |
| **SLA** | **:** | Stereolithography |
| **SLS** | **:** | Selective Laser Sintering |
| **SLM** | **:** | Selective Laser Melting |
| **TVL** | **:** | Tenth-value layer |
| **UV** | **:** | Ultraviolet Rays |
| **3D** | **:** | Three-Dimensional |
| **x** | **:** | Material Thickness |
| **Z** | **:** | The Number of Neutrons Passing Through the Sample |

## 1. INTRODUCTION

Radiation has become an integral part of our modern life. In order to meet the fundamental needs of contemporary society in health, energy, and science, radiation from both natural and artificial sources is employed. In the field of medicine, radiation plays a vital role in various applications such as diagnostic imaging techniques and cancer treatment. In cancer treatment, high-energy radiation affects the DNA of cells, halting the growth of cancerous cells, thus saving lives. In energy production, radiation triggers thermonuclear reactions in nuclear power plants, thereby providing a low-carbon, efficient source of energy. In the realm of science, radiation aids researchers in unraveling the mysteries of our world and the universe. However, despite the potential benefits of radiation, there are harmful effects as well. Radiation at high doses can damage cells and lead to genetic mutations. This dual nature of radiation underscores the importance of radiation protection and radiation shielding. On one hand, we use radiation to meet society's health and energy needs, and on the other hand, we must develop effective protection strategies and technologies to minimize the potential harms of radiation and protect human health. Scientific research on radiation exposure and its consequences further elucidates the importance of protection for general health and safety. Understanding and managing the potential impacts of radiation also ensures the healthy and safe use of radiation in technologies used in our daily lives and various industries.

The fundamental ways of protection from radiation are duration, distance, and shielding. Duration involves limiting the time of exposure to radiation; generally, the reduction of radiation exposure dose is directly related to reducing exposure time. Distance involves staying as far away as possible from the source of radiation; generally, radiation levels decrease as you move away from the source. Shielding involves using materials that block the passage of radiation. The choice of shielding materials usually depends on the type of radiation we want to stop. Radiation protection also includes the use of appropriate monitoring and detection devices to detect and measure the presence of radiation. Together, these measures play a vital role in protecting individuals and society from the possible harms of radiation exposure.

Among radiation protection strategies, the principles of time, distance, and shielding stand out. However, it's crucial to highlight that in certain circumstances, the creation of shielding can be more significant compared to the other principles. These situations typically involve the need for permanent protection; while time and distance mostly provide temporary protection, shielding offers a permanent form of protection. For instance, in situations where direct control over the radiation source is not feasible, or there's a continuous risk of radiation exposure, shielding provides an effective protection. Also, there may be cases where we have no direct control over the radiation source, and in these instances, shielding is usually the most effective protection strategy. These situations might involve medical or industrial applications; radiation sources are often used continuously in these types of applications, and therefore, creating shielding is essential. High-energy radiations, particularly gamma rays and high-energy beta particles, represent another significant situation. This type of radiation can penetrate deep into the skin and tissues, and therefore, forming an effective shield is usually the only way to protect from this type of radiation.

In conclusion, while time, distance, and shielding are fundamental principles of radiation protection, in certain situations, the weightage of shielding can be observed to be more substantial. These situations illustrate the critical role that shielding plays in protecting from radiation, and it can sometimes be more important than other protection strategies. The requirements for shielding applications increase proportionally depending on the diversity of technology. While sometimes large-scale shielding may be required, there are also instances where a need for light and small-scale shielding arises. Nowadays, there is a growing demand for complex and specific dimensions of shielding applications in fields such as spacecraft, nuclear medicine, etc. (Wilson et al., 1997; Baharul et al., 2020). The availability of three-dimensional (3D) printers to meet this need has been indicated by several studies in the literature (Woosley et al., 2018; Olsson et al., 2017; Viskadourakis et al., 2017; Oğul, 2022; Jain et al., 2018; Lee et al., 2018; Villani et al., 2021). However, the number of studies in this field is quite limited and there are no such studies in our country. With help of 3D printing technology, the compound boron nitride has been added into ABS filament, reporting a significant increase in neutron shielding capability from 50% to 72% (Woosley et al., 2018). They produced ABS polymer material with boron nitride additives and found that the prepared ABS sample's neutron shielding capability was significantly increased. They have contributed

a detailed study to the literature investigating the applicability of 3D printers in neutron radiation shielding, although they have not reported any results regarding gamma shielding. In another study, Olsson et al. (A. Olsson et al., 2017) produced ABS samples with boron carbide and also examined its mechanical properties in addition to its neutron shielding capability. It has been reported that complex shapes can be produced with 3D printing and desired new features can be obtained in final products. Again, the gamma shielding capability of the produced material was not reported. In a study published in 2017, Z. Viskadourakis et al. (Z. Viskadourakis et al., 2017) investigated the shielding characteristics of PLA with graphene oxide additives and ABS composites with carbon nanotubes for electromagnetic radiation. They have stated that 3D technology could be an effective method to create effective electromagnetic shields. In another study published in 2022, Oğul (2022) theoretically studied the use of PLA and ABS polymer materials in neutron shielding and suggested that 3D printers promise effective radiation shielding materials. In another study found in the literature, Jain et al. (2018) added carbon nanotubes into PLA and performed only mechanical tests such as hardness and material strength of the material, they did not conduct any research on radiation shielding capability. Lee et al. (Lee et al., 2018) investigated whether TPU, PLA, PVA, nylon and ABS polymers used in 3D printers can be used for gamma radiation shielding without any additives for very low gamma energies. Villani et al. (Villani et al., 2021), in their study, added tungsten and bismuth into the ABS material and examined their gamma shielding capabilities at different sample thicknesses. However, they did not provide an evaluation in terms of neutrons. In all studies mentioned in the literature, it was underlined that 3D technology could be an important method for radiation shielding. Currently, radiation shielding materials are produced with polymer materials using the casting method (Ozel et al., 2021; Mann et al., 2015). The biggest disadvantage of this method compared to 3D printers is the inability to provide millimetric dimensions offered by 3D printers and the difficulty in obtaining the desired complex shapes (Oğul, 2022).

As part of this thesis work, gadolinium oxide ($Gd_2O_3$) and erbium oxide ($Er_2O_3$) materials compounds were selected as additives at the nanoparticle size. The reason for choosing nano size compared to micron size is motivated by the fact that the nano additive allows the material to have a higher density, thus increasing the probability of interaction of incoming radiation with the material (Malekie and Hajiloo, 2017; Kavaz, 2019).

$Gd_2O_3$, one of the chosen additives, is notably used due to gadolinium (Gd). This element has the highest thermal neutron absorption cross-section among all elements and is used for regular fission distribution in nuclear reactor control rods. This feature is a significant advantage for the shielding of thermal neutrons. In addition to the listed properties, it is known that patients are given a gadolinium-based contrast agent to enhance image contrast for magnetic resonance (MR), one of the imaging techniques in nuclear medicine. In this context, it can be inferred that it can be used compared to toxic components in the literature from a human health perspective (Feifei, L., et al.,2019). The erbium (Er) element in the structure of the other additive, $Er_2O_3$, is known to be used in neutron-absorbing control rods in nuclear technology (Lamarsh J. et al., 2021; Mann et al., 2015). As Gd and Er elements also have high atomic numbers, they are expected to contribute positively to gamma-ray shielding. The reason for choosing the oxide forms of Gd and Er as additives is that the Gd and Er elements tend to bind the nonmetals in the polymer material, which could cause nonmetal gas release until saturation is reached (Obregon et al., 2013). This phenomenon is known to be due to the high electropositivity of Gd and Er and the high electronegativity of nonmetals (Obregon et al., 2013; Tantardini et al., 2021). It is thought that the $Er_2O_3$ compound will not cause this negative phenomenon. In addition to all of these, $Er_2O_3$ is used as an additive in infrared-absorbing glasses and goggles used by welders (Effendy et al., 2017). In light of all this information, it is anticipated that the gamma and neutron shielding functions of the selected polymer materials could be improved by adding $Gd_2O_3$ and $Er_2O_3$ materials. In short, it is accepted that $Gd_2O_3$ and $Er_2O_3$ materials are non-toxic and that an alternative shielding material to toxic additive-containing shielding materials will be produced within the scope of this thesis work.

In this thesis work, it is aimed to investigate the gamma and neutron shielding characteristics of ABS thermoplastics, known as 3D printer polymers with $Er_2O_3$ and $Gd_2O_3$ additives, using experimental, theoretical, and simulation methods at different material thicknesses and different radiation energies. To maintain integrity, the microstructures of the produced materials have also been examined. In the production of ABS polymer samples, two different production options have been compared by utilizing both casting type and 3D printing technology.

In this context, codes have been assigned to the samples produced both by the mold production technique and the 3D printing technique according to the added nano-oxide compound. The values in the codes represent the mass percentage of each element. The series produced with the mold production technique starts with the code "M", followed by filament samples produced from the Filament Extruder machine starting with the code "F", and the samples produced with the 3D printing technique starting with the code "P". The primary sample codes include: "M-ABS-0 (0% Additive), M-ABS-Er5 (5% Additive), M-ABS-Gd5 (5% Additive), M-ABS-Er10 (10% Additive), M-ABS-Gd10 (10% Additive), M-ABS-Er10Gd5 (10%, 5% Additive), M-ABS-Er5Gd10 (5%, 10% Additive), M-ABS-Er20 (20% Additive), M-ABS-Gd20 (20% Additive), P-ABS-0 (0% Additive), P-ABS-Er5 (5% Additive), P-ABS-Gd5 (5% Additive), P-ABS-Er10 (10% Additive), P-ABS-Gd10 (10% Additive), P-ABS-Er10Gd5 (10%, 5% Additive), P-ABS-Er5Gd10 (5%, 10% Additive), P-ABS-Er20 (20% Additive), P-ABS-Gd20 (20% Additive)."

These produced samples, fortified with nano-oxide compounds, were tested with various radioactive point sources ($^{241}$Am (59,5 keV), $^{133}$Ba (80,9, 276,3, 302,8, 356,0 and 383,8 keV), $^{22}$Na (511,0 and 1274,5 keV), $^{137}$Cs (661,6 keV), and $^{60}$Co (1173,2 and 1332,5 keV)) using experimental (HPGe detector system), theoretical (XCOM, EpiXS), and simulation (FLUKA, GEANT4) methods to determine their gamma radiation attenuation capabilities. The compatibility of each method with the experimental results was determined.

Also, within the scope of the thesis work, the neutron attenuation characteristics of all samples to be produced were evaluated with theoretical and simulation calculations. The SEM / EDS and TGA analyses of the produced samples were conducted. And the best performing shielding material was determined for each sample.

# 2. THEORETICAL FRAMEWORK

## 2.1. Radiation

Atoms, the fundamental building blocks of all matter in the universe, each contain a specific number of protons and neutrons. However, sometimes, atoms become unstable due to an imbalance in the number of protons and neutrons. These unstable atoms release various rays into their surroundings as they emit energy to stabilize their nuclei. This event of energy emission is referred to as radiation. Radiation spreads as energy packets in various forms - as waves, particles, or photons. These energy packets can take various forms, ranging from subatomic particles to the entire spectrum of electromagnetic waves. Each of these forms of energy leaves unique traces as they interact with the matter around them. Radiation is a universal phenomenon that is constantly present in nature and part of our lives. For instance, rays from the Sun, radio waves that facilitate radio and television communication, X-rays, and γ-rays used for medical imaging and industrial applications, even cosmic rays roaming around in the universe, are all types of radiation that we are exposed to in daily life. While many of these types of radiation are vital for facilitating our lives and expanding our scientific understanding, they can also pose potential risks to living beings. Therefore, the proper understanding and management of radiation are extremely important for public health and safety. This is particularly true in fields that heavily use radiation, such as nuclear technology and medical applications. In this context, continuous advancement of science and technology is required to mitigate the effects of radiation and make the most out of it. Radiation is a form of energy that can move through space and matter. This energy is disseminated either by particles or electromagnetic waves, depending on the characteristics of the radiation source. The definition of radiation typically relies on three main parameters:

- Energy: Radiation is divided into two based on the amount of its energy - low energy (non-ionizing) and high energy (ionizing). Ionizing radiation can cause ionization of atoms or molecules (loss of electrons). This can have harmful effects on living cells and can lead to radiation sickness or cancer. Non-ionizing radiation does not directly damage cells, but at high levels, it can cause tissue heating.

- Type: There are two main types of radiation: particle radiation and electromagnetic radiation. Particle radiation includes subatomic particles like alpha and beta particles. Electromagnetic radiation includes photons of energy at different wavelengths. This covers a broad range from radio waves to X-rays and gamma rays.
- Source: Radiation can be natural or artificial. Natural radiation can come from rocks and soil containing radioactive material, from cosmic rays, or from certain elements in the body (e.g., potassium-40). Artificial radiation arises from human activities, including medical procedures (like X-rays or radiation therapy), energy production (like nuclear power plants), scientific research, and military uses.

Radiation is divided into ionizing and non-ionizing radiation based on its ionizing property (Figure 2.1).

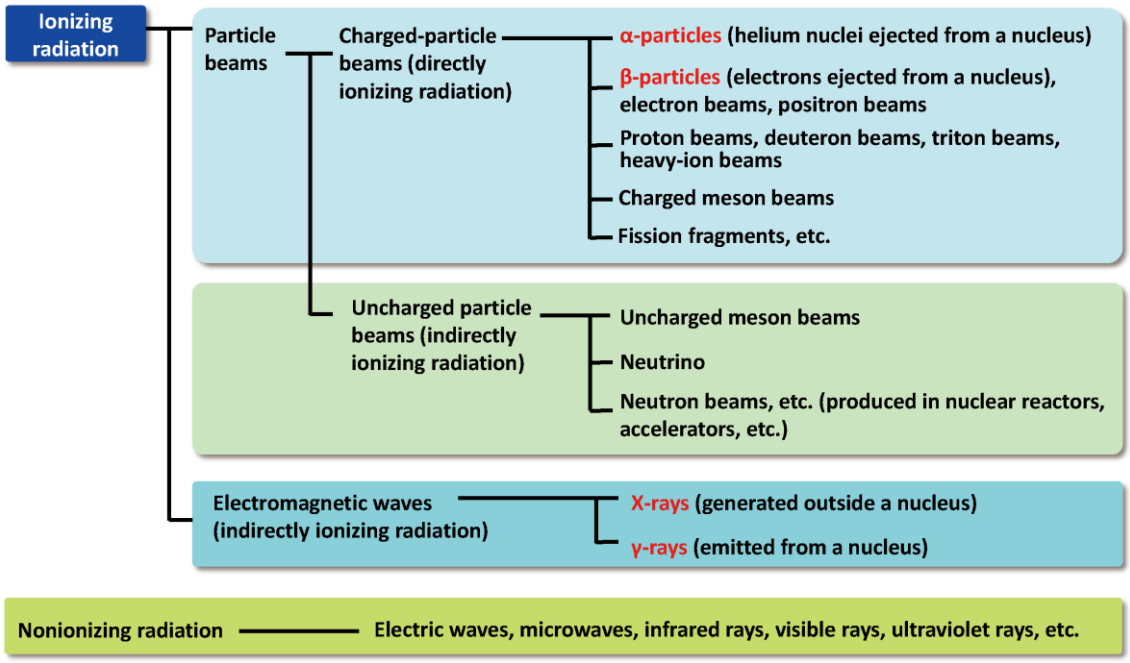



**Figure 2.1:** Classification of radiation based on its ionizing property (MOEJ, 2022).

### 2.1.1. Ionizing radiation

Ionizing radiation is radiation that possesses enough energy to ionize (that is, remove one or more electrons from) an atom or a molecule. The ionization of atoms or molecules can have a significant impact on chemical reactions and biological processes, and hence, ionizing radiation is often harmful for biological systems.

Ionizing radiation typically includes types of radiation that are high in energy and frequency, and these types are generally divided into two main categories: particle beams and electromagnetic waves. For example, alpha particles, beta particles, neutrons, and protons fall into the particle beam category, while gamma rays and X-rays belong to the electromagnetic wave category (Figure 2.2). This type of radiation can propagate through particles emitted as a result of the decay of an atomic nucleus or through high-energy photons generated as a result of high-energy processes. Ionizing radiation can interact with the surrounding material in various ways. These interactions typically occur through three mechanisms known as Compton scattering, the photoelectric effect, and pair production. These interactions will be explained in more detail in the following sections.

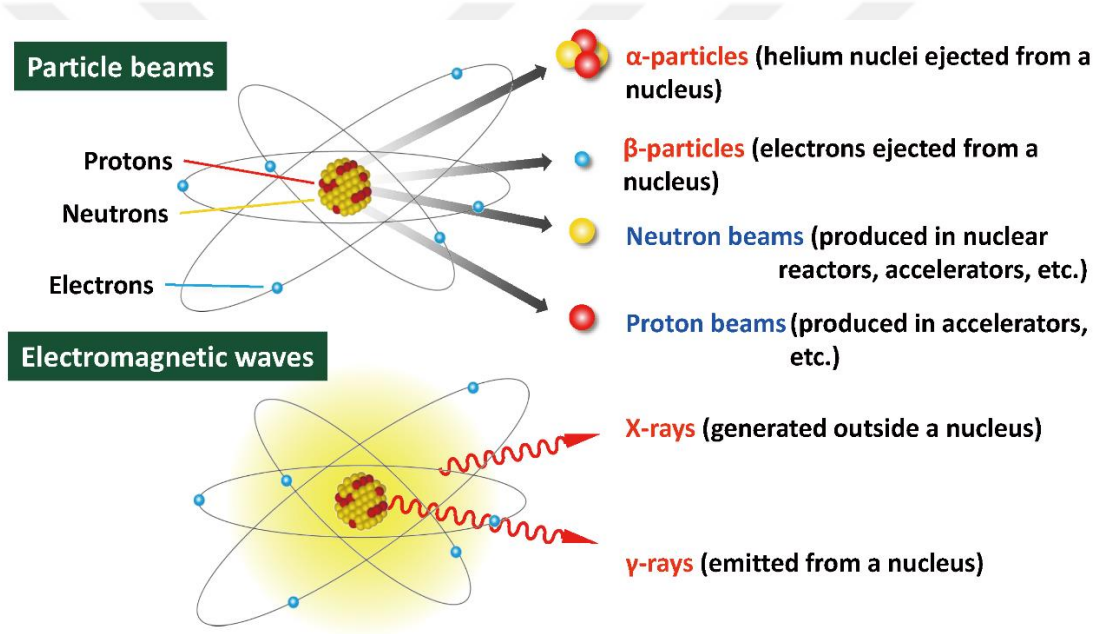



**Figure 2.2:** Types of Ionizing Radiation (MOEJ, 2022).

### 2.1.2. Non-ionizing radiation

Non-ionizing radiation is a type of radiation that does not have enough energy to ionize atoms or molecules. This type of radiation is found on the low-energy end of the electromagnetic spectrum and is typically present in the form of radio waves, microwaves, infrared rays, and visible light (Figure 2.3). This energy level is not strong enough to eject electrons from atoms or molecules, so unlike ionizing radiation, non-ionizing radiation does not cause direct atomic or molecular changes. However, with sufficient in-

tensity or prolonged exposure, non-ionizing radiation can have biological effects. For example, microwaves can cause heat in cells and infrared rays can lead to skin burns. Therefore, rigorous work should be carried out on the potential effects and control of non-ionizing radiation, and regulations should be made to ensure its safe use in various application fields and technologies.

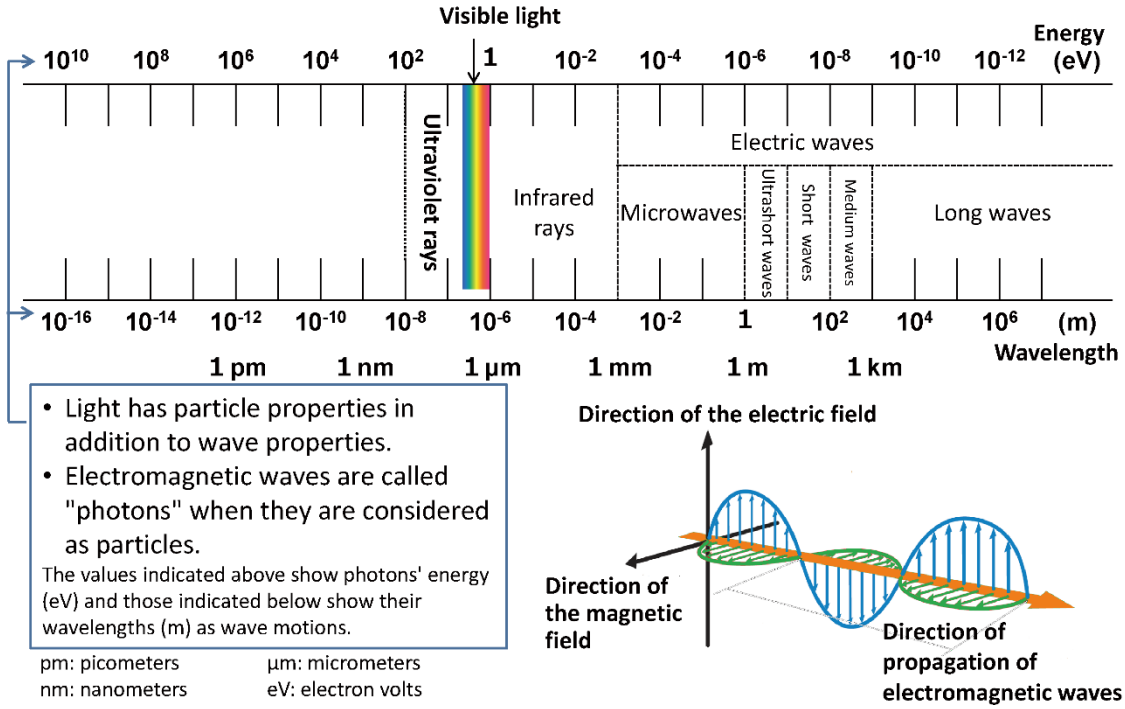
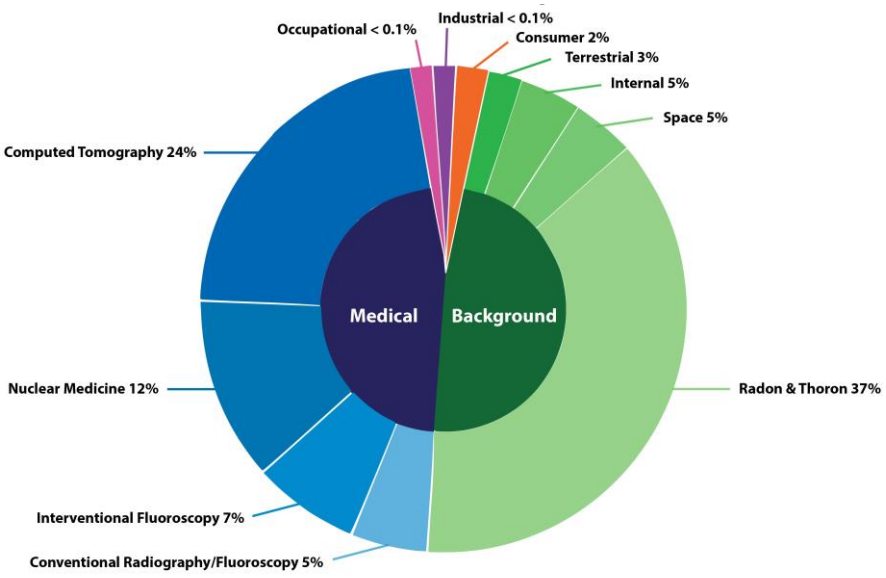



**Figure 2.3:** Types of Non-Ionizing Radiation (MOEJ, 2022).

## 2.2. Radiation Sources

Radiation can originate from both natural and artificial sources. Natural sources of radiation encompass radioactive materials in the universe and cosmic rays. For instance, natural radioactive elements such as radium, radon, and uranium can be found in soil, water, and air. Cosmic rays are high-energy particles that reach Earth from space. Artificial sources of radiation include medical radiography and radiotherapy, nuclear power plants, industrial radiography, and radioisotope production. While medical radiography and radiotherapy are used in the diagnosis and treatment of diseases, nuclear power plants are employed for electricity production, industrial radiography is used for material testing, and radioisotope production serves various industrial and medical applications. This diversity shows that radiation has a wide range of applications and also suggests the necessity of regulation and control in its use across these fields. To minimize

potential effects of radiation and to protect human health, radiation safety is a crucial subject, and the management of radiation sources is at the heart of engineering and regulatory activities in this field.




Average Annual Radiation Dose

| Sources | Radon & Thoron | Computed Tomography | Nuclear Medicine | Interventional Fluoroscopy | Space | Conventional Radiography/ Fluoroscopy | Internal | Terrestrial | Consumer | Occupational | Industrial |
|---|---|---|---|---|---|---|---|---|---|---|---|
| Units | | | | | | | | | | | |
| mrem (United States) | 228 mrem | 147 mrem | 77 mrem | 43 mrem | 33 mrem | 33 mrem | 29 mrem | 21 mrem | 13 mrem | 0.5 mrem | 0.3 mrem |
| mSv (International) | 2.28 mSv | 1.47 mSv | 0.77 mSv | 0.43 mSv | 0.33 mSv | 0.33mSv | 0.29 mSv | 0.21 mSv | 0.13 mSv | 0.005 mSv | 0.003 mSv |

**Figure 2.4:** Sources of radiation exposure (NCRP Report No. 160, 2022).

### 2.2.1. Natural sources of radiation

Natural sources of radiation include radioactive elements and cosmic rays that are constantly present in our environment and often constitute an unavoidable part of radiation exposure. Terrestrial radiation, or radiation originating from the earth, comes from radioactive elements such as uranium, thorium, and their decay products, as well as radon gas. These elements are naturally present in minerals and rocks in the Earth's crust. Cosmic rays are high-energy particles that are continually bombarding the Earth's atmosphere and originate from the sun as well as other stars and galaxies. Additionally, there are also sources of biological radiation, including natural radioactive elements found in the human body, such as carbon-14 and potassium-40. While radiation from natural sources is typically at low levels, it is significant from an environmental and public health perspective and should be taken into account in radiation protection and safety studies. Understanding the effects of radiation from these sources is crucial in developing radiation safety policies and protocols.

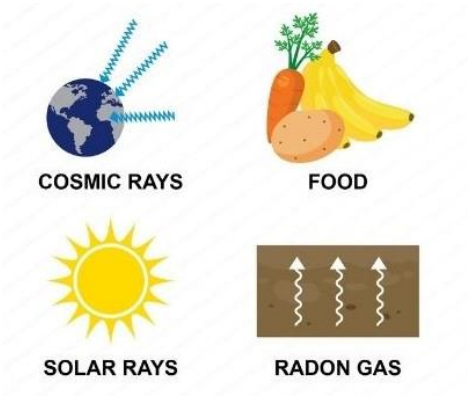



**Figure 2.5:** Natural sources of radiation (IAEA, 2021).

### 2.2.2. Artificial sources of radiation

Artificial sources of radiation are those radiation sources that are created typically for medical, industrial, and scientific applications, and are a consequence of human activities. Medical applications are often the largest source of artificial radiation and are used in radiological imaging procedures (such as X-rays, CT scans, PET scans, etc.) and radiation treatments (for instance, radiotherapy for cancer treatment). Industrial applications use radiation to test, measure, and inspect materials; for example, radiography is used to detect flaws in materials. In scientific applications, radiation is utilized for various experiments and research. Moreover, applications such as nuclear power plants and nuclear weapons also represent significant artificial sources of radiation. These sources play an important role in terms of public health and environmental safety. Therefore, the use, regulation, and control of artificial radiation sources constitute a fundamental aspect of nuclear engineering and radiation protection studies. Understanding and managing potential risks arising from artificial radiation sources is vital for developing effective radiation safety protocols and policies.

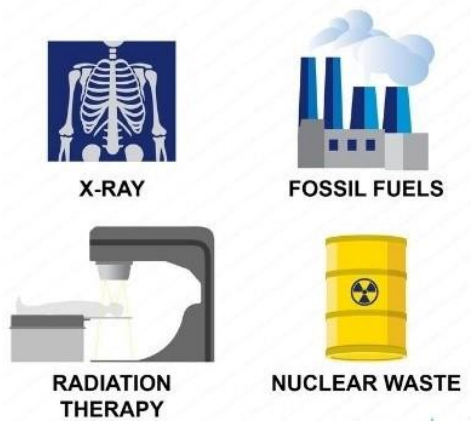



**Figure 2.6:** Artificial sources of radiation (IAEA, 2021).

## 2.3. Types of Radioactive Decay

Radioactive decay is a process where an atomic nucleus is unstable and releases energy to transition into a more stable state. This decay process is typically divided into three main types: alpha, beta, and gamma decays. Alpha decay is a process in which the atomic nucleus emits an alpha particle, which is a helium nucleus containing two protons and two neutrons. Beta decay is a process in which a neutron is converted into a proton, emitting an electron (beta particle) in the process. Gamma decay is a process where the energy level of the nucleus drops and a gamma ray is emitted to balance this energy reduction. Each type of decay has different energy and penetration capabilities. While alpha particles are generally high energy, they have the least penetration capability. Beta particles have slightly more penetration capability. Gamma rays have the highest penetration capability and can even pass through dense materials. Understanding the types of radioactive decay is important for applications in nuclear engineering fields like radiation protection and radioactive waste management.

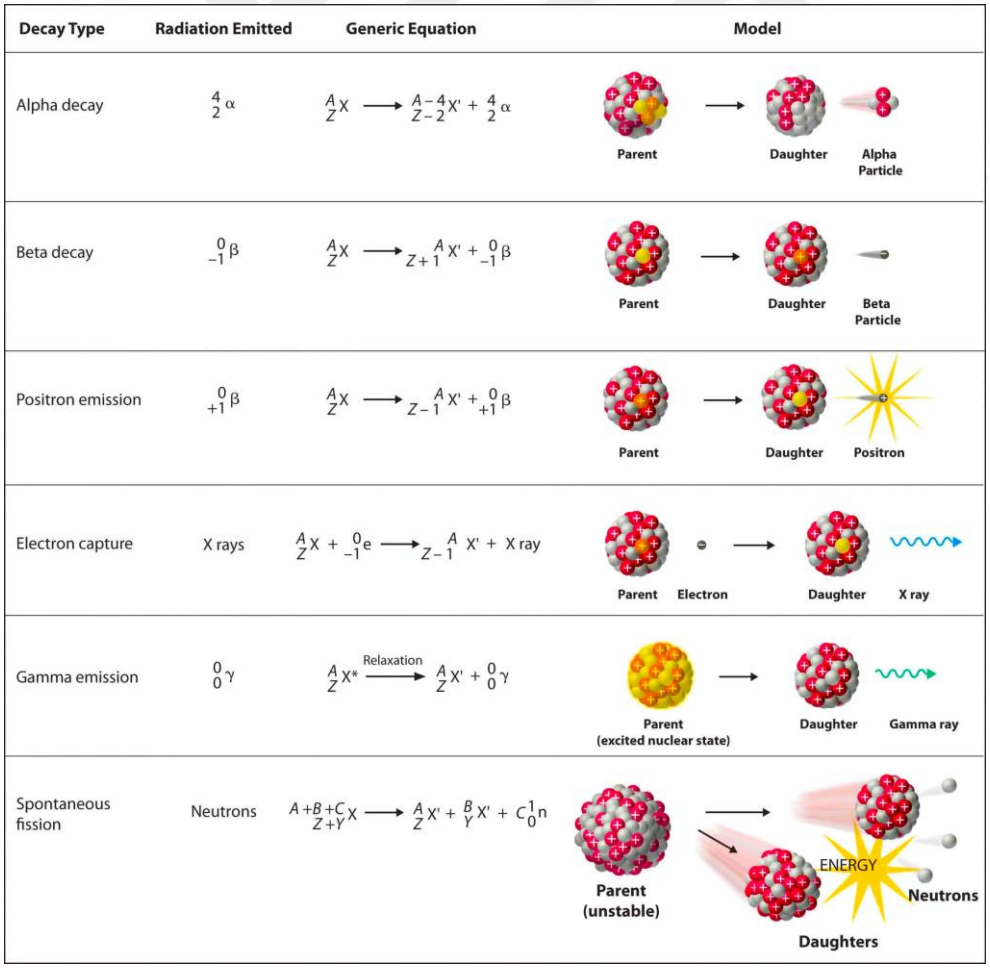



**Figure 2.7:** Types of radioactive decay (IAEA, 2021).

### 2.3.1. Alpha decay

Alpha decay is one of the radioactive decay processes and is predominantly observed in heavy atomic nuclei. In this process, the nucleus loses a mass of four units and suffers a loss of two units in proton number; this leads to a decrease in the atomic number (Z) by two units and the mass number (A) by four units. These losses correspond to the emission of an alpha particle (a helium nucleus consisting of two protons and two neutrons) from the nucleus. Alpha decay releases energy known as the Q value (the energy of the decay), in accordance with the principle of energy conservation. This energy is distributed as kinetic energy to the alpha particle and to the daughter atom nucleus produced as a result of the decay. This distribution occurs in such a way that the alpha particle, having a smaller mass, receives a large portion of the kinetic energy. Alpha decay occurs due to a mechanism known as quantum tunneling. This allows the nucleus to emit the alpha particle by overcoming the energy barrier. Alpha particles are usually a significant risk factor for biological systems, as they readily interact with the surrounding material.




**Figure 2.8:** Alpha Decay schematic (IAEA, 2019).

### 2.3.2. Beta decay

Beta decay is a type of radioactive decay of subatomic particles. During this decay process, a neutron in an atomic nucleus transforms into a proton, emitting an electron and an antineutrino (or in some cases, a positron and a neutrino) in the process. In this transformation, the atomic number of the nucleus increases by one while the total nucleon count (protons and neutrons) remains constant. A detailed analysis of beta decay involves topics in quantum mechanics and particle physics.

In particular, beta decay provides important insights about the fundamental physical force known as the weak force. The weak force governs the interactions of fermions - i.e., fundamental particles - and its existence makes beta decay possible. A thorough understanding of the interactions of the weak force allows for the very precise modeling of the beta decay process. This is especially important in nuclear engineering, as beta

decay is a process that has significant impacts on nuclear reactors and the nuclear fuel cycle.




**Figure 2.9:** Beta Decay schematic (IAEA, 2019).

### 2.3.3. Positron emission

Positron emission, or beta plus decay, is a type of radioactive decay. In this process, a proton in the atomic nucleus is converted into a neutron, and during this transformation, a positron and a neutrino are emitted. The positron is the antimatter counterpart of the electron and carries the same magnitude but opposite charge. This process occurs in proton-rich atoms and is typically found in radioisotopes with a low neutron/proton ratio, that is, those with a deficiency of neutrons. Positron emission is an important phenomenon widely utilized in nuclear engineering and medical imaging technologies (like PET) to understand physical and chemical processes and make imaging of these processes. It is based on the interaction of positrons with electrons, leading to an annihilation event. Both particles are converted into energy, which is expelled in the form of two gamma photons, typically of 511 keV energy each. These photons are emitted exactly 180 degrees apart from the nucleus and are used in PET scans. Understanding and controlling positron emission is very important for optimizing the operation of nuclear reactors and the nuclear fuel cycle.

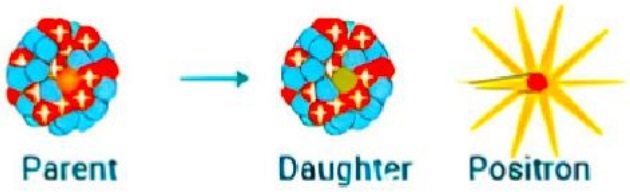



**Figure 2.10:** Positron emission schematic (IAEA, 2019).

### 2.3.4. Electron capture

Electron capture is another notable type of radioactive decay process, crucial in the field of nuclear engineering. In this process, an atomic nucleus captures one of its orbiting

electrons (usually from the innermost shell), which then combines with a proton to form a neutron, with the emission of an electron neutrino. Because the captured electron typically comes from the innermost, or K-shell, this process is often referred to as K-capture. Following the electron capture, the atomic number of the element decreases by one, transforming it into a new element. This process commonly occurs in proton-rich (neutron-deficient) isotopes where the transformation to a lower atomic number is energetically favorable. Additionally, this event often leads to an excited nucleus, which may drop to a lower energy state by emitting a gamma ray. Understanding electron capture is of great importance for applications such as nuclear reactors and medical isotopes production, and in various areas of research including astrophysics and neutrino studies.

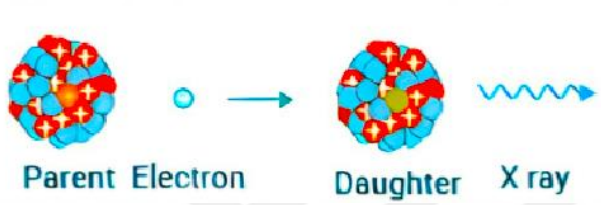



**Figure 2.11:** Electron capture schematic (IAEA, 2019).

### 2.3.5. Gamma emission

Gamma emission is a radioactive decay process that occurs during transitions between energy levels of an atomic nucleus. It involves an atomic nucleus transitioning from an excited (high-energy) state to a lower energy state. The difference in energy is expelled as a gamma-ray, a photon of very high energy. Gamma rays are the highest energy and shortest wavelength part of the electromagnetic spectrum. A range of processes, including nuclear reactions and radioactive decay, can lead to the production of gamma rays. Since the energy of gamma rays corresponds to the difference in energy levels of the nucleus, gamma spectra provide important information about the energy levels of a specific atomic nucleus. The emission and detection of gamma rays have significant applications in nuclear engineering, medical imaging, radiotherapy, and various areas of scientific research.

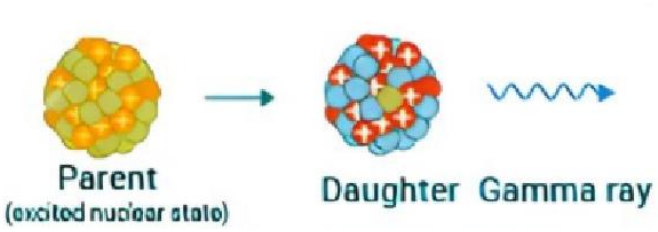



**Figure 2.12:** Gamma emission schematic (IAEA, 2019).

### 2.3.6. Spontaneous fission

Spontaneous fission is the random and spontaneous process of a particular heavy atomic nucleus, such as uranium-235, uranium-238, and plutonium-240, breaking apart due to instability. During this process, the atomic nucleus splits into lighter nuclei by emitting one or more neutrons, releasing energy in the process. Spontaneous fission plays a significant role in nuclear energy production and nuclear weapons technology. The occurrence of this process in a specific atom is quite rare, but when a sufficient number of atoms are present, fission events happen with enough frequency due to probability laws. The rate of spontaneous fission depends on the type and instability of the nucleus. Understanding spontaneous fission accurately is critical in nuclear reactor design and operation because the rate of neutron release directly affects the control of the reactor. Understanding the spontaneous fission process is also important in radioactive waste management and reducing the environmental impacts of nuclear energy.

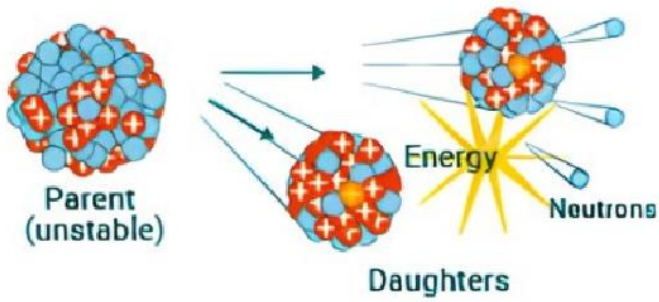



**Figure 2.13:** Spontaneous fission schematic (IAEA, 2019).

## 2.4. The Discovery and Characteristics of Gamma Rays

Gamma rays represent the most energetic and highest frequency portion of the electromagnetic spectrum. Discovered by the French physicist Paul Villard in 1900, gamma rays naturally occur as a result of radioactive decay. One characteristic of gamma rays is that, like other electromagnetic waves, their speed is equal to the speed of light. Additi-

onally, due to their higher energy compared to X-rays, gamma rays can easily penetrate through matter, making them useful in nuclear and particle physics applications, medical imaging, and cancer treatment. However, due to their high energy and high-frequency nature, gamma rays can also pose a significant radiation hazard. This requires nuclear engineers to take necessary precautions to minimize the effects of these rays and to use them safely and effectively.

### 2.4.1. Gamma sources

Gamma rays are produced as a result of various events such as nuclear decay of radioactive materials and high-energy particle collisions. Here are several main sources of gamma rays:

- Radioactive Decay: Many radioactive elements produce gamma rays during the decay process. This decay is the transition of an atomic nucleus to a more stable state and typically involves the emission of alpha or beta particles along with the release of gamma rays. For example, isotopes like cobalt-60 and cesium-137 are typical sources of gamma rays.




**Figure 2.14:** A representative visual of some radioactive gamma sources (U.S.-NRC, 2019).

**Table 2.1:** Some examples of gamma sources along with their half-life and main energy values

| Isotope | Symbol | Half-life | Main gamma-ray Energies (MeV) |
|---|---|---|---|
| Cesium-137 | $^{137}$Cs | 30,0 years | 0,662 |
| Barium-133 | $^{133}$Ba | 10,4 years | 0,384; 0,356; 0,303; 0,276; 0,081 |
| Cobalt-60 | $^{60}$Co | 5,26 years | 1,332; 1,173 |
| Sodium-22 | $^{22}$Na | 2,60 years | 1,275; 0,511 |
| Manganese-54 | $^{54}$Mn | 312 days | 0,835 |
| Zinc-65 | $^{65}$Zn | 244 days | 1,116 |
| Selenium-75 | $^{74}$Se | 120 days | 0,401; 0,280; 0,265; 0,136 |
| Yttrium-88 | $^{88}$Y | 107 days | 1,836; 0,898 |

**Continuation of Table 2.1…**

| | | | |
|---|---|---|---|
| Iridium-192 | $^{192}Ir$ | 74 days | 0,468; 0,316; 0,308; 0,296 |
| Antimony-124 | $^{124}Sb$ | 60 days | 2,091; 1,691; 0,723; 0,603; 0,121 |
| Mercury-203 | $^{203}Hg$ | 46 days | 0,279 |

**Source:** (Turgay, 2019).

- Cosmic Events: High-energy cosmic events also generate gamma rays. These events include supernova explosions, neutron stars, and black holes, which are some of the most energetic and violent events in the universe. These events can accelerate subatomic particles to speeds close to the speed of light, resulting in the production of gamma rays through collisions.

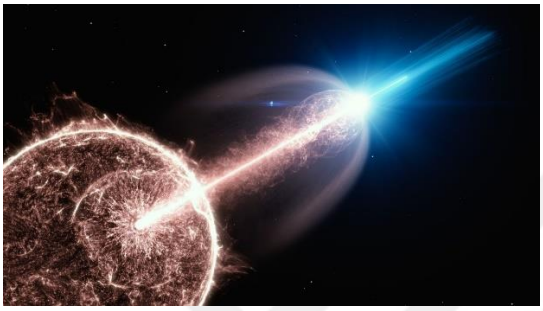


**Figure 2.15:** A representative visual of gamma-ray bursts (NASA, 2019).

- Nuclear Reactors and Weapons: Nuclear fusion and fission processes also produce gamma rays. Nuclear reactors generate a range of products during the fission process, and these products typically emit gamma rays. Additionally, the detonation of nuclear weapons also produces gamma rays.



**Figure 2.16:** A representative visual of nuclear power plant (U.S.-NRC, 2010).



**Figure 2.17:** A representative visual of nuclear weapon (U.S.-NRC, 2022).

- Particle Accelerators: Particle accelerators accelerate subatomic particles to high speeds, and the collision of these particles generates gamma rays. Particle accelerators are commonly used in physics research and certain medical applications.

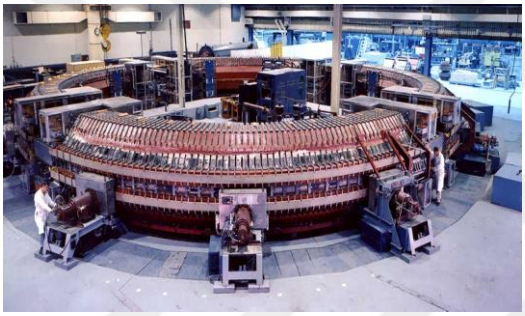


**Figure 2.18:** A representative visual of particle accelerator (CERN, 2015)

- Radiation Therapy: Another field where gamma rays are used is in medical applications, particularly in cancer treatment. Devices used in radiation therapy produce high-energy gamma rays to kill tumor cells.

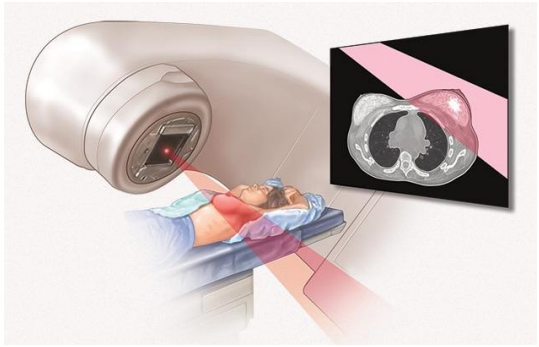


**Figure 2.19:** A representative visual of radiation therapy (U.S.-NRC, 2010).

These are the main sources of gamma rays, and gamma radiation has found various applications in nuclear engineering, astrophysics, and medicine.

## 2.5. The Discovery and Characteristics of Neutron Particles

Neutrons are fundamental components of an atomic nucleus and play a central role in nuclear physics due to their neutral charge and a range of properties. The discovery of neutrons is based on the remarkable work of the British physicist James Chadwick in 1932. Chadwick confirmed Ernest Rutherford's 1920 prediction by providing evidence for the existence of neutral components in the atomic nucleus. Neutrons, having no electrical charge, do not interact with other atoms, thus they play a balancing role among the positively charged protons within the atomic nucleus, thereby ensuring the stability of the atom.

Neutrons and protons together are called nucleons, and the mass number (A) of an atom represents the total number of these two particles. The rest mass of neutrons is slightly higher than that of protons (approximately one proton mass plus an electron mass), supporting the law of conservation of energy in beta decay processes.

Neutrons form the basis of nuclear fission and fusion processes, and these properties are of vital importance in the field of nuclear engineering. In the process of nuclear fission, a slow-moving (thermal) neutron collides with the nucleus of a fissile isotope, predominantly uranium-235 or plutonium-239. This collision leads to the splitting of the nucleus and the release of a large amount of energy. Additionally, more neutrons are released in this process, initiating a fission chain reaction. Neutrons are also key players in nuclear fusion processes. Fusion occurs when the nuclei of hydrogen isotopes, typically deuterium and tritium, combine. This fusion process results in the formation of a helium nucleus and a high-energy neutron. These properties of neutrons enable them to play a critical role in nuclear energy generation, radiation therapy, nuclear medical imaging, and materials science applications (Table 2.3). However, along with these properties, the control and management of neutrons need to be done correctly because the impact of high-energy neutrons on biological systems can pose significant health risks. Table 2.12 summarizes the fundamental properties of neutrons.

**Table 2.2:** The properties of neutrons

| | |
|---|---|
| **Discovered / Discovery Date:** | James Chadwick / 1932 |
| **Mass (akb)** | 1,008982 |
| **Mass (kg)** | $1{,}674 \times 10^{-27}$ kg |
| **Charge** | 0 |
| **Spin** | 1/2 |

**Continuation of Table 2.2…**

| | |
|---|---|
| **Lifetime** | 887 s. |
| **Nuclear decay equation** | $p^+$ , $e^+$ |
| **Diameter** | $1{,}45x10^{-13}$ cm |
| **Magnetic dipole moment** | μN= -1,935 JxT $^{-1}$ |
| **Antiparticle** | Antineutrino |
| **Half-life** | $t_{1/2}$ = 615 s. |

**Source:** (Korkut, 2019).

**Table 2.3:** Applications of Neutrons.

| | |
|---|---|
| **Physics and Chemistry Researchs** | High-energy plastic production. |
| **The production of crystalline materials.** | Material characterization. |
| **Medical diagnostic materials.** | Accelerator-Driven Systems (ADS). |
| **Superconductor production.** | Space exploration |
| **Cancer treatment** | Neutron activation analysis |
| **Determining the position of hydrogen atoms in molecules** | Medical isotope production |

**Source:** (Korkut, 2019).

Neutrons, being neutral particles, cannot be accelerated like charged particles such as protons. However, their energy can be reduced through collisions with atoms in matter. The energy, wavelength, and application areas of neutrons can be represented as shown in Table 2.4.

**Table 2.4:** Accepted neutron energy ranges encompassing the characteristics of advanced generation sources

| **Neutron Type** | **Energy Range (MeV)** | **Wavelength (Å)** | **Moderator Temperature (K)** | **Application Areas** |
|---|---|---|---|---|
| Ultra-cold neutrons | $<3x10^{-4}$ Mev | ≥500 | ≈5 | Basic properties of neutrons, ultra-low angle scattering |
| Very cold neutrons | $3x10^{-4}$ –0,1 | 30–500 | 5–20 | Spectroscopy and supermolecular structures |
| Cold neutrons | 0,1-5 | 4-30 | 20-100 | High-resolution spectroscopy |
| Thermal neutrons | 5-100 | 1-4 | 120-300 | Neutron diffraction spectroscopy |
| Epithermal neutrons | $100\text{-}10^3$ | 1-0.3 | 300 | High-energy spectroscopy |
| Resonant neutrons | $10^3\text{-}10^5$ | 0,3-0,03 | 300 | Intense inelastic scattering |

**Continuation of Table 2.4…**

| | | | | |
|---|---|---|---|---|
| Intermediate neutrons | $10^5$-$10^8$ | 0,03-9x$10^{-4}$ | - | Atomic physics, Device irradiation |
| Fast neutrons | $10^8$-$10^{10}$ | 9x$10^{-4}$-x$10^{-5}$ | - | Nuclear physics |
| Ultra-fast neutrons (Relativistic) | $10^{10}$-$3^{12}$ | 9x$10^{-5}$-5x$10^{-6}$ | - | Hadron physics |

**Source:** (Korkut, 2019).

The investigation of neutron-matter interactions is of fundamental importance in nuclear engineering and radiation protection strategies. These interactions are determined by two main parameters: microscopic and macroscopic cross-sections, which determine how neutrons will interact with a specific material. The microscopic cross-section represents the probability of an interaction between a neutron and a particular nucleus, while the macroscopic cross-section determines the overall interaction probability of a material and is calculated as the product of the number of atoms or molecules in a given volume and the microscopic cross-section.

Neutron interactions with matter are generally classified as elastic and inelastic scattering. Inelastic scattering is more effective with elements that have a high atomic number, such as iron-56, which enables the widespread use of materials containing iron and barium in neutron shielding. On the other hand, elastic scattering is more effective with light elements like hydrogen, indicating that materials rich in hydrogen, especially water, paraffin, and polyethylene, are excellent for neutron shielding. These interactions will be explained in more detail in the following sections.

### 2.5.1.Neutron sources

Neutron Sources can generate neutrons through various methods, including alpha-beryllium sources, photonuclear sources, spontaneous fission, nuclear reactions, and reactors.

#### 2.5.1.1.Alpha-neutron sources

Alpha-neutron sources play an important role in many compact laboratory experiments. These sources produce energetic alpha particles through a series of emitters and converters, which are used to trigger (α, n) reactions with various radioisotopes. In these (α, n) reactions, energetic alpha particles are directed towards target nuclei. If these particles manage to overcome the potential barriers, lighter nuclei emit a neutron.

These nuclei are typically light isotopes such as lithium, beryllium, boron, carbon, fluorine, and sodium. These light nuclei undergo bombardment by alpha particles to produce neutrons, forming the fundamental mechanism of alpha-neutron sources. These neutrons are then used for various experiments and measurements.

Alpha-neutron sources play a significant role in various fields such as nuclear physics, materials science, and medical applications. Specifically, neutrons are used to determine material properties, structure, and composition. Additionally, the selective ability of neutrons to kill cancer cells is utilized in medical applications such as Boron Neutron Capture Therapy (BNCT).

Each (α, n) source differs in the energy spectrum and intensity of the generated neutrons. Therefore, selecting the most suitable source for an experiment or application is important. Table 4 provides a comparative analysis of various (α, n) sources based on their relative intensity, aiding in determining which source is most suitable for a specific application.

**Table 2.5:** Q value and neutron yield for (α,n) reactions from light nuclei

| **Target** | **Reaction** | **Q-value (MeV)** | **Neutron Yield per $10^6$ α particles** |
|---|---|---|---|
| Natural Beryllium | $^{10}$Be (α,n) | +1,07 | 13 for $^{241}$Am-α particle |
| Beryllium-11 | $^{11}$Be (α,n) | +0,158 | 13 for $^{241}$Am-α particle |
| Berilyum-9 | $^{9}$Be (α,n) | +5,71 | 13 for $^{241}$Am-α particle |
| Fluorine | $^{10}$F (α,n) | -1,93 | 4,1 for $^{241}$Am-α particle |
| Carbon-13 | $^{13}$C (α,n) | +2,2 | 11 for $^{241}$Am-α particle |

**Source:** Topal, (2019).

### 2.5.1.2.Photon-neutron sources

Photon-neutron sources relate to gamma photons with energy levels exceeding approximately 7 MeV. A gamma photon at this energy level can trigger a (γ, n) reaction, meaning it can dislodge a neutron from the nucleus. This occurs when the neutron binding energy is surpassed by the energy of the gamma photon.

The fundamental mechanism of a photon-neutron source involves an energetic photon striking a target material and triggering a bremsstrahlung (braking radiation) event, leading to the production of neutrons. Bremsstrahlung is an event where an electron emits some of its energy in the form of X-rays or gamma rays when it approaches or orbits around a nucleus. An energetic photon can trigger this braking radiation, releasing neutrons within the target material.

The probability of a gamma photon triggering a (γ,n) reaction is directly related to the energy of the photon. In other words, a photon with higher energy will have a higher probability of triggering a (γ,n) reaction. These reactions occur when the energy of the photon is high enough to surpass the binding energy of the neutron.

Photon-neutron sources can produce neutrons over a broad energy spectrum, making them ideal for a range of applications including material characterization, radioactive waste analysis, cancer treatment, and nuclear physics experiments. However, the use of these sources requires careful monitoring and management from a radiation safety perspective, as high-energy photons and neutrons can pose serious health risks.

#### 2.5.1.3. Activation neutrons sources

Activation neutrons are associated with the decay processes of certain nuclei and are typically sourced from fission. Fission can be defined as the process of splitting an atomic nucleus, which results in the release of energy and typically multiple neutrons. These neutrons can propagate from an activated nucleus during the fission process or as a result of a delayed process. This latter group is known as delayed neutrons.

Activation neutrons primarily occur when an atomic nucleus captures a neutron and subsequently emits one or more neutrons. This process typically occurs when high-energy neutrons interact with the nucleus and often leads to the nucleus becoming more unstable. When unstable nuclei are activated by energetic neutrons, they can undergo various decay processes. These decay processes typically involve a form of radiation and often the emission of one or more neutrons. Activation neutrons result from the decay of these unstable nuclei. Activation neutrons are used in a range of important applications in nuclear physics and engineering. These include neutron activation analysis, radioactive waste management, and radiotherapy. They are also utilized in nuclear reactors for energy production and material testing. However, when working with activation neutrons, radiation safety must be considered. This entails implementing appropriate shielding, radiation monitoring, and safety procedures.

#### 2.5.1.4. Spontaneous fission neutron sources

Spontaneous fission is a process in which certain radioactive isotopes spontaneously undergo fragmentation. This process typically occurs when a nucleus has high energy and naturally decays, releasing energy. Spontaneous fission is often a decay mode for

heavy and unstable isotopes. Californium-252 is a significant example of spontaneous fission and is commonly used as a neutron source. This isotope undergoes an alpha decay with a half-life of approximately 2.65 years. However, about 3% of Californium-252's decays result from spontaneous fission events, which emit a series of energetic neutrons during the fission process. Due to its ability to produce these neutrons, Californium-252 is regarded as a valuable source in many applications. In nuclear reactors, fission neutrons are typically obtained as a direct result of a fission reaction. When a heavy nucleus, usually uranium-235 or plutonium-239, is struck by a high-energy neutron, it undergoes fragmentation, releasing two lighter nuclei and several energetic neutrons. These neutrons are utilized to trigger further fission reactions, enabling the sustained operation of a nuclear reactor. These processes allow for the utilization of neutrons from both Californium-252 and nuclear reactors in a variety of applications such as radioactive waste management, material analysis, medical treatments, and energy production. However, the use of such neutron sources requires radiation safety and protection measures.

#### 2.5.1.5. Nuclear reactions

Neutrons can be produced through a series of nuclear reactions. Such reactions can serve as a source of neutrons for various applications. Accelerators can also be used in the production of neutrons, which involves using particle accelerators to increase the energy levels of charged particles and initiate neutron-emitting nuclear reactions. However, the acceleration of charged particles is generally an energy-intensive process, which often makes accelerators less practical compared to radioactive decay sources. Radioactive decay is a process where neutrons are naturally emitted and is typically more energy-efficient. Neutron production typically occurs through the following types of nuclear reactions:

$^{3}H + d \rightarrow {}^{4}H + n$ Q = + 17,6 MeV (2.1)

$^{2}H + d \rightarrow {}^{3}H + n$ Q = + 3,3 MeV (2.2)

$^{9}Be + {}^{4}He \rightarrow {}^{12}C + n$ Q = + 5,7 MeV (2.3)

$^{7}Li + p \rightarrow {}^{7}Be + n$ Q = -1,6 MeV (2.4)

### 2.5.1.6. Nuclear reactors

In nuclear reactors, during the fission process, approximately $10^{14}$ neutrons are released per second. These neutrons typically have energy levels of 5-7 MeV. Since high-energy neutrons are not suitable for sustaining fission, a type of "moderator" is used to reduce their energy and make them more favorable for fission. Typical moderators can include substances like water, heavy water, or graphite. As the neutrons are slowed down and their energies decrease, they become "thermal neutrons." This state facilitates their interaction with fissile isotopes, such as uranium and thorium. When these fissile isotopes interact with thermal neutrons, they undergo fission due to their cross-sections (probability of interaction) with neutrons. As a result of the fission process, the mass energy of the material is converted into energy according to Einstein's famous equation $E=mc^2$. Additionally, these elements also have fertile isotopes that can undergo nuclear reactions with higher energy fast neutrons. Fast neutrons can trigger higher-energy fissions, thereby enabling greater energy production. Nuclear power plants, which generate electricity, control these fission processes through a series of control mechanisms and cooling systems. These systems ensure that the reaction remains under control and prevent potential overheating or critical situations. The design and operation of nuclear power plants typically involve addressing a range of complex issues, such as the energy of the fission process, reactor cooling, management of radioactive waste, and implementation of safety procedures.

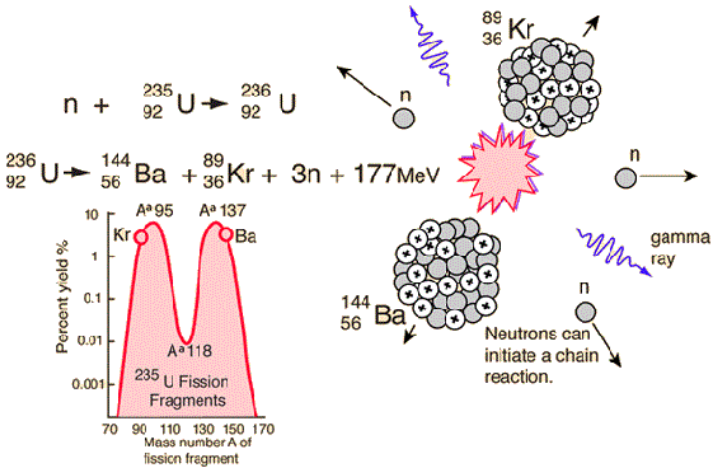



**Figure 2.20:** An example of a fission reaction observed in a reactor and the relationship graph between the mass numbers (A) of the newly formed nuclei after fission.

## 2.6. The Interaction of Radiation with Matter

Radiation can interact with the atomic and molecular structure of matter in various ways. These interactions typically occur in the forms of ionization or excitation. Ionization is the process where an energetic particle (such as an alpha particle, beta particle, or gamma ray) removes an electron from an atom or molecule, resulting in the formation of a positively charged ion and one or more free electrons. Ionization usually occurs as a result of interactions with high-energy radiation and can lead to radiation damage, radiation sickness, or genetic damage. Excitation, on the other hand, is the process where an energetic particle "excites" the electrons of an atom or molecule to higher energy levels. This excited state is usually unstable, and the electron quickly returns to its original energy level, emitting a photon (a light particle) in the process. These photons can typically be detected by measurement devices and can be used to determine the type, energy, and other characteristics of the radiation. In addition, radiation can also interact with the atomic nucleus of matter. Neutron scattering is an example of such interactions, where a neutron collides with an atomic nucleus and is scattered. These types of interactions are important for understanding the internal structure of matter and controlling the fission process in nuclear reactors. The interaction of radiation with matter depends on factors such as the duration of radiation exposure, the type and energy of the radiation encountered, and the material's ability to absorb and scatter radiation. These factors determine the resistance of matter to radiation damage and are of critical importance in nuclear engineering. Table 2.6 presents the types of radiation that arise as a result of various reactions, along with their characteristics.

**Table 2.6:** The types of fundamental radiation and their characteristics

| **Radiation Type** | **Charge** | **Energy Range** | **Air Range** | **Water Range** |
|---|---|---|---|---|
| Alpha (α) particles | +2 | 3-10 MeV | 2-10 m | 20-125 μm |
| Beta (+) particles | +1 | 0-3 MeV | 0-10 m | <1 cm |
| Beta (-) particles | -1 | 0-3 MeV | 0-10 m | <1 cm |
| Neutrons | 0 | 0-10 MeV | 0-100 m | 0-1 m |
| X-rays | 0 | 0,1-100 MeV | 0-10 m | mm-cm |
| Gamma rays | 0 | 0,01-10 MeV | 0-10 m | mm-10 cm |

**Source:** Subaşı, (2021).

### 2.6.1. Interaction mechanisms of photons with matter

Photons interact with matter through a series of interaction mechanisms. Rayleigh scattering primarily describes the interaction of low-energy photons (below a few keV) with atoms. The energy of the photon excites the outer electrons of the atom, but these electrons quickly return to their original energy levels, and the photon is scattered with almost the same energy (and thus frequency). The photoelectric effect is an interaction where a photon collides with one of the inner electrons of an atom and provides enough energy to remove it completely from the atom, creating a particle known as a photoelectron. This event is typically applicable to photons in the range of X-rays and gamma rays. Pair production is an interaction mechanism that is generally valid for photons with energies higher than 1.02 MeV. The photon loses its energy to create an electron-positron pair. This process involves the complete conversion of the photon's energy into particles, leading to the disappearance of the photon itself. Lastly, Compton scattering is a process where a photon collides with a free or outer-shell electron, transferring energy to the electron and causing it to transition to a higher energy state. The photon is scattered with lower energy (and thus lower frequency) after the collision. This process is generally applicable to photon energies ranging from meV to MeV. Understanding these interactions helps us comprehend how photons interact with matter, and their applications in nuclear engineering include radiation protection, radiation therapy, and radiation detection technologies.

#### 2.6.1.1. Photoelectric effect

The photoelectric effect is a phenomenon that was pivotal in the development of quantum mechanics and for which Albert Einstein received the Nobel Prize in 1905. It refers to situations where the energy of a photon is sufficient to eject an inner-shell electron from its bound energy level in an atom (Figure 2.21). The energy of the photon is divided into two components: the kinetic energy of the electron and the binding energy (BE) associated with its attachment to the atomic nucleus. Mathematically, this can be expressed as the photon's energy (hf) being equal to the sum of the electron's kinetic energy ($1/2\ mv^2$) and the binding energy (BE). The photoelectric effect is a significant area in nuclear engineering with applications in radiation protection, medical imaging (especially X-ray and gamma camera technologies), and even energy generation (such as solar cells). One of the most important aspects of this phenomenon is the direct rela-

tionship between the photon energy and the electron's kinetic energy, which is highly useful in X-ray spectroscopy and other energy-dispersive techniques. However, a complete understanding of the photoelectric effect also involves considering the complex nature of the interaction between photon energies and matter, taking into account the energy levels of materials and the behavior of electrons at these levels. This forms a critical part of modern nuclear engineering and is necessary to fully comprehend how matter interacts with radiation.

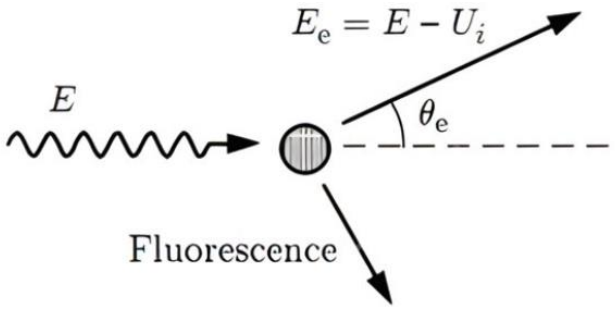



**Figure 2.21:** Photoelectric effect schematic (IAEA, 2019).

#### 2.6.1.2. Rayleigh scattering

Rayleigh scattering is a phenomenon that describes the interaction of low-energy photons (below a few keV) with atoms. In this interaction process, a photon is absorbed by one of the atom's electrons and immediately re-emitted. This absorption and re-emission process involves the temporary transition of the electron to a higher energy state and then returning to its original state. The energy level change causes the photon to deviate from its original path, giving rise to the term "scattering." (Figure 2.22). Rayleigh scattering conserves the energy and momentum of the photon. This means that the scattered photon has the same frequency as the original photon. However, other properties such as the scattering angle and polarization state of the scattered photon can vary. The characteristics of Rayleigh scattering depend on factors such as the electron density of the material and the energy levels of the electrons. In nuclear engineering, Rayleigh scattering is commonly used to understand the scattering of low-energy X-rays and gamma rays. It is also important for determining the interaction properties of materials with radiation and characterizing the structural properties of materials. It is particularly relevant in the design and analysis of materials that interact with low-energy radiation. A thorough understanding of Rayleigh scattering is crucial to comprehend how matter

interacts with radiation and how these interactions can affect the structure and properties of matter.

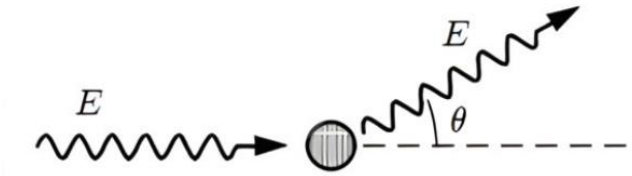



**Figure 2.22:** Rayleigh scattering schematic (IAEA, 2019).

### 2.6.1.3. Compton scattering

Compton scattering is a process in which a photon collides with a free or outer-shell electron, transferring energy to the electron and elevating it to a higher energy state. In this interaction, the incoming photon transfers energy and momentum to both the electron and the scattered photon. As a result of this energy transfer, the energy and frequency of the incoming photon decrease. This frequency shift depends on the energy difference between the initial and final states of the photon and is commonly referred to as Compton shift. After undergoing Compton scattering, the energy of the scattered photon decreases and the wavelength increases as it is deflected in a different direction from the incident angle. The change in wavelength is represented by the equation $\Delta\lambda = \lambda' - \lambda$, as shown in the image below:

$$\lambda-\lambda' = \frac{h}{m_0 c}(1-\cos\theta) = 0{,}024264(1-\cos\theta)\,\text{Å} \qquad (2.5)$$

Here, the term expressed as h/m0c is generally referred to as the Compton wavelength, with a numerical value of approximately 2,4264 x $10^{-10}$ cm. Compton scattering is particularly important for gamma rays in the intermediate energy range (0.5-1 MeV) and can also be observed at energies below 0.1 MeV in low-Z materials. The most significant consequence of Compton scattering is the change in energy of the photon, depending on the scattering angle. This characteristic is utilized in a technique called Compton spectroscopy, which is employed to measure the energy and intensity of radiation. Additionally, this interaction is used to determine the energy distribution and intensity of materials exposed to X-rays and gamma rays.

In nuclear engineering, Compton scattering is important in various applications, including radiation protection, radiation detection, and radiation-related risk assessments. It is employed to determine the energy distribution and intensity of radiation sources and materials interacting with radiation.

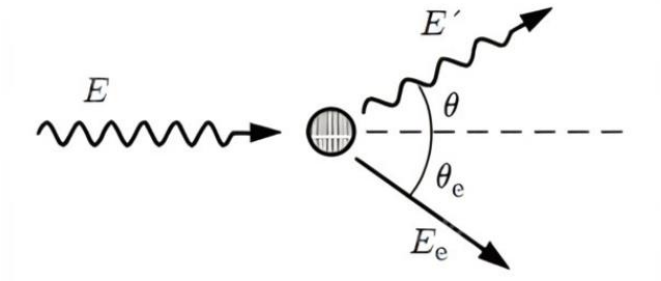



**Figure 2.23:** Compton scattering schematic (IAEA, 2019).

### 2.6.1.4. Pair production

Pair production refers to the interaction process of high-energy photons with matter. In this process, typically involving photons with energies greater than 1.022 MeV, a photon passing near an atomic nucleus or an electron utilizes its entire energy to create an electron-positron pair.

$$c = \nu\lambda \tag{2.6}$$

The relationship between the energy and wavelength of a photon is described by Planck's equation: E = hv = hc/λ, where E represents the energy of the photon, h is Planck's constant, v is the frequency of the photon, c is the speed of light, and λ is the wavelength of the photon. This equation indicates that as the energy of the photon increases, its wavelength decreases. In other words, a high-energy photon can have a wavelength comparable to the size of the nucleus, which is smaller than that of an atom.

The high energy of the photon can interact with particles within the nucleus, transferring its energy and rendering the nucleus unstable. During the process of using the photon's energy to create an electron and a positron, the entire energy of the photon is converted into the energies of the particles, leading to the complete annihilation of the photon. In this energy transfer process, the electron and positron each acquire an equal portion of the original energy of the photon, contributing to their respective rest mass energies.

Sometimes during pair production, the original nucleus may receive a certain amount of energy and momentum to ensure energy conservation. This is referred to as recoil of the

nucleus. Pair production is more commonly observed when the energy of the photon is greater than 1.022 MeV, which is the minimum energy required for the creation of an electron-positron pair. Understanding the process of pair production is important for comprehending how high-energy radiation interacts with matter, and it plays a significant role in radiation protection and detection applications.

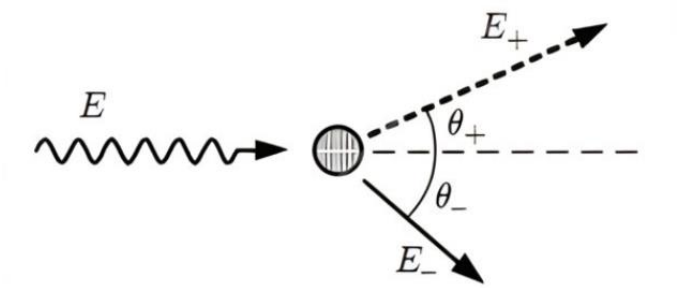



**Figure 2.24:** Pair production schematic (IAEA, 2019).

### 2.6.2. Interaction mechanisms of neutrons with matter

Neutrons, being neutral particles, interact with matter primarily through nuclear forces, giving rise to various mechanisms. The most common one is 1-) elastic scattering, which is a process where a neutron collides with a nucleus and transfers some or all of its kinetic energy to it. This can result in a change in the neutron's direction and a decrease in its speed. This process is significant in nuclear reactors where neutrons are slowed down, or "moderated," to lower energy levels, allowing for more fission events. 2-) Inelastic scattering is another mechanism where a neutron transfers energy to a nucleus, exciting it to a higher energy state. The excited nucleus typically emits gamma radiation as it returns to its ground state. This process is particularly important in the fast neutron region, typically above energies of 1 MeV. 3-) Charged particle reactions involve a neutron interacting with an atomic nucleus, releasing one or more charged particles. These reactions generally occur with high-energy neutrons and depend on the structure of the nucleus and the energy of the neutron. 4-) Radiative capture is the process in which a neutron is absorbed by a nucleus, which then emits gamma radiation. This process can lead to the transformation of elements, as the absorbing nucleus typically becomes a different isotope or even a different element. Radiative capture is often used in neutron activation analysis and plays a crucial role in the operation of thermal reactors, serving as a primary source of energy production and a means of controlling the neutron population. Finally, 5-) the fission process occurs when a neutron is absor-

bed by a heavy nucleus, causing the nucleus to split into two smaller nuclei, releasing a significant amount of energy, additional neutrons, and fission products. This mechanism forms the basis of nuclear energy and nuclear weapons. Understanding these interactions is important in nuclear engineering, especially in applications such as nuclear energy, radiation shielding, and nuclear instrumentation.

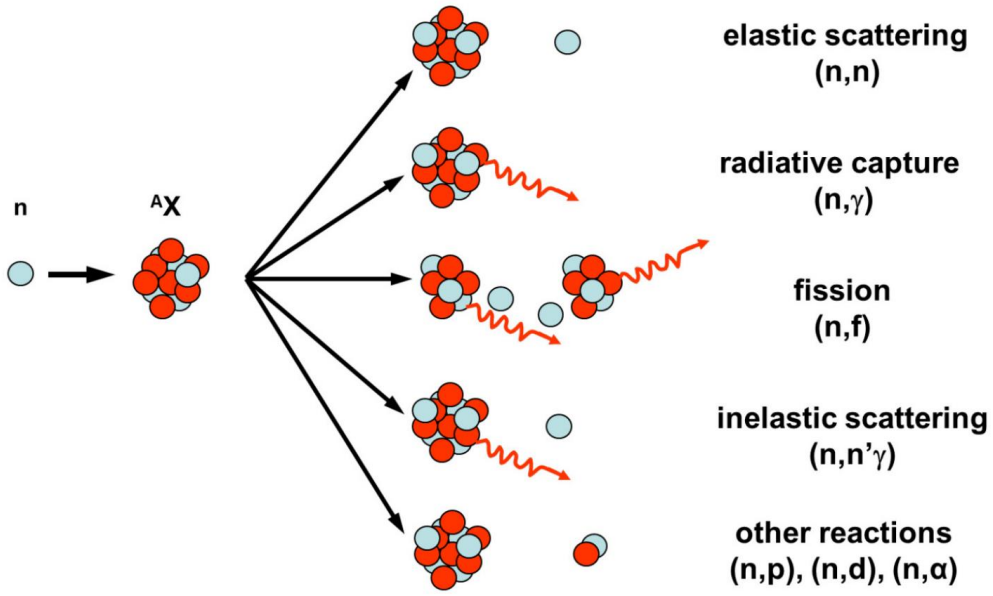



**Figure 2.25:** Interaction mechanisms of neutrons with matter (IAEA, 2019).

### 2.6.2.1. Scattering

A neutron scattering reaction takes place when a nucleus, upon being impacted by a neutron, emits another neutron. Although the initial and final neutrons may not be (and often are not) identical, the overall outcome of the reaction resembles the projectile neutron simply bouncing off or scattering from the nucleus. The two types of scattering reactions, elastic and inelastic scattering, are explained in the following paragraphs.

#### 2.6.2.1.1. Elastic scattering

Elastic scattering refers to the interaction (n,n) process where a neutron collides with an atomic nucleus and transfers a portion or all of its energy to the nucleus. This process follows the classical principles of conservation of kinetic energy and momentum. During the collision, the neutron and nucleus change their directions while preserving their energies and momenta. The characteristics of elastic scattering depend on factors such as the initial energy of the neutron and the mass number of the nucleus. High-energy neutrons are typically scattered at small angles, while low-energy neutrons are often

scattered at larger angles. Additionally, elastic scattering is generally proportional to the mass number of the nucleus, meaning larger nuclei tend to result in larger scattering angles. In nuclear engineering, elastic scattering is important in various applications, including radiation shielding and radiation detection technologies. This process determines the distribution and movement of neutrons within a material, which is crucial for determining the energy distribution and intensity of neutron sources and materials interacting with neutrons. A comprehensive understanding of elastic scattering plays a significant role in the design and analysis of neutron sources and materials interacting with neutrons.

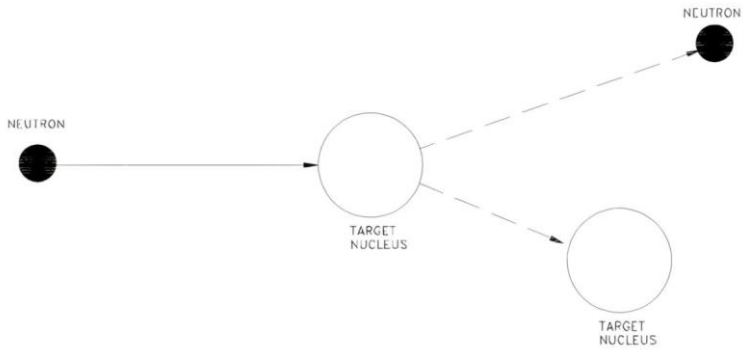



**Figure 2.26:** Elastic Scattering schematic (IAEA, 2019).

#### 2.6.2.1.2. Inelastic scattering

Inelastic scattering is a process in which a neutron collides with an atomic nucleus and transfers sufficient energy to the nucleus, thereby raising the nucleus to a higher energy state or an "excited" state. This interaction process is typically applicable to fast neutrons, meaning neutrons with energies generally above 1 MeV. After the collision, the nucleus, due to its increased energy, usually emits one or more gamma-ray photons. These gamma rays are a result of the nucleus transitioning from the excited state to its ground state. In this case, the energy of the nucleus is equal to the sum of the neutron's original energy and the energy emitted by the nucleus in the form of gamma-ray photons. This process is determined by the energy levels of the nucleus and the initial energy of the neutron. Different atomic nuclei may have different energy levels, and therefore, there are specific energy thresholds for inelastic scattering. Understanding inelastic scattering is important in nuclear reactors to comprehend the neutron energy spectrum, develop radiation protection strategies, and design radiation detectors. Additionally, the inelastic scattering process is significant in understanding how neutrons

move within materials, as the direction of the neutron can change during this process. A comprehensive understanding of this process is crucial in the design and analysis of neutron sources and materials interacting with neutrons.

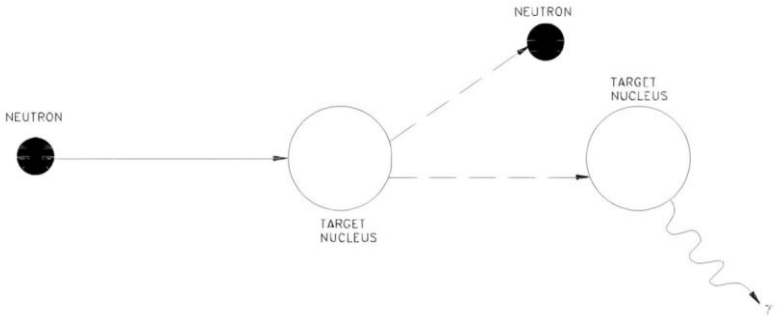



**Figure 2.27:** Inelastic Scattering schematic (IAEA, 2019).

### 2.6.2.2. Absorption interaction

#### 2.6.2.2.1. Radiative capture

Radiative capture is a process in which a neutron is absorbed by an atomic nucleus, resulting in the emission of one or more gamma ray photons. This process begins with the neutron entering the nucleus and causing it to transition to a higher energy level. Subsequently, the nucleus emits a gamma ray photon to lower its energy. Neutron absorption leads to the transformation of the nucleus into the next isotope or even a new element. Radiative capture typically occurs with thermal neutrons, which have very low energies (average kinetic energies around 0.025 eV). However, it can also take place in higher regions of the energy spectrum. This process is of vital importance in the control and operation of nuclear reactors. Radiative capture is used to control the neutron population and, consequently, adjust the reactor's power output. Additionally, this process plays a significant role in the production of specific isotopes, for example, for the generation of radioisotopes used in radiation therapy and medical imaging. Lastly, radiative capture is a valuable tool for measuring and understanding neutron interactions. The measurement and analysis of neutron interactions are crucial for determining the ability of materials to interact with neutrons and characterizing material properties. Radiative capture is a central component of these measurements and analyses.

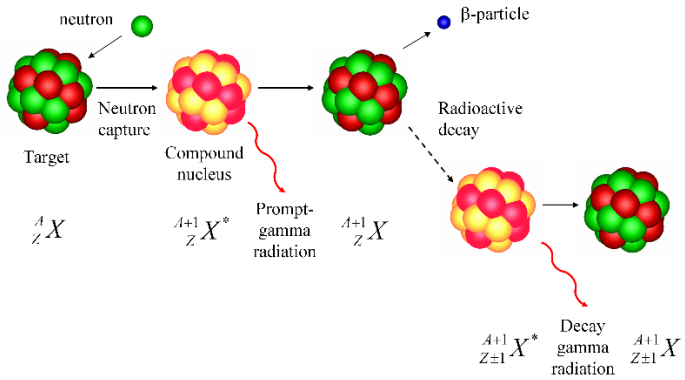



**Figure 2.28:** Radiative capture schematic (IAEA, 2019).

#### 2.6.2.2.2. Fission

Fission is a process where a neutron is typically absorbed by a heavy atomic nucleus, causing it to split into two fragments and releasing a significant amount of energy. This fission occurs to maximize the stability of the nucleus by increasing its energy. As a result of fission, typically two or more new nuclei, several neutrons, and a tremendous amount of energy are generated. The most well-known example of fission is the induced fission of uranium-235 by thermal neutrons. In this case, uranium-236, formed by the addition of a neutron, undergoes an energetic fission process, producing krypton and barium nuclei, three additional neutrons, and releasing approximately 200 MeV of energy. The fission process forms the basis of nuclear power generation and nuclear weapons. Additionally, the detection and analysis of fission products play a critical role in fields such as nuclear forensics and nuclear material accounting. Moreover, fission neutrons sustain the chain reaction necessary to maintain the criticality of nuclear reactors. Therefore, a comprehensive understanding of the fission process is a vital component of nuclear engineering and nuclear sciences.

### 2.6.2.3. Transfer interaction

#### 2.6.2.3.1. Charged particle reactions

Charged particle reactions involve the interaction of a neutron with an atomic nucleus, resulting in the release of one or more charged particles. These reactions typically occur with high-energy neutrons and are dependent on the structure of the nucleus and the energy of the neutron. One example is the (n, p) reaction, known as a neutron-proton reaction. In this reaction, a neutron is absorbed by a nucleus, and a proton is released.

This is a type of neutron capture process where the nucleus undergoes a transformation from one element to another. For example, a neutron can be absorbed by a carbon-13 nucleus, resulting in the release of a proton and the formation of carbon-14.

Another example is the (n, α) reaction, where a neutron is absorbed by a nucleus, and an alpha particle (a helium nucleus consisting of two protons and two neutrons) is released. These types of reactions are dependent on the energy states of the nucleus and the energy of the neutron, and they typically occur with high-energy neutrons. Charged particle reactions are important in understanding neutron interactions and neutron spectrum, and they play a significant role in nuclear energy production, radiation protection, and the design of radiation detectors.

$$ {}^{1}_{0}n + {}^{10}_{5}B \rightarrow {}^{7}_{3}Li + {}^{4}_{2}He \tag{2.6} $$

## 2.7. Radiation Units

Radiation units are of vital importance for measuring and characterizing various aspects of radiation. The effects of radiation are measured and quantified through parameters such as dose, dose rate, activity, and exposure, each defined by specific radiation units. These units are indispensable tools for understanding the quantity and impact of radiation.

They are used in various applications including the safe operation of nuclear facilities, development of radiation protection strategies, medical radiation practices, and environmental radiation monitoring and assessment. Radiation units enable us to understand and manage the potential effects of radiation on humans and the environment. Furthermore, these units provide a worldwide standard for determining and comparing levels of radiation exposure and associated risks. This allows scientists, engineers, and policymakers to make radiation-related decisions based on scientific evidence.

Lastly, radiation units play a crucial role in the development and implementation of radiation-related laws and regulations. They enable us to measure and quantify the quantity and impact of radiation, informing the creation of policies and practices based on this information.

### 2.7.1. Activity unit

Activity measures the number of decays per unit time of a radioactive material and is a fundamental concept in radiation physics. The unit of activity is expressed as

"becquerel" (Bq), which represents one decay per second. Previously, an older unit commonly used was the "curie" (Ci), which is approximately equal to 3.7 x $10^{10}$ becquerels, or corresponds to 3.7 x $10^{10}$ decays per second. The unit of activity is important in various applications. For example, in radiation therapy, medical imaging, environmental monitoring, and other areas where radioactive sources are used, measuring the activity of radioactive sources is necessary. It is also used to determine and manage the concentration of radioactive isotopes and neutron flux in nuclear reactors. Measuring activity is particularly important in the management and storage of radioactive materials, as it is a critical parameter for assessing radiation exposure and the potential effects of radioactive sources on human health and the environment. Activity measurements are used to guide safety protocols, radiation protection strategies, and radioactive waste management practices.

### 2.7.2. Irradiation dose unit

The unit "Roentgen" (R) is a specific measurement unit for radiation exposure, representing the amount of X-ray and gamma radiation that produces an electric charge of 2.58x$10^{-4}$ Coulombs (C) per kilogram of air under normal conditions (0 °C and 760 mm Hg pressure). This is expressed as

1 Roentgen (R) = 2.58x$10^{-4}$ C/kg (2.8)

The Roentgen unit is typically used for X-ray and gamma radiation with energies below 3 MeV. However, it is not used for radiation from particle types such as alpha and beta particles. Interestingly, these measurements are independent of the speed of radiation. This is an important point to consider when determining radiation exposure, as it takes into account the interaction of radiation with energy and matter. It indicates that the Roentgen unit is suitable as an exposure measurement only for specific types and energies of radiation.

### 2.7.3. Absorbed dose unit

The radiation unit Absorbed Dose is a radiation unit that measures the degree of irradiation of a specific material with a specific amount of energy. The energy of radiation is defined as the amount of energy applied to a surface or material and is commonly measured in the unit "Gray" (Gy). One Gray is defined as the absorbed dose of radiation resulting from the deposition of 1 joule of energy in 1 kilogram of material. Gray is par-

ticularly important in medical applications, such as radiation therapy, as it is used to measure the radiation dose delivered to tissues. This is critical for assessing the effectiveness of radiation therapy treatment and potential side effects for the patient.

Additionally, the Gray unit is used in industrial applications, such as nuclear power plants and radioactive waste facilities. In these types of facilities, Gray measurements are performed to determine and manage radiation exposure levels for workers and the surrounding environment. Another common unit of absorbed dose is the "Rad" (Radiation Absorbed Dose), where 1 rad is defined as the absorbed dose of radiation resulting from the deposition of 100 ergs of energy in 1 gram of material. However, the Gray unit, used within the SI unit system, is more commonly used in modern applications and scientific literature. The conversion between these two units is as follows: 1 Gy = 100 rad. Therefore, Gray and rad can often be used interchangeably to determine radiation dose.

### 2.7.4. Equivalent dose unit

Among radiation units, Equivalent Dose plays an important role in measuring the biological effects of radiation. Equivalent dose is obtained by multiplying the absorbed dose of radiation in an organ or tissue by a factor that corresponds to the biological effect of the radiation type. This factor is called the radiation weighting factor or quality factor and is used to account for the biological effects of different types of radiation (e.g., alpha particles, beta particles, neutrons, gamma rays, and X-rays). The SI unit for equivalent dose is the Sievert (Sv), although the Rem (roentgen equivalent man) unit is also commonly used. The equivalence of 1 Sv to 100 Rem is valid. Equivalent dose is a critical parameter in radiation protection applications where the biological effect of radiation combines with the radiation dose. This unit allows us to better understand the relationship between radiation exposure and its biological effects. Since different types and energies of radiation have varying effects on biological tissues, the equivalent dose plays a critical role in converting these effects into a standardized measurement, enabling the development of radiation protection strategies and risk assessments.

### 2.7.5. Effective dose unit

One of the radiation units, Effective Dose is used to assess the potential biological effects of radiation on specific organs or tissues. Effective dose provides a standardization by taking into account factors such as different types of radiation and the sensitivity of

exposed organs to radiation. Effective dose is obtained by weighting the equivalent doses received by each organ or tissue according to their sensitivity to radiation. These weighting factors consider the organ's radiation sensitivity and potential health effects that may arise from radiation exposure. The SI unit for effective dose is the Sievert (Sv). The use of effective dose in radiation protection and the assessment of biological effects allows for a comprehensive evaluation of the potential harmful effects of radiation. Effective dose is a vital measurement for predicting and managing health risks associated with exposure to radiation on organs and tissues. Therefore, radiation safety and health physicists often utilize effective dose measurements in radiation exposure and risk management planning.

### 2.8. Methods of Protection Against Radiation

Radiation protection is of vital importance considering the wide range of applications and potential hazards associated with radiation. The principle of ALARA (As Low As Reasonably Achievable) has been developed as the fundamental basis for protecting against the harmful effects of radiation. According to this principle, the aim is to minimize exposure to radiation by implementing measures that keep the dose as low as reasonably achievable.

To achieve this, several key principles are followed:

- Minimizing Exposure Time: Limiting the duration of exposure to radiation is crucial in reducing overall dose. Minimize the time spent in areas with high radiation levels or when working with radiation-emitting devices.
- Maximizing Distance: Increasing the distance between oneself and the radiation source significantly decreases radiation exposure. Maintaining a safe distance from the radiation source is important in minimizing the dose received.
- Effective Shielding: The use of appropriate shielding materials is essential to block or attenuate radiation. Materials such as lead, concrete, and other dense substances are commonly used for effective radiation shielding. Ensuring that shielding is properly designed and positioned provides additional protection.
- Contamination Control: Preventing the entry of radioactive materials into the body is critical. Proper personal protective equipment, including gloves, masks, and specialized clothing, should be used when handling radioactive substances. Practicing

good hygiene and following decontamination procedures minimize the risk of ingestion or inhalation.

- Radiation Monitoring: Regularly monitoring radiation levels in the environment, workplaces, or areas where radiation exposure is possible is necessary. This enables compliance with safety regulations and allows for early detection of any radiation hazards.
- Education and Training: Proper education and training on radiation safety are essential for individuals working with or around radiation. Understanding the risks, safety protocols, and emergency procedures is vital to effectively minimize exposure and respond to potential incidents.
- Compliance with Regulations: Adherence to local regulations and guidelines related to radiation safety is crucial. Ensuring that facilities, equipment, and practices comply with established standards helps maintain a safe working environment.

By following the ALARA principle and implementing these measures, it is possible to minimize radiation exposure and protect against its potential hazards. A comprehensive approach that considers these factors is essential to ensure the safety and well-being of individuals working with radiation.

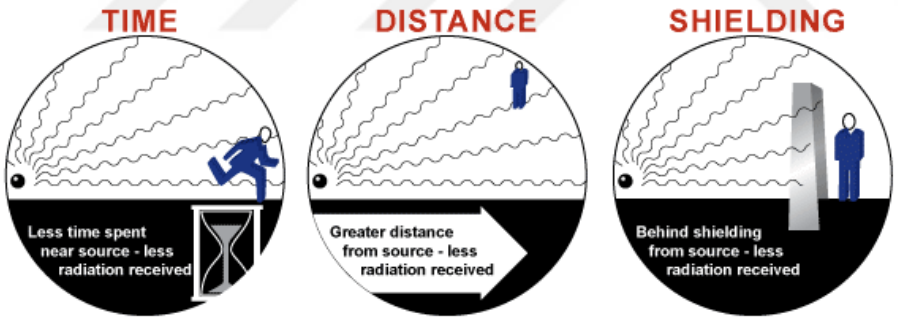



**Figure 2.29:** Methods of protection against radiation (IAEA, 2019).

### 2.8.1. Time rule

The "time rule," which is one of the fundamental principles of radiation protection, means minimizing the duration of radiation exposure. This principle is based on the fact that radiation dose is directly proportional to the duration of exposure; that is, the less time spent, the lower the radiation dose received. Implementing the time rule is important, especially for radiation workers or individuals at risk of exposure to radioactive materials. It is recommended for radiation workers to plan in advance how much time they will spend in radiation areas and to limit their interactions with radiation to a mi-

nimum and as necessary. Furthermore, radiation workers often learn to perform their tasks quickly and efficiently, reducing the time spent in radiation fields. This is an important strategy to avoid high radiation doses and minimize potential harmful effects of radiation. This strategy is typically supported by thoughtful analysis of procedures and careful planning of workflows and protocols. This, in turn, is part of the time principle in radiation protection.

### 2.8.2. Distance rule

The "distance rule," which is one of the fundamental principles of radiation protection, refers to maintaining as much distance as possible from a radiation source. This rule is based on the fact that radiation intensity decreases rapidly as the distance from the source increases, following the inverse square law. This phenomenon states that radiation intensity decreases rapidly as the square of the distance from the radiation source increases. This principle implies that doubling the distance from a radiation source reduces the radiation intensity to one-fourth. This helps significantly reduce the radiation dose received when the exposure time remains constant. The distance rule is of critical importance for radiation workers and individuals at risk of exposure to radioactive materials. It is recommended for radiation workers to stay as far away as possible from radiation sources and minimize physical contact with them. This is an integral part of radiation protection strategies and helps minimize the potential health effects of radiation.

### 2.8.3. Shielding rule

One of the key aspects of radiation protection strategies is the "shielding rule." This rule suggests the use of appropriate shielding to absorb or block radiation. Shielding involves placing a barrier between a radiation source and an individual that can stop or absorb the radiation. The choice of shielding material depends on the type and energy of radiation. Alpha and beta particles can generally be stopped by low-density materials such as paper or plastic, while gamma rays and neutrons typically require denser materials such as heavy metals (e.g., lead) or concrete for effective shielding. Shielding materials typically absorb radiation and convert its energy, often into heat. This energy is then safely dissipated into the surroundings. Shielding is an important component of radiation protection strategies and can significantly reduce an individual's radiation

exposure. Shielding is particularly crucial in high-radiation environments, such as nuclear power plants or radiological medical applications.

### 2.9. Radiation Shielding

Radiation shields are typically selected based on the type and energy level of the radiation being encountered. Radiation shields are primarily composed of materials that can stop or attenuate alpha, beta, gamma, and neutron radiation.

- Alpha radiation: Alpha radiation consists of high-energy nuclei emitted from radioactive materials. These particles are large and heavy, so for shielding, a thin layer of paper or even air is often sufficient.

- Beta radiation: Beta radiation consists of electrons or positrons emitted from radioactive materials. Low-density materials such as plastic, glass, or aluminum are typically used to stop beta particles.

- Gamma radiation: Gamma rays are high-energy photons emitted from atomic nuclei. Shielding gamma radiation usually requires heavy metals, especially lead. However, materials like concrete and water can also be effective gamma shields.

- Neutron radiation: Neutrons are neutral-charged particles emitted from radioactive materials or nuclear reactions. Typically, heavy hydrogen-containing materials (e.g., water or polyethylene) or concrete are used to stop neutrons. In special cases, materials like beryllium or iron can also be used depending on the speed of the neutrons.

The effectiveness of radiation shields is often measured by the half-thickness value, which indicates how thick a particular material needs to be to reduce the intensity of a radiation beam by half. Therefore, the design and selection of radiation shields vary depending on the type, energy, intensity, and other factors of the radiation being encountered. Radiation shields are generally divided into two main categories: Passive shields and active shields.

### 2.9.1. Passive shields

Passive shields utilize material properties to limit the effects of radiation. These shields are made of materials that can absorb, scatter, or block radiation. Lead, concrete, water, and various plastics are among the passive shield materials. They are selected based on the type and energy of radiation. Passive shields are used in nuclear reactors, medical radiation equipment, and for the transportation and storage of radioactive materials.

#### 2.9.1.1. Passive radiation shielding categories

Passive Radiation shielding categories can be classified based on their applications as follows:

- Primary Shielding: This category includes shields that are used to block direct radiation from the radiation source. These shields are made of high-density materials that prevent the transmission of radiation, providing protection. Examples of materials used in this category are lead, concrete, or steel.

- Secondary Shielding: This category involves shields used to control the reflections and scatter of radiation emitted from the source. These shields prevent the spread of radiation, ensuring protection. Specialized materials can be used to prevent the reflection of radiation from walls in a room, for instance.

- Personal Shielding: This category encompasses personal protective equipment used by individuals to protect themselves from radiation. Examples include lead aprons, lead glasses, gloves, and other personal protective gear. These equipment items reduce the individual's exposure level, providing protection.

- Structural Shielding: This category includes shields that are structurally integrated into buildings or facilities to protect against radiation.

These shields prevent radiation from entering the building or facility. Examples of this category include reactor shields in nuclear power plants or specially designed rooms in radiology laboratories. These shielding categories are utilized as part of radiation protection strategies and are selected based on the radiation source, type, and intensity.

### 2.9.2. Active shields

Active shields use energy to reduce the effects of radiation. These shields typically measure the radiation field and adjust the energy as needed. Active shields often involve electronic and control systems. They are used, especially in high-radiation environments, to continuously monitor and adjust radiation levels. Active shields are employed in nuclear power plants and radiation therapy applications.

Both types of shields have their own advantages and are usually used together as part of a radiation protection strategy. The choice of shield type depends on the source, type, intensity of radiation, and the individual's exposure time to that radiation.

### 2.9.3. Radiation shielding types based on their purposes

Radiation shielding types based on their purposes of use are as follows:

- Medical Shielding: Used in medical facilities to protect patients, healthcare professionals, and the public from radiation exposure during diagnostic imaging procedures, radiation therapy, and nuclear medicine applications.
- Industrial Shielding: Applied in industrial settings such as nuclear power plants, research laboratories, and industrial radiography facilities to protect workers and the surrounding environment from radiation hazards.
- Transportation Shielding: Utilized in the transportation of radioactive materials to prevent radiation leakage and ensure the safety of the public and transport personnel.
- Military and Defense Shielding: Used in military and defense applications to protect personnel, equipment, and critical infrastructure from radiation hazards associated with nuclear weapons, reactors, and other radioactive sources.
- Space Shielding: Deployed in space exploration missions to shield astronauts and equipment from the harmful effects of cosmic radiation.
- Nuclear Waste Shielding: Employed in the containment and storage of nuclear waste materials to prevent radiation leakage and protect the environment and future generations.

Please note that these are general categories and there may be additional specialized shielding types based on specific applications.

### 2.9.4. Slowing down and absorption of gamma rays

When gamma rays interact with matter, several outcomes can occur: absorption, scattering, or no interaction at all. The interaction mechanism of gamma rays with matter is schematically shown in (Figure 2.30). Let's delve into the details:

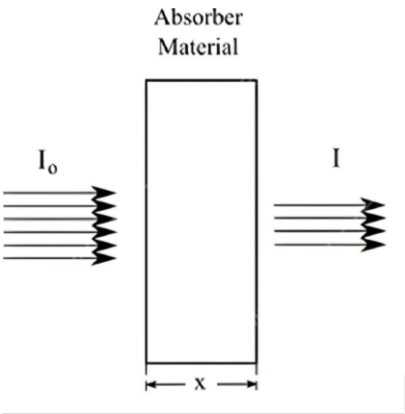



**Figure 2.30:** Mechanisms of photon attenuation (IAEA, 2017)

The mathematical calculation of the change in photon energies is done using the Beer-Lambert (2.9) equation;

$$-\frac{dI}{dx} = \mu I \tag{2.9}$$

Here, when the intensity of photons passing through a material with a thickness of x is arranged as I(x) and integrated;

$$\int_{I_0}^{I(X)} \left(\frac{dI}{I}\right) = \int_{0}^{X} -\mu dx \tag{2.10}$$

The expression is obtained. By utilizing the properties of logarithms;

$$\ln I(x) - \ln I_0 = -\mu x \tag{2.11}$$

It is expressed in the form. Here, $I_0$ represents the intensity of photons incident on the shielding material, I(x) represents the intensity of photons passing through the shielding material with a thickness of x, and μ represents the linear attenuation coefficient. This exponential relationship signifies that photons can never be completely absorbed by the absorber material but can be reduced to very low values. Alongside the linear attenuation coefficient, another expression that helps understand the radiation shielding capabilities of materials is the mass attenuation coefficient ($\mu_m=\mu/\rho$), which represents the ratio of the linear attenuation coefficient to the material density.

The unit of the linear attenuation coefficient is $cm^{-1}$, and the unit of the mass attenuation coefficient is $cm^2/g$. Other useful definitions used in photon absorption are the half-value layer (HVL) and the tenth-value layer (TVL). The half-value layer represents the thickness of the absorber material required to reduce the incident photon intensity by half, while the tenth-value layer represents the thickness of the absorber material required to reduce the incident photon intensity by one-tenth. According to the Beer-Lambert equation, the half-value layer can be expressed as.

$$\frac{I(x)}{I_0} = \frac{1}{2} = I_0 e^{-\mu x_{1/2}} \tag{2.12}$$

It is expressed as $x_{1/2}$. If $x_{1/2}$ is solved, it can be written as;

$$HVL = \frac{\ln(2)}{\mu} \tag{2.13}$$

Similarly, for the tenth value layer (TVL), it can be obtained by;

$$TVL = \frac{\ln(10)}{\mu} \tag{2.14}$$

The equation allows us to obtain the HVL and TVL values, which are useful expressions for comparing the radiation shielding performance of different materials and for designing effective shields.

To gain a more detailed understanding through deeper research, it's necessary to consider parameters of the chosen material such as the effective atomic number (Zeff), effective electron density (NE), and radiation protection efficiency (RPE). These parameters are defined in Equations 2.15, 2.16, and 2.17.

$$RPE = \left(1 - \frac{I}{I_0}\right)100 \tag{2.15}$$

Radiation protection efficiency (RPE) is a parameter used to quantify the effectiveness of a material in shielding against or attenuating ionizing radiation. It is a measure of how well a material can absorb or deflect radiation, thereby protecting surrounding areas or organisms from the harmful effects of that radiation. The higher the RPE, the more efficient the material is at providing protection against radiation.

$$Z_{eff} = \frac{\sum_i f_i A_i (\frac{\mu}{\rho}) i}{\sum_j f_j \frac{A_j}{z_j} (\frac{\mu}{\rho}) j} \tag{2.16}$$

The effective atomic number (Zeff) is used to determine the effect of a material on radiation interactions. It can be thought of as a weighted average of the atomic numbers of the material's components. A high Zeff value generally implies that the material will interact more intensively with radiation.

$$N_E = N_A \frac{Z_{eff}}{< A >} \tag{2.17}$$

Effective electron density ($N_E$) is a parameter that indicates the number of free electrons per unit volume in a material. It is used to evaluate a material's ability to interact with and attenuate ionizing radiation, since these interactions largely occur with the electrons in a material. Higher $N_E$ values usually correspond to greater attenuation of ionizing radiation.

In addition, calculation of energy absorption buildup factor and exposure buildup factor; First of all, we have calculated the equivalent atomic number ($Z_{eq}$) for each sample which illustrates the properties of the composite material in terms of equivalent element. The values of $Z_{eq}$ vary with respect to the values of photon energy and can be calculated using the following formula ;

$$Z_{eq} = \frac{Z_1(\log R_2 - \log R) + Z_2(\log R - \log R_1)}{(\log R_2 - \log R_1)} \tag{2.18}$$

where $Z_1$ and $Z_2$ are the atomic numbers of elements corresponding to the ratios $R_1$ and $R_2$ respectively, R is the ratio of Compton partial mass attenuation coefficients ($\mu_{Compton}$) to the total mass attenuation coefficients ($\mu_{Total}$) for the chosen samples at specific energy value.

The second step is to find the five G-P fitting parameters (b, c, a, $X_k$ and d) for the selected bricks which can be estimated using the same logarithmic interpolation as that for $Z_{eq}$ ;

$$h = \frac{h_1(\log Z_2 - \log Z) + h_2(\log Z - \log Z_1)}{(\log Z_2 - \log Z_1)} \tag{2.19}$$

where h represents the G-P fitting coefficient function which is correspond to the calculated $Z_{eq}$, $h_1$ and $h_2$ represent the values of G-P fitting parameters corresponding to the atomic numbers $Z_1$ and $Z_2$, respectively. The values $h_1$ and $h_2$ are provided by the American nuclear society ANSI/ANS-6.4.3 (ANS, 1991) for energy range 0.015–15 MeV up to penetration depth 40 mean free path (mfp).

Finally, the calculated G-P parameters are used to calculate EABF and EBF using the G-P compatibility equation.

$$B(E,x)=\begin{cases}1+\dfrac{b-1}{K-1}(K^{x}-1), & \mathrm{K}\neq 1\\ 1+(B-1)x, & \mathrm{K}=1\end{cases} \tag{2.20}$$

where,

$$K(E,x)=cx^{a}+d\,\frac{\tanh(x/X_{k}-2)-\tanh(-2)}{1-\tanh(-2)},\ x\le 40\ \text{mfp} \tag{2.21}$$

where x is the penetration depth in mfp, E is the energy of the incident photon, K is the photon dose multiplicative factor and represent the spectrum shape change, and (b, c, a, Xk, d) are the calculated G-P fitting parameters in the previous step.

Energy Absorption Buildup Factor (EABF) and Exposure Buildup Factor (EBF) are two different terms used to evaluate the interaction of radiation with materials. Both terms play an important role in radiation protection and radiation dosimetry, but they address different aspects:

**1.** Energy Absorption Buildup Factor:

- The Energy Absorption Buildup Factor measures how much energy is absorbed by a material from radiation passing through it, considering not only the primary radiation initially present but also radiation scattered within the material.
- The Energy Absorption Buildup Factor specifies the ratio between the total energy absorbed in the material and the energy absorbed from primary (incident) radiation alone.
- This factor takes into account the accumulation of radiation and the transfer of energy within the material. This is particularly important in applications such as radiotherapy and medical imaging, as it is important to understand how much energy is absorbed by body tissues when exposed to radiation.

**2.** Exposure Buildup Factor:

- The Exposure Buildup Factor measures the accumulation of radiation in a material due to scattering and secondary radiation production as the radiation passes through the material.
- The Exposure Buildup Factor indicates how much the exposure level (intensity) of radiation increases as it passes through a certain material, compared to primary radiation alone.

- Exposure buildup factors are important in radiation protection and radiation detection applications, particularly in the design of protective barriers and in evaluating radiation hazards.

Differences:

- The Energy Absorption Buildup Factor focuses on energy transfer, while the Exposure Buildup Factor focuses on the intensity of radiation.
- The Energy Absorption Buildup Factor takes into account the amount of energy absorbed within the material; the Exposure Buildup Factor evaluates the intensity of radiation progressing through the material.

Both factors are used to understand how radiation interacts within a material, but they have different aspects and criteria.

### 2.9.5. Slowing down and absorption of neutron particles

All types of radiation undergo weakening or attenuation after passing through a material. The magnitude of this attenuation varies depending on the energy of the radiation, the properties of the target material, and the thickness. Neutrons, being electrically neutral, can easily penetrate into the depths of matter. When neutrons collide with light nuclei, they can undergo a process called moderation or slowing down. As neutrons pass through a material, they slow down through nuclear reactions and eventually lose their energy by being absorbed. Fast neutrons can induce reactions such as proton, alpha, or 2 neutron reactions, after which they slow down. Similarly, thermal or slow neutrons can be captured and absorbed in the material through elastic and inelastic interactions.

$$dI(x) = -\sum_t dx \tag{2.22}$$

Here, I represents the number of neutrons passing through the area. Its unit is neutrons per square centimeter per second ($n/cm^2s$). $\Sigma_t$ is the macroscopic total cross-section, which is the product of the material's total cross-section and the number of particles. The total cross-section includes all interactions such as absorption, scattering, and transmission, and it varies for each material. The absorption cross-section includes interactions like fission, (n,α), (n,2n), (n,p), (n,γ), while the scattering cross-section refers to elastic and inelastic interactions. Its unit is $cm^{-1}$.

Dividing equation (2.19) by the number of neutrons per unit area ("I") on both sides, we can rewrite it as:

$$\frac{dI}{I} = -\sum_t dx \tag{2.23}$$

If we take the integral of both sides of equation (2.16) with respect to their respective components, we get:

$$\int_{I_0}^{I} \frac{dI}{I} = \int_0^x \sum_t dx \tag{2.24}$$

If we solve equation (2.20) by specifying the integral limits, we obtain:

$$\ln(I / I_0) = -\sum_t x \tag{2.25}$$

$$I = I_0 e^{-\sum_t x} \tag{2.26}$$

Here, $I_0$ represents the initial radiation intensity without any absorbing material. I is the attenuated radiation intensity by the barrier, with the unit of interactions/cm$^2$s, and x is the thickness of the material. During absorption, neutrons with low energies or different cross-sections may be generated.

Additionally, to theoretically evaluate the materials, effective neutron removal cross-sections are being calculated. The larger this cross-section is, the more effective the neutron shielding capability will be.

$$\sum_R = \sum_i \rho_i (\sum_{R/\rho})_i \tag{2.27}$$

$$\sum_{R/\rho} = \sum_i w_i (\sum_{R/\rho})_i \tag{2.28}$$

"$w_i$" represents the mass fraction of each element, while "ρ" denotes density. The Effective Neutron Removal Cross-Section is a parameter used in nuclear physics to quantify the probability of a neutron interaction with a target, leading to the removal of the neutron from the system. Essentially, it represents the "target size" seen by a neutron when it interacts with a material. A larger cross-section indicates a higher probability of neutron interaction, hence greater neutron shielding effectiveness.

When neutrons interact with matter, two parameters are involved: microscopic and macroscopic cross-section parameters. The probability of neutron interaction with a particle or nucleus is referred to as the neutron microscopic cross-section. It can be divided into two groups: absorption and scattering. The macroscopic cross-section is the product of the microscopic cross-section and the number of atoms or molecules per unit volume of the element or compound. The average free path between two collisions of neutron particles within the material depends on the mean free path, which is an important parameter in shielding.

### 2.9.6. Commonly used materials in radiation shielding

Materials used in radiation shielding are special materials selected to absorb or scatter radiation in order to protect against its effects. These materials should have specific properties to reduce or block the impact of different types of radiation. Here are some commonly used materials in radiation shielding:

#### 2.9.6.1. Lead (Pb)

Lead, which is one of the most commonly occurring elements on Earth, forms five oxide compounds in nature (PbO, $Pb_2O_3$, $PbO_4$, $PbO_2$, and $Pb_2O$). Its density is 11.34 $g/cm^3$. Lead is a material with high density that effectively stops gamma rays. It can also absorb alpha and beta particles. It has high density and excellent radiation absorption capabilities, making it an effective choice for shielding against radiation. Lead's radiation shielding properties are attributed to its high density, which impedes the passage of radiation and reduces its harmful effects. When radiation beams penetrate lead, they interact with the atoms in the material and get absorbed, minimizing the propagation of radiation. Lead also has a tendency to scatter radiation. As radiation beams pass through lead shielding, they disperse, further diminishing the spread of radiation. Additionally, lead rapidly absorbs radiation and effectively retains the energy, preventing its outward transmission. Radiation shielding structures often consist of lead panels and lead coatings. Lead panels are assembled to impede the transmission and absorb the energy of radiation, while lead coatings are used around devices containing radiation sources to prevent their outward emission. Radiation shielding plays a vital role in preventing harm to humans and the environment from harmful radiation emitted by radiation sources. Lead is frequently chosen as a preferred material for this purpose. However, it is important to follow the recommendations of experts and adhere to local regulations regarding radiation shielding and protection.

While lead is an effective material for radiation shielding, it should also be considered as a potential toxic substance. Lead is a toxic element that poses serious risks to human health. Prolonged and high-level exposure to lead can have adverse effects on various organs and systems, including the nervous system, kidneys, blood, and circulatory system. Symptoms of lead poisoning may include fatigue, headaches, abdominal pain, memory problems, nerve damage, and behavioral changes.



**Figure 2.31:** The mineral appearance of lead metal (PUBCHEM, 2017).

### 2.9.6.2. Concrete

Concrete is a durable construction material widely used in the construction industry. It can also be effectively used for radiation shielding purposes. Concrete has the ability to absorb and limit the spread of radiation. Its high density effectively blocks the passage of radiation and absorbs its energy. The aggregates (gravel, sand, stone, etc.) and cement matrix within concrete help disperse and limit the effects of radiation. Concrete shields can be designed in various forms to block radiation. Reinforced concrete structures, commonly known as reinforced concrete, are often used for radiation shielding. Reinforcement with steel rebars enhances the effectiveness of concrete as a radiation shield by further dispersing and absorbing the radiation.The thickness of concrete shields can vary depending on the radiation source and protection requirements. Higher radiation levels may require thicker concrete shields. The design of concrete shields should be optimized based on the type and propagation characteristics of the radiation source. Concrete shields offer advantages such as cost-effectiveness, ease of application, and durability. Concrete is a widely available material with a wide range of applications, and it can be easily shaped. Additionally, concrete shields are resistant to fire and other external factors. The use of concrete in radiation shielding is important in fields such as medical radiation therapy, nuclear power facilities, and research laboratories. The radiation shielding properties of concrete aim to control radiation and protect human health. However, the design and implementation of concrete shields should be carried out in accordance with expert recommendations and relevant regulations.

Despite being a useful material for radiation shielding, concrete has some ergonomic disadvantages. Particularly, thick and dense concrete shields can create a significant burden in terms of transportation, installation, and maintenance. This is an important consideration for ensuring worker safety and operational efficiency. Handling and installing heavy concrete shields can increase the risk of injuries for workers. Moreover, special equipment and techniques may be required for the placement and repositioning

of the shields. The large size and weight of concrete shields can occupy space and restrict the use of limited areas, potentially causing congestion. The dimensions and weight of concrete shields can also affect the load-bearing capacity of structures. Therefore, the weight of concrete in radiation shielding can be considered a disadvantage from an ergonomic standpoint. It is important to take these challenges into account and implement appropriate measures to protect workers and ensure effective operations. Solutions such as alternative materials or lightweight concrete composites can help mitigate the drawbacks of heavy concrete shields and improve ergonomics.



**Figure 2.32:** An example concrete picture (PUBCHEM, 2017).

The classification of concrete based on density is provided in (Table 2.7);

**Table 2.7:** Classification of concrete based on density

| **Concrete Type** | **Density (kg/m$^3$)** |
|---|---|
| Lightweight | 800-2000 |
| Normal | 2000-2600 |
| Heavy | >2600 |

**Source:** (Sürücü, 2019).

### 2.9.6.3. Steel

Steel is a widely used material in the construction industry due to its durability, high strength, and workability. It is also effective for radiation shielding purposes. Steel is considered an effective material for radiation shielding. Its high density creates a protective barrier that prevents the penetration of radiation. Radiation interacts with the atoms of the steel material, absorbing its energy and reducing the spread of radiation. Steel is particularly efficient in absorbing high-energy radiation types like gamma rays. Steel shields can be designed in various forms to block radiation. Commonly used forms include steel plates, steel-reinforced concrete structures, or steel shields. The steel material

disperses radiation energy, limiting its propagation and reducing exposure to surrounding individuals and the environment. The design of steel shields depends on factors such as thickness and density to reduce the impact of radiation. Thicker and denser steel shields may be required for higher radiation levels. During the design process, consideration is given to the radiation source, its propagation characteristics, and the required level of protection. Steel shields find applications in various fields, including nuclear power plants, radiation therapy centers, nuclear research laboratories, and nuclear waste storage facilities. The durability and strength of steel provide effective long-term protection. However, there are some factors to consider when using steel shields. For instance, steel is a heavy material, which can make transportation, installation, and maintenance challenging. Additionally, steel shields may interact with other factors such as electromagnetic fields, leading to behavioral changes. In radiation shielding, the effective use of steel requires careful design and implementation. Proper consideration should be given to the recommended thickness, density, and placement by experts. Local regulations and safety standards should also be followed. This ensures that steel shields are used effectively to control radiation and protect human health.



**Figure 2.33:** An example concrete picture (PUBCHEM, 2017).

#### 2.9.6.4. Boron (B)

Boron can be utilized in various forms for its radiation shielding properties. Compounds such as boron carbide, boron oxide, boron hydride, and borosilicate glass are employed in the construction of radiation shields. These compounds absorb radiation and disperse its energy, preventing its propagation. Despite being a lightweight material, boron exhibits high resistance and can be effectively used in radiation shielding. Its high heat resistance is particularly crucial for shielding radiation sources operating at elevated temperatures. Moreover, boron shields can provide a thinner profile compared to other materials, offering advantages in terms of portability and ease of use. The radiation shielding

properties of boron support its application in various fields, including nuclear facilities, medical radiation therapy, and radiographic imaging. Proper utilization of boron in the design of radiation shields enables effective control of radiation sources and reduction of exposure risks. However, decisions regarding radiation shields and the use of boron should be made in accordance with expert recommendations and local regulations.



**Figure 2.34:** The mineral appearance of boron (PUBCHEM, 2017).

#### 2.9.6.5. Paraffin

Paraffin, also known as paraffin wax, is a material that can provide moderate shielding against gamma rays. It is a low-density material commonly used in radiation shielding applications, particularly for its ability to slow down or moderate fast neutrons. Paraffin is often used in combination with other neutron-absorbing materials to enhance the overall shielding effectiveness. It is frequently utilized in research facilities, nuclear reactors, and medical settings for neutron radiation protection. Please note that the translation provided is a general description of paraffin's use in radiation shielding. The specific application and effectiveness of paraffin as a shield may vary depending on the radiation source, energy, and desired level of protection.



**Figure 2.35:** An example paraffin picture (PUBCHEM, 2017).

#### 2.9.6.6. Polymethylmethacrylate (PMMA)

Polymethylmethacrylate (PMMA), a transparent thermoplastic polymer, is widely known by its trade name "acrylic" or "plexiglass". It possesses unique properties that make it suitable for various applications, including radiation shielding. PMMA is an excellent material for radiation shielding due to its high transparency to visible light and its ability to attenuate ionizing radiation. It has a relatively low atomic number, which makes it an effective shield against gamma rays and X-rays. PMMA's molecular structure allows it to absorb and scatter radiation energy, reducing its penetration depth and protecting individuals from harmful radiation exposure. The effectiveness of PMMA as a radiation shield depends on its thickness and density. Thicker PMMA sheets provide greater shielding against radiation, while increasing the density enhances its radiation absorption capabilities. The design of PMMA shielding should consider the specific radiation source, energy level, and desired level of protection. PMMA shields find applications in various fields, including medical imaging, nuclear medicine, and radiation therapy. In medical imaging, PMMA is used as a protective barrier for patients and healthcare professionals during X-ray examinations. In nuclear medicine, it is utilized as shielding material for radiation sources such as radioisotopes. PMMA is also used in radiation therapy to protect surrounding healthy tissues from the effects of ionizing radiation during treatment. In addition to its radiation shielding properties, PMMA offers other advantages. It is lightweight, easy to handle, and can be easily fabricated into different shapes and sizes. PMMA is also resistant to chemicals, weathering, and impact, making it a durable choice for radiation shielding applications. It is important to note that the design and implementation of PMMA shielding should adhere to relevant safety regulations and guidelines. Proper thickness and density calculations, as well as structural considerations, are essential to ensure effective radiation protection. In conclusion, PMMA is a versatile material with excellent radiation shielding properties. Its transparency, radiation absorption capabilities, and ease of use make it a valuable choice for various radiation shielding applications. By utilizing PMMA shields, individuals and professionals can be safeguarded against the harmful effects of ionizing radiation while performing their tasks safely and efficiently.



**Figure 2.36:** An example Polymethylmethacrylate picture (PUBCHEM, 2017).

### 2.9.6.7. Polyethylene (PE)

Polyethylene is a versatile thermoplastic polymer that is widely used in various industries and applications. It is a synthetic material composed of ethylene monomers, which are derived from petroleum. Polyethylene is known for its excellent combination of properties, including flexibility, toughness, chemical resistance, and low electrical conductivity. While it is primarily used for packaging, pipes, and other general-purpose applications, it also exhibits certain radiation shielding properties that make it suitable for use in radiation shielding applications. Polyethylene's radiation shielding properties stem from its high hydrogen content. Hydrogen atoms, which are abundant in polyethylene, have a high scattering cross-section for ionizing radiation, especially for neutrons and gamma rays. When exposed to radiation, polyethylene molecules scatter and absorb the radiation, effectively reducing its penetration and protecting against potential harmful effects. The hydrogen atoms in polyethylene act as a barrier, dispersing the energy of the radiation and minimizing its ability to pass through the material. In radiation shielding applications, polyethylene is commonly used in the form of sheets, blocks, or composite materials. These materials can be tailored to achieve the desired level of radiation attenuation by adjusting the thickness and density. Polyethylene-based radiation shields are employed in various industries, including nuclear power plants, medical facilities, research laboratories, and industrial settings where radiation sources are present. Polyethylene's advantages as a radiation shielding material include its lightweight nature, ease of handling and fabrication, and cost-effectiveness. It is relatively easy to mold, cut, and shape polyethylene into different forms, allowing for customized shielding solutions. Additionally, polyethylene is resistant to corrosion, moisture, and many chemicals, making it a durable and long-lasting choice for radiation shielding applications.

However, it is important to note that while polyethylene provides effective shielding against certain types of ionizing radiation, it may not be suitable for all radiation sources or high-energy radiation. The thickness and composition of the polyethylene shield should be carefully designed and evaluated based on the specific radiation source, energy level, and shielding requirements. Consulting with radiation safety experts and following applicable regulations and guidelines is crucial to ensure the proper design and use of polyethylene radiation shields. In conclusion, polyethylene is a versatile polymer with various desirable properties, including its potential for radiation shielding. Its high hydrogen content enables effective scattering and absorption of ionizing radiation, making it a suitable material for attenuating radiation exposure. Polyethylene-based radiation shields offer advantages such as lightweight construction, ease of handling, and cost-effectiveness, but proper design and evaluation are necessary to ensure optimal shielding performance for specific radiation sources and applications.



**Figure 2.37:** An example Polymethylmethacrylate picture (PUBCHEM, 2017)

#### 2.9.6.8. Bismuth (Bi)

Bismuth is a chemical element with the symbol Bi and atomic number 83. It is a dense, brittle metal that has been widely used for its radiation shielding properties. Bismuth is highly regarded for its excellent radiation shielding properties. It has a high atomic number, which means it has a large number of protons and electrons in its atomic structure. This characteristic makes bismuth an effective material for attenuating and absorbing ionizing radiation, such as gamma rays and X-rays. The high density of bismuth further enhances its radiation shielding capabilities, as it allows for increased interaction and absorption of radiation energy. One of the notable features of bismuth is its ability to attenuate and scatter radiation without producing significant secondary radiation. This is important in radiation shielding applications as it helps minimize the risk of creating additional scattered radiation that could potentially harm individuals in the surro-

unding area. Bismuth's radiation shielding effectiveness can be optimized by utilizing appropriate thicknesses and configurations based on the specific radiation source and desired level of protection. Bismuth-based shielding materials are commonly used in various industries and applications that involve radiation protection. In medical settings, bismuth shields are utilized to protect patients and medical professionals during diagnostic imaging procedures, such as X-rays and CT scans. Bismuth is also employed in nuclear power plants, research facilities, and industrial applications where radiation sources are present. Additionally, bismuth alloys are used in radiation therapy to shield healthy tissues and organs from the effects of ionizing radiation during cancer treatments. Apart from its radiation shielding properties, bismuth offers several other advantages. It is non-toxic and has low environmental impact compared to some other heavy metals used for radiation shielding. Bismuth is also malleable and can be easily shaped into various forms, allowing for flexibility in design and installation. In conclusion, bismuth is a valuable element for radiation shielding due to its high atomic number, density, and ability to attenuate ionizing radiation effectively. Its use in various industries and applications demonstrates its significance in ensuring the safety and protection of individuals exposed to radiation. By utilizing bismuth-based shielding materials, the risks associated with ionizing radiation can be minimized, providing a safer environment for workers, patients, and the general public.

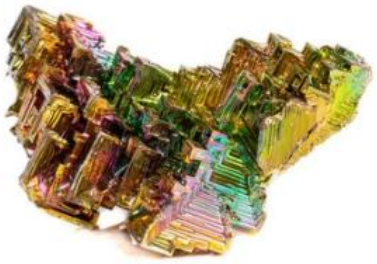


**Figure 2.38:** The mineral appearance of bismuth (PUBCHEM, 2017).

### 2.9.6.9. Tungsten (W)

Tungsten, atomic number 74, is a dense and heavy metal that possesses exceptional radiation shielding properties, making it an ideal material for radiation shielding applications. Tungsten is widely recognized for its outstanding radiation shielding capabilities. It has the highest melting point of all metals, excellent thermal stability, and remarkable density, which allows it to effectively attenuate and absorb ionizing radiation. Due to its

high atomic number and density, tungsten is particularly efficient at blocking high-energy gamma rays and X-rays, preventing their penetration and reducing their harmful effects on living organisms. The unique properties of tungsten contribute to its superior radiation shielding performance. Its high atomic number results in strong interactions with incoming radiation, as the nuclei of tungsten atoms effectively scatter and absorb radiation particles. Tungsten's density further enhances its radiation attenuation properties, as denser materials provide greater resistance to the passage of radiation. This makes tungsten an ideal choice for applications requiring high-density radiation shielding, such as medical imaging, radiation therapy, nuclear power plants, and industrial radiography. Tungsten alloys, which consist of tungsten combined with other metals such as nickel, iron, or copper, are commonly used in radiation shielding applications. These alloys offer enhanced mechanical strength, improved workability, and increased resistance to corrosion, while still retaining the excellent radiation attenuation properties of tungsten. Tungsten alloys are utilized in the construction of radiation shielding containers, collimators, and protective barriers, providing effective and reliable protection against ionizing radiation. In addition to its exceptional radiation shielding properties, tungsten is also known for its non-toxic nature and resistance to environmental degradation. These qualities make it a safe and durable material for long-term radiation shielding applications. Tungsten's high melting point and stability allow it to withstand extreme temperatures and harsh environments, ensuring its performance and integrity over extended periods of use. In conclusion, tungsten is a highly effective material for radiation shielding due to its high atomic number, density, and stability. Its ability to attenuate and absorb ionizing radiation, particularly gamma rays and X-rays, makes it invaluable in various fields where radiation protection is essential. Tungsten and tungsten alloys are widely employed in medical, industrial, and nuclear applications to safeguard personnel, patients, and the general public from the harmful effects of ionizing radiation. By utilizing tungsten-based radiation shielding solutions, the risks associated with radiation exposure can be effectively minimized, ensuring the safety and well-being of individuals working in radiation-prone environments.



**Figure 2.39:** The mineral appearance of tungsten (PUBCHEM, 2017)

### 2.9.6.10. Cadmium (Cd)

Cadmium is a chemical element with atomic number 48. It is used in various applications due to its radiation shielding properties. Cadmium is considered an effective material for radiation shielding due to its ability to absorb and attenuate radiation. Its high atomic number and density allow cadmium to effectively block the transmission of radiation. By absorbing radiation energy, cadmium disperses it, reducing the risk of exposure to individuals and the environment. Cadmium shields can be used in different forms for radiation protection. Typically, cadmium is used in steel alloys. When combined with steel, cadmium enhances its shielding capabilities and limits radiation propagation. Cadmium-containing steel is commonly used in nuclear power plants, radiation therapy centers, radiographic testing devices, and other applications involving radiation sources. Cadmium is particularly effective in absorbing thermal neutrons, making it valuable for thermal neutron absorption in nuclear reactors and radiography devices. By absorbing thermal neutrons and dissipating their energy, cadmium contributes to reactor control and neutron shielding processes. In addition to its radiation shielding properties, cadmium offers advantages such as low toxicity and chemical stability. It is considered an environmentally friendly material and can be safely used in various industries. Its high melting point and chemical resistance make it suitable for long-term applications.

In conclusion, cadmium is utilized as an effective material for radiation shielding. Its high atomic number, density, and thermal neutron absorption capability make cadmium suitable for blocking and reducing the propagation of radiation. The use of cadmium in various applications helps mitigate risks associated with radiation sources and protects human health. However, it is essential to consider the toxic properties of cadmium and implement appropriate safety measures.



**Figure 21.40:** The mineral appearance of cadmium (PUBCHEM, 2017).

### 2.9.6.11. Barium (Ba)

Barium is a chemical element with atomic number 56 and symbol Ba. It is a soft, silvery-white metal that belongs to the alkaline earth metal group. Barium has several applications, including its use in radiation shielding due to its high atomic number and density. Barium is an effective material for radiation shielding due to its ability to absorb and attenuate ionizing radiation. Its high atomic number (56) and density (approximately 3,6 g/cm³) make it an ideal choice for blocking the penetration of radiation. Barium's dense atomic structure allows it to effectively scatter and absorb radiation energy, thereby reducing the potential harmful effects of ionizing radiation. Barium shielding materials are commonly used in medical imaging, industrial radiography, and nuclear power applications. In medical imaging, such as X-ray and computed tomography (CT) scans, barium compounds are often used as contrast agents to enhance the visibility of specific body tissues or organs. Barium's radiation shielding properties help protect surrounding tissues from unnecessary radiation exposure during these procedures. In industrial radiography, barium-based shielding materials, such as barium sulfate, are utilized to provide protection against gamma rays and X-rays. These shielding materials are often used in radiography rooms, non-destructive testing facilities, and industrial settings where radiation sources are present. Barium's high atomic number and density effectively absorb and scatter radiation, minimizing the risk of exposure to workers and the environment. It is important to note that barium, like other heavy metals, can be toxic if ingested or inhaled in certain forms. Proper safety measures and handling protocols should be followed to ensure the safe use and disposal of barium-based radiation shielding materials. Additionally, regulatory guidelines and standards should be adhered to when incorporating barium shielding in radiation-related applications.

In summary, barium is an effective radiation shielding material due to its high atomic number and density. Its ability to absorb and scatter ionizing radiation makes it valuable for protecting against the harmful effects of radiation exposure. However, proper safety precautions must be taken when handling barium-based materials to mitigate any potential health risks associated with their toxicity.



**Figure 21.41:** The mineral appearance of barium (PUBCHEM, 2017)

### 2.9.6.12. Gadolinium (Gd)

Gadolinium is a chemical element with the symbol Gd and atomic number 64. It is part of a group of elements known as lanthanides and is generally classified as a rare earth element. Gadolinium is not found in its free form in nature, but it can be found in minerals such as monazite and bastnasite. Due to its high neutron absorption cross-section, gadolinium is used as a control rod in nuclear reactors. Additionally, gadolinium-based compounds are used as contrast agents in magnetic resonance imaging (MRI), making it an important application in medicine. When it comes to radiation shielding, gadolinium's high neutron absorption capacity makes it particularly effective as a shielding material against neutron radiation. This makes gadolinium an ideal material for the construction of control rods used in nuclear reactors as it can effectively absorb neutrons and thus control the rate of nuclear reactions. This absorption capacity is due to gadolinium's high thermal neutron absorption cross-section, which means it can effectively capture the majority of thermal neutrons. Interaction of neutrons with gadolinium nuclei enhances its energy absorption and scattering capacity, thereby reducing the harmful effects of radiation. However, gadolinium does not provide significant protection against gamma rays, as it lacks sufficient electron density to effectively absorb or scatter high-energy photons. Therefore, while gadolinium is commonly used for neutron shielding, it is often used in conjunction with another material, such as lead, for protection against gamma rays. However, gadolinium's high atomic number and density can

provide some degree of protection against certain gamma rays in specific scenarios. Nevertheless, gadolinium is primarily preferred as a shielding material against neutron radiation and is less effective against other types of radiation.



**Figure 2.42:** The mineral appearance of gadolinium (PUBCHEM, 2017)

### 2.9.6.13. Erbium (Er)

Erbium is a chemical element with atomic number 68 and symbol Er in the periodic table. It belongs to the lanthanide series of rare earth elements. Erbium is typically not found in its free state in nature, but it is present in some rare earth minerals, especially xenotime and gadolinite. Erbium and its compounds are commonly used in the glass and ceramic industry because they can impart a pleasing pink color to these materials. Additionally, erbium-doped fiber amplifiers (EDFAs) are used in the telecommunications industry as they utilize specific optical properties of erbium to amplify optical signals. Furthermore, erbium is used in the production of certain lasers used in medical and dental applications. When it comes to radiation shielding, erbium is primarily used as an absorber for thermal neutrons. Neutrons interact with atomic nuclei, and when a neutron is captured by an erbium atom, a gamma ray is emitted. This property makes erbium particularly suitable as a shielding material for neutron radiation. However, erbium has limited ability to block other types of radiation, especially high-energy photons (gamma rays and X-rays). This is because the electrons of erbium atoms do not have sufficient density to absorb or scatter high-energy photons effectively. Therefore, erbium is generally combined with another shielding material that contains heavy elements to provide additional protection against gamma and X-ray radiation. A similar strategy is often employed to provide protection against high-energy particle radiation.

In conclusion, erbium is a material commonly used in neutron shielding, but protection against other types of radiation usually requires its combination with other materials.

The radiation absorption properties of erbium can be significant for both industrial and scientific applications.



**Figure 2.43:** The mineral appearance of erbium (PUBCHEM, 2017)

### 2.9.6.14. Antimony (Sb)

Antimony is a chemical element with the symbol Sb and atomic number 51. It is commonly found in nature as antimony sulfide ($Sb_2S_3$). It is widely used as a material for radiation shielding. Antimony possesses high density and a relatively high atomic weight, which makes it effective in blocking the passage of radiation. Particles emitted from a radiation source interact with the antimony material, absorbing their energy and limiting the spread of radiation. Consequently, antimony serves as an effective barrier in reducing the risk of radiation exposure. Moreover, antimony exhibits the ability to absorb neutrons. Neutrons interact with the nuclei of antimony atoms, leading to their absorption. This property can be utilized in controlling neutron radiation from nuclear reactors and other neutron sources. The radiation shielding performance of antimony depends on the thickness and density of the material. Thicker and denser antimony shields provide better protection against higher levels of radiation. The design of radiation shields should be optimized based on the characteristics of the radiation source and its propagation. Although antimony is widely used as a material for radiation shielding, it has some disadvantages. For instance, antimony metal itself can be toxic and pose health risks. Additionally, due to its high density, antimony is heavy and brittle, which may present challenges during transportation and assembly processes. In conclusion, antimony can be effectively employed in radiation shielding. Its high density and neutron absorption capability contribute to controlling radiation exposure. However, considerations should be given to the toxic risks associated with antimony and the material properties. Proper design, placement, and safety measures ensure that antimony shields are an effective tool in protecting individuals and the environment from radiation.



**Figure 2.44:** The mineral appearance of antimony (PUBCHEM, 2017)

### 2.9.6.15. Tin (Sn)

Tin (Sn) is a chemical element with the atomic number 50 and is symbolized by "Sn." It is a malleable and ductile post-transition metal known for its two stable allotropes (two different forms of variable structure) at room temperature: white tin and gray tin. Tin is resistant to water and air, making it a useful protective material. Additionally, its low toxicity and chemical reactivity make it applicable in a range of uses. The use of tin in radiation shielding is notable, particularly for its ability to provide protection against gamma rays and X-rays. These types of radiation can cause damage by displacing electrons from energy levels and ionizing atoms. The high atomic number and density of tin help prevent such energetic radiation from causing this type of damage. Tin acts by absorbing and scattering energetic radiation, protecting the electrons and atoms of the material it interacts with. When radiation strikes a thick layer of material, the electrons of tin absorb the energy, which then dissipates into space surrounding the tin atoms. This energy distribution prevents the radiation from penetrating deeper layers of the material and thus prevents it from causing harm inside the material. Additionally, the tin atoms absorb and later release energy, aiding in the dispersion of energetic radiation. The combination of these processes allows tin to be effective in radiation shielding. However, it is important to note that tin is not completely radiation-proof; even a thick layer of tin may not absorb all high-energy radiation, and therefore it is often used in conjunction with other materials in radiation shielding.



**Figure 2.45:** The mineral appearance of tin (PUBCHEM, 2017)

## 2.10. Polymers

Polymers are large molecules with repeating structures of units called monomers, which can be found in nature and synthesized in laboratories.

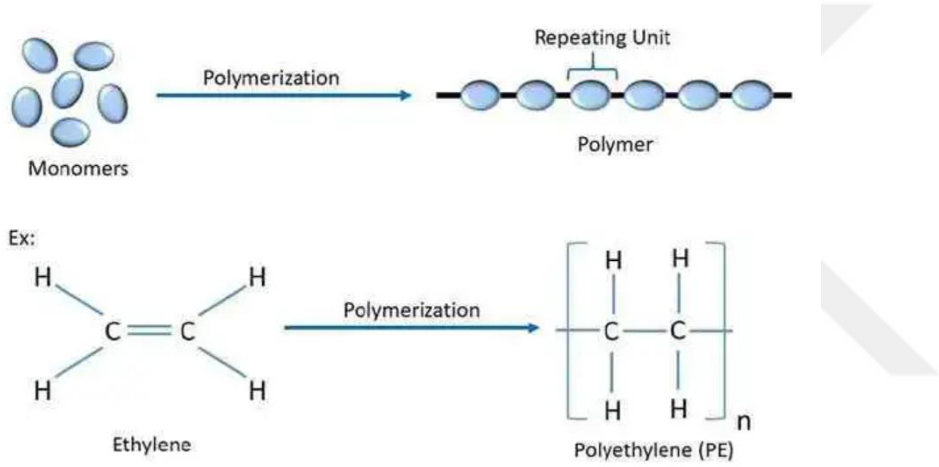



**Figure 2.46:** Polymerization schematic (PUBCHEM, 2017)

Natural polymers are found in plant and animal cells and include substances with biological functions such as proteins, nucleic acids, carbohydrates, and rubber. On the other hand, synthetic polymers are produced from petrochemicals and other organic molecules under laboratory conditions, and they are often used as high-performance materials. These include plastics, synthetic fibers, elastomers, resins, and adhesives. Polymers have a wide range of applications, which depend on the specific physical and chemical properties of the polymer. For example, thermoplastic polymers soften when heated and harden again when cooled, making them recyclable and capable of being reshaped. Thermoset polymers, on the other hand, permanently harden when heated and cannot be reversed, making them ideal for high-temperature applications. Elastomers are generally flexible and capable of returning to their original shape, making them suitable for rub-

ber products and elastic fibers. Lastly, fibers are often high-strength polymers with low stretching capacity, making them suitable for textiles and composite materials.

The diversity of polymers makes them an important component of materials science. They are widely used in biomedical devices, electronics, automotive industry, construction, textiles, packaging, and many other sectors. The science and engineering of polymers require a multidisciplinary approach to understand, develop, and control their properties and processes, often encompassing chemistry, physics, materials science, and engineering. Additionally, in the context of environmental sustainability, the development of polymers derived from biodegradable and renewable sources plays a significant role in designing next-generation materials.

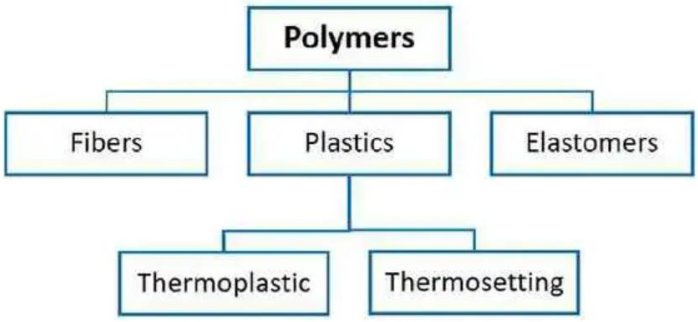



**Figure 21.47:** Classification of polymers (PUBCHEM, 2017).

### 2.10.1. Fibers

Polymer-based fibers are highly flexible and durable materials, typically composed of natural or synthetic polymers. These fibers are characterized by their high tensile strength and relatively small diameter compared to their length. Synthetic polymer fibers, in particular, exhibit unique properties such as chemical resistance, heat resistance, abrasion resistance, lightweight, and dimensional stability. Polymer fibers are commonly made from synthetic polymers such as polyester, polyamide (nylon), polypropylene, polyacrylonitrile, and polyurethane. Each polymer type possesses its own distinctive characteristics. For instance, polyester fibers find wide applications due to their chemical and heat resistance, high resistance to abrasion, and dimensional stability. Nylon fibers, on the other hand, are preferred for their high strength and flexibility, excellent abrasion resistance, and low density. Another important feature of polymer fibers is their ability to resist external influences. They exhibit resistance to chemicals, UV radiation, and microorganisms. However, the level of resistance depends on the specific polymer used and the processing techniques applied.

Fibers are commonly combined using techniques such as spinning, weaving, knitting, or braiding to create textile products. They are also used in the production of nonwoven materials, composite materials, and even high-performance industrial products. These applications allow for the production of a wide range of products with different mechanical and physical properties. Biodegradable polymer fibers, in particular, hold significant potential in terms of sustainability and environmental impact. They can be composed of natural polymers derived from plant or animal sources (such as cellulose or proteins) or synthetic biopolymers produced through biotechnological processes. These types of fibers can be utilized in various applications as environmentally friendly, renewable, and sustainable materials, ranging from clothing and packaging to agricultural coatings and medical applications.



**Figure 2.48:** Carbon Fiber Reinforced Polymer fabric (PUBCHEM, 2017)

### 2.10.2. Elastomers

Elastomers are a subcategory of polymers known for their high flexibility and elasticity properties. These materials can quickly return to their original shapes upon the removal of an applied force, which gives them the behavior similar to "rubber." The unique properties of elastomers arise from their molecular-level rubber-like structure: long, flexible polymer chains forming an irregular, amorphous structure. This structure allows the material to be resistant to large deformations, making elastomers flexible and durable against applied stresses. Elastomers are typically produced synthetically and encompass various polymer types such as polybutene, polyisoprene, polychloroprene (neoprene), styrene-butadiene, and polyurethane. The properties of these materials can vary significantly depending on the selection of initial monomers, polymerization process, and the formation of cross-links. The wide range of properties exhibited by elastomers enables their utilization in diverse industries ranging from automotive to medical applications,

electrical and electronics, and the construction sector. Elastomers are preferred for their excellent elasticity, high impact resistance, good insulation properties, excellent friction and wear resistance, and stability across a wide temperature range. However, these materials are generally sensitive to high temperatures and particularly susceptible to oxidation and ozone effects, limiting their use in some cases. Various modification techniques and material design strategies are employed to overcome these challenges and further enhance the properties of elastomers. These strategies may involve the use of different monomers and fillers, adjusting the density of cross-linking, and modifying the chemical structure of the polymer through engineering methods. In this way, the properties of elastomers can be optimized and made suitable for a wider range of applications.



**Figure 2.49:** Polybutene material (PUBCHEM, 2017)

### 2.10.3. Plastics

Plastics form the most common and diverse subgroup within the polymer class and have a wide range of applications. As synthetic or semi-synthetic materials, these substances are typically obtained through the polymerization of one or more monomers. Some typical characteristics of plastics include high strength, lightness, chemical resistance, electrical insulation, and low thermal conductivity. However, the properties of different plastic types depend largely on the monomers and polymerization processes used, as well as the additives and processing methods employed. Many plastic types offer excellent dimensional stability and chemical resistance over a wide temperature range. For example, polyolefins like polyethylene and polypropylene are relatively low-cost, lightweight materials that are resistant to chemicals and suitable for various molding techniques. Polystyrene provides high rigidity, transparency, and excellent processability, making it useful in packaging, insulation, and consumer goods. Engineering plastics such as polymethyl methacrylate (PMMA) and polycarbonate offer high strength, heat

resistance, and optical properties, making them ideal for optical lenses, automotive components, and high-performance industrial applications. Additionally, biodegradable or bio-based versions of plastics are also available. These materials involve the polymerization of monomers derived from sustainable sources and/or are biodegradable under specific conditions. Such materials hold significant potential, particularly for reducing the environmental impact of plastic waste. However, the environmental impact of plastics is a significant concern throughout their life cycle. This includes the extraction and processing of raw materials as well as the management and disposal of plastic waste. Therefore, various strategies have been developed to enhance the sustainability of plastics, including recycling, energy recovery, the development of biodegradable plastics, and the adoption of environmentally friendly production methods.



**Figure 2.50:** Polymethyl methacrylate (PMMA) material (PUBCHEM, 2017)

### 2.10.4. Termosets

Termosets are a significant subclass of polymer materials that are preferred in many applications due to their unique properties. Termosets are polymers that chemically crosslink and harden when heat is applied. This crosslinking process is typically referred to as "curing" and is often an irreversible process. Therefore, once a thermoset polymer has gone through the curing process, it cannot be melted or reshaped. This characteristic of thermosets offers a range of excellent material properties. For example, thermosets typically exhibit high temperature resistance, superior resistance to chemicals and wear, high surface hardness, and excellent electrical insulation properties. These properties make thermosets an ideal material across a wide range of applications, from automotive and aerospace applications to electronic components, adhesives, and coatings. For instance, epoxy resins are used in a wide range of applications due to their excellent mechanical properties, high heat and chemical resistance, and excellent adhesive properties. Phenol formaldehyde resins (phenolics) and urethanes provide high hardness, excellent heat resistance, and excellent electrical insulation. Polyester resins

and vinyl esters, on the other hand, offer excellent chemical resistance and high strength properties, making them widely used in the production of composite materials. However, the irreversible nature of thermosets poses challenges in terms of managing and recycling used thermoset waste. This is a concern due to environmental impacts and waste management issues. In recent years, various research efforts have been focused on developing recyclable or "reprocessable" thermosets. These advancements have the potential to reduce the environmental impact of thermoset materials and constitute an important research area in polymer science.



**Figure 2.51:** Phenol formaldehyde resins (phenolics) material (PUBCHEM, 2017).

### 2.10.5. Thermoplastics

Thermoplastics constitute the largest and most diverse subgroup within the polymer class. Thermoplastic polymers are materials that soften when heated and harden again when cooled. This property allows thermoplastics to be repeatedly melted and reshaped, making them an ideal material for many applications. They are commonly used in various shaping techniques such as injection molding, extrusion, blow molding, and thermoforming. Thermoplastics can be composed of various polymer types, each with its own unique characteristics. For example, polyolefins like polyethylene and polypropylene are relatively low-cost, lightweight materials that are resistant to chemicals and provide high heat resistance. Polystyrene offers good rigidity and excellent transparency, while PVC (polyvinyl chloride) exhibits high chemical resistance and excellent flame retardant properties. More complex and engineering-grade thermoplastics also exist, including polycarbonates, nylons, polyurethanes, polyethylene terephthalate (PET), and high-performance polymers. These materials are characterized by their ability to enhance high strength, heat resistance, chemical resistance, and/or specific mechanical properties. Another important characteristic of thermoplastics is their recyclability. Ther-

moplastics can be recycled through mechanical or chemical processes or incinerated for energy recovery. However, the efficiency and environmental impact of recycling processes depend on the type of plastic used, waste management systems, and local infrastructure. The wide variety and ability to be repeatedly reshaped make thermoplastics ideal for a wide range of applications—primarily in packaging, automotive, electronics, medical devices, toys, and many other consumer goods. However, the environmental impact of plastic waste and recycling challenges raise significant concerns for the sustainability of these materials. Therefore, numerous research and development efforts are underway to develop more sustainable versions of thermoplastics and improve recycling processes.



**Figure 2.52:** Polyvinyl chloride (PVC) pipes (PUBCHEM, 2017)

## 2.11. 3D Printers and Filaments

### 2.11.1. 3D printers

Three-dimensional (3D) printing refers to the process of printing a solid form of a 3D model of an object, created through computer-aided design programs (such as AutoCAD, Solid Work, etc.) or 3D scanners. 3D physical products are formed by stacking two-dimensional layers that make up the object. The devices that carry out this process are called 3D printers. Today, 3D prints can be made using many different types of raw materials. The main factor distinguishing 3D printing technologies is the processing methods of the layers that make up an object and the type of raw material used. While some 3D printing methods use the raw material by melting or softening it, others harden a photo-reactive resin layer-by-layer with a laser or UV (Ultraviolet) light source. The American Society for Testing and Materials (ASTM) categorizes additive manufactu-

ring processes according to standard terminology. According to ASTM, 3D printing technologies have been produced using material extrusion, powder bed fusion, binder jetting, and vat photopolymerization techniques, using biologically non-inert tissues, synthetic and natural polymers, natural and inorganic ceramic materials, or newly developed biodegradable, biocompatible, and bio-emulative materials. Among the most preferred 3D printers are those using FDM (Fused Deposition Modeling), SLS (Selective Laser Sintering), SLA (Stereolithography), DLP (Digital Light Processing), SLM (Selective Laser Melting), and EBM (Electron Beam Melting) printing technologies. FDM is a popular additive manufacturing technique with extensive application areas in many industries, from medical prosthetics to automotive and aviation. However, parts produced with FDM can form internal voids and porous structures, which can potentially lead to a decrease in mechanical properties. 3D printers, unlike traditional methods, have the ability to produce a wide variety of geometric shapes without the need for finishing work such as cutting and arranging, hence are widely used in many sectors. Considering various materials and geometric features, 3D printer technologies used for prototype production or rapid prototyping may vary. For example, the method of fused deposition modeling uses thermoplastics as filament raw material and works based on the principle of accumulating molten thermoplastic layer by layer. Various industries use such filament types, and the most popular ones are usually polylactic acid (PLA), acrylonitrile butadiene styrene (ABS), and polyamide (PA). 3D printing can be defined as a manufacturing technology developed to shorten product development times, produce small batch sizes, and produce physical models of complex geometric structures with high precision and low cost. As it requires repeatability and high precision in engineering tissue structure, it is often the preferred method. The establishment of the first manufacturing institute in the United States, the National Additive Manufacturing Innovation Institute, which has had a significant impact on bioprinter technology and research, has increased the use of 3D printing in biological research. The 3D printer market is continuously growing. From a market of $8.5 billion in 2018, it is expected to reach approximately $51.7 billion in 2026. The use of polymer filament is also rapidly increasing and reached a value of $1.3 billion in 2018, this figure is expected to rise to $4.4 billion by 2023.

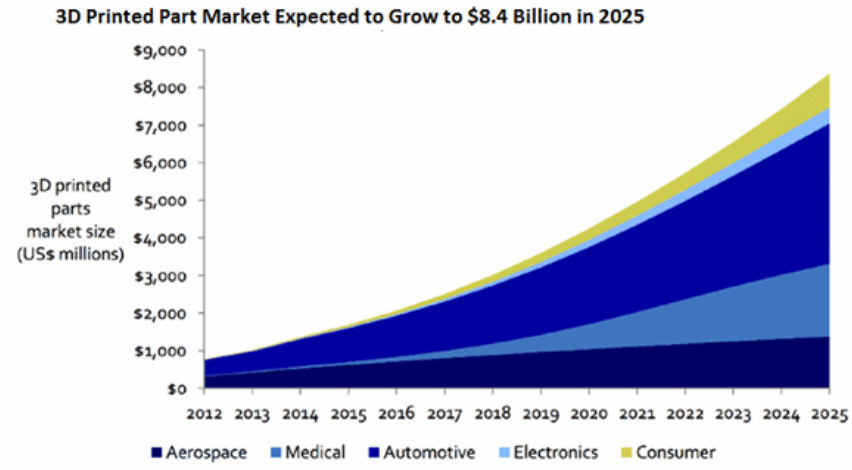



**Figure 2.53:** 3D Printing Market from 2012 to 2025 (Olam, 2021).

In this assessment, attention should be paid not only to individual use but also to the use in sectors such as medical, automotive, military, and consumer goods. Polymer-based filaments (PLA, ABS, PETG, etc.) used by FDM 3D printers offer certain advantages and disadvantages. Enhancing the printability and properties of filaments will greatly assist in the transition of these printers to general products. However, for many applications, the properties of filaments used alone often do not meet the requirements of the application. Therefore, to produce FDM-based products with desired properties, multiple materials can be combined to improve the properties of a certain filament. Such composite filaments expand the use of 3D printers using FDM technology. For instance, for neutron shielding, it is thought that such composite filaments can reach targeted properties by being combined with suitable alloys.

### 2.11.2. 3D printer filaments

3D printer filaments are of critical importance for both the current industry and future technological advancements. It is anticipated that the use of these filaments will revolutionize the industry with customized production, rapid prototyping, and accelerated manufacturing processes. Especially in cases where complex geometries and high customization levels are economically or technically challenging with traditional manufacturing techniques, 3D printing offers a significant advantage with filament technology.

Furthermore, 3D printer filaments have the potential to create a revolution in space exploration and in-space manufacturing. The limited resources and high transportation costs in space increase the importance of 3D printing technology and particularly filaments that can be produced through in-situ resource utilization (ISRU). This opens up

possibilities for directly converting materials found on other planets such as the Moon or Mars into 3D printer filaments and enabling the production of structures and tools adapted to space living conditions.

Additionally, environmentally friendly filaments and those made from recyclable materials can play a crucial role in transitioning to sustainable production and a circular economy. Biodegradable filaments and filaments made from recycled materials can enhance resource efficiency and reduce waste. Moreover, the development of new materials and composites allows for a wide range of applications and the attainment of previously unachievable properties. This can open doors to new industrial applications and lead to faster, more efficient, and environmentally friendly manufacturing processes.

#### 2.11.2.1. Acrylonitrile butadiene styrene (ABS) filament

Acrylonitrile Butadiene Styrene (ABS) possesses unique and superior characteristics among three-dimensional (3D) printing filaments. ABS is a copolymer obtained through the polymerization of acrylonitrile, butadiene, and styrene, and it stands out with features such as durability, rigidity, and high temperature resistance. These properties give ABS a broader range of applications compared to other popular filament types such as Polylactic Acid (PLA) or Thermoplastic Urethane (TPU). The wide melting temperature range of ABS (approximately 210-250°C) makes it an ideal choice for challenging 3D printing applications. This allows ABS to be preferred for producing more durable and long-lasting objects compared to materials like PLA that have lower melting temperatures. Its high temperature tolerance makes ABS more resistant to thermal deformation, making it an excellent option for producing parts that need to operate at high temperatures. Additionally, ABS can be easily processed on surfaces and is resistant to abrasive chemicals, making it popular in a wide range of industrial applications such as automotive, electronics, and toy industries. The surface quality and ease of post-processing of ABS result in smoother and more professional outcomes compared to other materials like PLA or PETG. Lastly, ABS has environmental implications due to the emission of harmful fumes and gases during the printing process. However, these issues can be managed effectively with proper ventilation. Despite the sustainability challenges of ABS, its durability, processability, and wide range of applications make it an ideal material for 3D printing and suitable for more demanding applications compared to other filament types.

### 2.11.2.2. Polylactic acid (PLA) filament

Polylactic Acid (PLA) is a commonly used thermoplastic filament in the three-dimensional (3D) printing industry. PLA is a sustainable material that is biodegradable and derived from renewable sources such as corn starch, sweet potatoes, or sugarcane. These characteristics provide significant advantages to PLA in terms of environmental impact compared to other popular 3D printing filaments, especially petroleum-based ones like ABS. The melting temperature of PLA filament typically ranges from 180 to 220°C. This relatively low melting temperature makes PLA particularly user-friendly for beginners in 3D printing because it allows for less precise control of the printer's nozzle and bed temperatures. PLA also has high dimensional stability, making it an ideal choice for detailed and precise 3D printing applications. However, the relatively low melting temperature and lower durability of PLA limit its performance under higher temperature and mechanical stress conditions. Nevertheless, these disadvantages are balanced by PLA's excellent workability, wide range of color options, low impact and shrinkage rates, and generally pleasant odor. In conclusion, PLA is an excellent filament choice for 3D printing applications that prioritize sustainability, workability, and ease of use. These characteristics make PLA a more popular option compared to other filament types, particularly in prototyping, education, and hobbyist 3D printing applications.

### 2.11.2.3.Thermoplastic polyurethane (TPU) filament

Thermoplastic Polyurethane (TPU) is a flexible filament type commonly used in 3D printing. This polyurethane material is known for its flexibility and high impact resistance, distinguishing it from other filaments such as ABS (Acrylonitrile Butadiene Styrene) or PLA (Polylactic Acid), which are harder and less flexible. TPU's unique properties make it ideal for printing flexible objects, impact-absorbing parts, or components requiring high wear resistance. TPU typically has a melting point of around 220-250°C, making it compatible with various 3D printing technologies. However, the flexibility of TPU can pose certain challenges during the printing process as it can make it difficult to feed properly through the 3D printer's extruder. This means that TPU generally requires high precision and experience in 3D printing. Additionally, due to its excellent wear resistance, flexibility, and impact resistance, TPU has a wide range of applications in various industries, including automotive, footwear, and electronics. For example, TPU is commonly used in the production of automotive parts, phone cases, and other elasto-

meric products. In conclusion, TPU offers a unique material option for 3D printing, especially for applications requiring flexibility and impact resistance. However, the unique challenges presented by TPU during the printing process require careful settings and often more experience to effectively use this material in 3D printing.

#### 2.11.2.4. Polyethylene terephthalate glycol-modified (PETG) filament

Polyethylene Terephthalate Glycol-modified (PETG) is a commonly used thermoplastic filament in three-dimensional (3D) printing. PETG is a polymer that offers a range of superior properties compared to other popular 3D printing filaments like PLA (Polylactic Acid) and ABS (Acrylonitrile Butadiene Styrene). It is known for its high impact resistance, excellent transparency, and ease of use. The melting temperature of PETG filament typically ranges from 220 to 250°C. This allows PETG to have higher temperature resistance than PLA while not reaching the same high melting point as ABS. It enables the production of parts that can operate within a wide temperature range. Furthermore, PETG has the advantage of lower shrinkage compared to other filaments such as PLA and ABS. This provides PETG with higher dimensional stability during 3D printing, allowing for the production of more precise and detailed objects. Additionally, PETG's transparency makes it particularly suitable for optical applications and lighting components. Moreover, PETG is often preferred for applications like food and beverage packaging due to its FDA approval for food safety. In conclusion, PETG is a versatile filament option for 3D printing applications, offering a wide range of applications, excellent mechanical and thermal properties, and ease of use. These characteristics make PETG a popular choice, especially in industrial and professional 3D printing applications, compared to other filament types.

#### 2.11.2.5. Polyvinyl alcohol (PVA) filament

Polyvinyl Alcohol (PVA) is a commonly used support material filament in the three-dimensional (3D) printing industry. PVA is known for its solubility in water and good compatibility with other thermoplastics such as PLA (Polylactic Acid) or PETG (Polyethylene Terephthalate Glycol). These properties enable PVA to be used as a support material in the 3D printing of objects with complex geometries. The melting temperature of PVA filament typically ranges from 180 to 210°C. This allows PVA to be printed at a lower temperature than PLA while not reaching the same high melting point as

PETG. It enables the production of parts that can operate within a wide temperature range. However, PVA's solubility can pose certain challenges during the printing process as it can make it difficult to feed properly through the 3D printer's extruder. This means that PVA generally requires high precision and experience in 3D printing.

PVA's water solubility allows for easy removal of support materials after the printing process is complete. This feature makes PVA an ideal choice for specialized applications that require properties such as air permeability, solubility, and adhesion.

In conclusion, PVA offers an excellent option as a support material in 3D printing applications due to its water solubility and broad compatibility range. However, effective use of PVA in 3D printing requires careful control and experience.

#### 2.11.2.6. Nylon filament

Nylon is a thermoplastic filament commonly used in three-dimensional (3D) printing. Chemically known as polyamide, nylon stands out with its excellent strength, low friction, and high temperature resistance. These properties make nylon suitable for a wide range of applications compared to other popular 3D printing filaments such as ABS (Acrylonitrile Butadiene Styrene) or PLA (Polylactic Acid). The melting temperature of nylon typically ranges from 220 to 270°C. This high melting temperature allows nylon to be used in the production of parts that operate at high temperatures. Nylon also has high impact resistance and excellent wear resistance, making it an ideal choice for 3D printing applications that require strength and durability. However, nylon's water solubility can pose certain challenges that limit its usage. In particular, nylon filament's susceptibility to moisture requires special attention in terms of storage and handling. This means that careful settings and experience are required to effectively use nylon in 3D printing. Lastly, nylon's wide range of applications allows it to be used in various industries such as automotive, aerospace, electronics, and textiles. These applications rely on nylon's excellent mechanical properties and broad processing range. In conclusion, nylon offers superior material properties for 3D printing applications, especially those requiring strength, durability, and high temperature resistance. However, unique challenges like moisture sensitivity require careful control and experience to effectively use nylon in 3D printing.

## 2.12. Nanomaterials

Nanomaterials are typically materials with sizes smaller than 100 nanometers (nm), and at this scale, significant and sometimes unexpected changes occur in material properties. The unique properties of nanomaterials make them highly valuable in various scientific and engineering applications, placing them at the forefront of materials science and nanotechnology research. The significance of nanomaterials primarily stems from their enhanced or novel properties. This is often associated with distinct interactions between atoms or molecules within the material at the nanoscale. As a result, nanomaterials can exhibit significantly different physical and chemical properties compared to the same materials at larger scales. Nanomaterials can find applications in various industries such as energy storage and conversion, environmental protection, information technology, biomedical, and pharmaceutical applications. For example, nanomaterials play a crucial role in energy applications like solar cells and energy storage systems, where they can enhance energy efficiency and reduce environmental impacts. Nanomaterials also contribute to the development of more effective drug delivery systems and biomedical applications used in early disease diagnosis. In conclusion, the development and utilization of nanomaterials make significant contributions to scientific research and technological advancements. The unique properties of these materials play a critical role in applications across diverse industries, addressing global challenges in the areas of environment, energy, health, and information technology.

## 2.13. Polymer Matrix Nanocomposites (PMNC)

Polymer matrix nanocomposites (PMNCs) are advanced materials composed of a polymer matrix combined with nanoscale fillers. These fillers typically include materials such as graphene, nanosilica, metal oxide nanoparticles, and nanoclays or nanotubes, and they are usually dispersed homogeneously within the matrix material, often at a scale of a few nanometers. PMNCs can exhibit significantly enhanced mechanical, thermal, optical, and electrical properties depending on the choice of filler material and its distribution and orientation within the matrix. The improvements in the mechanical properties of PMNCs are often attributed to the high surface area of the nanofillers, which enables strong interactions with the matrix material, thereby enhancing the overall strength, hardness, and durability of the composite. Furthermore, the high surface energy and fine structure of the fillers facilitate the formation of stronger and more ef-

fective bonding with the matrix, resulting in higher strength and stiffness values. In terms of thermal properties, nanofillers are typically known to possess high thermal conductivity, and their incorporation into PMNCs can enhance the overall thermal conductivity of the composites. These properties enhance the usability of the composites in high-temperature applications. PMNCs can also be used in optoelectronic and energy applications due to the specific optical and electrical properties of the nanofillers. For instance, certain nanofillers like carbon nanotubes or graphene can provide high electrical conductivity and optical efficiency to the composites. This wide range of properties enables the utilization of PMNCs in a variety of industries and applications, including automotive, electronics, energy, and environmental engineering, among others. However, harnessing and utilizing the advanced properties of PMNCs requires careful attention to factors such as the selection, distribution, and alignment of nanofillers within the matrix. This necessitates the development of various techniques and methods for the design and production of PMNCs, further emphasizing their scientific and industrial significance.

### 2.13.1. Methods for the synthesis of polymer nanocomposites

There are various methods for synthesizing polymer nanocomposites. Here are some commonly used polymerization methods for nanocomposites:

#### 2.13.1.1. Sol-gel method

The sol-gel method involves dispersing nanoparticles into a polymer matrix. In this method, a solution is prepared, and nanofillers, along with monomers that will form the polymer matrix, are included. The solution is then slowly subjected to polymerization, resulting in the formation of a gel. The gel can be further converted into a solid nanocomposite material through drying and sintering steps.

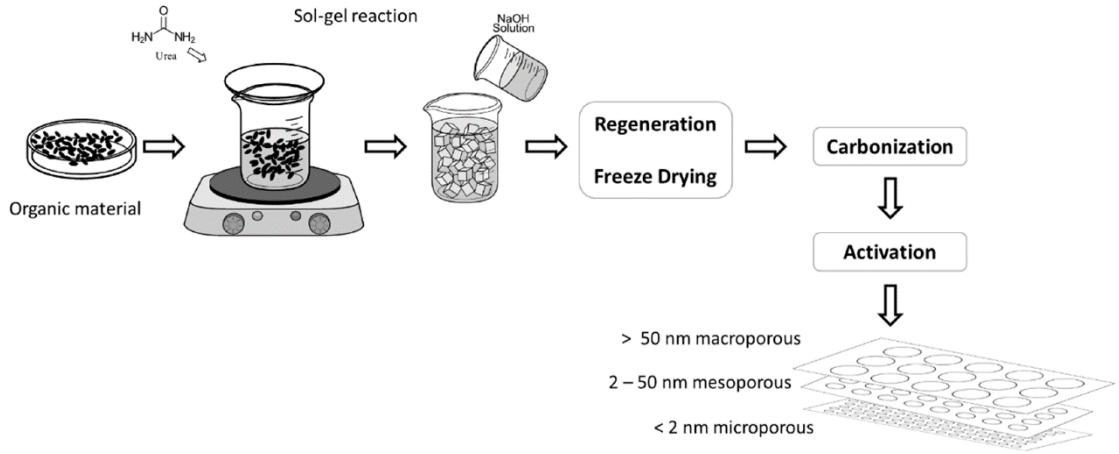



**Figure 2.54:** Schematic illustration of the nanocomposite sol-gel polymerization (PUBCHEM, 2017).

### 2.13.1.2. In-situ polymerization method

In this method, nanofillers are created within the polymer matrix during the polymerization reaction itself. For example, suitable monomers for polymerization are placed in a reaction environment along with nanofillers. As the monomers polymerize, the nanofillers become integrated into the matrix, forming a nanocomposite polymer.

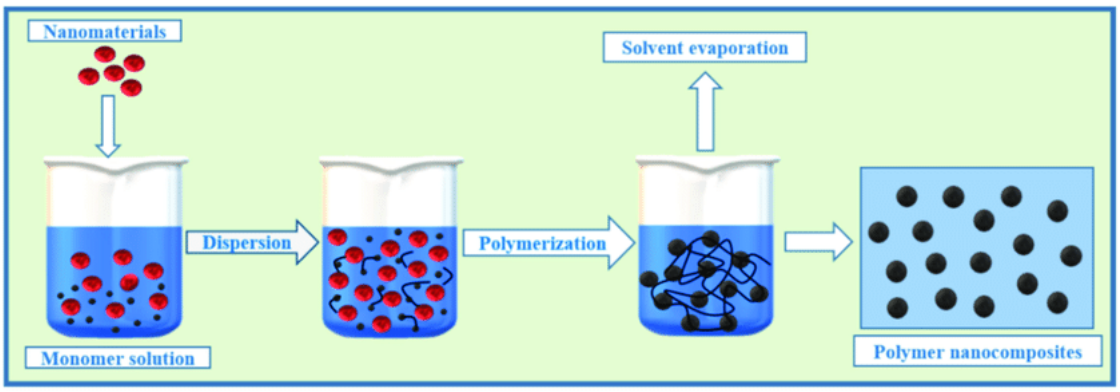



**Figure 21.55:** Schematic illustration of the in-situ polymerization metod

### 2.13.1.3. Mechanical mixing method

In this method, the polymer matrix and nanofillers are mechanically mixed. For instance, nanofillers in the form of powder or nanoparticles are added to the polymer matrix, and a mechanical mixing process (such as stirring, grinding, or fractionation) is used to ac-

hieve a homogeneous distribution. Subsequently, this mixture is transformed into a solid structure through processes like polymerization or sintering.

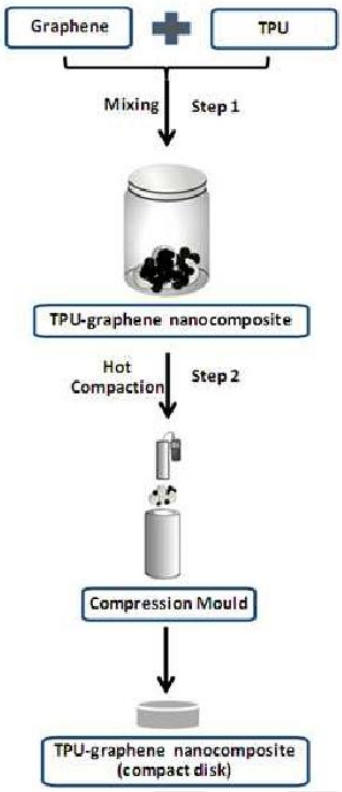



**Figure 2.56:** A Schematic illustration of the dry (mechanical) mixing metod (PUBCHEM, 2017).

### 2.13.1.4. Electrostatic self-assembly method

This method involves the orderly assembly of nanofillers into the polymer matrix using electrostatic interactions. Nanofillers are positioned within the matrix through ionic interactions or electrostatic attraction/repulsion, creating a regular structure. The choice of these methods will depend on factors such as the specific nanofillers used, the polymer matrix, the intended application, and the desired material properties. Each method has its advantages and disadvantages, and the appropriate method should be determined based on specific requirements.

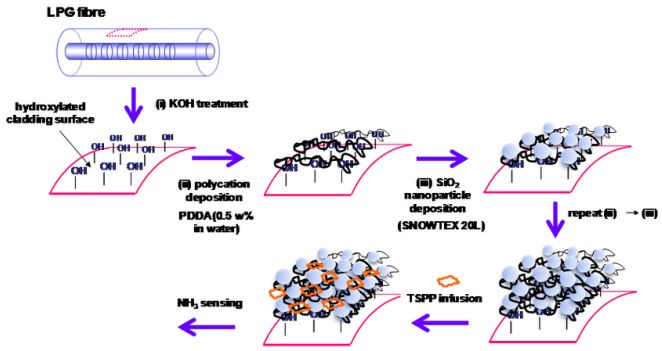



**Figure 21.57:** A Schematic illustration of the Electrostatic self-assembly method

## 3. MATERIALS AND METHODS

In order to perform motivated work in the earlier sections, unique codes have been assigned to the samples produced both by the mold production technique and the 3D printing technique according to the nanpowder additives. The values in the codes represent the mass percentage of each element. The series produced with the mold production technique starts with the code "M", followed by filament samples produced from the Filament Extruder machine starting with the code "F", and the samples produced with the 3D printing technique starting with the code "P". The sample codes include: "M-ABS-0 (0% Additive), M-ABS-Er5 (5% Additive), M-ABS-Gd5 (5% Additive), M-ABS-Er10 (10% Additive), M-ABS-Gd10 (10% Additive), M-ABS-Er10Gd5 (10%, 5% Additive), M-ABS-Er5Gd10 (5%, 10% Additive), M-ABS-Er20 (20% Additive), M-ABS-Gd20 (20% Additive), F-ABS-0 (0% Additive), F-ABS-Er5 (5% Additive), F-ABS-Gd5 (5% Additive), F-ABS-Er10 (10% Additive), F-ABS-Gd10 (10% Additive), F-ABS-Er10Gd5 (10%, 5% Additive), F-ABS-Er5Gd10 (5%, 10% Additive), F-ABS-Er20 (20% Additive), F-ABS-Gd20 (20% Additive), P-ABS-0 (0% Additive), P-ABS-Er5 (5% Additive), P-ABS-Gd5 (5% Additive), P-ABS-Er10 (10% Additive), P-ABS-Gd10 (10% Additive), P-ABS-Er10Gd5 (10%, 5% Additive), P-ABS-Er5Gd10 (5%, 10% Additive), P-ABS-Er20 (20% Additive), P-ABS-Gd20 (20% Additive)." These produced samples, fortified with nano-oxide compounds, were tested with various radioactive point sources ($^{241}$Am (59,5 keV), $^{133}$Ba (80,9, 276,3, 302,8, 356,0 and 383,8 keV), $^{22}$Na (511,0 and 1274,5 keV), $^{137}$Cs (661,6 keV), and $^{60}$Co (1173,2 and 1332,5 keV)) using experimental (HPGe detector system), theoretical (XCOM, EpiXS), and simulation (FLUKA, GEANT4) methods to determine their gamma radiation attenuation capabilities. The compatibility of each method with the experimental results was determined.
Also, within the scope of the thesis work, the neutron attenuation characteristics of all samples to be produced were evaluated with theoretical and simulation calculations. The SEM / EDS and TGA structural analyses of the produced samples were additionally conducted.

## 3.1. Materials

### 3.1.1. Acrylonitrile butadiene styrene granules

Acrylonitrile Butadiene Styrene (ABS) is a thermoplastic polymer with a wide range of applications due to its durability, mechanical properties, and chemical resistance. In this paragraph, I will focus on the features of ABS used in filament and granule forms. Mechanical properties are an important factor in the use of ABS in filament and granule forms. ABS stands out with its high impact resistance, which makes the material resistant to sudden shocks and collisions in various applications. Additionally, the hardness and strength of ABS resist forces applied to surfaces and provide durability against tensile or bending forces.The color options for ABS in filament and granule forms typically vary. Standard neutral colors such as black, white, or gray are available, but different color options can be obtained by adding pigments. This allows ABS to be more aesthetically suitable for a variety of applications and provides more options for designers. The temperature range of ABS in filament and granule forms is also important. ABS material generally melts between 210 and 250°C and can be easily shaped at this temperature. The ABS that melts when heated solidifies again when cooled, forming a durable structure. Therefore, ABS in filament and granule forms is commonly used in production methods such as 3D printing and injection molding. The density of ABS typically ranges from 1,05 to 1,07 g/cm³. The low density of ABS provides various advantages. Firstly, the lightweight nature of ABS is an important characteristic. This lightweight property facilitates the transportation, processing, and utilization of the material. Additionally, the low density offers cost advantages as it requires less material usage, thereby reducing production costs. In conclusion, ABS in filament and granule forms is a preferred polymer in applications such as 3D printing and injection molding due to its durability, mechanical properties, and color diversity. With its high impact resistance, various color options, and shapability, ABS is a successful choice in production processes and design projects. The ABS granules used within the scope of the thesis study were obtained from RIIZ company (Kayseri, Turkey). Below, tables are provided that describe the chemical, mechanical, thermal, and electrical properties of ABS in more detail.



**Figure 3.1:** ABS granules (PUBCHEM, 2017).

**Table 3.1:** Chemical properties of ABS

| **Property** | **Level of Resistance** |
|---|---|
| Resistance to Diluted Acid and Alkalis | Very Good |
| Resistance to Aliphatic Hydrocarbons | Moderate |
| Resistance to Aromatic Hydrocarbons | Poor |
| Resistance to Halogenated Hydrocarbons | Poor |
| Resistance to Alcohols | Poor |

**Table 3.2:** Mechanical Properties of ABS

| **Property** | **Value** |
|---|---|
| Elongation at Break | 10 - 50 % |
| Elongation at Yield | 1,7 - 6 % |
| Flexibility (Flexural Modulus) | 1,6 – 2,4 GPa |
| Hardness Shore D | 100 |
| Stiffness (Flexural Modulus) | 1,6 – 2,4 GPa |
| Strength at Break (Tensile) | 29,8 - 43 MPa |
| Strength at Yield (Tensile) | 29,6 - 48 MPa |
| Toughness (Notched Izod Impact at Room Temperature) | 200 - 215 J/m |
| Toughness at Low Temperature (Notc-hed Izod Impact at Low Temperature) | 20 - 160 J/m |
| Young Modulus | 1,79 - 3.2 GPa |

**Table 3.3:** Thermal properties of ABS

| Property | Value |
|---|---|
| Max Service Temperature | 61,9 – 76,9 °C |
| Insulator or Conductor | Insulator |
| Specific Heat Capability | $1{,}39e^{3}$ – $1{,}92e^{3}$ J/kg °C |
| Thermal Expansion Coefficient | $8{,}46e^{-5}$ – $2{,}34e^{-4}$ strain/°C |

**Table 3.4 :** Electrical Properties of ABS

| **Property** | **Value** |
|---|---|
| Arc Resistance | 60 - 120 sec |
| Dielectric Constant | 2,7 – 3,2 |
| Dielectric Strength | 15,7 - 34 kV/mm |
| Dissipation Factor | 50 - 190 x $10^{-4}$ |
| Volume Resistivity | 14 - 16 x $10^{15}$ Ohm.cm |

### 3.1.2. Pure Acetone

Acetone is a colorless, volatile, and flammable compound with the chemical formula $(CH_3)_2CO$. It has a slight sweet odor. On an industrial scale, acetone is primarily produced through the oxidation of cumene with cumene hydroperoxide and is abundantly available worldwide, making it an economical and accessible solvent. Due to its chemical and physical properties, acetone has the ability to dissolve a variety of compounds, especially polymers, oils, resins, and other organic substances. Its ability to dissolve ABS (Acrylonitrile Butadiene Styrene) is particularly notable due to its interaction with the acrylonitrile and styrene components present in this polymer. However, some polymers, particularly polyolefins such as polyethylene and polypropylene, are not soluble in acetone. This is because these polymers have low solubility parameters for acetone, and the ability of acetone molecules to spread within the polymer matrix of these materials is limited. The environmental impact of acetone is also an important consideration. The evaporation of acetone can contribute to photochemical reactions in the atmosphere, affecting air quality. Nevertheless, its non-toxic nature and rapid biodegradation make it a more environmentally acceptable solvent. However, the discharge of acetone into wastewater can have negative effects on aquatic life, highlighting the need for careful management. Overall, acetone is a versatile and effective solvent both in practical and environmental aspects, but it should always be used with appropriate safety and environmental protection measures. The pure acetone solvent used within the scope of the thesis study were obtained from RIIZ company (Kayseri, Turkey).

**Table 3.5 :** Material properties of acetone

| **Chemical Properties** | **Description** |
|---|---|
| Chemical Formula | $(CH_3)_2CO$ |
| Molecular Weight | 58,08 g/mol |
| Appearance | Colorless |
| Odor | Slightly sweet |

**Continuation of Table 3.5…**

| | |
|---|---|
| Density | 0,79 g/cm³ |
| Boiling Point | 56,5°C |
| Melting Point | -94,9°C |
| Flash Point | 465°C |
| Solubility | Highly soluble in water; miscible with most organic solvents |
| Acidity/Alkalinity (pH) | Varies depending on the concentration of hydrogen ions |
| Flammability | Flammable. Should be used with caution and kept away from open flames |
| Chemical Stability | Stable. Does not decompose under normal conditions |
| Reactivity | Stable against oxidation. Can react with certain metals and bases |
| Toxicity | Harmful to human health. Prolonged or high-dose exposure may cause irritation to the skin, eyes, and respiratory tract. Appropriate safety precautions should be taken. |
| Environmental Impact | The evaporation of acetone can contribute to photochemical reactions in the atmosphere. Discharge into wastewater can have a negative impact on aquatic life. Proper management and waste disposal should be carried out with caution. |

### 3.1.3. Erbium oxide ($Er_2O_3$) nanopowder

Erbium oxide ($Er_2O_3$) is the oxide of erbium, which is one of the rare earth elements. It exhibits notable properties such as high thermal and chemical stability, wide bandgap, and low absorption coefficient. The density of this material is approximately 8.64 g/cm³, making it effective for gamma and neutron shielding in nuclear technology. Erbium oxide typically has a cubic (Face-Centered Cubic, FCC) crystal structure, where atoms are located at the corners and surfaces of a cube. This crystal structure determines many properties of the material and affects its performance in various applications. Erbium oxide, when in the nanoscale, allows for the optimization of these properties for many applications. It finds wide usage in optoelectronics, fiber optics, biomedical, and energy fields. In optical communication systems, erbium oxide is used to amplify the power of light carrying information. At the nanoscale, erbium oxide provides more effective light scattering and helps achieve a better signal-to-noise ratio. In the biomedical field, nanoscale erbium oxide is utilized in cell labeling and imaging technologies, acting as an effective biological marker. In the energy field, erbium oxide is employed to enhance the performance of solar cells. At the nano-level, this material facilitates more efficient light absorption by the cells, thereby improving energy conversion. In the context of nuclear technology, erbium oxide plays a significant role in gamma and neutron shielding. Erbium, used as a neutron absorber in nuclear reactors, regulates the energy production process and reduces radioactive pollution. Erbium oxide is added to fuel rods in

nuclear reactors, where it absorbs neutrons and controls the operation of the reactor. Additionally, erbium oxide is employed as high-density radiation protection material. This material provides protection against high-energy gamma rays in nuclear facilities, radiation therapy centers, and space applications. These properties make erbium oxide a versatile material in the field of nuclear technology.



**Figure 3.2 :** Erbium oxide nanopowder (PUBCHEM, 2017).

**Table 3.6 :** Chemical properties of erbium oxide nanopowder

| **Chemical Properties** | **Description** |
|---|---|
| Chemical Formula | $Er_2O_3$ |
| Purity | 99,95% |
| Erbium (Er) Ions | +3 charge |
| Oxygen (O) Ions | -2 charge |
| Chemical Stability | Chemically stable and resistant to most acids and bases |
| Solubility | Insoluble in water, but can undergo hydrolysis in the presence of acids to form hydroxide ions |

**Table 3.7 :** Physical properties of erbium oxide nanopowder

| **Physical Properties** | **Description** |
|---|---|
| Appearance | Pink powder |
| Particle Size | 110 nm |
| Crystal Structure | Cubic (Face-Centered Cubic, FCC) |
| Density | 8.64 g/cm³ |
| Melting Point | 2,344°C |
| Boiling Point | Approximately 3,300°C |
| Thermal Stability | Exhibits high thermal stability and typically does not decompose at high temperatures |
| Surface Area | High surface area, advantageous for the development of catalytic and optical properties |

### 3.1.4. Gadolinium oxide ($Gd_2O_3$) nanopowder

Gadolinium oxide ($Gd_2O_3$) is the oxide of the element gadolinium and belongs to the family of rare earth metal oxides. It is known for its high turbostability, thermal and chemical stability, and neutron capture ability. The density of gadolinium oxide is approximately 7.41 g/cm³, and it typically exhibits a cubic crystal structure, although in some cases it can also show a monoclinic structure. At the nanoscale, many of these properties are further enhanced in gadolinium oxide, providing high-performance capabilities for a range of applications. In the biomedical field, gadolinium oxide nanoparticles are used as contrast agents in magnetic resonance imaging (MRI), allowing for clearer images of tissues and organs. Additionally, these nanoparticles are also utilized for targeted drug delivery. In the field of nuclear technology, gadolinium oxide plays a significant role. Gadolinium is known for its high thermal neutron capture cross-section, which enables its use as a control rod material in nuclear reactors. Gadolinium oxide is employed to regulate the neutron flux in the reactor and ensure its safe operation. Moreover, gadolinium oxide serves as an effective shielding material against gamma rays and neutrons, making it suitable for radiation shielding in nuclear facilities, medical radiation therapy centers, and research facilities. In summary, the nanoscale and macroscale properties of gadolinium oxide enable its effective and versatile utilization in various fields. The used additives, $Gd_2O_3$ nanopowder (99.95% purity, particle size: 95 nm) were purchased from Nanografi Company (Turkiye)



**Figure 3.3 :** Gadolinium oxide nanopowder

**Table 3.8 :** Physical-chemical1 properties of gadolinium oxide nanopowder

| **Physical- Chemical Properties** | **Description** |
|---|---|
| Appearance | White powder |
| Particle Size | 95 nm |
| Crystal Structure | Cubic (Face-Centered Cubic, FCC) |
| Density | 7,40 g/cm³ |
| Melting Point | 2,425°C |
| Boiling Point | Approximately 3,200°C |

**Continuation of Table 3.8…**

| | |
|---|---|
| Thermal Stability | Exhibits high thermal stability and does not decompose at high temperatures |
| Surface Area | High surface area, advantageous for the development of catalytic and optical properties |

### 3.1.5. Steel casting molds

Steel casting molds are an essential component of the casting process in polymer production, and they have a significant impact on quality, efficiency, and product features. The type of casting plays a decisive role in determining the shape, size, internal structure, and physical properties of the polymer. Firstly, steel molds provide very high precision and repeatability. This allows the dimensions and shape tolerances of the produced polymer parts to be extremely tight. Secondly, steel casting molds are usually extremely durable. This means that the same mold can be used for long periods, which typically leads to lower production costs. Finally, the use of steel casting molds increases speed and efficiency in polymer production processes. This is because steel molds provide fast and effective cooling, which can significantly shorten casting times. Therefore, the use of steel casting molds can enhance the overall quality, speed, and cost-effectiveness of polymer production processes. The technical drawing of the mold is shown in Figures 3.4 and 3.5.

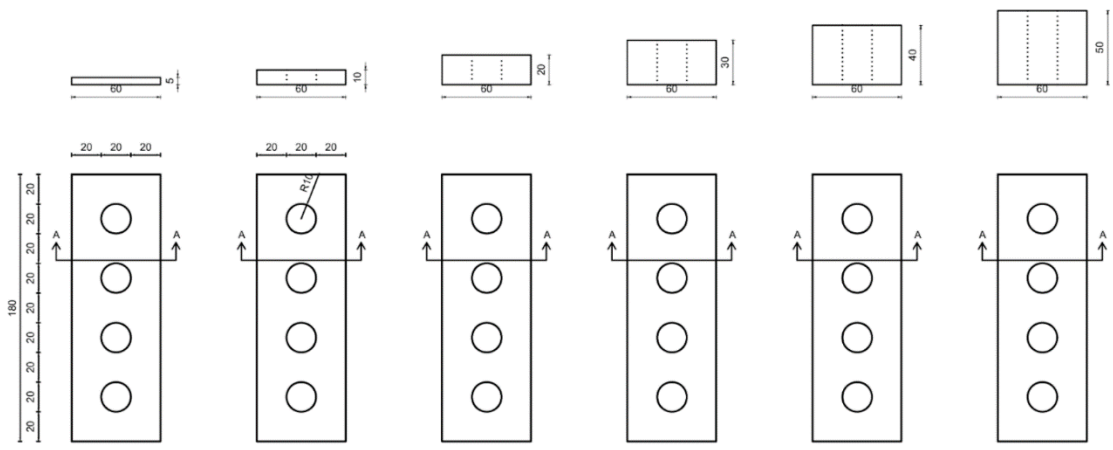



**Figure 3.4** The technical drawing visual of the internal components of the casting mold

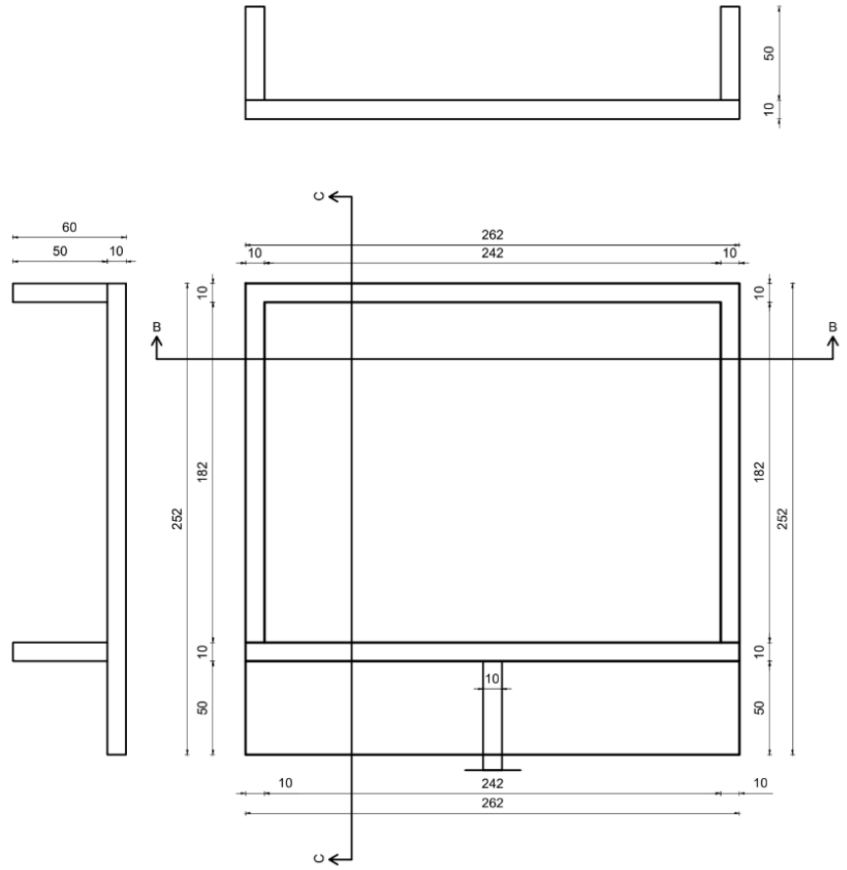



**Figure 3.5 :** The technical drawing visual of the external components of the casting mold.

### 3.1.6. Twin-screw extruder machine

The twin-screw extruder plays a crucial role in advanced polymer processing operations, such as composite filament production. This extruder consists of two screws and a cylindrical body. Each screw rotates and moves forward at separate speeds, facilitating the mixing, dispersion, and homogenization of materials. The twin-screw extruder offers a range of significant advantages for composite material production. The two screws can distribute fillers or additives within the material more homogeneously. Additionally, the increased mixing and material passage in this system provide an excellent blend, enhancing the mechanical properties and homogeneity of the product. Furthermore, the twin-screw extruder can better control material flow and reduce viscosity fluctuations, offering more stable performance during the production process. Due to these characteristics, the twin-screw extruder is a piece of equipment commonly used in applications like composite filament production, ensuring composite materials possess excellent mechanical properties and a homogeneous structure. A twin-screw extruder from Gulnar Mac-

hines, Turkey (with a screw diameter of 16 mm and L/D = 40) was used to fabricate the filaments at the Erciyes University Nanotechnology Research Center (ERNAM).

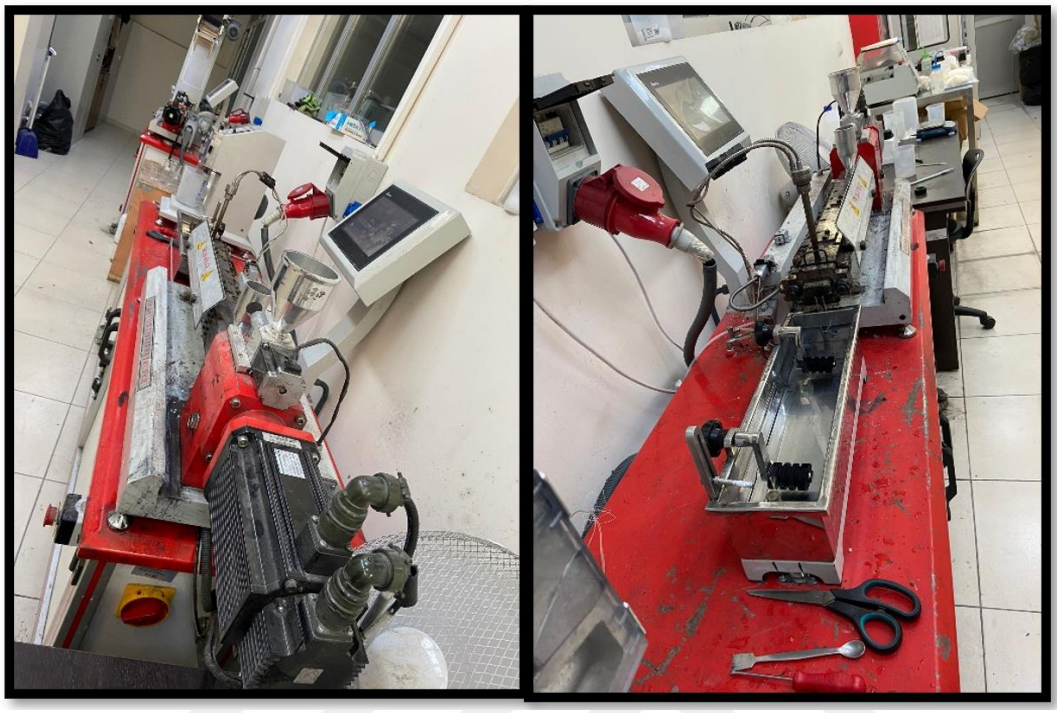


**Figure 3.6:** The twin-screw extruder device's general visual from the right and left sides.

**Table 3.9:** Specifications of twin-screw extruder

| **Property** | **Description** |
|---|---|
| Screw Number | 2 |
| Screw Speed | Independently adjustable to desired speed |
| Screw Diameter | Typically designed symmetrically and customizable 30, 40, 50, etc. (Customizable) |
| Screw Length (L/D Ratio) | 20:1, 25:1, 30:1, etc. (Customizable) |
| Body Material | Hardened steel or special alloys for high durability (High carbon steel, alloyed steel, etc.) |
| Mixing Capability | Can homogeneously mix materials with different movements and rotation speeds between the two screws |
| Material Feeding | Suitable conveyor or feeding systems for controlled material feeding |
| Motor Power (kW) | 5-100, etc. (Varies depending on model and application) |
| Thermal Control | Heating and cooling zones for maintaining optimum processing temperature |
| Flow Control | Can control material flow with screw rotation speed and feed rate adjustments |
| Suitable Applications | Production of composite filaments, processing polymer blends, granule or pellet production |

### 3.1.7. Thermostatic drying oven

Thermostatic drying ovens serve the purpose of drying materials at a specific temperature and are typically used in industrial and laboratory applications. Their functions and purposes include:

- Material Drying: Different types of materials (such as coatings, paints, varnishes, polymers, ceramics, etc.) may require drying. Thermostatic drying ovens help achieve the desired properties of products by allowing materials to dry at the required temperature and duration.
- Laboratory Applications: Professionals working in fields like biology, chemistry, and medicine may need to dry samples or remove moisture during experiments. Thermostatic drying ovens provide precise temperature control for such laboratory processes.
- Analytical Studies: Some analytical tests or characterization studies may involve drying samples at specific temperatures. These ovens can be used to optimize analysis processes.
- Moisture Removal: For products, materials, or components sensitive to moisture content, these ovens can be used to eliminate moisture. For instance, they can reduce the moisture content in electronic components or protect sensitive materials from moisture-induced degradation.
- Heat Treatment: Certain materials can acquire specific properties through heat treatment. Thermostatic ovens enable controlled thermal processing of materials.

These ovens may possess features like temperature control, timing, and humidity adjustment. This allows users to precisely control their processes and achieve desired outcomes.



**Figure 3.7:** Thermostatic Drying Oven owned by Sinop University's Scientific and Technological Research Application and Research Center

**Table 3.10:** Specifications of thermostatic drying oven

| **Property** | **Description** |
|---|---|
| Capacity | 48 L |
| Temperature | Ambient +5° to 220°C |
| Dimensions (D x W x H) Interior | 29 x 41 x 41 cm |
| Width | 45,72 cm |
| Width Interior | 40,64 cm |

Using a drying oven and a precision scale, the mass changes of each sample were analyzed depending on the temperature. These analyses were conducted by exposing the samples to fixed temperatures of 120°C, 140°C, 160°C, 180°C, 200°C, and 220°C, each for a duration of 10 minutes. The masses of the samples that were not exposed to these temperature levels were compared with the mass changes of the samples held at the respective temperatures. The evaluation of the study commenced considering that 3D printers typically have an average bed temperature of 110°C. Taking into account the information that the material of the samples, ABS, has a melting temperature range of 210-250°C, the highest temperature level was determined as 220°C.

### 3.1.8. Hammer mill grinder

Hammer mills are a type of grinding equipment often used for processes such as polymer fragmentation. These mills utilize a series of rapidly rotating hammers to break down material into smaller pieces. As the hammers inside rotate, the fed polymer parts are continually struck and broken down by the hammers.

The operating principle of hammer mills is to reduce the material using impact forces. The material enters from the top of the mill and is broken into smaller pieces by the

rapid movement of the hammers. These pieces then pass through a sieve at the bottom of the mill as they exit. This sieve prevents pieces larger than a certain size from passing through, controlling the size of the final product. There are several advantages to using hammer mills for polymer grinding. Firstly, these mills are generally quite durable and demonstrate good resistance to heavy load conditions. Secondly, hammer mills typically operate at high efficiency and speed, which increases the speed and efficiency of polymer fragmentation. Thirdly, hammer mills can usually process a wide variety of materials, making them usable with a range of different materials including polymers.



**Figure 3.8 :** Hammer mill grinder

**Table 3.11 :** Specifications of hammer mill Grinder

| **Feature** | **Hammer Mill Grinder (for Polymers)** |
|---|---|
| Function | Grinds polymer material to desired size |
| Advantages | High capacity, uniform and consistent product size, energy efficiency |
| Disadvantages | Product waste can occur in case of over-grinding, processing of low moisture or hard materials might be difficult |
| Applications | Plastic recycling, pre-processing of polymer-based materials for production |
| Key Components | A rotating rotor (with hammers), a grinding chamber, a sieve (controls the output size of the material) |
| Operating Principle | The polymer is broken down and ground by hammers via a rapidly rotating rotor. Once it reaches the desired size, the material passes through the sieve and is collected. |

### 3.1.9. Scanning Electron Microscope

Scanning Electron Microscopy and Energy Dispersive Spectroscopy (SEM-EDS) is a powerful analytical tool combination for characterizing additive polymer samples. Scanning Electron Microscopy (SEM) is used to examine the surface structure and morphology of the sample, while Energy Dispersive Spectroscopy (EDS) is used for elemental analysis. SEM directs high-energy electron beams towards the surface of the sample, and these electrons are backscattered from the surface of the sample. The signals obtained from these scattering events are detected by detectors and used to form an image. SEM is used to visualize in detail the surface topography, morphology, porosity, and distribution of additives in additive polymer samples. EDS, on the other hand, is a spectroscopy used in conjunction with SEM. This technique analyzes the characteristic X-rays that arise at the points where the electron beam interacts with the surface of the sample. These X-rays are used to determine the elemental composition of the sample. EDS is a powerful tool for determining the chemical composition, elemental distribution, and concentration of additives in additive polymer samples. This allows for the evaluation of important features such as the homogeneity, distribution, and quantity of additives. SEM-EDS offers various advantages in the characterization of additive polymers. Thanks to its high resolution and magnification capability, a detailed image of the surface topography of the sample is obtained. Also, with EDS analysis, the composition and elemental distribution of the additives can be determined. This information is important for optimizing production processes of additive polymer samples, assessing their performance, and ensuring quality control. In conclusion, SEM-EDS is a powerful analytical tool combination for characterizing additive polymer samples. These methods are used to examine the surface morphology of additive polymer samples, visualize the distribution of additives, and perform elemental analysis. This enables a better understanding of the structural and chemical properties of additive polymers and facilitates progress in areas such as material design, production, and performance optimization. SEM analyses were performed with the JEOL, JSM-5300 scanning electron microscope, which belongs to the Central Research Laboratory of the Karadeniz Technical University. The samples were cut to be exposed to the electron beam. In order for images to be obtained from the samples, all the samples were coated with gold palladium under vacuum conditions. The images were taken at 10 kV and 100X magnification on a 100 μm scale.

SEM images are an important analysis that allows gaining information about the surface morphologies of the produced samples. With this analysis, it is possible to examine possible cracks on the sample surface, particle size, and similar features.

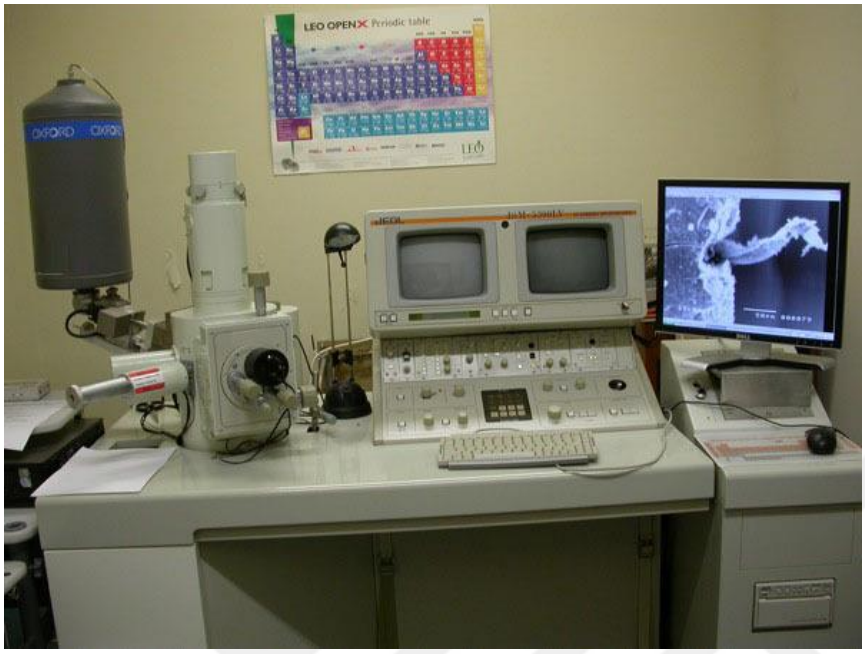



**Figure 3.9:** JEOL, JSM-5300 scanning electron microscope owned by Karadeniz Technical University

**Table 3.12:** Characteristics of a Scanning Electron Microscope

| **Features** | **Description** |
|---|---|
| Resolution | Provides high resolution at the nanometer level |
| Magnification range | Typically capable of magnifications ranging from 10x to 300,000x |
| Operating principle | Scans the surface of the specimen using electron beams |
| Types of specimens | Capable of examining solid, liquid, and gas-phase specimens |
| Surface topography | Enables detailed visualization of the specimen's surface morphology |
| Composition analysis | Can perform elemental analysis using Energy Dispersive Spectroscopy (EDS) |
| Sample preparation | Requires proper cutting and coating of specimens |
| Environmental conditions | Can operate under ultra-high vacuum (UHV) or atmospheric conditions |
| Data acquisition time | Varies typically from minutes to hours |
| Application areas | Material science, nanotechnology, biology, surface science, etc |

### 3.1.10. Thermogravimetric Analyzer (TGA)

The Thermogravimetric Analyzer (TGA) is a highly sensitive instrument utilized as one of the thermal analysis methods. Designed with the purpose of investigating thermal degradation, weight loss, and chemical changes in materials, the TGA's fundamental function is to precisely measure weight changes during the controlled heating or cooling of a sample. These measurements can be employed to ascertain alterations in sample composition, decomposition or degradation reactions, moisture content, gas emissions, and thermal stability. TGA analysis finds diverse applications in various fields such as comprehending the thermal degradation behavior of polymers, evaluating the effects of additives, and determining the composition of biological samples. This instrument plays a crucial role in advancing material science, characterizing novel materials, and enhancing industrial processes, encompassing vital realms of research. The temperature-dependent mass losses of the materials were obtained using the computer-controlled PerkinElmer Diamond thermogravimetric analysis system, which belongs to Erciyes University Nanotechnology Research Center (ERNAM) (Figure 3.10). The analyses were conducted under a nitrogen atmosphere, with a heating rate of 20 °C/min and ceramic sample crucibles within the range of 40-800 °C.



**Figure 3.10:** Perkin-Elmer, Diamond thermogravimetric analysis system owned by Erciyes University Nanotechnology research center

## 3.2. Methods

### 3.2.1. Sample production

The sample production process has been executed in a certain sequential order of stages. Initially, the traditional mold casting technique was employed, and a nanocomposite

sample was produced. In this stage, nanoscale materials were homogeneously distributed in a macro-scale structure, creating a critical basis for subsequent stages. In the second stage, nanocomposite filament production was performed using a twin-screw extruder. Thermoplastic materials were melted at a certain temperature and then cooled at a designated diameter to form a filament with the assistance of a twin-screw extruder. Twin-screw extruders have ensured the homogeneous mixing of the material and the flawless structure of the filament. Finally, sample production from the nanocomposite filament produced with the twin-screw extruder has been accomplished. This process has generally been executed using extrusion or 3D printing technologies, and the final sample was designed to have a specific geometry. These stages have been carried out in a particular sequence, and each has played a significant role in determining the final characteristics of the sample. Quality control mechanisms have been carefully implemented at every stage, and errors have been minimized. Thanks to these meticulous applications, it has been ensured that the sample obtained in the end possesses the desired features. The samples intended to have radiation shielding properties for the M series were determined to have ABS polymer matrix and nano additive ratios along with their corresponding density values as specified theoretically in Table 3.13 and 3.14.

**Table 3.13:** Percentage of nanoparticle additive and density table for M-Series polymer samples

| **Sample Code** | **ABS (%)** | **$Gd_2O_3$ (%)** | **$Er_2O_3$ (%)** | **Density ($g/cm^3$)** |
|---|---|---|---|---|
| M-ABS-0 | 100 | 0 | 0 | 1,0500 |
| M-ABS-Er5 | 95 | 0 | 5 | 1,0982 |
| M-ABS-Gd5 | 95 | 5 | 0 | 1,0971 |
| M-ABS-Er10 | 90 | 0 | 10 | 1,1511 |
| M-ABS-Gd10 | 90 | 10 | 0 | 1,1486 |
| M-ABS-Er10Gd5 | 85 | 5 | 10 | 1,2080 |
| M-ABS-Er5Gd10 | 85 | 10 | 5 | 1,2066 |
| M-ABS-Er20 | 80 | 0 | 20 | 1,2738 |
| M-ABS-Gd20 | 80 | 20 | 0 | 1,2676 |

**Table 3.14**: Percentage of nanoparticle additive and density table for P-Series polymer samples

| **Sample Code** | **ABS (%)** | **$Gd_2O_3$ (%)** | **$Er_2O_3$ (%)** | **Density ($g/cm^3$)** |
|---|---|---|---|---|
| P-ABS-0 | 100 | 0 | 0 | 1,0442 |
| P-ABS-Er5 | 95 | 0 | 5 | 1,0768 |
| P-ABS-Gd5 | 95 | 5 | 0 | 1,0756 |
| P-ABS-Er10 | 90 | 0 | 10 | 1,1289 |
| P-ABS-Gd10 | 90 | 10 | 0 | 1,1261 |
| P-ABS-Er10Gd5 | 85 | 5 | 10 | 1,1843 |

**Continuation of Table 3.14…**

| | | | | |
|---|---|---|---|---|
| P-ABS-Er5Gd10 | 85 | 10 | 5 | 1,1829 |
| P-ABS-Er20 | 80 | 0 | 20 | 1,2490 |
| P-ABS-Gd20 | 80 | 20 | 0 | 1,2428 |

### 3.2.1.1.Sample production with nano powder additive using casting type technique

Casting Type Nano Powder-Enhanced Polymer Sample Production involves the creation of samples that incorporate nano-sized powders as additives in polymer materials through the casting process. This innovative approach aims to enhance the mechanical, thermal, and electrical properties of polymers, opening up new possibilities for various applications. The production process begins with the careful selection of a polymer matrix suitable for the desired application, followed by the dispersion of nano-sized powders within the polymer matrix. The nano powders, typically metallic or ceramic in nature, are added in controlled quantities to achieve the desired material properties. The mixture is then subjected to a casting process, where it is carefully poured into a mold and allowed to solidify. The resulting nano powder-enhanced polymer samples exhibit improved strength, stiffness, thermal stability, electrical conductivity, and other desired characteristics, making them highly attractive for a range of industries such as aerospace, automotive, electronics, and biomedical. This advanced production technique paves the way for the development of next-generation polymer composites with enhanced performance and multifunctional properties, contributing to advancements in materials science and engineering.

The process of creating ABS samples in a casting type involves four separate steps, each performed with meticulous attention to detail. Each of these steps is crucial for achieving sample homogeneity, obtaining desired properties, and ensuring quality control.

1. The first step involves accurately weighing a specified amount of ABS (Acrylonitrile Butadiene Styrene) granules. It's crucial to use a precision scale in this process, as the accuracy of the specified weight will directly affect the quality of the solution to be obtained (For example, 200 mL of pure acetone will be added to 100 g of ABS granules).
2. Subsequently, the weighed ABS granules are placed into a jar that can be tightly sealed. It is vital that the jar can be tightly sealed because the lid must be completely closed to prevent evaporation of the solution during the mixing process with acetone.

3. In the next step, a specified amount of pure acetone is measured using a graduated liquid volume cylinder. Accurate measurement of the exact amount of pure acetone is necessary for the ABS to dissolve completely and homogeneously.
4. The measured acetone is then added to the jar containing the ABS granules. This mixture is left to stand for 24 hours to allow the ABS to dissolve completely in the acetone. During this time, the acetone reacts with the ABS granules to dissolve them.
5. After the waiting period, a magnetic stirrer is used to ensure homogeneity of the obtained viscous solution and to increase its consistency. The magnetic stirrer mixes the solution continuously and at a steady speed, allowing all granules to dissolve completely and the solution to mix homogeneously. This mixing operation is carried out for 15 minutes to achieve optimal results.

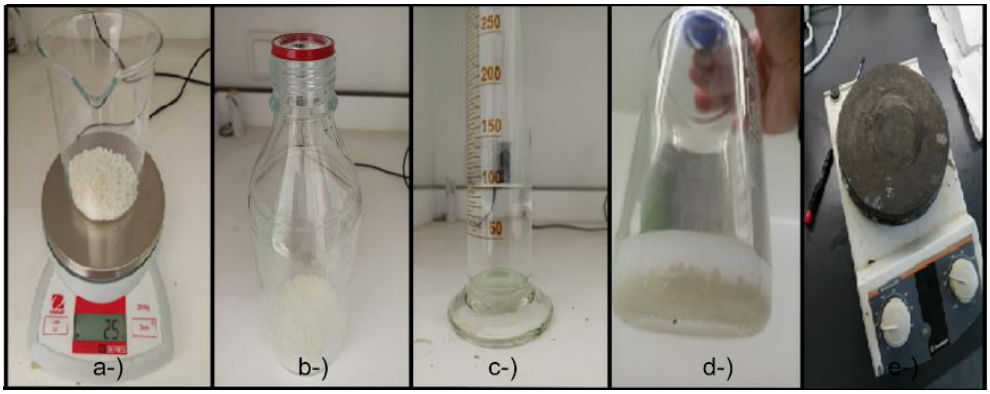



**Figure 3.11:** a-) The process involves precisely weighing a specified amount of ABS granules, b-) The weighed ABS granules are then placed in a pre-selected jar that can be tightly sealed, c-) Using a graduated liquid volume cylinder, a desired amount of pure acetone is measured, d-) The measured acetone is added to the jar containing the ABS granules and left for 24 hours to allow the ABS to dissolve completely in the acetone, e-) A magnetic stirrer is then used to increase the homogeneity and consistency of the resulting solution.

6. The nanopowders are added to the solution considering the values given in Table 3.13, mixed, and subjected to magnetic stirring for 30 minutes to evenly distribute the particles.
7. Before being poured into the molds depicted in Figure 1.2, the molds are cleaned of dust and dirt and are coated with a mold-release wax. The purpose of this procedure is to ensure easy removal of the sample from the mold.
8. The mold is then heated to 80°C, and while maintaining a stable temperature, the solution is poured into the mold. This process aids in facilitating the evaporation of the pure acetone that remains in the viscous state.

**9.** To prevent the formation of acetone bubbles, the solution is stirred until solidification is observed.

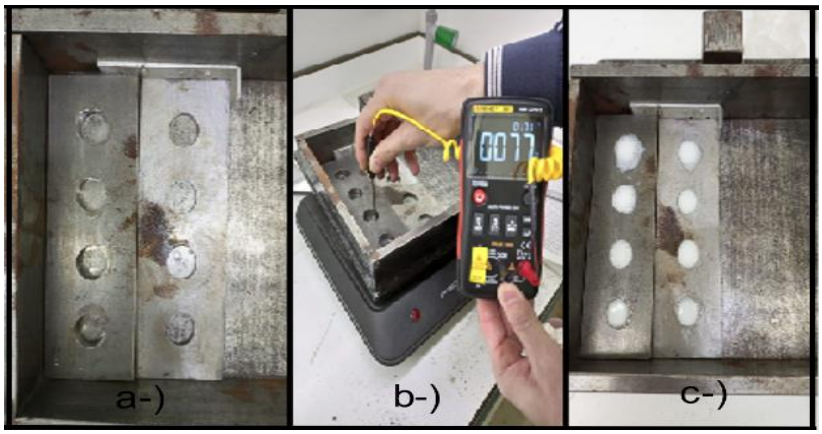



**Figure 3.12:** a-) The molds were positioned and waxed with a mold-release agent to ensure the easy removal of the samples. b-) Before initiating the casting process, the casting mold was heated until it reached the desired temperature (80°C). c-) The solution was poured into the casting mold.

**10.** Then, the dried composite will be extracted in the form of pellets with dimensions of 10 mm (thickness) x 20 mm (diameter) and 20 mm (thickness) x 20 mm (diameter), and to ensure no residual solvent is left, it underwent a drying process in an extra drying oven at 80 °C. The final form of the samples is provided in Figure 3.13




**Figure 3.13:** Samples of casting type composite specimens enhanced with nano-powder additives; 1) M-ABS-0 (0% Additive), 2) M-ABS-Er5 (5% Additive), 3) M-ABS-Er10 (10% Additive), 4) M-ABS-Er20 (20% Additive), 5) M-ABS-Er5Gd10 (5%, 10% Additive), 6) M-ABS-Gd5 (5% Additive), 7) M-ABS-Gd10 (10% Additive), 8) M-ABS-Gd20 (20% Additive), 9) M-ABS-Er10Gd5 (10%, 5% Additive)

### 3.2.1.2. Filament production with twin-screw extrusion incorporating nanoparticles

In order to achieve both the benefits of nanotoxicity reduction and time savings, a dilution method was employed for the production of ABS filament with additives. Granules were initially produced with a composition of 80% polymer and 20% nanotoxicant for each relevant parameter. Subsequently, these granules were diluted with additional polymer reinforcement to achieve dilutions of 10% and then 5%, before being transformed into filament form. This process allowed each filament product to be blended with a dual mixture, ensuring a homogeneous mixture within the structure.

1. Measurement of granule size
2. Measurement of additive added to the granule
3. Combination of granule and nanoparticles for twin-screw extrusion
4. Conversion of granule into filament form
5. Recycling of granule through a hammer mill grinder to enhance filament homogeneity
6. Extrusion of nanoparticle-enhanced granule
7. Conversion of granule back into filament form
8. Obtaining filament windings

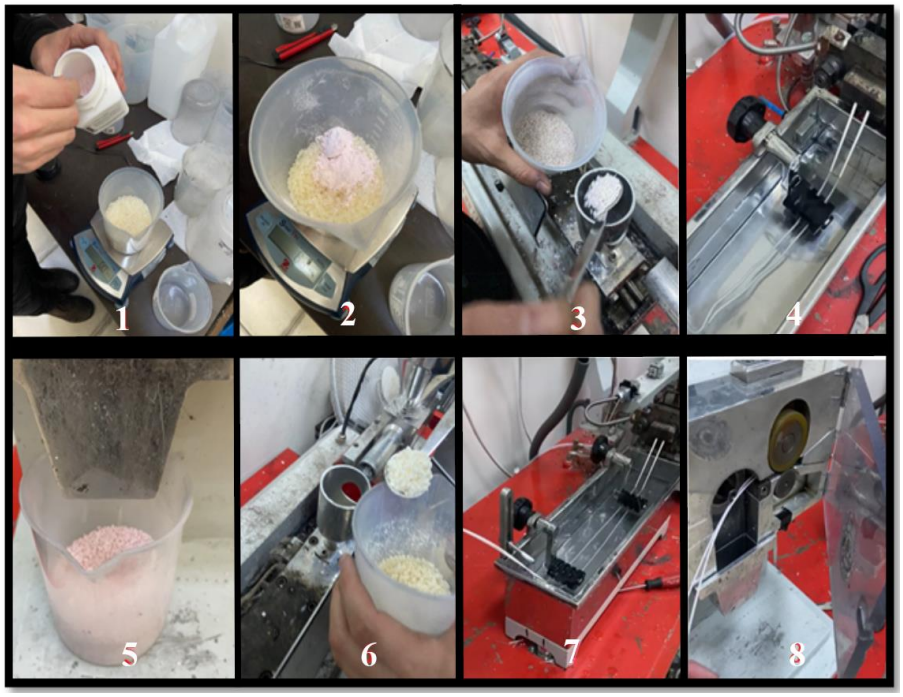



**Figure 3.14 :** 1) Measurement of granule size, 2) Measurement of additive added to the granule, 3) Combination of granule and nanoparticles for twin-screw extrusion 4) Conversion of granule

into filament form 5) Recycling of granule through a hammer mill grinder to enhance filament homogeneity 6) Extrusion of nanoparticle-enhanced granule 7) Conversion of granule back into filament form 8) Obtaining filament windings

As a result, the obtained filament outputs have a diameter range that varies approximately between 1.55mm and 1.98mm. The visual representations of the obtained filament samples are provided in Figure 3.12.

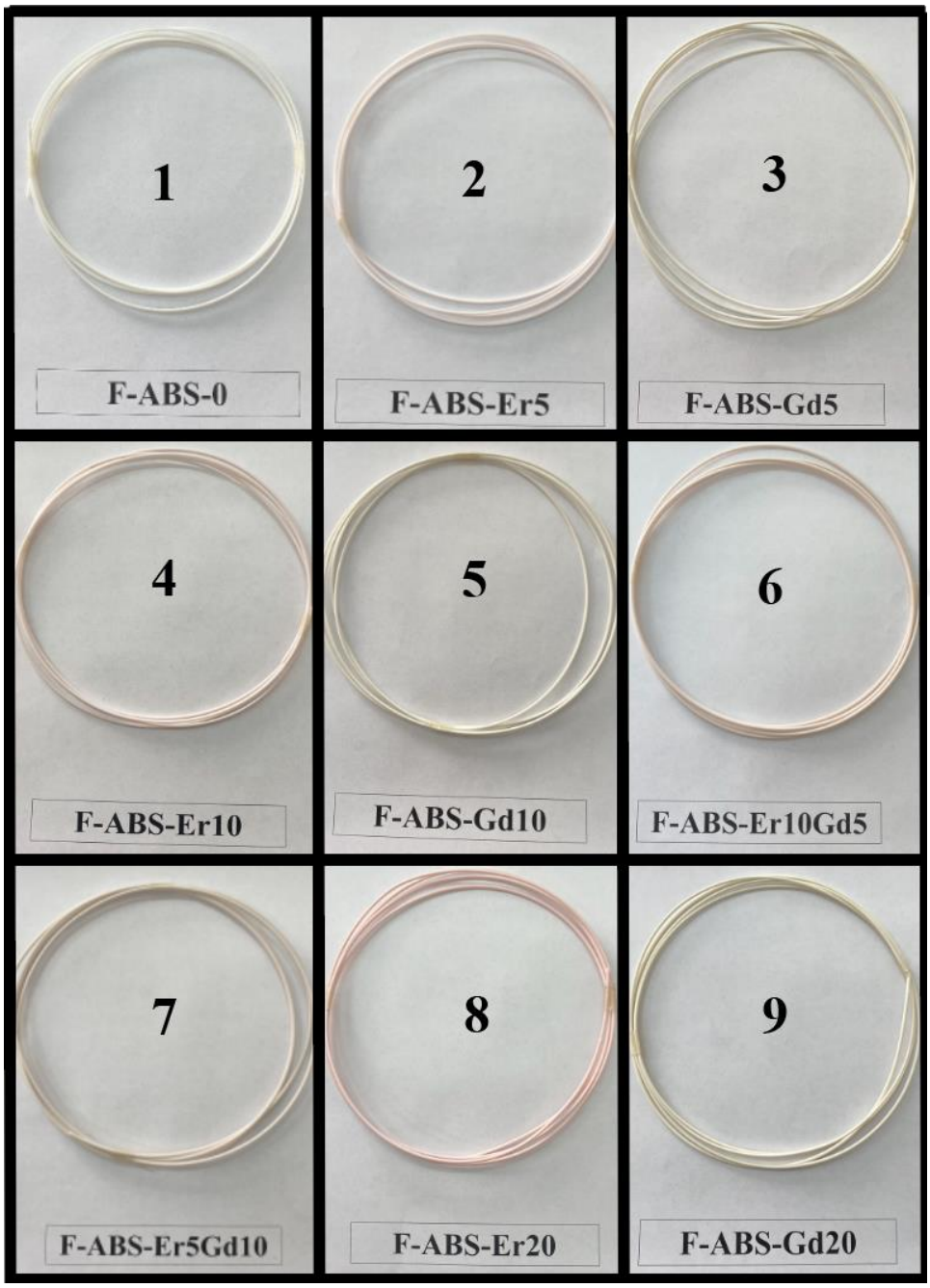



**Figure 3.15 :** Samples of F-series filament specimens enhanced with nano-powder additives; 1) F-ABS-0 (0% Additive), 2) F-ABS-Er5 (5% Additive), 3) F-ABS-Gd5 (5% Additive), 4) F-ABS-Er10 (10% Additive), 5) F-ABS-Gd10 (10% Additive), 6) F-ABS-Er10Gd5 (10%, 5%

Additive), 7) F-ABS-Er5Gd10 (5%, 10% Additive), 8) F-ABS-Er20 (20% Additive), 9) F-ABS-Gd20 (20% Additive)

#### 3.2.1.3. Sample production from nanocomposite filament with 3D printing technique.

ABS filaments with added nanoparticles were produced using a twin-screw extruder, and then samples were fabricated using a creality CR-10 Smart Pro 3D Direct Drive printer owned by Erciyes University anotechnology Application and Research Center (Kayseri, Turkey).

This printer model enables the adjustment of temperature and filament thickness settings for various materials such as 1.75mm/ABS/TPU/PETG/PLA/Carbon fiber to achieve desired sample outputs. The choice of this printer is attributed to its steel hotend component, which facilitates the smooth printing of filament blends containing different additives. The samples were printed with a 100% fill ratio on a 3D printer. An object or sample with a 100% fill ratio is often challenging or impractical to achieve through 3D printing. The reason behind this is that 3D printing involves adding material in layers to create an object, and ensuring that there are no gaps or air pockets between these layers can be extremely difficult. In practice, several factors, including the flowability of the material, printing parameters, and design considerations, can lead to the formation of some voids or air bubbles within the object during the 3D printing process.



**Figure 3.16 :** The Creality CR-10 Smart Pro 3D Direct Drive printer

The final form of the samples is provided in Figure 3.18

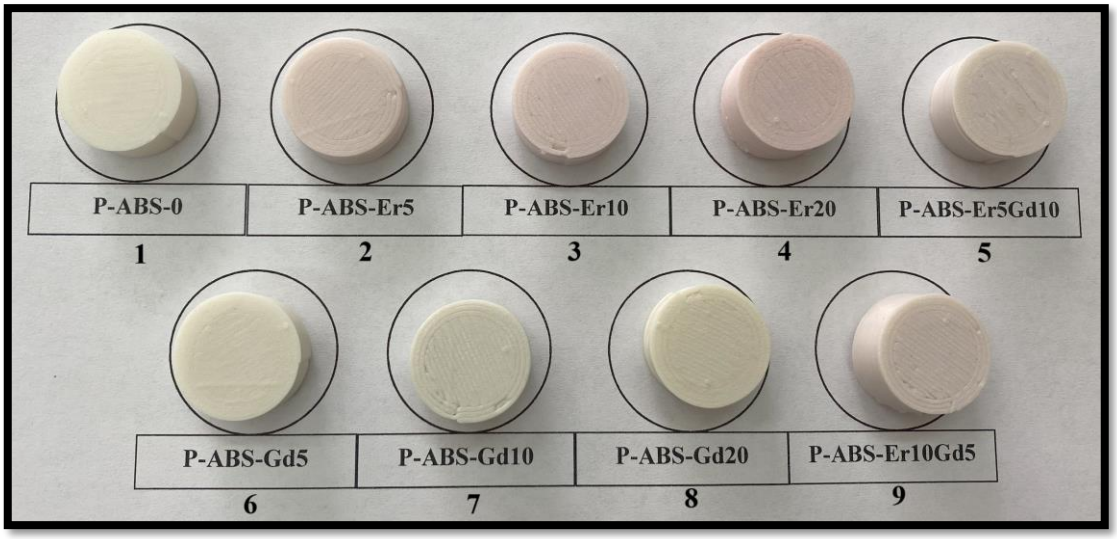



**Figure 3.17:** Samples of casting type composite specimens enhanced with nano-powder additives; 1) P-ABS-0 (0% Additive), 2) P-ABS-Er5 (5% Additive), 3) P-ABS-Er10 (10% Additive), 4) P-ABS-Er20 (20% Additive), 5) P-ABS-Er5Gd10 (5%, 10% Additive), 6) P-ABS-Gd5 (5% Additive), 7) P-ABS-Gd10 (10% Additive), 8) P-ABS-Gd20 (20% Additive), 9) P-ABS-Er10Gd5 (10%, 5% Additive)

### 3.2.2. Sample density measurement

The density of the obtained sample was determined using the Archimedes method. In this method, the sample was first weighed using a precise scale. Then, the sample was immersed in a liquid, and the amount of liquid displaced by the sample was measured. According to the Archimedes principle, the sample applies a force on the liquid, resulting in a displacement. The amount of liquid displaced determines the sample's volume, which is used for density calculation. To determine the density of the sample, the known density of a reference liquid (such as water) was used. Taking into account the displacement of the sample and the density of the reference liquid, the density of the sample was calculated. The density data obtained through this method were subjected to statistical analysis, and the results demonstrated high accuracy and repeatability.



**Figure 3.18 :** The Archimedes Density Kit

The experimental densities obtained for the M-Series and P-Series are provided in Table 3.15.

**Table 3.15 :** The experimental densities obtained for the M-Series and P-Series using the Archimedes method

| **Sample** | **Density of the M (Molded)-Series (g/cm$^3$)** | **Density of the P (Printed)-Series (g/cm$^3$)** |
|---|---|---|
| ABS-0 | 1,0500 | 1,0442 |
| ABS-Er5 | 1,0982 | 1,0768 |
| ABS-Gd5 | 1,0971 | 1,0756 |
| ABS-Er10 | 1,1511 | 1,1289 |
| ABS-Gd10 | 1,1486 | 1,1261 |
| ABS-Er10Gd5 | 1,2080 | 1,1843 |
| ABS-Er5Gd10 | 1,2066 | 1,1829 |
| ABS-Er20 | 1,2738 | 1,2490 |
| ABS-Gd20 | 1,2676 | 1,2428 |

When examining the relative difference between the M-Series and P-Series, a maximum difference of 1,95 is observed between the values.

### 3.2.3. Structural analysis

Thus far in this study, we have investigated the integration and distribution of erbium oxide ($Er_2O_3$) and gadolinium oxide ($Gd_2O_3$) nanoparticles into the ABS (Acrylonitrile Butadiene Styrene) plastic matrix. Initially, erbium oxide and gadolinium oxide nanoparticles were mixed into the ABS matrix at predetermined proportions (%5, %10, and %20). Samples at these ratios were prepared and produced using two distinct production processes. In the first method, we employed the casting mold technique. A sol-gel process was utilized to prepare a mixture of ABS and nanoparticles at the specified ratios. The mixture was then poured into a casting mold and solidified. In the second method, we utilized the extrusion process. Based on the specified ratios of ABS and nanoparticles, an additive filament was produced. This filament was then converted into a sample in a predetermined format using a 3D printer. All prepared samples were imaged using a Scanning Electron Microscope (SEM). This technique was employed to determine the extent of homogeneous distribution of the nanoparticles within the ABS matrix. Additionally, we conducted elemental mapping using Energy Dispersive Spectroscopy (EDS). These analyses were used to ascertain the exact position and distribution of the nanoparticles within the ABS matrix. Thus, we were able to determine the effectiveness of nanoparticle integration into the ABS matrix and understand the impact of this integration on the overall properties of the samples. The backscattered electron (BSE) method has been used to image samples. Back-scattered electrons are reflected back from the samples, and most electrons do not lose their energy on the specimen surface. Therefore, it is assumed that BSEs make elastic interactions with specimens. Secondary electrons originate from the surface of the specimens. Hence, it is interpreted that SEs are derived from inelastic interactions. The SEM analyses were carried out using a scanning JEOL, JSM-5300 electron microscope, and the samples were cut to be exposed to the electron beam. In order to obtain microscopic images of the samples, each sample was subjected to a coating process with a gold-palladium alloy in a vacuum environment. The imaging process was carried out under an accelerating voltage of 10 kilovolts (kV), using a 100X objective magnification and displaying the images at a scale of 100 micrometers (μm). SEM imaging is a crucial analysis that provides information about the surface morphologies of the produced samples. With this analysis, it is possible to examine features such as potential cracks on the sample surface and particle size.

### 3.2.4. Thermal analysis

Thus far in this study, Many types of plastics offer high thermal resistance properties, making them suitable for use in high-temperature environments or conditions where frequent temperature fluctuations occur. Particularly, thermoplastics can have higher thermal resistance compared to thermosets, and as a result, they are widely preferred in industries such as automotive, aerospace, electronics, and medical devices. Strong thermal resistance enhances the durability of plastic materials, ensuring long lifespan and consistent performance. Thanks to these attributes, plastics are considered a significant option for designing and producing critical components with wide-ranging applications in modern industries. ABS (Acrylonitrile Butadiene Styrene) is a significant plastic material that offers excellent thermal resistance properties. Its high temperature stability enables successful application in various fields. The thermal resistance of this material provides a valuable advantage, particularly in meeting the demands of industrial and commercial sectors. ABS plastics can be used across a wide range of applications, from automotive components to medical devices. Moreover, ABS's exceptional processability and durability enhance product longevity while ensuring consistent performance. Therefore, the thermal resistance of ABS plastics stands out as a reliable and effective option in industrial design and manufacturing processes. Thermal analysis consists of two separate analytical methods. Firstly, utilizing a drying oven and precision scale belonging to Sinop University's Scientific and Technological Research Application and Research Center, mass changes occurring in relation to temperature were analyzed for each sample of nanopowder-modified polymer produced through M-series and P-series manufacturing. These analyses were carried out by subjecting the samples to fixed temperatures of 120°C, 140°C, 160°C, 180°C, 200°C, and 220°C, holding them at each temperature level for 10 minutes. The masses of the samples not exposed to these temperature levels were examined by comparing them with the mass changes of the samples held at the respective temperatures. The evaluation of the study was initiated considering the typical average bed temperature of 110°C for 3D printers. Taking into account the information that the material of the samples, ABS, has a melting temperature range of 210-250°C, the highest temperature level was determined as 220°C. In the second phase, samples from the P-series, including previously untreated P-ABS-0, P-ABS-Er20, and P-ABS-Gd20 samples determined to exhibit the highest radiation shielding performance based on theoretical and experimental results, were subjected to

thermal analysis through the Thermogravimetric Analysis (TGA) device at Erciyes University Nanotechnology Research Center (ERNAM) through a service provision. Time- and temperature-dependent (25-650°C) mass loss percentages were analyzed to interpret material characterization in greater detail and at higher temperatures. This additional analysis allows for a more comprehensive interpretation of material characterization across an extended temperature range.

### 3.2.5. Radiation shielding analysis

#### 3.2.5.1. Gamma radiation shielding analysis

These produced samples, fortified with nano-oxide compounds, were tested with various radioactive point sources ($^{241}$Am (59,5 keV), $^{133}$Ba (80,9, 276,3, 302,8, 356,0 ve 383,8 keV), $^{22}$Na (511,0 and 1274,5 keV), $^{137}$Cs (661,6 keV), ve $^{60}$Co (1173,2 and 1332,5 keV)) using experimental (HPGe detector system), theoretical (XCOM, EpiXS), and simulation (FLUKA, GEANT4) methods to determine their gamma radiation attenuation capabilities. The theoretical atomic percentage table for pure and nanopowder additive-incorporated samples for theoretical and simulation gamma and neutron radiation shielding analyses is given in Table 3.16. This table is applicable to both the M series and the P series, as the only difference between the two structures stems from the void ratio coefficient in material production.

**Table 3.16 :** Element Distribution Table by Weight Percentage

| Sample | C (%) | H (%) | O (%) | N (%) | Er (%) | Gd (%) |
|---|---|---|---|---|---|---|
| ABS-0 | 85,2623 | 8,1091 | 0,0000 | 6,6286 | 0,0000 | 0,0000 |
| ABS-Er5 | 80,9992 | 7,7036 | 0,6274 | 6,2972 | 4,3726 | 0,0000 |
| ABS-Gd5 | 80,9992 | 7,7036 | 0,6622 | 6,2972 | 0,0000 | 4,338 |
| ABS-Er10 | 76,7361 | 7,2982 | 1,2548 | 5,9657 | 8,7452 | 0,0000 |
| ABS-Gd10 | 76,7361 | 7,2982 | 1,3241 | 5,9657 | 0,0000 | 8,6759 |
| ABS-Er10Gd5 | 72,4732 | 6,8927 | 1,9168 | 5,6343 | 8,7452 | 4,338 |
| ABS-Er5Gd10 | 72,4732 | 6,8927 | 1,9515 | 5,6343 | 4,3726 | 8,6759 |
| ABS-Er20 | 68,2098 | 6,4873 | 2,5096 | 5,3029 | 17,4904 | 0,0000 |
| ABS-Gd20 | 68,2098 | 6,4873 | 2,6482 | 5,3029 | 0,0000 | 17,3518 |

##### 3.2.5.1.1. High-purity germanium detectors (HPGe) analysis

High-purity germanium detectors (HPGe) are ideal tools for gamma spectroscopy and are commonly used for the detection of radioactive materials. They derive their name from the high-purity (typically 99,999% or higher) germanium crystals they are made of.

These detectors provide remarkable sensitivity and energy resolution, allowing for the determination of the energies of incoming gamma rays. The operating principle involves the interaction of gamma rays with the germanium atoms in the detector, causing the energy levels of electrons to rise. As the electrons transition to lower energy levels, this energy difference is detected as an electrical signal, which corresponds to the energy of the gamma ray. However, the high performance of HPGe detectors comes with certain requirements that make their use somewhat challenging. These include operating at very low temperatures (typically around the temperature of liquid nitrogen) and the difficulty of decontaminating the detectors from radioactive impurities. High-purity germanium detectors (HPGe) from Kastamonu University Scientific and Technological Research Application and Research Center have been selected for radiation shielding tests.




**Figure 3.19:** HPGe detector owned by Kastamonu University Scientific and Technological Research Application and Research Center

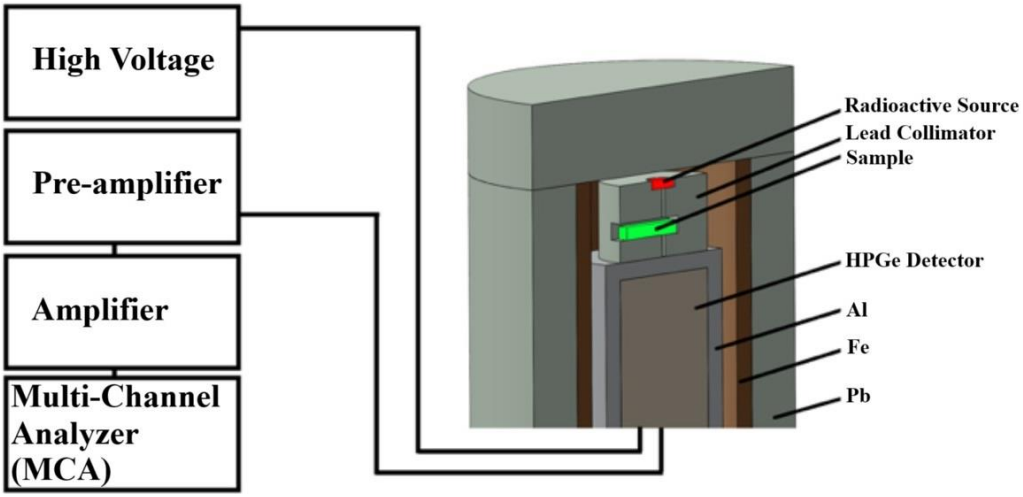



**Figure 3.20:** Cross-sectional view of the HPGe detector

**Table 3.17:** Technical specifications for HPGe

| **Technical Specifications** | **Value** |
|---|---|
| Brand | ORTEC |
| Model | GEM40P4-83 |
| Range | 40 keV - 10 MeV |
| Efficiency | 40% |
| Resolution | 1,85 KeV / 1,33 MeV ($^{60}$Co – FWHM) |

While conducting the radiation shielding material test using an HPGe detector, the following steps were followed to obtain the linear attenuation coefficient (μ):

**1)** The radiation shielding material to be tested was properly prepared and placed inside the detector.

**2)** Radioactive sources with specific energies ($^{241}$Am (59,5 keV), $^{133}$Ba (80,9, 276,3, 302,8, 356,0 and 383,8 keV), $^{22}$Na (511,0 and 1274,5 keV), $^{137}$Cs (661,6 keV), ve $^{60}$Co (1173,2 and 1332,5 keV)) were used to measure the gamma rays passing through the radiation shielding material. These sources emit gamma rays with various energies within the tested energy range.

**3)** The HPGe detector was positioned behind the material, and the energies of the detected gamma rays were recorded.

**4)** Using the recorded energies of the detected gamma rays and the corresponding output signals from the detector, an energy-output curve was established. This curve represents the relationship between the detector's output and the incoming gamma ray energies.

**5)** The linear attenuation coefficient (μ) was calculated using the energy-output curve.

This method is commonly used to experimentally determine the linear attenuation coefficient (μ) in radiation shielding material tests. In accordance with the Beer-Lambert law formula mentioned in Section 2.9.4, measurements will be conducted on the gamma spectrometer both with and without a sample for 1000 seconds to obtain the I and $I_0$ values. To yield more precise results, these measurements will be repeated three times. The resulting spectra will be analyzed using the MAESTRO and Microcal Origin programs, and the experimental gamma shielding parameters will be determined.

#### 3.2.5.1.2. WinXCom analysis

WinXCOM is a database developed by NIST (National Institute of Standards and Technology) that models the interactions between photons (X-rays and gamma rays) and materials. WinXCOM operates over an energy range of 1 keV to 100 GeV and allows users to adjust parameters such as photon energy, material composition, and density. WinXCOM is used to calculate mass attenuation coefficients and energy absorption coefficients, which are critical in radiation shielding design. WinXCOM is based on various theoretical models and experimental data. For instance, it utilizes the Klein-Nishina formula for photon scattering calculations, Scofield's cross-section calculations for the photoelectric effect, and the Bethe-Heitler theory for pair production. WinXCOM employs elemental cross-section data and sometimes complex number theory in making these calculations. Scientists and engineers can use WinXCOM in areas such as radiation protection, medical imaging, material analysis, and nuclear power plant design. WinXCOM also offers an API (Application Programming Interface) that can be accessed through a web-based interface and integrated with programming languages. The mass attenuation coefficient characterizes how a material attenuates the intensity of a photon or X-ray beam as it passes through the material. The method for calculating the mass attenuation coefficient using WinXCOM is described below:

**1)** Accessing the WinXCOM Website: The WinXCOM National Institute of Standards and Technology (NIST) website can be accessed to perform the calculations.

**2)** Selecting the Material: Once on the WinXCOM page, you can select the material for which you want to calculate the mass attenuation coefficient. You can choose elements, compounds, or mixtures.

**3)** Selecting the Energy Range: Enter the energy range for which you want to calculate the mass attenuation coefficients (e.g., entering an energy range between 59.5 keV and 1332.5 keV).

**4)** Submit the Form: After selecting the material and entering the energy range, submit the form. WinXCOM will perform the calculations and display the mass attenuation coefficients.

**5)** Interpreting the Results: Examine the presented data. Mass attenuation coefficients are usually given in units of $cm^2/g$. The output data can usually be downloaded in various formats and used for further analysis.

WinXCOM provides theoretical values based on established physical models. In practical applications, there may be some differences between the theoretical values and experimental measurements.

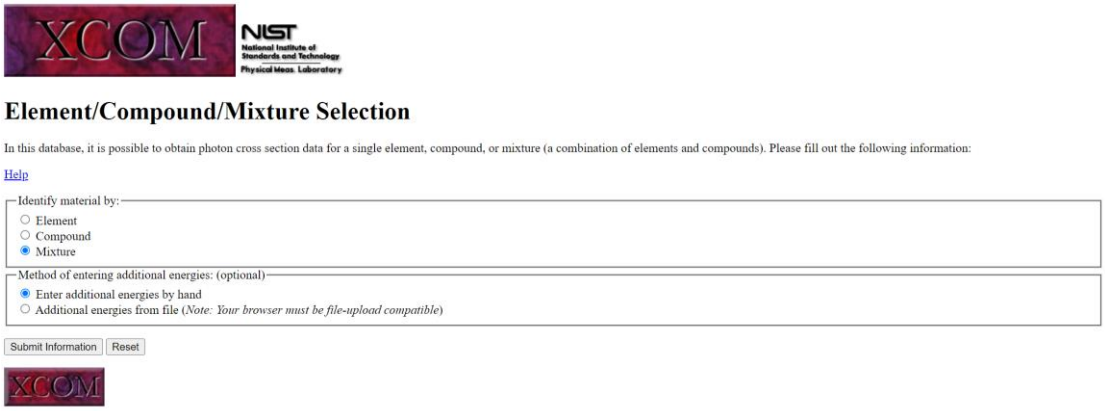



**Figure 3.21 :** WinXCOM user interface page

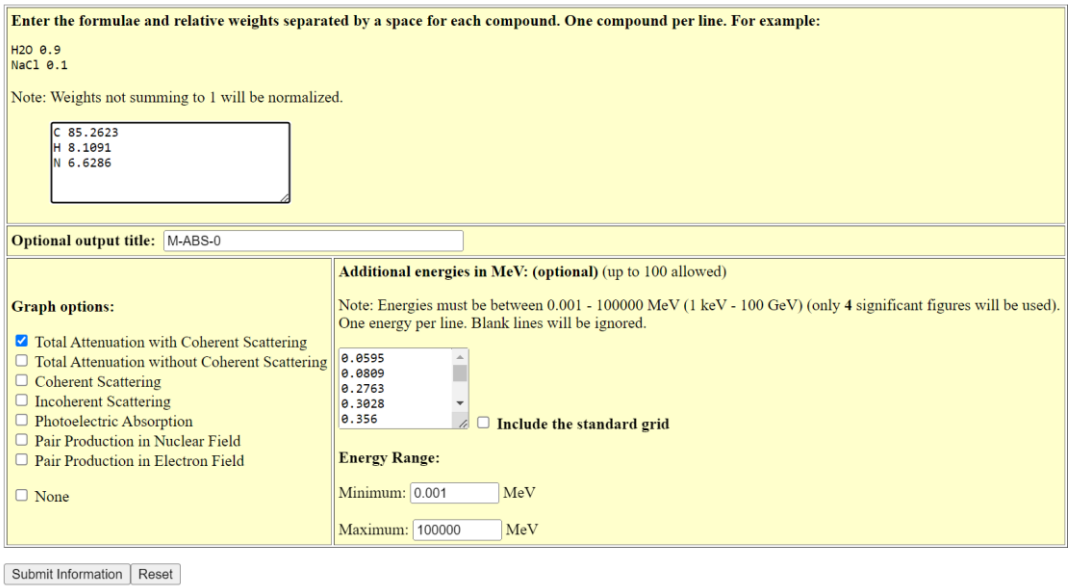



**Figure 3.22 :** WinXCOM material content identification interface

#### 3.2.5.1.3. EpiXS analysis

EpiXS is a Windows-based program for photon attenuation, dosimetry, and shielding calculations. It is designed to assist physicists and engineers in determining the interaction of photons with different materials, which is important for applications such as radiation protection, medical imaging, and materials analysis. One key input for EpiXS is the energy range, which specifies the range of photon energies for which the calculations are performed. This is crucial because the interaction of photons with matter significantly varies with energy. Typical energy ranges can vary from a few keV (kilo-electron volts) to several MeV (mega-electron volts), depending on the application. EpiXS likely utilizes established libraries of cross-sectional data for photon interactions with matter. One such library used is EPICS2017 (ENDF/B-VIII) and EPDL97 (ENDF/B-VI.8) databases, which provide photon interaction cross sections for a wide range of elements and compounds. By utilizing such libraries, EpiXS can provide accurate and reliable calculations for various materials and photon energies.

To calculate the linear attenuation coefficient and mass attenuation coefficient, the following steps are followed:

**1)** Opening the Program: Open the EpiXS program.

**2)** Material Selection: In the program's interface, select the material for which you want to make the calculation. This can be elements, compounds, or mixtures.

**3)** Energy Range Determination: Enter the energy range of the photons. The energy range allows for the calculation of the attenuation coefficient at different energies.

**4)** Calculation Type Selection: Select either the linear attenuation coefficient or the mass attenuation coefficient from the options.

**5)** Starting the Calculation: Click the relevant button or enter the command to start the calculation. The program will calculate the attenuation coefficient for the selected material and energy range.

**6)** Reviewing the Results: Once the calculations are complete, review the results

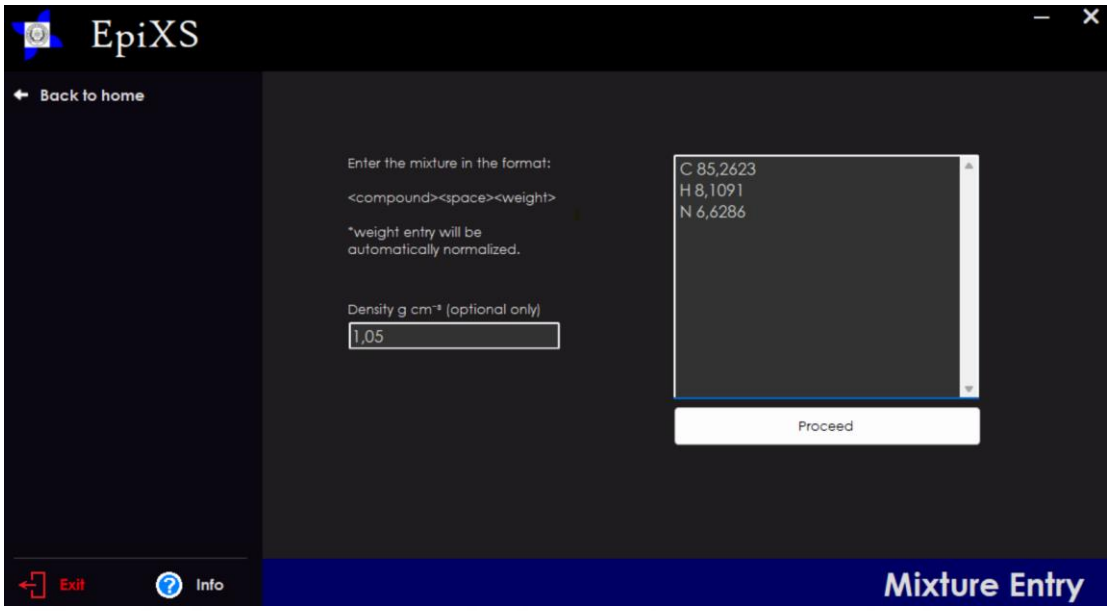



**Figure 3.23 :** EpiXS user interface page

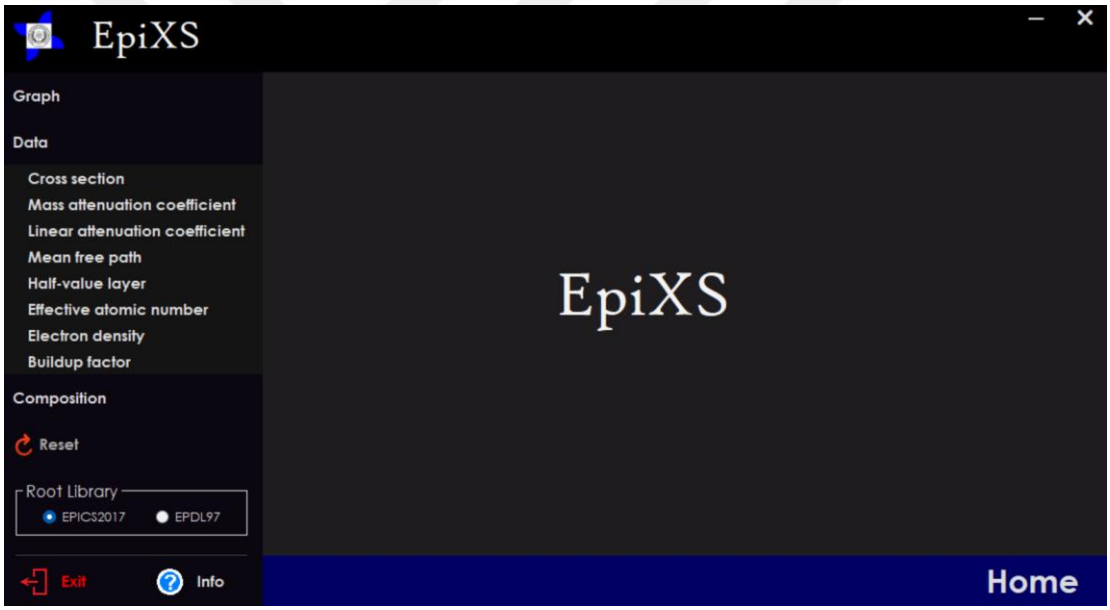



**Figure 3.24 :** EpiXS material content identification interface

### 3.2.5.1.3. GEANT4 (gamma) analysis

GEANT4 is a comprehensive C++ library developed for high-energy physics simulations, and it is also used in various fields such as radiation shielding, medical physics, and space engineering. In radiation shielding studies related to gamma photons, the "G4EmStandardPhysics_option4" (Testem13) model of GEANT4's "electromagnetic" package allows for detailed and accurate simulation of photon-matter interactions. This package covers photon interaction processes such as photoelectric effect, Compton scat-

tering, and pair production. In this model, evaluated data libraries such as ENDF (Evaluated Nuclear Data File) and EPDL (Evaluated Photon Data Library) are utilized for photon cross-section data, ensuring high reliability and accuracy in calculations. This feature of GEANT4 enables researchers who want to analyze the distribution of physical quantities within materials, such as energy spectra, angular distributions, and energy depositions. Furthermore, using Monte Carlo methods in GEANT4, it is possible to investigate radiation shielding performance for complex geometries and different material combinations. This is particularly critical for understanding and optimizing the interaction of high-energy gamma photons with complex structures and materials. The modular structure of GEANT4 allows researchers to customize photon interaction mechanisms and material responses, facilitating detailed analysis. GEANT4 uses various libraries and models to ensure accurate simulation of different interactions, providing values for cross-sections, energy losses, and other physical quantities. Some of the libraries used by GEANT4 include:

- G4NDL (GEANT4 Neutron Data Library): Evaluated data library for neutron interactions. It is used to model thermal and fast neutron interactions.
- G4EMLOW (Low Energy Electromagnetic Physics): Contains data sets for low-energy electromagnetic interactions involving photons, electrons, and positrons.
- G4PhotonEvaporation and G4RadioactiveDecay: Used to model atomic nucleus decay processes and gamma emissions.
- G4SAIDDATA: Data library used for modeling elastic scattering interactions.
- G4ABLA: Used for heavy ion and nuclear decay processes.
- G4PII: Data library for ionization and excitation processes.
- G4RealSurface: Data library used for modeling surface interactions.
- G4ENSDFSTATE (Evaluated Nuclear Structure Data File): Contains nuclear structure data.

These libraries and data sets are integrated within GEANT4 to model and simulate various physical processes. Furthermore, GEANT4 allows users to integrate their own data and models, making it a flexible and customizable simulation tool.

In this study, the GEANT4 simulation software was carefully installed on the Linux operating system to establish the foundation of a complex simulation environment. After the installation, GEANT4 was meticulously configured to recognize the components of the examined examples, which includes identifying both the natural elements of the

samples and those to be integrated. The focus of the study was on hadronic interactions, for which the "electromagnetic/TestEm13" package within GEANT4 was used. This package is particularly capable of simulating photon interactions and provides in-depth information crucial for understanding the passage of radiation through materials, which is important for understanding the shielding capabilities of materials.For material definitions, the "DetectorConstruction.cc" file located in the "electromagnetic/TestEm13/src" directory plays a central role. This file is of key importance for the simulation environment to recognize the compositions of materials.The specific path to this file is "geant4.10.07.p02-install/share/Geant4-10.7.2/examples/extended/ electromagnetic/TestEm13/src/DetectorConstruction.cc". Once accessed, a meticulous process was carried out to define both the naturally occurring elements in the materials used in this research and the synthesized composites for this study. By utilizing the GEANT4 simulation environment, carefully configuring it with the necessary material definitions, and using the "electromagnetic/TestEm13" package, this study is well-prepared to provide an in-depth analysis of the shielding properties of materials against gamma radiation. This is essential for the development of new materials with enhanced shielding capabilities. To work with gamma rays using the GEANT4 simulation tool on the electromagnetic/TestEm13 example, the following steps are followed:

- Setting Environment Variables: Configure the necessary environment variables for GEANT4 to function. This includes setting directory paths where GEANT4 is installed and other required settings.
- Example Utilization: Navigate to the examples/extended/electromagnetic/TestEm13 folder in the directory where GEANT4 is installed. This example is used for simulating electromagnetic interactions, particularly with gamma rays.
- Compiling the Code: In this folder, use tools such as CMake and make to compile the code. Typically, this involves creating a build directory and then generating configuration files with CMake.
- Setting Simulation Parameters: Before running the TestEm13 example, examine the source code and set the required simulation parameters. These may include parameters such as photon energy, type of material, and geometry to be used for the simulation.
- Starting the Simulation: Run the compiled application. This triggers the execution of the simulation and generates outputs.

- Evaluating Results: Once the simulation is complete, examine the generated outputs. These could be in the form of data files or visualized geometry.Analysis and Reporting: Analyze the obtained data and report the results in an appropriate format.

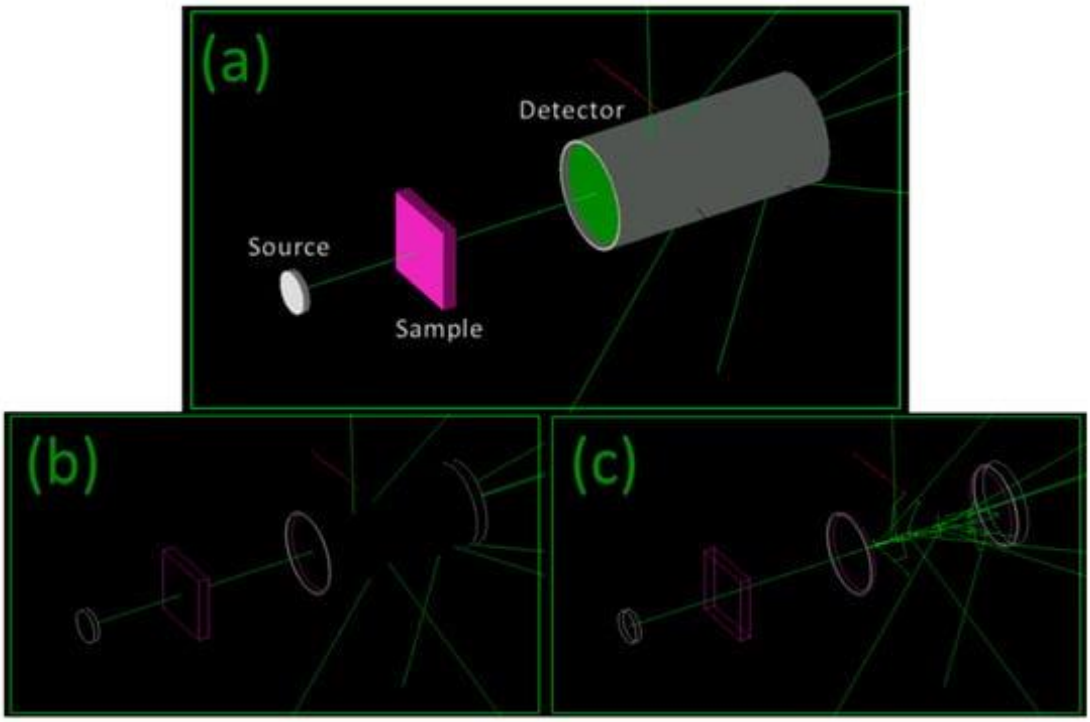



**Figure 3.25 :** Geant4 visualization of the developed code. (a) Solid surface view, (b) wire frame view, (c) hidden edges view.

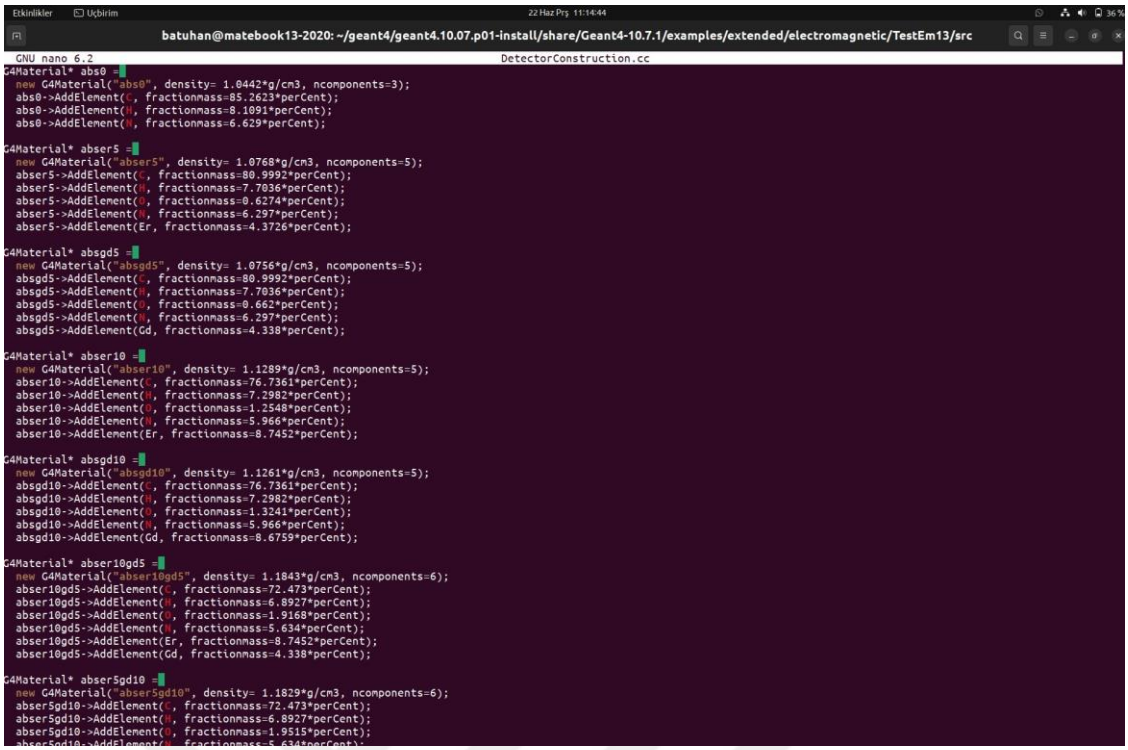



**Figure 3.26 :** Nanopowder-additive and non-additive samples defined in the GEANT4 terminal interface

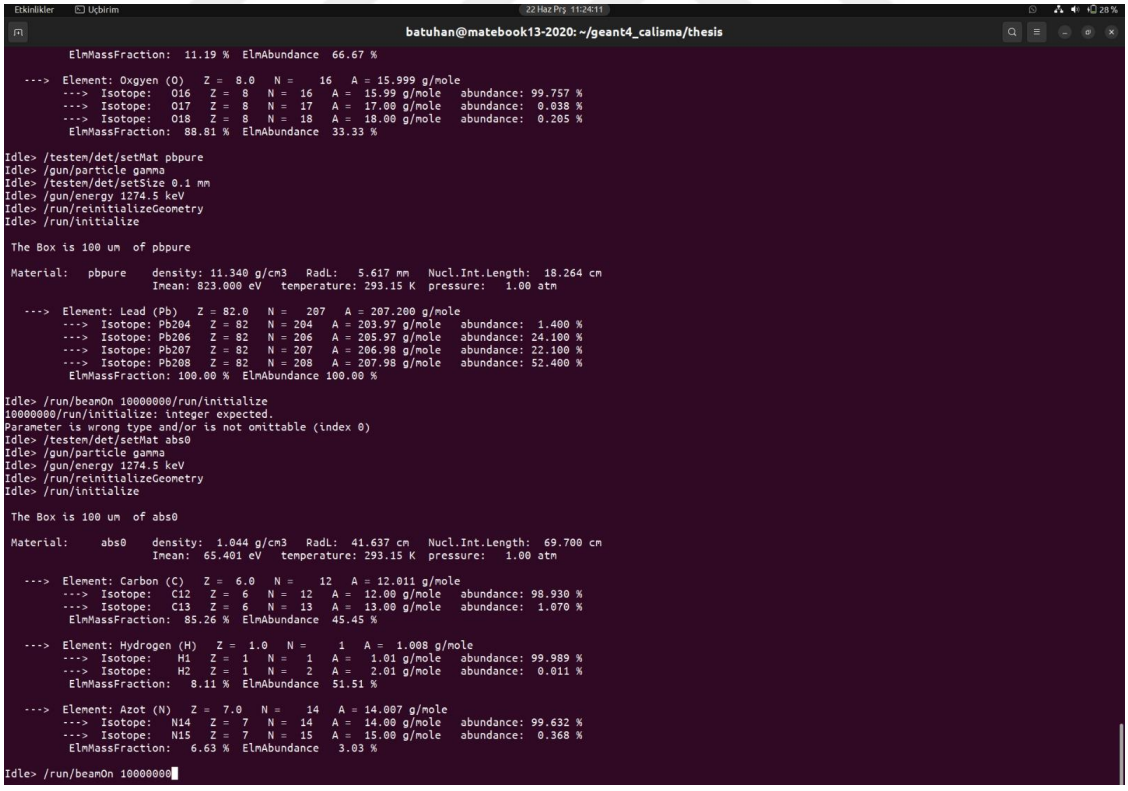



**Figure 3.27 :** Command and parameters for starting the GEANT4 simulation program

The experimental setup has been modeled to work with a point-like radiation source ($^{241}$Am (59,5 keV), $^{133}$Ba (80,9, 276,3, 302,8, 356,0 and 383,8 keV), $^{22}$Na (511,0 and 1274,5 keV), $^{137}$Cs (661,6 keV), ve $^{60}$Co (1173,2 and 1332,5 keV)), and the physical and chemical properties of the selected samples have been integrated into this modeling process. A total of 10,000,000 gamma photons have been bombarded onto each sample. The Geant4 platform will provide outputs based on the data obtained from this experiment, including parameters such as mass attenuation coefficient, number of gamma rays passing through the sample, and linear attenuation coefficient. The results obtained from this study have been compared with experimental data and theoretical findings available in the literature to assess the reliability and validity of the results.

#### 3.2.5.1.4. FLUKA (gamma) analysis

FLUKA is a simulation program that works on the Monte Carlo principle to calculate particle interactions with matter. It is written in the Fortran programming language and is used on the Linux operating system. FLUKA was initially developed by J. Rant and H. Geibel in 1962 for shielding design in hadron accelerators. Its first generation was developed between 1962 and 1978. A. Ferrari and A. Fassó are currently working on expanding the energy range of particles in the FLUKA program. FLUKA finds applications in various fields such as accelerator shielding design, accelerator-driven systems, activation studies, cosmic rays, and many others. The program considers interactions such as hadron-hadron, hadron-nucleus, nucleus-nucleus, electromagnetic-muon, and neutrino interactions. Additionally, FLUKA calculates particle transport in magnetic fields, Boolean and Voxel geometries, and provides detailed neutron transport and interaction calculations (Böhlen et al., 2014). In radiation shielding studies, particularly for gamma photons, FLUKA (FLUktuierende KAskade) is an invaluable tool with its extensive capabilities in particle interactions and transport. Originating from high-energy physics, FLUKA has evolved into a versatile Monte Carlo simulation package for various applications, including radiation shielding. Considering gamma photon interactions, it is essential to take into account various physical processes such as photoelectric absorption, Compton scattering, and pair production. FLUKA's comprehensive libraries and models address these interactions accurately, incorporating updated cross-section data. In a typical radiation shielding study performed using FLUKA, the user defines the problem geometry, which may include materials used in shielding and the

source of gamma photons. Through the simulation, controlled by parameters adjustable by the user, a detailed tracking of gamma photons is performed. Moreover, FLUKA offers scoring features that facilitate the acquisition of relevant information such as energy deposition or flux. For the assessment of the shielding material's effectiveness, recording the attenuated gamma radiation is fundamental. FLUKA operates in a broad energy range from 1 keV to 1000 TeV, making it particularly useful for gamma photons. Finally, through robust post-processing and data analysis tools, the simulated data can be meticulously analyzed to evaluate the shielding capabilities of materials for gamma photons. This method offers researchers the opportunity to optimize shielding configurations and materials, contributing to the safer handling and management of ionizing radiations. FLUKA is a comprehensive Monte Carlo simulation package, and it utilizes several libraries for various physical interactions and processes. As of my last knowledge update in September 2021, the following libraries are among those used in FLUKA:

- ENDF/B-VII: Evaluated Nuclear Data File, it's used for neutron cross-sections and other nuclear data.
- JENDL: Japanese Evaluated Nuclear Data Library, similar to ENDF but developed by Japan for nuclear data.
- PEANUT: Precise Event-by-event Analysis of Nuclear-reactions and Transmutations, FLUKA's own model for low-energy neutrons (19 MeV down to thermal energies).
- EMF: Electromagnetic processes by FLUKA, it is a collection of models for electromagnetic interactions.
- DPMJET: A library used for high energy hadronic interactions, especially for energies beyond 5 GeV.
- RQMD: Relativistic Quantum Molecular Dynamics, used for intermediate-energy hadronic interactions.
- EVALUATED NUCLEAR DATA LIBRARY (NDL): Provides cross-sections and angular distributions for several processes such as neutron reactions and proton interactions.

**Table 3.18:** FLUKA Unit System

| **Physical Quantity** | **Unit** |
|---|---|
| Distance | cm |
| Surface Area | $cm^2$ |
| Volume | $cm^3$ |
| Energy | GeV |
| Momentum | GeV/c |
| Temperature | K |
| Solid Angle | sr |
| Magnetic Field | T |
| Electric Field | kV/cm |
| Time | s |
| Activity | Bq |
| Linear Energy Transfer (LET) | keV / (μmg / $cm^3$) |
| Equivalent Dose | pSv |

The process of calculating the linear attenuation coefficient for gamma rays in FLUKA is outlined step by step below:

**1)** Create a New Project: Initiate a new project in FLUKA. This is typically done through FLUKA's user interface.

**2)** Define Geometry and Materials: The geometry and materials for your simulation are defined. Defining material properties is critical for calculating the linear attenuation coefficient.

**3)** Set Up Photon Source: The photon (gamma) source is defined. This includes the energy spectrum, direction, and intensity of the photons to be irradiated.

**4)** Set Physics Lists: In FLUKA, appropriate physics lists and models are selected. Ensure that electromagnetic interactions are accurately modeled for gamma rays.

**5)** Set Outputs: How outputs containing the linear attenuation coefficient will be recorded is set up. This may include various information such as energy spectrum, number of photons passing through, and other parameters.

**6)** Start Simulation: Once all parameters are set, the simulation is launched. FLUKA will simulate the interaction of photons with the material and write the results to output files.

**7)** Analyze Results: Once the simulation is complete, analyze the output files and determine the linear attenuation coefficient.

Reporting and Evaluation: Organize the results and evaluate the linear attenuation coefficient by comparing it with other materials or theoretical values.

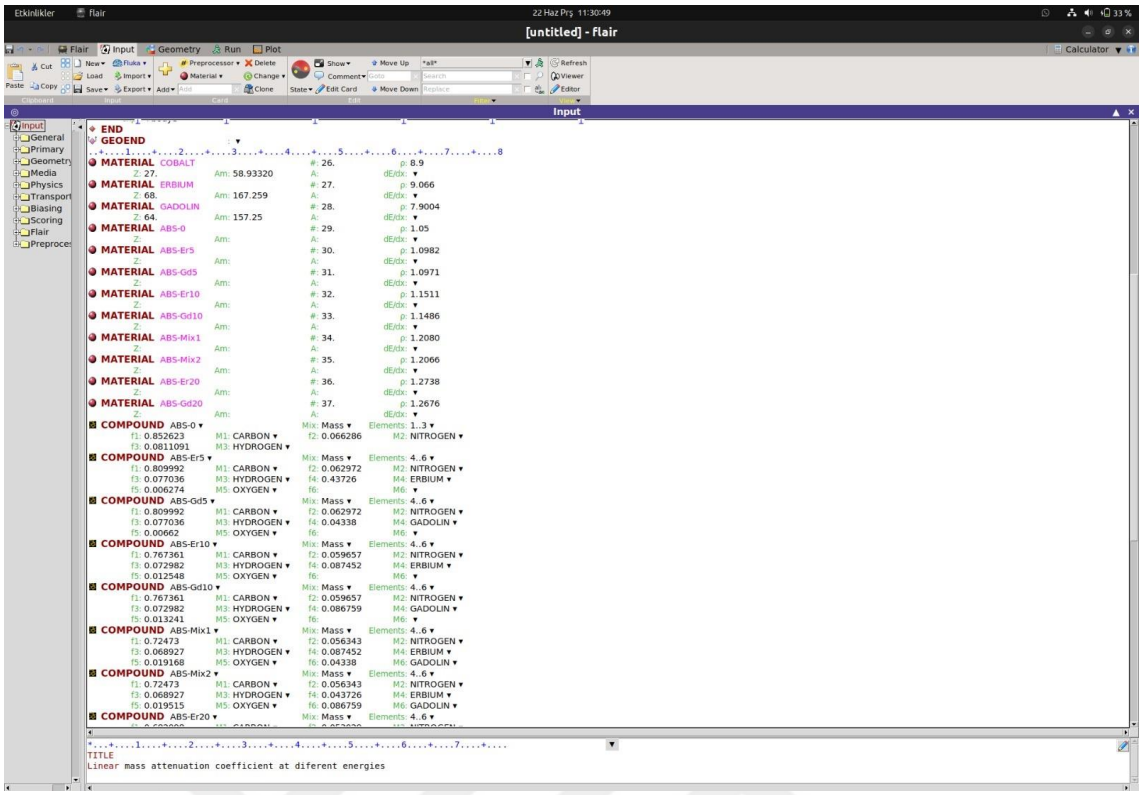



**Figure 3.28 :** Flair material content identification interface for Fluka access

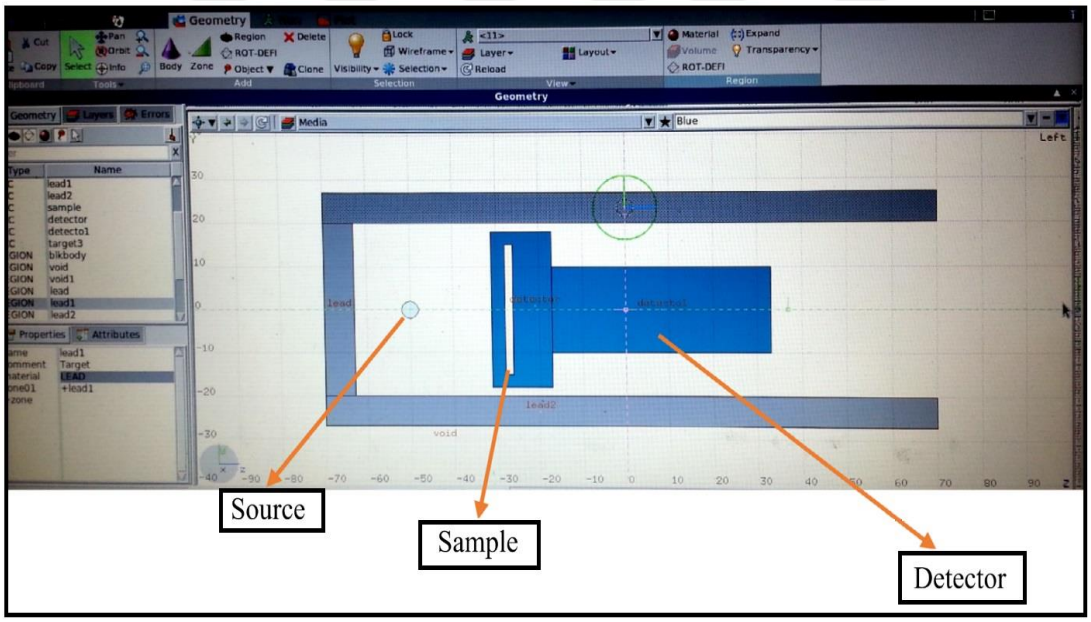



**Figure 3.29 :** Screenshot of flair interface for left view of simulation

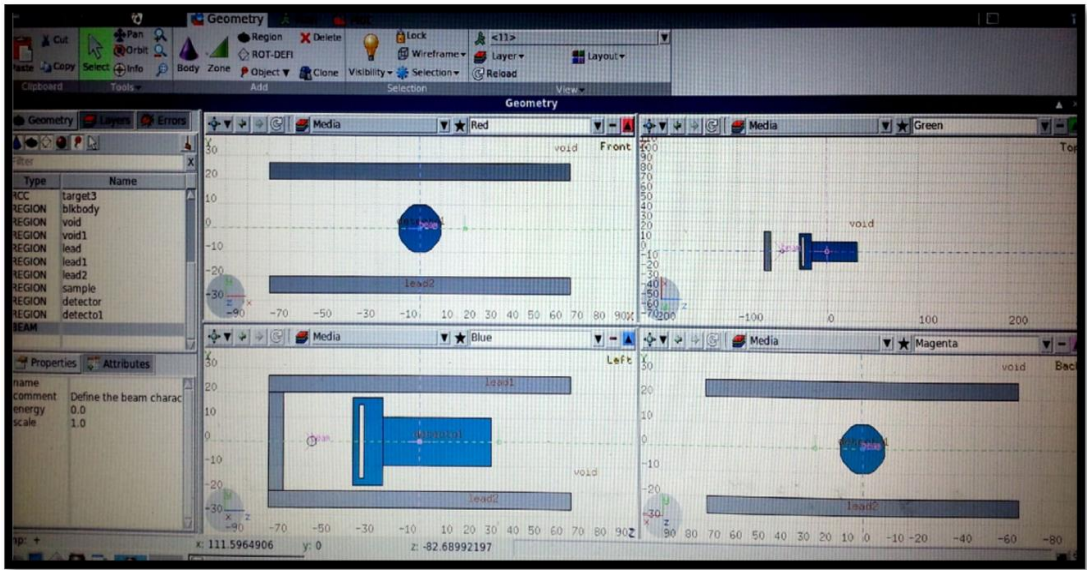



**Figure 3.30 :** Screenshot of flair interface for four views of simulation

The experimental setup has been modeled to work with a point-like radiation source ($^{241}$Am (59,5 keV), $^{133}$Ba (80,9, 276,3, 302,8, 356,0 and 383,8 keV), $^{22}$Na (511,0 and 1274,5 keV), $^{137}$Cs (661,6 keV), ve $^{60}$Co (1173,2 and 1332,5 keV)), and the physical and chemical properties of the selected samples have been integrated into this modeling process. A total of 10,000,000 gamma photons have been bombarded onto each sample. The FLUKA platform will provide outputs based on the data obtained from this experiment, including parameters such as mass attenuation coefficient, number of gamma rays passing through the sample, and linear attenuation coefficient. The results obtained from this study have been compared with experimental data and theoretical findings available in the literature to assess the reliability and validity of the results.

### 3.2.5.2. Neutron radiation shielding analysis

This section of the thesis does not contain experimental results. For it to be a comprehensive study, the neutron shielding properties of the produced samples will be evaluated both through simulations and theoretically. As a result, a clear interpretation regarding the effectiveness of a material that can be used in gamma shielding for neutron shielding has been enabled. In this context, effective neutron removal cross-sections have been calculated in order to evaluate the materials theoretically. It has been observed that the larger this cross-section is, the more effective the neutron shielding capability. To interpret the obtained results, a comparison will be made with concrete and paraffin blocks (of the same thickness as the sample used), which are commonly used in

shielding. This value can be calculated using the equations in Section 2.9.5. The neutron shielding evaluation of the prepared samples will be conducted through simulation using the GEANT4 and FLUKA programs, which are also used for gamma shielding. 10,000,000 neutrons at 4,5 MeV will be directed onto the samples, and the number of neutrons passing through each sample will be determined. The materials' neutron shielding capabilities have been compared to ordinary concrete and paraffin blocks based on the number of neutrons passing through. In this context, the variation in the number of neutrons passing through the M series and P series materials has been simulated for different energy values (0.1 MeV, 0.5 MeV, 1 MeV, 3 MeV, 4,5 MeV, 6 MeV, and 10 MeV). The effect of sample thickness on neutron shielding has been considered as another comparison parameter. In this regard, simulations will be produced for different sample thicknesses (1 mm, 3 mm, 5 mm, 7 mm, 9 mm, 11 mm, 13 mm, 15 mm, 17 mm, 19 mm) at 4,5 MeV energy, and the results have been graphed for each sample, compared to the results for concrete and paraffin.

#### 3.2.5.2.1. GEANT4 (neutron) analysis

In this study, similar to gamma calculations, the GEANT4 simulation program was used for neutron collisions and the estimation of radiation penetration (transportation) through the material. After the installation of the GEANT4 simulation program on the Linux operating system, the contributions present in the samples and the percentages of the additional elements to be included were defined in the GEANT4 program. Material definitions were made in the "DetectorConstruction.cc" document located in the "hadronic/Hadr03/src" directory. The path followed for this process is geant4.10.07.p02-install/share/Geant4-10.7.2/examples/extended/hadronic/Hadr03/src. After accessing the "DetectorConstruction.cc" document, all elements present in the materials used in this research and newly created composites were defined. Based on this data, suitable definitions were made in the "DetectorConstruction.cc" document using the C++ programming language. Table 3.16 provides the chemical compositions and mass percentages of ABS polymers, including both doped and undoped sample ratios.

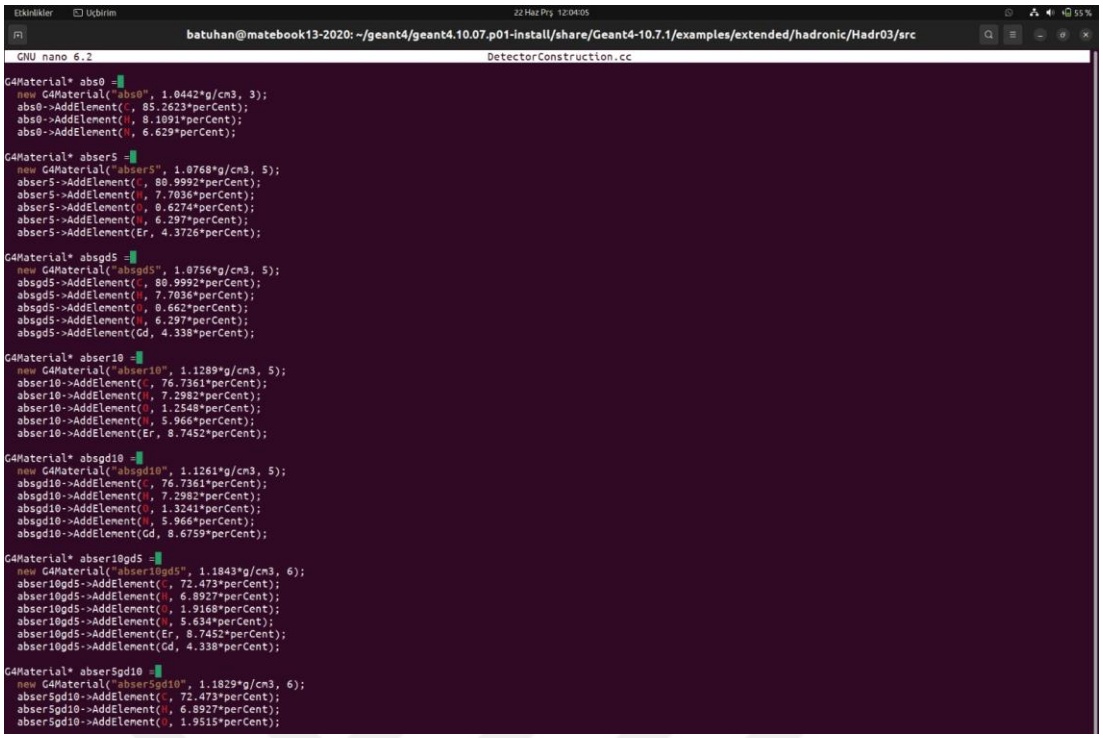



**Figure 3.31 :** Nanopowder-additive and non-additive samples defined in the GEANT4 (neutron) terminal in-terface

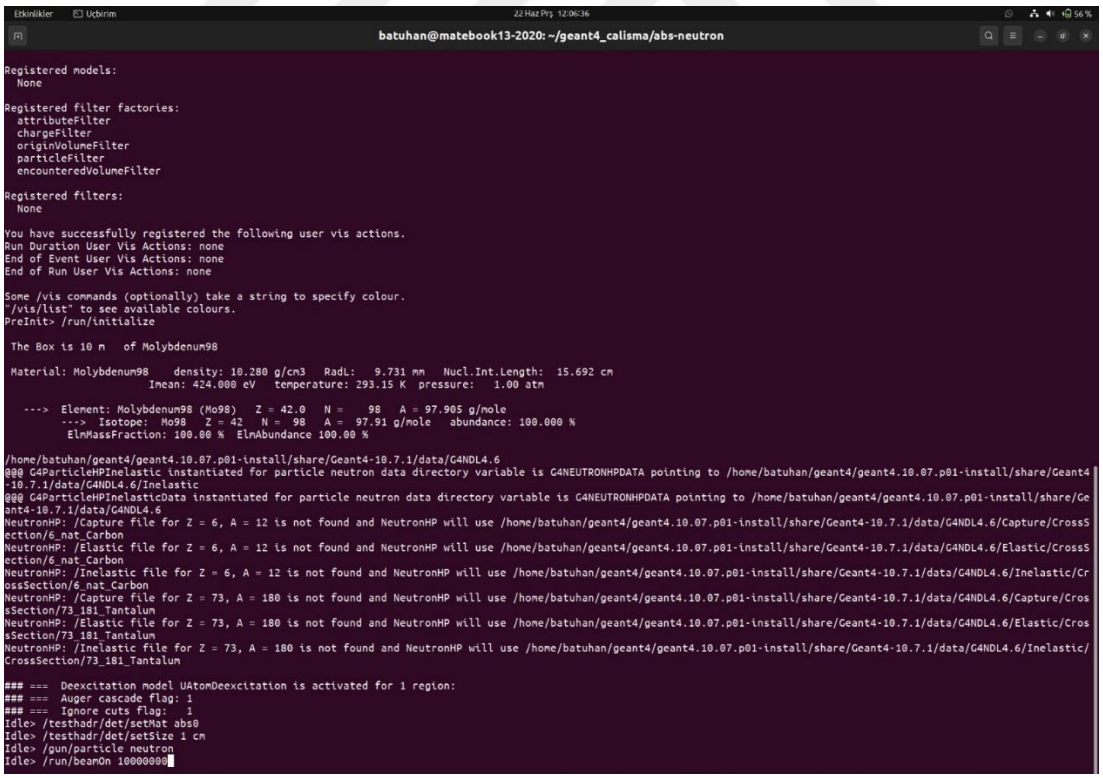



**Figure 3.32 :** Command and parameters for starting the GEANT4 simulation program

#### 3.2.5.2.2. FLUKA (neutron) analysis

In the FLUKA simulation study, doped ABS polymers to be defined were configured through an input file created using the Flair interface in the FLUKA program. In Flair, the particle type we will use is neutron, and the energy of the neutron was defined in GeV in accordance with our study. A total of 10,000,000 neutrons with an energy of 4,5 MeV will be directed at the samples, and the number of neutrons passing through each sample has been determined. Based on the number of neutrons transmitted, a comparison of the neutron shielding effectiveness of the materials has been made with ordinary concrete and paraffin blocks. The variation of the number of transmitted neutrons with energy has been determined by simulating the results at 0,1 MeV, 0,5 MeV, 1 MeV, 3 MeV, 4,5 MeV, 6 MeV, and 10 MeV. The effect of sample thickness on neutron shielding has been considered as another comparative parameter. In this context, simulations will be performed for different sample thicknesses (1 mm, 3 mm, 5 mm, 7 mm, 9 mm, 11 mm, 13 mm, 15 mm, 17 mm, 19 mm) at an energy of 4,5 MeV, and the results will be graphically compared with the results for concrete and paraffin.

#### 3.2.5.2.3. Effective neutron removal cross section analysis using analytical calculation method

In this section, the neutron shielding properties of produced samples will be comprehensively analyzed through simulation and theoretical assessment. The ultimate goal is to acquire insights into the effectiveness of materials usable for neutron shielding, which can also be employed in gamma shielding. To achieve this objective, effective neutron capture cross-sections will be calculated as a theoretical measure to evaluate the materials. A larger value of this cross-section indicates a more potent neutron shielding capability. To interpret the obtained results effectively, a comparative analysis will be conducted with commonly used shielding materials such as lead, concrete, and paraffin blocks (with the same thickness as the utilized samples). The neutron removal cross-section helps us determine how effectively a material can absorb and capture neutrons. This assists in preventing the uncontrolled spread of neutrons, thereby reducing environmental and human health risks. Additionally, it prevents neutrons from interacting with other materials, entering into reactions, and sustaining nuclear chain reactions.

# 4. RESULTS

## 4.1. Gamma Radiation Shielding Analysis Results

### 4.1.1. M-series (molded samples) gamma shielding results

#### 4.1.1.1. Linear attenuation coefficient (LAC) results for the M-series

In this study, the Linear Attenuation Coefficient (LAC) values of the M series samples were experimentally determined. These measurements were carried out using a High-Purity Germanium (HPGe) detector at 11 different energy levels ranging from 59.5 keV to 1332.5 keV. Details of this study, including the statistical uncertainties associated with the experimental measurements, have been explained in previous sections of the document. To enhance the credibility of the experimental findings, they were supported by two distinct sets of theoretical calculations and validated through two separate Monte Carlo simulation programs. The LAC results for our samples are presented in Tables 4.1 to 4.9. Additionally, Figure 5.1 provides a graphical representation of the data presented in the tables. As evident from the graphs and tables, there is an exponential decrease in the LAC value with the increase in gamma energy. Furthermore, a comparative analysis among the experimental, theoretical, and simulation data demonstrates a high degree of congruence, with the largest discrepancy being approximately 6-7%.

**Table 4.1:** Linear attenuation coefficient (LAC) results for the M-ABS-0

| Energy (keV) | Experimental ($cm^{-1}$) | Uncertainty | EpiXS ($cm^{-1}$) | Xcom ($cm^{-1}$) | Geant4 ($cm^{-1}$) | FLUKA ($cm^{-1}$) |
|---|---|---|---|---|---|---|
| 59,5 | 0,1920 | 0,0171 | 0,1979 | 0,1979 | 0,1884 | 0,1982 |
| 80,9 | 0,1832 | 0,0135 | 0,1813 | 0,1813 | 0,1759 | 0,1815 |
| 276,3 | 0,1203 | 0,0073 | 0,1245 | 0,1246 | 0,1236 | 0,1247 |
| 302,8 | 0,1142 | 0,0139 | 0,1204 | 0,1204 | 0,1197 | 0,1205 |
| 356 | 0,1144 | 0,0133 | 0,1132 | 0,1133 | 0,1129 | 0,1133 |
| 383,8 | 0,1016 | 0,0152 | 0,1100 | 0,1100 | 0,1098 | 0,1100 |
| 511 | 0,0909 | 0,0085 | 0,0978 | 0,0979 | 0,0982 | 0,0980 |
| 661,6 | 0,0837 | 0,0173 | 0,0874 | 0,0875 | 0,0880 | 0,0876 |
| 1173,2 | 0,0628 | 0,0178 | 0,0665 | 0,0667 | 0,0669 | 0,0668 |
| 1274,5 | 0,0627 | 0,0159 | 0,0638 | 0,0639 | 0,0641 | 0,0640 |
| 1332,5 | 0,0622 | 0,0142 | 0,0623 | 0,0624 | 0,0627 | 0,0624 |

**Table 4.2**: Linear attenuation coefficient (LAC) results for the M-ABS-Er5

| Energy (keV) | Experimental ($cm^{-1}$) | Uncertainty | EpiXS ($cm^{-1}$) | Xcom ($cm^{-1}$) | Geant4 ($cm^{-1}$) | FLUKA ($cm^{-1}$) |
|---|---|---|---|---|---|---|
| 59,5 | 0,8129 | 0,0139 | 0,8588 | 0,8656 | 0,8345 | 0,8665 |
| 80,9 | 0,4628 | 0,0096 | 0,4838 | 0,4834 | 0,4678 | 0,4840 |
| 276,3 | 0,1347 | 0,0081 | 0,1398 | 0,1399 | 0,1377 | 0,1399 |
| 302,8 | 0,1284 | 0,0101 | 0,1333 | 0,1333 | 0,1316 | 0,1332 |
| 356 | 0,1168 | 0,0097 | 0,1228 | 0,1229 | 0,1219 | 0,1229 |
| 383,8 | 0,1135 | 0,0191 | 0,1185 | 0,1185 | 0,1178 | 0,1185 |
| 511 | 0,0968 | 0,0094 | 0,1035 | 0,1036 | 0,1036 | 0,1035 |
| 661,6 | 0,0859 | 0,0157 | 0,0917 | 0,0918 | 0,0921 | 0,0916 |

**Continuation of Table 4.2…**

| | | | | | | |
|---|---|---|---|---|---|---|
| 1173,2 | 0,0653 | 0,0192 | 0,0692 | 0,0693 | 0,0696 | 0,0694 |
| 1274,5 | 0,0627 | 0,0111 | 0,0663 | 0,0664 | 0,0666 | 0,0664 |
| 1332,5 | 0,0647 | 0,0141 | 0,0648 | 0,0649 | 0,0651 | 0,0649 |

**Table 4.3:** Linear attenuation coefficient (LAC) results for the M-ABS-Gd5

| Energy (keV) | Experimental ($cm^{-1}$) | Uncertainty | EpiXS ($cm^{-1}$) | Xcom ($cm^{-1}$) | Geant4 ($cm^{-1}$) | FLUKA ($cm^{-1}$) |
|---|---|---|---|---|---|---|
| 59,5 | 0,7466 | 0,0178 | 0,7698 | 0,7694 | 0,7450 | 0,7700 |
| 80,9 | 0,4047 | 0,0106 | 0,4394 | 0,4388 | 0,4234 | 0,4392 |
| 276,3 | 0,1293 | 0,0103 | 0,1378 | 0,1378 | 0,1358 | 0,1376 |
| 302,8 | 0,1228 | 0,0140 | 0,1316 | 0,1316 | 0,1300 | 0,1311 |
| 356 | 0,1182 | 0,0112 | 0,1216 | 0,1218 | 0,1207 | 0,1214 |
| 383,8 | 0,1115 | 0,0155 | 0,1176 | 0,1176 | 0,1169 | 0,1176 |
| 511 | 0,1115 | 0,0087 | 0,1030 | 0,1031 | 0,1031 | 0,1031 |
| 661,6 | 0,0882 | 0,0078 | 0,0914 | 0,0915 | 0,0918 | 0,0914 |
| 1173,2 | 0,0644 | 0,0095 | 0,0691 | 0,0692 | 0,0694 | 0,0694 |
| 1274,5 | 0,0713 | 0,0168 | 0,0662 | 0,0663 | 0,0665 | 0,0663 |
| 1332,5 | 0,0647 | 0,0100 | 0,0647 | 0,0648 | 0,0650 | 0,0647 |

**Table 4.4:** Linear attenuation coefficient (LAC) results for the M-ABS-Er10

| Energy (keV) | Experimental ($cm^{-1}$) | Uncertainty | EpiXS ($cm^{-1}$) | Xcom ($cm^{-1}$) | Geant4 ($cm^{-1}$) | FLUKA ($cm^{-1}$) |
|---|---|---|---|---|---|---|
| 59,5 | 1,4929 | 0,0185 | 1,5833 | 1,5978 | 1,5427 | 1,5736 |
| 80,9 | 0,7729 | 0,0173 | 0,8154 | 0,8148 | 0,7879 | 0,8150 |
| 276,3 | 0,1676 | 0,0146 | 0,1566 | 0,1567 | 0,1532 | 0,1567 |
| 302,8 | 0,1363 | 0,0165 | 0,1473 | 0,1473 | 0,1446 | 0,1475 |
| 356 | 0,1241 | 0,0178 | 0,1333 | 0,1335 | 0,1317 | 0,1336 |
| 383,8 | 0,1176 | 0,0081 | 0,1279 | 0,1279 | 0,1264 | 0,1277 |
| 511 | 0,1008 | 0,0121 | 0,1098 | 0,1099 | 0,1095 | 0,1099 |
| 661,6 | 0,0895 | 0,0111 | 0,0964 | 0,0965 | 0,0966 | 0,0964 |
| 1173,2 | 0,0669 | 0,0107 | 0,0721 | 0,0723 | 0,0725 | 0,0721 |
| 1274,5 | 0,0648 | 0,0106 | 0,0691 | 0,0692 | 0,0694 | 0,0693 |
| 1332,5 | 0,0622 | 0,0095 | 0,0675 | 0,0676 | 0,0678 | 0,0676 |

**Table 4.5:** Linear attenuation coefficient (LAC) results for the M-ABS-Gd10

| Energy (keV) | Experimental ($cm^{-1}$) | Uncertainty | EpiXS ($cm^{-1}$) | Xcom ($cm^{-1}$) | Geant4 ($cm^{-1}$) | FLUKA ($cm^{-1}$) |
|---|---|---|---|---|---|---|
| 59,5 | 1,4842 | 0,0126 | 1,3954 | 1,5827 | 1,3538 | 1,4155 |
| 80,9 | 0,7492 | 0,0147 | 0,7218 | 0,8080 | 0,6941 | 0,7333 |
| 276,3 | 0,1492 | 0,0149 | 0,1523 | 0,1562 | 0,1491 | 0,1553 |
| 302,8 | 0,1419 | 0,0123 | 0,1438 | 0,1469 | 0,1413 | 0,1451 |
| 356 | 0,1418 | 0,0151 | 0,1309 | 0,1331 | 0,1294 | 0,1305 |
| 383,8 | 0,1297 | 0,0159 | 0,1258 | 0,1275 | 0,1245 | 0,1253 |
| 511 | 0,1089 | 0,0103 | 0,1087 | 0,1096 | 0,1084 | 0,1088 |
| 661,6 | 0,1038 | 0,0201 | 0,0957 | 0,0963 | 0,0960 | 0,0960 |
| 1173,2 | 0,0686 | 0,0096 | 0,0718 | 0,0721 | 0,0722 | 0,0721 |
| 1274,5 | 0,0670 | 0,0119 | 0,0688 | 0,0691 | 0,0691 | 0,0691 |
| 1332,5 | 0,0680 | 0,0150 | 0,0672 | 0,0675 | 0,0675 | 0,0675 |

**Table 4.6:** Linear attenuation coefficient (LAC) results for the M-ABS-Er10Gd5

| Energy (keV) | Experimental ($cm^{-1}$) | Uncertainty | EpiXS ($cm^{-1}$) | Xcom ($cm^{-1}$) | Geant4 ($cm^{-1}$) | FLUKA ($cm^{-1}$) |
|---|---|---|---|---|---|---|
| 59,5 | 2,1475 | 0,0168 | 2,2814 | 2,2963 | 2,2232 | 2,2414 |
| 80,9 | 1,0437 | 0,0111 | 1,1310 | 1,1296 | 1,0905 | 1,1312 |
| 276,3 | 0,1639 | 0,0176 | 0,1728 | 0,1729 | 0,1681 | 0,1729 |
| 302,8 | 0,1573 | 0,0095 | 0,1610 | 0,1610 | 0,1571 | 0,1609 |
| 356 | 0,1549 | 0,0174 | 0,1437 | 0,1439 | 0,1412 | 0,1439 |
| 383,8 | 0,1441 | 0,0106 | 0,1371 | 0,1371 | 0,1350 | 0,1371 |
| 511 | 0,1176 | 0,0106 | 0,1161 | 0,1162 | 0,1154 | 0,1163 |
| 661,6 | 0,1038 | 0,0180 | 0,1012 | 0,1014 | 0,1012 | 0,1012 |
| 1173,2 | 0,0719 | 0,0150 | 0,0752 | 0,0753 | 0,0755 | 0,0753 |
| 1274,5 | 0,0735 | 0,0185 | 0,0720 | 0,0721 | 0,0723 | 0,0720 |
| 1332,5 | 0,0721 | 0,0173 | 0,0703 | 0,0705 | 0,0706 | 0,0705 |

**Table 4.7:** Linear attenuation coefficient (LAC) results for the M-ABS-Er5Gd10

| Energy (keV) | Experimental ($cm^{-1}$) | Uncertainty | EpiXS ($cm^{-1}$) | Xcom ($cm^{-1}$) | Geant4 ($cm^{-1}$) | FLUKA ($cm^{-1}$) |
|---|---|---|---|---|---|---|
| 59,5 | 2,0590 | 0,0146 | 2,1819 | 2,1887 | 2,1220 | 2,1662 |
| 80,9 | 0,9878 | 0,0086 | 1,0815 | 1,0796 | 1,0410 | 1,0811 |
| 276,3 | 0,1658 | 0,0142 | 0,1705 | 0,1705 | 0,1660 | 0,1704 |
| 302,8 | 0,1516 | 0,0139 | 0,1591 | 0,1591 | 0,1554 | 0,1589 |
| 356 | 0,1517 | 0,0086 | 0,1424 | 0,1425 | 0,1400 | 0,1423 |
| 383,8 | 0,1399 | 0,0158 | 0,1360 | 0,1360 | 0,1340 | 0,1359 |
| 511 | 0,1183 | 0,0092 | 0,1155 | 0,1156 | 0,1149 | 0,1156 |
| 661,6 | 0,0966 | 0,0079 | 0,1009 | 0,1010 | 0,1009 | 0,1009 |
| 1173,2 | 0,0719 | 0,0171 | 0,0750 | 0,0752 | 0,0756 | 0,0756 |
| 1274,5 | 0,0713 | 0,0127 | 0,0719 | 0,0720 | 0,0721 | 0,0719 |
| 1332,5 | 0,0713 | 0,0163 | 0,0702 | 0,0703 | 0,0704 | 0,0703 |

**Table 4.8:** Linear attenuation coefficient (LAC) results for the M-ABS-Er20

| Energy (keV) | Experimental ($cm^{-1}$) | Uncertainty | EpiXS ($cm^{-1}$) | Xcom ($cm^{-1}$) | Geant4 ($cm^{-1}$) | FLUKA ($cm^{-1}$) |
|---|---|---|---|---|---|---|
| 59,5 | 3,1199 | 0,0074 | 3,2640 | 3,2953 | 3,1856 | 3,2762 |
| 80,9 | 1,4755 | 0,0186 | 1,5847 | 1,5833 | 1,5305 | 1,5604 |
| 276,3 | 0,1883 | 0,0097 | 0,1956 | 0,1957 | 0,1892 | 0,1949 |
| 302,8 | 0,1663 | 0,0149 | 0,1800 | 0,1800 | 0,1747 | 0,1800 |
| 356 | 0,1662 | 0,0149 | 0,1578 | 0,1580 | 0,1544 | 0,1578 |
| 383,8 | 0,1544 | 0,0183 | 0,1495 | 0,1495 | 0,1466 | 0,1494 |
| 511 | 0,1265 | 0,0130 | 0,1244 | 0,1245 | 0,1232 | 0,1244 |
| 661,6 | 0,1038 | 0,0178 | 0,1074 | 0,1075 | 0,1071 | 0,1072 |
| 1173,2 | 0,0768 | 0,0098 | 0,0789 | 0,0791 | 0,0792 | 0,0791 |
| 1274,5 | 0,0800 | 0,0148 | 0,0756 | 0,0757 | 0,0757 | 0,0757 |
| 1332,5 | 0,0771 | 0,0183 | 0,0738 | 0,0739 | 0,0740 | 0,0739 |

**Table 4.9:** Linear attenuation coefficient (LAC) results for the M-ABS-Gd20

| Energy (keV) | Experimental ($cm^{-1}$) | Uncertainty | EpiXS ($cm^{-1}$) | Xcom ($cm^{-1}$) | Geant4 ($cm^{-1}$) | FLUKA ($cm^{-1}$) |
|---|---|---|---|---|---|---|
| 59,5 | 2,7369 | 0,0095 | 2,8411 | 2,8394 | 2,7608 | 2,8179 |
| 80,9 | 1,2516 | 0,0193 | 1,3744 | 1,3715 | 1,3197 | 1,3690 |
| 276,3 | 0,1960 | 0,0160 | 0,1858 | 0,1858 | 0,1800 | 0,1858 |
| 302,8 | 0,1746 | 0,0175 | 0,1721 | 0,1720 | 0,1673 | 0,1720 |
| 356 | 0,1628 | 0,0099 | 0,1524 | 0,1525 | 0,1493 | 0,1524 |
| 383,8 | 0,1503 | 0,0169 | 0,1449 | 0,1450 | 0,1423 | 0,1449 |
| 511 | 0,1136 | 0,0171 | 0,1218 | 0,1219 | 0,1208 | 0,1218 |
| 661,6 | 0,1033 | 0,0149 | 0,1057 | 0,1059 | 0,1056 | 0,1056 |
| 1173,2 | 0,0752 | 0,0121 | 0,0782 | 0,0784 | 0,0785 | 0,0784 |
| 1274,5 | 0,0691 | 0,0110 | 0,0749 | 0,0750 | 0,0751 | 0,0749 |
| 1332,5 | 0,0755 | 0,0143 | 0,0731 | 0,0733 | 0,0734 | 0,0733 |

#### 4.1.1.2. Mass attenuation coefficient (MAC) results for the M-series

The mass attenuation coefficient (MAC) values of the M series samples were determined by dividing the experimentally measured linear attenuation coefficient (LAC) values by the experimentally measured density values. Details of this study, including the statistical uncertainties associated with the experimental measurements, have been explained in previous sections of the document. To enhance the credibility of the experimental findings, they were supported by two distinct sets of theoretical calculations and validated through two separate Monte Carlo simulation programs. The MAC results for

our samples are presented in Tables 4.10 to 4.18. Additionally, Figure 5.3 provides a graphical representation of the data presented in the tables. As evident from the graphs and tables, there is an exponential decrease in the MAC value with the increase in gamma energy. Furthermore, a comparative analysis among the experimental, theoretical, and simulation data demonstrates a high degree of congruence, with the largest discrepancy being approximately 6-7%.

**Table 4.10:** Mass attenuation coefficient (MAC) results for the M-ABS-0

| Energy (keV) | Experimental ($cm^2/g$) | Uncertainty | EpiXS ($cm^2/g$) | Xcom ($cm^2/g$) | Geant4 ($cm^2/g$) | FLUKA ($cm^2/g$) |
|---|---|---|---|---|---|---|
| 59,5 | 0,18284 | 0,01629 | 0,18845 | 0,18850 | 0,17943 | 0,18878 |
| 80,9 | 0,17447 | 0,01286 | 0,17262 | 0,17270 | 0,16756 | 0,17282 |
| 276,3 | 0,11461 | 0,00695 | 0,11856 | 0,11870 | 0,11771 | 0,11876 |
| 302,8 | 0,10878 | 0,01324 | 0,11470 | 0,11470 | 0,11402 | 0,11480 |
| 356 | 0,10896 | 0,01267 | 0,10777 | 0,10790 | 0,10757 | 0,10787 |
| 383,8 | 0,09675 | 0,01448 | 0,10475 | 0,10480 | 0,10459 | 0,10480 |
| 511 | 0,08653 | 0,00810 | 0,09317 | 0,09324 | 0,09350 | 0,09334 |
| 661,6 | 0,07975 | 0,01648 | 0,08325 | 0,08334 | 0,08380 | 0,08344 |
| 1173,2 | 0,05980 | 0,01695 | 0,06336 | 0,06348 | 0,06375 | 0,06358 |
| 1274,5 | 0,05967 | 0,01514 | 0,06076 | 0,06083 | 0,06108 | 0,06093 |
| 1332,5 | 0,05926 | 0,01352 | 0,05934 | 0,05946 | 0,05967 | 0,05946 |

**Table 4.11:** Mass attenuation coefficient (MAC) results for the M-ABS-Er5

| Energy (keV) | Experimental ($cm^2/g$) | Uncertainty | EpiXS ($cm^2/g$) | Xcom ($cm^2/g$) | Geant4 ($cm^2/g$) | FLUKA ($cm^2/g$) |
|---|---|---|---|---|---|---|
| 59,5 | 0,7402 | 0,0127 | 0,7819 | 0,7882 | 0,7598 | 0,7890 |
| 80,9 | 0,4214 | 0,0087 | 0,4405 | 0,4402 | 0,4260 | 0,4407 |
| 276,3 | 0,1226 | 0,0074 | 0,1273 | 0,1274 | 0,1254 | 0,1274 |
| 302,8 | 0,1169 | 0,0092 | 0,1214 | 0,1214 | 0,1198 | 0,1213 |
| 356 | 0,1063 | 0,0088 | 0,1118 | 0,1119 | 0,1110 | 0,1119 |
| 383,8 | 0,1034 | 0,0174 | 0,1079 | 0,1079 | 0,1072 | 0,1079 |
| 511 | 0,0882 | 0,0086 | 0,0943 | 0,0944 | 0,0943 | 0,0943 |
| 661,6 | 0,0783 | 0,0143 | 0,0835 | 0,0836 | 0,0839 | 0,0834 |
| 1173,2 | 0,0594 | 0,0175 | 0,0630 | 0,0631 | 0,0633 | 0,0632 |
| 1274,5 | 0,0570 | 0,0101 | 0,0604 | 0,0605 | 0,0607 | 0,0605 |
| 1332,5 | 0,0589 | 0,0128 | 0,0590 | 0,0591 | 0,0593 | 0,0591 |

**Table 4.12:** Mass attenuation coefficient (MAC) results for the M-ABS-Gd5

| Energy (keV) | Experimental ($cm^2/g$) | Uncertainty | EpiXS ($cm^2/g$) | Xcom ($cm^2/g$) | Geant4 ($cm^2/g$) | FLUKA ($cm^2/g$) |
|---|---|---|---|---|---|---|
| 59,5 | 0,6805 | 0,0163 | 0,7017 | 0,7013 | 0,6791 | 0,7019 |
| 80,9 | 0,3689 | 0,0097 | 0,4005 | 0,4000 | 0,3859 | 0,4003 |
| 276,3 | 0,1178 | 0,0094 | 0,1256 | 0,1256 | 0,1238 | 0,1255 |
| 302,8 | 0,1120 | 0,0127 | 0,1200 | 0,1200 | 0,1185 | 0,1195 |
| 356 | 0,1077 | 0,0102 | 0,1109 | 0,1110 | 0,1100 | 0,1107 |
| 383,8 | 0,1017 | 0,0141 | 0,1072 | 0,1072 | 0,1065 | 0,1072 |
| 511 | 0,1017 | 0,0079 | 0,0939 | 0,0940 | 0,0940 | 0,0940 |
| 661,6 | 0,0804 | 0,0072 | 0,0833 | 0,0834 | 0,0837 | 0,0833 |
| 1173,2 | 0,0587 | 0,0086 | 0,0630 | 0,0631 | 0,0633 | 0,0632 |
| 1274,5 | 0,0650 | 0,0153 | 0,0603 | 0,0604 | 0,0606 | 0,0604 |
| 1332,5 | 0,0590 | 0,0092 | 0,0589 | 0,0591 | 0,0592 | 0,0590 |

**Table 4.13:** Mass attenuation coefficient (MAC) results for the M-ABS-Er10

| Energy (keV) | Experimental ($cm^2/g$) | Uncertainty | EpiXS ($cm^2/g$) | Xcom ($cm^2/g$) | Geant4 ($cm^2/g$) | FLUKA ($cm^2/g$) |
|---|---|---|---|---|---|---|
| 59,5 | 1,2969 | 0,0161 | 1,3754 | 1,3880 | 1,3402 | 1,3670 |
| 80,9 | 0,6715 | 0,0150 | 0,7084 | 0,7078 | 0,6844 | 0,7080 |
| 276,3 | 0,1456 | 0,0127 | 0,1361 | 0,1361 | 0,1331 | 0,1361 |
| 302,8 | 0,1184 | 0,0143 | 0,1280 | 0,1280 | 0,1256 | 0,1281 |
| 356 | 0,1078 | 0,0155 | 0,1158 | 0,1160 | 0,1144 | 0,1161 |
| 383,8 | 0,1021 | 0,0070 | 0,1111 | 0,1111 | 0,1098 | 0,1109 |
| 511 | 0,0876 | 0,0105 | 0,0954 | 0,0955 | 0,0951 | 0,0955 |
| 661,6 | 0,0777 | 0,0096 | 0,0838 | 0,0839 | 0,0839 | 0,0838 |
| 1173,2 | 0,0581 | 0,0093 | 0,0627 | 0,0628 | 0,0629 | 0,0627 |
| 1274,5 | 0,0563 | 0,0092 | 0,0600 | 0,0601 | 0,0603 | 0,0602 |
| 1332,5 | 0,0541 | 0,0083 | 0,0586 | 0,0587 | 0,0589 | 0,0587 |

**Table 4.14:** Mass attenuation coefficient (MAC) results for the M-ABS-Gd10

| Energy (keV) | Experimental ($cm^2/g$) | Uncertainty | EpiXS ($cm^2/g$) | Xcom ($cm^2/g$) | Geant4 ($cm^2/g$) | FLUKA ($cm^2/g$) |
|---|---|---|---|---|---|---|
| 59,5 | 1,2922 | 0,0110 | 1,2149 | 1,3780 | 1,1787 | 1,2324 |
| 80,9 | 0,6523 | 0,0128 | 0,6285 | 0,7035 | 0,6043 | 0,6385 |
| 276,3 | 0,1299 | 0,0130 | 0,1326 | 0,1360 | 0,1298 | 0,1352 |
| 302,8 | 0,1236 | 0,0107 | 0,1252 | 0,1279 | 0,1230 | 0,1263 |
| 356 | 0,1235 | 0,0131 | 0,1140 | 0,1159 | 0,1127 | 0,1136 |
| 383,8 | 0,1129 | 0,0138 | 0,1095 | 0,1110 | 0,1084 | 0,1090 |
| 511 | 0,0948 | 0,0090 | 0,0946 | 0,0955 | 0,0944 | 0,0947 |
| 661,6 | 0,0904 | 0,0175 | 0,0833 | 0,0839 | 0,0836 | 0,0835 |
| 1173,2 | 0,0597 | 0,0084 | 0,0625 | 0,0628 | 0,0628 | 0,0628 |
| 1274,5 | 0,0583 | 0,0104 | 0,0599 | 0,0601 | 0,0602 | 0,0601 |
| 1332,5 | 0,0592 | 0,0131 | 0,0585 | 0,0587 | 0,0588 | 0,0587 |

**Table 4.15:** Mass attenuation coefficient (MAC) results for the M-ABS-Er10Gd5

| Energy (keV) | Experimental ($cm^2/g$) | Uncertainty | EpiXS ($cm^2/g$) | Xcom ($cm^2/g$) | Geant4 ($cm^2/g$) | FLUKA ($cm^2/g$) |
|---|---|---|---|---|---|---|
| 59,5 | 1,7778 | 0,0139 | 1,8887 | 1,9010 | 1,8405 | 1,8555 |
| 80,9 | 0,8640 | 0,0092 | 0,9363 | 0,9351 | 0,9028 | 0,9365 |
| 276,3 | 0,1357 | 0,0146 | 0,1431 | 0,1431 | 0,1392 | 0,1431 |
| 302,8 | 0,1302 | 0,0079 | 0,1333 | 0,1333 | 0,1301 | 0,1332 |
| 356 | 0,1282 | 0,0144 | 0,1189 | 0,1191 | 0,1169 | 0,1191 |
| 383,8 | 0,1193 | 0,0088 | 0,1135 | 0,1135 | 0,1118 | 0,1135 |
| 511 | 0,0974 | 0,0088 | 0,0961 | 0,0962 | 0,0956 | 0,0963 |
| 661,6 | 0,0859 | 0,0149 | 0,0838 | 0,0839 | 0,0838 | 0,0838 |
| 1173,2 | 0,0595 | 0,0124 | 0,0623 | 0,0624 | 0,0625 | 0,0624 |
| 1274,5 | 0,0608 | 0,0153 | 0,0596 | 0,0597 | 0,0598 | 0,0596 |
| 1332,5 | 0,0597 | 0,0143 | 0,0582 | 0,0583 | 0,0584 | 0,0583 |

**Table 4.16:** Mass attenuation coefficient (MAC) results for the M-ABS-Er5Gd10

| Energy (keV) | Experimental ($cm^2/g$) | Uncertainty | EpiXS ($cm^2/g$) | Xcom ($cm^2/g$) | Geant4 ($cm^2/g$) | FLUKA ($cm^2/g$) |
|---|---|---|---|---|---|---|
| 59,5 | 1,7065 | 0,0121 | 1,8084 | 1,8140 | 1,7587 | 1,7954 |
| 80,9 | 0,8187 | 0,0071 | 0,8963 | 0,8948 | 0,8628 | 0,8960 |
| 276,3 | 0,1374 | 0,0118 | 0,1413 | 0,1413 | 0,1376 | 0,1412 |
| 302,8 | 0,1256 | 0,0115 | 0,1319 | 0,1319 | 0,1288 | 0,1317 |
| 356 | 0,1258 | 0,0071 | 0,1180 | 0,1181 | 0,1161 | 0,1179 |
| 383,8 | 0,1160 | 0,0131 | 0,1127 | 0,1127 | 0,1111 | 0,1126 |
| 511 | 0,0981 | 0,0076 | 0,0958 | 0,0958 | 0,0952 | 0,0958 |
| 661,6 | 0,0801 | 0,0065 | 0,0836 | 0,0837 | 0,0836 | 0,0836 |
| 1173,2 | 0,0596 | 0,0142 | 0,0622 | 0,0623 | 0,0626 | 0,0626 |
| 1274,5 | 0,0591 | 0,0105 | 0,0596 | 0,0597 | 0,0598 | 0,0596 |
| 1332,5 | 0,0591 | 0,0135 | 0,0582 | 0,0583 | 0,0584 | 0,0583 |

**Table 4.17:** Mass attenuation coefficient (MAC) results for the M-ABS-Er20

| Energy (keV) | Experimental ($cm^2/g$) | Uncertainty | EpiXS ($cm^2/g$) | Xcom ($cm^2/g$) | Geant4 ($cm^2/g$) | FLUKA ($cm^2/g$) |
|---|---|---|---|---|---|---|
| 59,5 | 2,4493 | 0,0058 | 2,5624 | 2,5870 | 2,5009 | 2,5720 |
| 80,9 | 1,1584 | 0,0146 | 1,2441 | 1,2430 | 1,2015 | 1,2250 |
| 276,3 | 0,1478 | 0,0076 | 0,1536 | 0,1536 | 0,1485 | 0,1530 |
| 302,8 | 0,1306 | 0,0117 | 0,1413 | 0,1413 | 0,1372 | 0,1413 |
| 356 | 0,1305 | 0,0117 | 0,1239 | 0,1240 | 0,1212 | 0,1239 |
| 383,8 | 0,1213 | 0,0144 | 0,1174 | 0,1174 | 0,1151 | 0,1173 |
| 511 | 0,0993 | 0,0102 | 0,0976 | 0,0977 | 0,0967 | 0,0976 |
| 661,6 | 0,0815 | 0,0140 | 0,0843 | 0,0844 | 0,0841 | 0,0842 |
| 1173,2 | 0,0603 | 0,0077 | 0,0620 | 0,0621 | 0,0621 | 0,0621 |
| 1274,5 | 0,0628 | 0,0116 | 0,0593 | 0,0594 | 0,0595 | 0,0595 |
| 1332,5 | 0,0606 | 0,0144 | 0,0579 | 0,0580 | 0,0581 | 0,0580 |

**Table 4.18:** Mass attenuation coefficient (MAC) results for the M-ABS-Gd20

| Energy (keV) | Experimental ($cm^2/g$) | Uncertainty | EpiXS ($cm^2/g$) | Xcom ($cm^2/g$) | Geant4 ($cm^2/g$) | FLUKA ($cm^2/g$) |
|---|---|---|---|---|---|---|
| 59,5 | 2,1591 | 0,0075 | 2,2413 | 2,2400 | 2,1780 | 2,2230 |
| 80,9 | 0,9873 | 0,0152 | 1,0843 | 1,0820 | 1,0411 | 1,0800 |
| 276,3 | 0,1546 | 0,0126 | 0,1466 | 0,1466 | 0,1420 | 0,1466 |
| 302,8 | 0,1377 | 0,0138 | 0,1358 | 0,1357 | 0,1320 | 0,1357 |
| 356 | 0,1284 | 0,0078 | 0,1202 | 0,1203 | 0,1178 | 0,1202 |
| 383,8 | 0,1186 | 0,0133 | 0,1143 | 0,1144 | 0,1123 | 0,1143 |
| 511 | 0,0896 | 0,0135 | 0,0961 | 0,0962 | 0,0953 | 0,0961 |
| 661,6 | 0,0815 | 0,0118 | 0,0834 | 0,0835 | 0,0833 | 0,0833 |
| 1173,2 | 0,0593 | 0,0095 | 0,0617 | 0,0618 | 0,0619 | 0,0618 |
| 1274,5 | 0,0545 | 0,0087 | 0,0591 | 0,0592 | 0,0593 | 0,0591 |
| 1332,5 | 0,0595 | 0,0113 | 0,0577 | 0,0578 | 0,0579 | 0,0578 |

### 4.1.1.3. Half value layer (HVL) results for the M-series

Following the MAC values, the other results to be presented are the half-value layers (HVL) of the samples. The half-value layer, in other words, can be expressed as the thickness of the sample required to reduce the radiation intensity incident on the sample to half. The smaller this value, the better the gamma radiation shielding capability of the sample. HVL values are provided in Tables 4.19 to 4.27. Table figures can be seen in Figure 5.5 and Figure y.y in the Results section. When the tables are examined, it is observed that as gamma energy increases, the HVL value also increases. There is alignment among the experimental, theoretical, and simulation results, with the maximum discrepancy being around 6-7%.

**Table 4.19:** Half value layer (HVL) results for the M-ABS-0

| Energy (keV) | Experimental (cm) | EpiXS (cm) | Xcom (cm) | Geant4 (cm) | FLUKA (cm) |
|---|---|---|---|---|---|
| 59,5 | 3,6104 | 3,5031 | 3,5021 | 3,6791 | 3,4969 |
| 80,9 | 3,7838 | 3,8242 | 3,8225 | 3,9397 | 3,8198 |
| 276,3 | 5,7596 | 5,5680 | 5,5614 | 5,6082 | 5,5587 |
| 302,8 | 6,0685 | 5,7553 | 5,7554 | 5,7897 | 5,7503 |
| 356 | 6,0584 | 6,1255 | 6,1181 | 6,1368 | 6,1198 |
| 383,8 | 6,8229 | 6,3018 | 6,2990 | 6,3117 | 6,2990 |
| 511 | 7,6290 | 7,0854 | 7,0800 | 7,0602 | 7,0724 |

| | | | | | |
|---|---|---|---|---|---|
| 661,6 | 8,2779 | 7,9292 | 7,9210 | 7,8780 | 7,9116 |
| 1173,2 | 11,0385 | 10,4185 | 10,3992 | 10,3551 | 10,3828 |
| 1274,5 | 11,0636 | 10,8650 | 10,8522 | 10,8085 | 10,8344 |
| 1332,5 | 11,1401 | 11,1239 | 11,1023 | 11,0637 | 11,1023 |

**Table 4.20:** Half value layer (HVL) results for the M-ABS-Er5

| Energy (keV) | Experimental (cm) | EpiXS (cm) | Xcom (cm) | Geant4 (cm) | FLUKA (cm) |
|---|---|---|---|---|---|
| 59,5 | 0,8527 | 0,8072 | 0,8007 | 0,8306 | 0,7999 |
| 80,9 | 1,4977 | 1,4328 | 1,4338 | 1,4816 | 1,4321 |
| 276,3 | 5,1475 | 4,9575 | 4,9540 | 5,0326 | 4,9540 |
| 302,8 | 5,3995 | 5,2010 | 5,1989 | 5,2683 | 5,2032 |
| 356 | 5,9364 | 5,6452 | 5,6403 | 5,6875 | 5,6403 |
| 383,8 | 6,1047 | 5,8485 | 5,8493 | 5,8864 | 5,8493 |
| 511 | 7,1592 | 6,6941 | 6,6887 | 6,6927 | 6,6941 |
| 661,6 | 8,0652 | 7,5576 | 7,5496 | 7,5256 | 7,5677 |
| 1173,2 | 10,6217 | 10,0159 | 9,9975 | 9,9631 | 9,9817 |
| 1274,5 | 11,0636 | 10,4498 | 10,4373 | 10,4029 | 10,4373 |
| 1332,5 | 10,7144 | 10,7004 | 10,6793 | 10,6495 | 10,6793 |

**Table 4.21:** Half value layer (HVL) results for the M-ABS-Gd5

| Energy (keV) | Experimental (cm) | EpiXS (cm) | Xcom (cm) | Geant4 (cm) | FLUKA (cm) |
|---|---|---|---|---|---|
| 59,5 | 0,9285 | 0,9004 | 0,9009 | 0,9304 | 0,9002 |
| 80,9 | 1,7126 | 1,5774 | 1,5795 | 1,6371 | 1,5782 |
| 276,3 | 5,3622 | 5,0319 | 5,0303 | 5,1047 | 5,0359 |
| 302,8 | 5,6425 | 5,2665 | 5,2651 | 5,3313 | 5,2871 |
| 356 | 5,8654 | 5,6982 | 5,6920 | 5,7422 | 5,7085 |
| 383,8 | 6,2143 | 5,8964 | 5,8938 | 5,9314 | 5,8938 |
| 511 | 6,2141 | 6,7282 | 6,7228 | 6,7245 | 6,7228 |
| 661,6 | 7,8628 | 7,5850 | 7,5766 | 7,5507 | 7,5848 |
| 1173,2 | 10,7572 | 10,0363 | 10,0176 | 9,9823 | 9,9902 |
| 1274,5 | 9,7203 | 10,4700 | 10,4570 | 10,4220 | 10,4565 |
| 1332,5 | 10,7144 | 10,7207 | 10,6996 | 10,6687 | 10,7068 |

**Table 4.22:** Half value layer (HVL) results for the M-ABS-Er10

| Energy (keV) | Experimental (cm) | EpiXS (cm) | Xcom (cm) | Geant4 (cm) | FLUKA (cm) |
|---|---|---|---|---|---|
| 59,5 | 0,4643 | 0,4378 | 0,4338 | 0,4493 | 0,4405 |
| 80,9 | 0,8968 | 0,8501 | 0,8507 | 0,8798 | 0,8505 |
| 276,3 | 4,1351 | 4,4255 | 4,4243 | 4,5234 | 4,4243 |
| 302,8 | 5,0847 | 4,7042 | 4,7043 | 4,7946 | 4,7006 |
| 356 | 5,5859 | 5,1984 | 5,1909 | 5,2649 | 5,1865 |
| 383,8 | 5,8961 | 5,4211 | 5,4199 | 5,4821 | 5,4297 |
| 511 | 6,8755 | 6,3120 | 6,3065 | 6,3312 | 6,3065 |
| 661,6 | 7,7459 | 7,1883 | 7,1804 | 7,1737 | 7,1883 |
| 1173,2 | 10,3603 | 9,6089 | 9,5899 | 9,5660 | 9,6089 |
| 1274,5 | 10,6953 | 10,0296 | 10,0174 | 9,9917 | 10,0008 |
| 1332,5 | 11,1401 | 10,2717 | 10,2511 | 10,2297 | 10,2511 |

**Table 4.23:** Half value layer (HVL) results for the M-ABS-Gd10

| Energy (keV) | Experimental (cm) | EpiXS (cm) | Xcom (cm) | Geant4 (cm) | FLUKA (cm) |
|---|---|---|---|---|---|
| 59,5 | 0,4670 | 0,4967 | 0,4379 | 0,5120 | 0,4897 |
| 80,9 | 0,9252 | 0,9603 | 0,8578 | 0,9986 | 0,9452 |
| 276,3 | 4,6465 | 4,5523 | 4,4374 | 4,6479 | 4,4636 |
| 302,8 | 4,8840 | 4,8188 | 4,7184 | 4,9059 | 4,7769 |
| 356 | 4,8883 | 5,2943 | 5,2069 | 5,3562 | 5,3130 |
| 383,8 | 5,3440 | 5,5088 | 5,4368 | 5,5656 | 5,5341 |
| 511 | 6,3678 | 6,3766 | 6,3225 | 6,3921 | 6,3718 |
| 661,6 | 6,6787 | 7,2412 | 7,1963 | 7,2223 | 7,2232 |
| 1173,2 | 10,1112 | 9,6490 | 9,6111 | 9,6037 | 9,6111 |
| 1274,5 | 10,3500 | 10,0696 | 10,0379 | 10,0296 | 10,0379 |
| 1332,5 | 10,1935 | 10,3118 | 10,2738 | 10,2676 | 10,2738 |

**Table 4.24:** Half value layer (HVL) results for the M-ABS-Er10Gd5

| Energy (keV) | Experimental (cm) | EpiXS (cm) | Xcom (cm) | Geant4 (cm) | FLUKA (cm) |
|---|---|---|---|---|---|
| 59,5 | 0,3228 | 0,3038 | 0,3019 | 0,3118 | 0,3093 |
| 80,9 | 0,6641 | 0,6129 | 0,6136 | 0,6356 | 0,6127 |
| 276,3 | 4,2288 | 4,0108 | 4,0099 | 4,1226 | 4,0099 |
| 302,8 | 4,4068 | 4,3058 | 4,3047 | 4,4113 | 4,3079 |
| 356 | 4,4743 | 4,8244 | 4,8180 | 4,9078 | 4,8180 |
| 383,8 | 4,8114 | 5,0568 | 5,0557 | 5,1344 | 5,0557 |
| 511 | 5,8925 | 5,9691 | 5,9642 | 6,0047 | 5,9580 |
| 661,6 | 6,6787 | 6,8467 | 6,8385 | 6,8460 | 6,8460 |
| 1173,2 | 9,6460 | 9,2170 | 9,2002 | 9,1824 | 9,2002 |
| 1274,5 | 9,4325 | 9,6241 | 9,6117 | 9,5937 | 9,6241 |
| 1332,5 | 9,6075 | 9,8575 | 9,8375 | 9,8228 | 9,8375 |

**Table 4.25:** Half value layer (HVL) results for the M-ABS-Er5Gd10

| Energy (keV) | Experimental (cm) | EpiXS (cm) | Xcom (cm) | Geant4 (cm) | FLUKA (cm) |
|---|---|---|---|---|---|
| 59,5 | 0,3366 | 0,3177 | 0,3167 | 0,3267 | 0,3200 |
| 80,9 | 0,7017 | 0,6409 | 0,6420 | 0,6659 | 0,6411 |
| 276,3 | 4,1815 | 4,0652 | 4,0657 | 4,1766 | 4,0686 |
| 302,8 | 4,5722 | 4,3560 | 4,3555 | 4,4606 | 4,3621 |
| 356 | 4,5679 | 4,8678 | 4,8644 | 4,9495 | 4,8726 |
| 383,8 | 4,9531 | 5,0970 | 5,0975 | 5,1732 | 5,1020 |
| 511 | 5,8587 | 5,9996 | 5,9955 | 6,0336 | 5,9955 |
| 661,6 | 7,1748 | 6,8721 | 6,8636 | 6,8694 | 6,8694 |
| 1173,2 | 9,6460 | 9,2368 | 9,2198 | 9,1718 | 9,1718 |
| 1274,5 | 9,7203 | 9,6439 | 9,6309 | 9,6124 | 9,6439 |
| 1332,5 | 9,7194 | 9,8773 | 9,8573 | 9,8418 | 9,8573 |

**Table 4.26:** Half value layer (HVL) results for the M-ABS-Er20

| Energy (keV) | Experimental (cm) | EpiXS (cm) | Xcom (cm) | Geant4 (cm) | FLUKA (cm) |
|---|---|---|---|---|---|
| 59,5 | 0,2222 | 0,2124 | 0,2103 | 0,2176 | 0,2116 |
| 80,9 | 0,4698 | 0,4374 | 0,4378 | 0,4529 | 0,4442 |
| 276,3 | 3,6806 | 3,5434 | 3,5427 | 3,6636 | 3,5566 |
| 302,8 | 4,1682 | 3,8510 | 3,8511 | 3,9673 | 3,8511 |
| 356 | 4,1697 | 4,3921 | 4,3884 | 4,4905 | 4,3921 |
| 383,8 | 4,4879 | 4,6351 | 4,6351 | 4,7285 | 4,6391 |
| 511 | 5,4798 | 5,5740 | 5,5691 | 5,6265 | 5,5740 |
| 661,6 | 6,6787 | 6,4565 | 6,4481 | 6,4719 | 6,4642 |
| 1173,2 | 9,0209 | 8,7810 | 8,7640 | 8,7564 | 8,7640 |
| 1274,5 | 8,6597 | 9,1739 | 9,1609 | 9,1526 | 9,1526 |
| 1332,5 | 8,9848 | 9,3982 | 9,3788 | 9,3726 | 9,3788 |

**Table 4.27:** Half value layer (HVL) results for the M-ABS-Gd20

| Energy (keV) | Experimental (cm) | EpiXS (cm) | Xcom (cm) | Geant4 (cm) | FLUKA (cm) |
|---|---|---|---|---|---|
| 59,5 | 0,2533 | 0,2440 | 0,2441 | 0,2511 | 0,2460 |
| 80,9 | 0,5538 | 0,5043 | 0,5054 | 0,5252 | 0,5063 |
| 276,3 | 3,5372 | 3,7308 | 3,7300 | 3,8514 | 3,7300 |
| 302,8 | 3,9710 | 4,0276 | 4,0296 | 4,1429 | 4,0296 |
| 356 | 4,2582 | 4,5492 | 4,5455 | 4,6431 | 4,5492 |
| 383,8 | 4,6123 | 4,7823 | 4,7799 | 4,8710 | 4,7823 |
| 511 | 6,1033 | 5,6896 | 5,6860 | 5,7366 | 5,6919 |
| 661,6 | 6,7078 | 6,5546 | 6,5464 | 6,5629 | 6,5629 |
| 1173,2 | 9,2204 | 8,8591 | 8,8425 | 8,8302 | 8,8425 |
| 1274,5 | 10,0256 | 9,2520 | 9,2400 | 9,2267 | 9,2520 |
| 1332,5 | 9,1835 | 9,4767 | 9,4573 | 9,4470 | 9,4573 |

#### 4.1.1.4. Tenth value layer (TVL) results for the M-series

Following the HVL values, the other results to be presented are the tenth value layers (TVL) of the samples. Tenth Value Layer" (Tenth Value Layer - TVL) is a term used in the field of radiation shielding or radiation protection. TVL denotes how much a specific type or energy of radiation can reduce or block the thickness of a protective material, allowing only one-tenth (10%) of the radiation to pass through. This term is used to measure how much radiation decreases or will decrease as it passes through shielding material The smaller this value, the better the gamma radiation shielding capability of the sample. When the tables are examined, it is observed that as gamma energy increases, the TVL value also increases. There is alignment among the experimental, theoretical, and simulation results, with the maximum discrepancy being around 6-7%.

**Table 4.28:** Tenth value layer (TVL) results for the M-ABS-0

| Energy (keV) | Experimental (cm) | EpiXS (cm) | Xcom (cm) | Geant4 (cm) | FLUKA (cm) |
|---|---|---|---|---|---|
| 59,5 | 11,9935 | 11,6370 | 11,6336 | 12,2217 | 11,6166 |
| 80,9 | 12,5694 | 12,7037 | 12,6980 | 13,0875 | 12,6890 |
| 276,3 | 19,1331 | 18,4966 | 18,4746 | 18,6300 | 18,4654 |
| 302,8 | 20,1591 | 19,1187 | 19,1189 | 19,2329 | 19,1021 |
| 356 | 20,1257 | 20,3483 | 20,3238 | 20,3862 | 20,3295 |
| 383,8 | 22,6652 | 20,9342 | 20,9250 | 20,9670 | 20,9250 |
| 511 | 25,3430 | 23,5371 | 23,5193 | 23,4534 | 23,4941 |
| 661,6 | 27,4987 | 26,3402 | 26,3132 | 26,1703 | 26,2816 |
| 1173,2 | 36,6690 | 34,6095 | 34,5453 | 34,3990 | 34,4910 |
| 1274,5 | 36,7526 | 36,0927 | 36,0503 | 35,9051 | 35,9911 |
| 1332,5 | 37,0065 | 36,9527 | 36,8809 | 36,7529 | 36,8809 |

**Table 4.29:** Tenth value layer (TVL) results for the M-ABS-Er5

| Energy (keV) | Experimental (cm) | EpiXS (cm) | Xcom (cm) | Geant4 (cm) | FLUKA (cm) |
|---|---|---|---|---|---|
| 59,5 | 2,8326 | 2,6813 | 2,6600 | 2,7594 | 2,6573 |
| 80,9 | 4,9754 | 4,7597 | 4,7629 | 4,9218 | 4,7575 |
| 276,3 | 17,0996 | 16,4685 | 16,4570 | 16,7181 | 16,4570 |
| 302,8 | 17,9369 | 17,2773 | 17,2703 | 17,5010 | 17,2846 |
| 356 | 19,7203 | 18,7531 | 18,7365 | 18,8935 | 18,7365 |
| 383,8 | 20,2793 | 19,4284 | 19,4311 | 19,5543 | 19,4311 |
| 511 | 23,7823 | 22,2374 | 22,2193 | 22,2325 | 22,2374 |
| 661,6 | 26,7922 | 25,1059 | 25,0791 | 24,9996 | 25,1393 |
| 1173,2 | 35,2844 | 33,2722 | 33,2111 | 33,0968 | 33,1586 |
| 1274,5 | 36,7526 | 34,7135 | 34,6720 | 34,5577 | 34,6720 |
| 1332,5 | 35,5924 | 35,5459 | 35,4757 | 35,3770 | 35,4757 |

**Table 4.30:** Tenth value layer (TVL) results for the M-ABS-Gd5

| Energy (keV) | Experimental (cm) | EpiXS (cm) | Xcom (cm) | Geant4 (cm) | FLUKA (cm) |
|---|---|---|---|---|---|
| 59,5 | 3,0843 | 2,9912 | 2,9928 | 3,0907 | 2,9903 |
| 80,9 | 5,6890 | 5,2400 | 5,2471 | 5,4382 | 5,2426 |
| 276,3 | 17,8128 | 16,7155 | 16,7104 | 16,9575 | 16,7288 |
| 302,8 | 18,7439 | 17,4950 | 17,4902 | 17,7101 | 17,5634 |
| 356 | 19,4844 | 18,9292 | 18,9084 | 19,0751 | 18,9634 |
| 383,8 | 20,6433 | 19,5876 | 19,5786 | 19,7036 | 19,5786 |
| 511 | 20,6427 | 22,3507 | 22,3327 | 22,3384 | 22,3327 |

| | | | | | |
|---|---|---|---|---|---|
| 661,6 | 26,1196 | 25,1969 | 25,1688 | 25,0828 | 25,1960 |
| 1173,2 | 35,7346 | 33,3397 | 33,2778 | 33,1605 | 33,1867 |
| 1274,5 | 32,2902 | 34,7807 | 34,7373 | 34,6210 | 34,7356 |
| 1332,5 | 35,5924 | 35,6133 | 35,5432 | 35,4406 | 35,5673 |

**Table 4.31:** Tenth value layer (TVL) results for the M-ABS-Er10

| Energy (keV) | Experimental (cm) | EpiXS (cm) | Xcom (cm) | Geant4 (cm) | FLUKA (cm) |
|---|---|---|---|---|---|
| 59,5 | 1,5424 | 1,4543 | 1,4411 | 1,4925 | 1,4633 |
| 80,9 | 2,9790 | 2,8238 | 2,8261 | 2,9226 | 2,8253 |
| 276,3 | 13,7364 | 14,7011 | 14,6972 | 15,0263 | 14,6972 |
| 302,8 | 16,8909 | 15,6272 | 15,6273 | 15,9272 | 15,6151 |
| 356 | 18,5560 | 17,2688 | 17,2439 | 17,4897 | 17,2291 |
| 383,8 | 19,5866 | 18,0083 | 18,0045 | 18,2110 | 18,0369 |
| 511 | 22,8400 | 20,9681 | 20,9499 | 21,0318 | 20,9499 |
| 661,6 | 25,7314 | 23,8792 | 23,8528 | 23,8306 | 23,8792 |
| 1173,2 | 34,4163 | 31,9200 | 31,8569 | 31,7774 | 31,9200 |
| 1274,5 | 35,5291 | 33,3176 | 33,2772 | 33,1916 | 33,2220 |
| 1332,5 | 37,0065 | 34,1217 | 34,0534 | 33,9822 | 34,0534 |

**Table 4.32:** Tenth value layer (TVL) results for the M-ABS-Gd10

| Energy (keV) | Experimental (cm) | EpiXS (cm) | Xcom (cm) | Geant4 (cm) | FLUKA (cm) |
|---|---|---|---|---|---|
| 59,5 | 1,5514 | 1,6501 | 1,4548 | 1,7008 | 1,6267 |
| 80,9 | 3,0734 | 3,1899 | 2,8496 | 3,3173 | 3,1399 |
| 276,3 | 15,4353 | 15,1225 | 14,7406 | 15,4399 | 14,8278 |
| 302,8 | 16,2242 | 16,0078 | 15,6741 | 16,2972 | 15,8684 |
| 356 | 16,2387 | 17,5874 | 17,2970 | 17,7928 | 17,6493 |
| 383,8 | 17,7524 | 18,2999 | 18,0605 | 18,4886 | 18,3838 |
| 511 | 21,1535 | 21,1827 | 21,0028 | 21,2339 | 21,1667 |
| 661,6 | 22,1863 | 24,0547 | 23,9055 | 23,9919 | 23,9948 |
| 1173,2 | 33,5885 | 32,0533 | 31,9274 | 31,9030 | 31,9274 |
| 1274,5 | 34,3820 | 33,4506 | 33,3453 | 33,3176 | 33,3453 |
| 1332,5 | 33,8620 | 34,2552 | 34,1287 | 34,1084 | 34,1287 |

**Table 4.33:** Tenth value layer (TVL) results for the M-ABS-Er10Gd5

| Energy (keV) | Experimental (cm) | EpiXS (cm) | Xcom (cm) | Geant4 (cm) | FLUKA (cm) |
|---|---|---|---|---|---|
| 59,5 | 1,0722 | 1,0093 | 1,0027 | 1,0357 | 1,0273 |
| 80,9 | 2,2062 | 2,0359 | 2,0385 | 2,1115 | 2,0354 |
| 276,3 | 14,0479 | 13,3237 | 13,3206 | 13,6948 | 13,3206 |
| 302,8 | 14,6392 | 14,3035 | 14,3000 | 14,6539 | 14,3107 |
| 356 | 14,8631 | 16,0264 | 16,0049 | 16,3033 | 16,0049 |
| 383,8 | 15,9830 | 16,7984 | 16,7946 | 17,0561 | 16,7946 |
| 511 | 19,5744 | 19,8288 | 19,8128 | 19,9471 | 19,7922 |
| 661,6 | 22,1863 | 22,7441 | 22,7170 | 22,7419 | 22,7419 |
| 1173,2 | 32,0433 | 30,6183 | 30,5625 | 30,5033 | 30,5625 |
| 1274,5 | 31,3340 | 31,9706 | 31,9294 | 31,8696 | 31,9706 |
| 1332,5 | 31,9153 | 32,7458 | 32,6793 | 32,6307 | 32,6793 |

**Table 4.34:** Tenth value layer (TVL) results for the M-ABS-Er5Gd10

| Energy (keV) | Experimental (cm) | EpiXS (cm) | Xcom (cm) | Geant4 (cm) | FLUKA (cm) |
|---|---|---|---|---|---|
| 59,5 | 1,1183 | 1,0553 | 1,0520 | 1,0851 | 1,0629 |
| 80,9 | 2,3311 | 2,1291 | 2,1328 | 2,2120 | 2,1298 |
| 276,3 | 13,8905 | 13,5043 | 13,5060 | 13,8742 | 13,5156 |
| 302,8 | 15,1885 | 14,4703 | 14,4685 | 14,8179 | 14,4905 |
| 356 | 15,1741 | 16,1705 | 16,1592 | 16,4418 | 16,1866 |
| 383,8 | 16,4540 | 16,9319 | 16,9334 | 17,1850 | 16,9485 |
| 511 | 19,4622 | 19,9303 | 19,9165 | 20,0432 | 19,9165 |
| 661,6 | 23,8340 | 22,8287 | 22,8004 | 22,8198 | 22,8198 |
| 1173,2 | 32,0433 | 30,6841 | 30,6275 | 30,4680 | 30,4680 |
| 1274,5 | 32,2902 | 32,0362 | 31,9932 | 31,9317 | 32,0362 |
| 1332,5 | 32,2872 | 32,8117 | 32,7453 | 32,6937 | 32,7453 |

**Table 4.35:** Tenth value layer (TVL) results for the M-ABS-Er20

| Energy (keV) | Experimental (cm) | EpiXS (cm) | Xcom (cm) | Geant4 (cm) | FLUKA (cm) |
|---|---|---|---|---|---|
| 59,5 | 0,7380 | 0,7054 | 0,6987 | 0,7228 | 0,7028 |
| 80,9 | 1,5605 | 1,4530 | 1,4543 | 1,5045 | 1,4756 |
| 276,3 | 12,2267 | 11,7709 | 11,7686 | 12,1703 | 11,8147 |
| 302,8 | 13,8464 | 12,7929 | 12,7930 | 13,1791 | 12,7930 |
| 356 | 13,8514 | 14,5902 | 14,5778 | 14,9171 | 14,5902 |
| 383,8 | 14,9084 | 15,3975 | 15,3974 | 15,7078 | 15,4106 |
| 511 | 18,2036 | 18,5163 | 18,5002 | 18,6909 | 18,5163 |
| 661,6 | 22,1863 | 21,4481 | 21,4202 | 21,4992 | 21,4736 |
| 1173,2 | 29,9668 | 29,1700 | 29,1134 | 29,0881 | 29,1134 |
| 1274,5 | 28,7670 | 30,4751 | 30,4318 | 30,4042 | 30,4042 |
| 1332,5 | 29,8468 | 31,2201 | 31,1557 | 31,1353 | 31,1557 |

**Table 4.36:** Tenth value layer (TVL) results for the M-ABS-Gd20

| Energy (keV) | Experimental (cm) | EpiXS (cm) | Xcom (cm) | Geant4 (cm) | FLUKA (cm) |
|---|---|---|---|---|---|
| 59,5 | 0,8413 | 0,8105 | 0,8109 | 0,8340 | 0,8171 |
| 80,9 | 1,8398 | 1,6753 | 1,6788 | 1,7448 | 1,7448 |
| 276,3 | 11,7504 | 12,3933 | 12,3908 | 12,7940 | 12,7940 |
| 302,8 | 13,1914 | 13,3795 | 13,3861 | 13,7624 | 13,7624 |
| 356 | 14,1456 | 15,1122 | 15,0997 | 15,4241 | 15,4241 |
| 383,8 | 15,3217 | 15,8864 | 15,8785 | 16,1812 | 16,1812 |
| 511 | 20,2746 | 18,9003 | 18,8884 | 19,0566 | 19,0566 |
| 661,6 | 22,2829 | 21,7740 | 21,7467 | 21,8015 | 21,8015 |
| 1173,2 | 30,6296 | 29,4293 | 29,3742 | 29,3334 | 29,3334 |
| 1274,5 | 33,3044 | 30,7345 | 30,6945 | 30,6504 | 30,6504 |
| 1332,5 | 30,5070 | 31,4809 | 31,4164 | 31,3822 | 31,3822 |

### 4.1.1.5. Mean free path (MFP) results for the M-series

Following the TVL values, the other results to be presented are the mean free path (MFP) of the samples. Mean Free Path (MFP) is an important concept in radiation shielding or radiation protection. MFP measures how far radiation travels without interactions as it progresses through a substance. It defines the radiation's mean free path within a material, and the length of this path is a critical factor in shielding materials and designs. This term is used to measure how much radiation decreases or will decrease as it passes through shielding material The smaller this value, the better the gamma radiation shielding capability of the sample. When the tables are examined, it is observed that as gamma energy increases, the MFP value also increases. There is alignment among the experimental, theoretical, and simulation results, with the maximum discrepancy being around 6-7%.

**Table 4.37:** Mean free path (MFP) results for the the M-ABS-0

| Energy (keV) | Experimental (cm) | EpiXS (cm) | Xcom (cm) | Geant4 (cm) | FLUKA (cm) |
|---|---|---|---|---|---|
| 59,5 | 5,2087 | 5,0539 | 5,0524 | 5,3078 | 5,0450 |
| 80,9 | 5,4588 | 5,5171 | 5,5147 | 5,6838 | 5,5108 |
| 276,3 | 8,3094 | 8,0330 | 8,0234 | 8,0909 | 8,0194 |
| 302,8 | 8,7550 | 8,3032 | 8,3032 | 8,3528 | 8,2959 |
| 356 | 8,7405 | 8,8372 | 8,8265 | 8,8536 | 8,8290 |
| 383,8 | 9,8434 | 9,0916 | 9,0876 | 9,1059 | 9,0876 |
| 511 | 11,0063 | 10,2220 | 10,2143 | 10,1857 | 10,2034 |
| 661,6 | 11,9425 | 11,4394 | 11,4277 | 11,3656 | 11,4140 |
| 1173,2 | 15,9251 | 15,0307 | 15,0029 | 14,9393 | 14,9793 |
| 1274,5 | 15,9614 | 15,6749 | 15,6564 | 15,5934 | 15,6307 |
| 1332,5 | 16,0717 | 16,0483 | 16,0172 | 15,9616 | 16,0172 |

**Table 4.38:** Mean free path (MFP) results for the the M-ABS-Er5

| Energy (keV) | Experimental (cm) | EpiXS (cm) | Xcom (cm) | Geant4 (cm) | FLUKA (cm) |
|---|---|---|---|---|---|
| 59,5 | 1,2302 | 1,1645 | 1,1552 | 1,1984 | 1,1541 |
| 80,9 | 2,1608 | 2,0671 | 2,0685 | 2,1375 | 2,0661 |
| 276,3 | 7,4263 | 7,1522 | 7,1472 | 7,2606 | 7,1472 |
| 302,8 | 7,7899 | 7,5034 | 7,5004 | 7,6006 | 7,5066 |
| 356 | 8,5644 | 8,1444 | 8,1372 | 8,2054 | 8,1372 |
| 383,8 | 8,8072 | 8,4376 | 8,4388 | 8,4923 | 8,4388 |
| 511 | 10,3285 | 9,6576 | 9,6497 | 9,6555 | 9,6576 |
| 661,6 | 11,6357 | 10,9034 | 10,8917 | 10,8572 | 10,9179 |
| 1173,2 | 15,3238 | 14,4499 | 14,4234 | 14,3738 | 14,4006 |
| 1274,5 | 15,9614 | 15,0759 | 15,0579 | 15,0082 | 15,0579 |
| 1332,5 | 15,4576 | 15,4374 | 15,4069 | 15,3640 | 15,4069 |

**Table 4.39:** Mean free path (MFP) results for the the M-ABS-Gd5

| Energy (keV) | Experimental (cm) | EpiXS (cm) | Xcom (cm) | Geant4 (cm) | FLUKA (cm) |
|---|---|---|---|---|---|
| 59,5 | 1,3395 | 1,2991 | 1,2997 | 1,3423 | 1,2987 |
| 80,9 | 2,4707 | 2,2757 | 2,2788 | 2,3618 | 2,2768 |
| 276,3 | 7,7360 | 7,2594 | 7,2572 | 7,3645 | 7,2652 |
| 302,8 | 8,1404 | 7,5980 | 7,5959 | 7,6914 | 7,6277 |
| 356 | 8,4620 | 8,2208 | 8,2118 | 8,2842 | 8,2357 |
| 383,8 | 8,9653 | 8,5068 | 8,5029 | 8,5572 | 8,5029 |
| 511 | 8,9650 | 9,7068 | 9,6990 | 9,7015 | 9,6990 |
| 661,6 | 11,3436 | 10,9429 | 10,9307 | 10,8933 | 10,9425 |
| 1173,2 | 15,5193 | 14,4793 | 14,4523 | 14,4014 | 14,4128 |
| 1274,5 | 14,0235 | 15,1051 | 15,0862 | 15,0357 | 15,0855 |
| 1332,5 | 15,4576 | 15,4667 | 15,4362 | 15,3917 | 15,4467 |

**Table 4.40:** Mean free path (MFP) results for the the M-ABS-Er10

| Energy (keV) | Experimental (cm) | EpiXS (cm) | Xcom (cm) | Geant4 (cm) | FLUKA (cm) |
|---|---|---|---|---|---|
| 59,5 | 0,6699 | 0,6316 | 0,6259 | 0,6482 | 0,6355 |
| 80,9 | 1,2937 | 1,2264 | 1,2273 | 1,2693 | 1,2270 |
| 276,3 | 5,9656 | 6,3846 | 6,3829 | 6,5258 | 6,3829 |
| 302,8 | 7,3356 | 6,7868 | 6,7869 | 6,9171 | 6,7816 |
| 356 | 8,0588 | 7,4997 | 7,4889 | 7,5957 | 7,4825 |
| 383,8 | 8,5063 | 7,8209 | 7,8192 | 7,9089 | 7,8333 |
| 511 | 9,9193 | 9,1063 | 9,0984 | 9,1340 | 9,0984 |
| 661,6 | 11,1750 | 10,3706 | 10,3591 | 10,3495 | 10,3706 |
| 1173,2 | 14,9468 | 13,8627 | 13,8353 | 13,8008 | 13,8627 |
| 1274,5 | 15,4301 | 14,4697 | 14,4521 | 14,4149 | 14,4281 |
| 1332,5 | 16,0717 | 14,8189 | 14,7892 | 14,7583 | 14,7892 |

**Table 4.41:** Mean free path (MFP) results for the the M-ABS-Gd10

| Energy (keV) | Experimental (cm) | EpiXS (cm) | Xcom (cm) | Geant4 (cm) | FLUKA (cm) |
|---|---|---|---|---|---|
| 59,5 | 0,6738 | 0,7166 | 0,6318 | 0,7386 | 0,7065 |
| 80,9 | 1,3348 | 1,3854 | 1,2376 | 1,4407 | 1,3637 |
| 276,3 | 6,7035 | 6,5676 | 6,4018 | 6,7055 | 6,4396 |
| 302,8 | 7,0461 | 6,9521 | 6,8072 | 7,0778 | 6,8916 |
| 356 | 7,0524 | 7,6381 | 7,5120 | 7,7273 | 7,6650 |
| 383,8 | 7,7098 | 7,9475 | 7,8436 | 8,0295 | 7,9840 |
| 511 | 9,1868 | 9,1995 | 9,1214 | 9,2218 | 9,1926 |
| 661,6 | 9,6354 | 10,4468 | 10,3820 | 10,4196 | 10,4208 |
| 1173,2 | 14,5873 | 13,9206 | 13,8659 | 13,8553 | 13,8659 |
| 1274,5 | 14,9319 | 14,5274 | 14,4817 | 14,4696 | 14,4817 |
| 1332,5 | 14,7061 | 14,8768 | 14,8219 | 14,8131 | 14,8219 |

**Table 4.42:** Mean free path (MFP) results for the the M-ABS-Er10Gd5

| Energy (keV) | Experimental (cm) | EpiXS (cm) | Xcom (cm) | Geant4 (cm) | FLUKA (cm) |
|---|---|---|---|---|---|
| 59,5 | 0,4657 | 0,4383 | 0,4355 | 0,4498 | 0,4462 |
| 80,9 | 0,9581 | 0,8842 | 0,8853 | 0,9170 | 0,8840 |
| 276,3 | 6,1009 | 5,7864 | 5,7851 | 5,9476 | 5,7851 |
| 302,8 | 6,3577 | 6,2119 | 6,2104 | 6,3641 | 6,2151 |
| 356 | 6,4550 | 6,9602 | 6,9508 | 7,0804 | 6,9508 |
| 383,8 | 6,9413 | 7,2955 | 7,2938 | 7,4074 | 7,2938 |
| 511 | 8,5011 | 8,6115 | 8,6046 | 8,6629 | 8,5956 |
| 661,6 | 9,6354 | 9,8776 | 9,8659 | 9,8767 | 9,8767 |
| 1173,2 | 13,9162 | 13,2974 | 13,2731 | 13,2474 | 13,2731 |
| 1274,5 | 13,6082 | 13,8846 | 13,8668 | 13,8408 | 13,8846 |
| 1332,5 | 13,8607 | 14,2213 | 14,1924 | 14,1713 | 14,1924 |

**Table 4.43:** Mean free path (MFP) results for the the M-ABS-Er5Gd10

| Energy (keV) | Experimental (cm) | EpiXS (cm) | Xcom (cm) | Geant4 (cm) | FLUKA (cm) |
|---|---|---|---|---|---|
| 59,5 | 0,4857 | 0,4583 | 0,4569 | 0,4713 | 0,4616 |
| 80,9 | 1,0124 | 0,9247 | 0,9262 | 0,9606 | 0,9250 |
| 276,3 | 6,0326 | 5,8648 | 5,8656 | 6,0255 | 5,8697 |
| 302,8 | 6,5963 | 6,2844 | 6,2836 | 6,4353 | 6,2931 |
| 356 | 6,5900 | 7,0228 | 7,0178 | 7,1406 | 7,0297 |
| 383,8 | 7,1459 | 7,3534 | 7,3541 | 7,4634 | 7,3606 |
| 511 | 8,4523 | 8,6556 | 8,6496 | 8,7047 | 8,6496 |
| 661,6 | 10,3510 | 9,9144 | 9,9021 | 9,9105 | 9,9105 |
| 1173,2 | 13,9162 | 13,3259 | 13,3013 | 13,2321 | 13,2321 |
| 1274,5 | 14,0235 | 13,9131 | 13,8945 | 13,8678 | 13,9131 |
| 1332,5 | 14,0221 | 14,2500 | 14,2211 | 14,1987 | 14,2211 |

**Table 4.44:** Mean free path (MFP) results for the the M-ABS-Er20

| Energy (keV) | Experimental (cm) | EpiXS (cm) | Xcom (cm) | Geant4 (cm) | FLUKA (cm) |
|---|---|---|---|---|---|
| 59,5 | 0,3205 | 0,3064 | 0,3035 | 0,3139 | 0,3052 |
| 80,9 | 0,6777 | 0,6310 | 0,6316 | 0,6534 | 0,6409 |
| 276,3 | 5,3100 | 5,1121 | 5,1110 | 5,2855 | 5,1311 |
| 302,8 | 6,0134 | 5,5559 | 5,5559 | 5,7236 | 5,5559 |
| 356 | 6,0156 | 6,3364 | 6,3311 | 6,4784 | 6,3364 |
| 383,8 | 6,4746 | 6,6870 | 6,6870 | 6,8218 | 6,6928 |
| 511 | 7,9057 | 8,0415 | 8,0345 | 8,1173 | 8,0415 |
| 661,6 | 9,6354 | 9,3148 | 9,3027 | 9,3370 | 9,3259 |
| 1173,2 | 13,0144 | 12,6684 | 12,6438 | 12,6328 | 12,6438 |
| 1274,5 | 12,4933 | 13,2352 | 13,2164 | 13,2044 | 13,2044 |
| 1332,5 | 12,9623 | 13,5587 | 13,5307 | 13,5219 | 13,5307 |

**Table 4.45:** Mean free path (MFP) results for the the M-ABS-Er20

| Energy (keV) | Experimental (cm) | EpiXS (cm) | Xcom (cm) | Geant4 (cm) | FLUKA (cm) |
|---|---|---|---|---|---|
| 59,5 | 0,3205 | 0,3064 | 0,3035 | 0,3139 | 0,3052 |
| 80,9 | 0,6777 | 0,6310 | 0,6316 | 0,6534 | 0,6409 |
| 276,3 | 5,3100 | 5,1121 | 5,1110 | 5,2855 | 5,1311 |
| 302,8 | 6,0134 | 5,5559 | 5,5559 | 5,7236 | 5,5559 |
| 356 | 6,0156 | 6,3364 | 6,3311 | 6,4784 | 6,3364 |
| 383,8 | 6,4746 | 6,6870 | 6,6870 | 6,8218 | 6,6928 |
| 511 | 7,9057 | 8,0415 | 8,0345 | 8,1173 | 8,0415 |
| 661,6 | 9,6354 | 9,3148 | 9,3027 | 9,3370 | 9,3259 |
| 1173,2 | 13,0144 | 12,6684 | 12,6438 | 12,6328 | 12,6438 |
| 1274,5 | 12,4933 | 13,2352 | 13,2164 | 13,2044 | 13,2044 |
| 1332,5 | 12,9623 | 13,5587 | 13,5307 | 13,5219 | 13,5307 |

**Table 4.46:** Mean free path (MFP) results for the the M-ABS-Gd20

| Energy (keV) | Experimental (cm) | EpiXS (cm) | Xcom (cm) | Geant4 (cm) | FLUKA (cm) |
|---|---|---|---|---|---|
| 59,5 | 0,3654 | 0,3520 | 0,3522 | 0,3622 | 0,3549 |
| 80,9 | 0,7990 | 0,7276 | 0,7291 | 0,7578 | 0,7305 |
| 276,3 | 5,1031 | 5,3823 | 5,3813 | 5,5564 | 5,3813 |
| 302,8 | 5,7289 | 5,8107 | 5,8135 | 5,9769 | 5,8135 |
| 356 | 6,1433 | 6,5631 | 6,5577 | 6,6986 | 6,5631 |
| 383,8 | 6,6541 | 6,8994 | 6,8959 | 7,0274 | 6,8994 |
| 511 | 8,8051 | 8,2083 | 8,2031 | 8,2762 | 8,2117 |
| 661,6 | 9,6773 | 9,4563 | 9,4445 | 9,4683 | 9,4683 |
| 1173,2 | 13,3022 | 12,7810 | 12,7570 | 12,7393 | 12,7570 |
| 1274,5 | 14,4639 | 13,3478 | 13,3304 | 13,3113 | 13,3478 |
| 1332,5 | 13,2490 | 13,6720 | 13,6440 | 13,6291 | 13,6440 |

#### 4.1.1.6. Radiation protection efficiency (RPE) results for the M-series

Radiation protection efficiency (RPE) is regarded as a significant topic in both academic and industrial contexts, aimed at the management and reduction of radiation exposure. This concept finds importance across various domains such as nuclear energy, medical imaging, and industrial applications, where the protection of radiation workers and the general public is paramount. RPE aims to minimize potential health risks resulting from exposure by assessing the radiation absorption capabilities of materials. In this context, the significance of RPE encompasses the preservation of health standards, adherence to legal regulations, and cost-effectiveness considerations. Aspects like worker safety, environmental impact, and long-term health outcomes constitute fundamental components emphasized by RPE. Therefore, radiation protection efficiency emerges as a multidisciplinary area of research and application within academic literature, demanding a safety-oriented approach.

**Table 4.47:** Radiation Protection Efficiency (RPE) 0,50 mm = 0,05 cm (FLUKA) results for the M series

| Energy (keV) | M-ABS-0 | M-ABS-Er5 | M-ABS-Gd5 | M-ABS-Er10 | M-ABS-Gd10 | M-ABS-Er10Gd5 | M-ABS-Er5Gd10 | M-ABS-Er20 | M-ABS-Gd20 |
|---|---|---|---|---|---|---|---|---|---|
| 59,5 | 0,9376 | 4,0865 | 3,6565 | 7,4237 | 6,5451 | 10,5206 | 10,0664 | 14,7244 | 12,8937 |
| 80,9 | 0,8758 | 2,3120 | 2,0948 | 3,8627 | 3,4111 | 5,3066 | 5,0717 | 7,3669 | 6,3855 |
| 276,3 | 0,6161 | 0,6863 | 0,6766 | 0,7633 | 0,7429 | 0,8372 | 0,8264 | 0,9415 | 0,8958 |
| 302,8 | 0,5968 | 0,6557 | 0,6480 | 0,7202 | 0,7039 | 0,7826 | 0,7740 | 0,8698 | 0,8331 |
| 356 | 0,5632 | 0,6075 | 0,6017 | 0,6561 | 0,6450 | 0,7037 | 0,6978 | 0,7688 | 0,7436 |
| 383,8 | 0,5476 | 0,5870 | 0,5826 | 0,6302 | 0,6208 | 0,6727 | 0,6677 | 0,7303 | 0,7090 |
| 511 | 0,4897 | 0,5165 | 0,5141 | 0,5459 | 0,5407 | 0,5755 | 0,5728 | 0,6141 | 0,6023 |
| 661,6 | 0,4390 | 0,4595 | 0,4579 | 0,4819 | 0,4787 | 0,5050 | 0,5032 | 0,5341 | 0,5267 |
| 1173,2 | 0,3341 | 0,3473 | 0,3466 | 0,3616 | 0,3602 | 0,3767 | 0,3772 | 0,3950 | 0,3917 |
| 1274,5 | 0,3201 | 0,3326 | 0,3320 | 0,3463 | 0,3450 | 0,3606 | 0,3599 | 0,3779 | 0,3749 |
| 1332,5 | 0,3128 | 0,3249 | 0,3243 | 0,3382 | 0,3370 | 0,3522 | 0,3515 | 0,3691 | 0,3662 |

**Table 4.48:** Radiation Protection Efficiency (RPE) 0,75 mm = 0,075 cm (FLUKA) results for the M series

| Energy (keV) | M-ABS-0 | M-ABS-Er5 | M-ABS-Gd5 | M-ABS-Er10 | M-ABS-Gd10 | M-ABS-Er10Gd5 | M-ABS-Er5Gd10 | M-ABS-Er20 | M-ABS-Gd20 |
|---|---|---|---|---|---|---|---|---|---|
| 59,5 | 1,4031 | 6,0667 | 5,4342 | 10,9262 | 9,6553 | 15,3583 | 14,7130 | 21,2525 | 18,7031 |
| 80,9 | 1,3109 | 3,4479 | 3,1257 | 5,7377 | 5,0727 | 7,8533 | 7,5103 | 10,8442 | 9,4236 |
| 276,3 | 0,9227 | 1,0277 | 1,0132 | 1,1427 | 1,1123 | 1,2531 | 1,2370 | 1,4090 | 1,3407 |
| 302,8 | 0,8939 | 0,9819 | 0,9704 | 1,0784 | 1,0541 | 1,1716 | 1,1587 | 1,3018 | 1,2470 |
| 356 | 0,8435 | 0,9099 | 0,9013 | 0,9825 | 0,9659 | 1,0537 | 1,0448 | 1,1510 | 1,1134 |
| 383,8 | 0,8203 | 0,8793 | 0,8726 | 0,9438 | 0,9297 | 1,0074 | 0,9999 | 1,0934 | 1,0616 |
| 511 | 0,7336 | 0,7738 | 0,7701 | 0,8177 | 0,8100 | 0,8620 | 0,8579 | 0,9197 | 0,9021 |
| 661,6 | 0,6577 | 0,6884 | 0,6861 | 0,7221 | 0,7172 | 0,7565 | 0,7539 | 0,8000 | 0,7890 |
| 1173,2 | 0,5008 | 0,5204 | 0,5194 | 0,5420 | 0,5398 | 0,5645 | 0,5652 | 0,5919 | 0,5870 |
| 1274,5 | 0,4798 | 0,4985 | 0,4976 | 0,5189 | 0,5170 | 0,5404 | 0,5394 | 0,5664 | 0,5618 |
| 1332,5 | 0,4688 | 0,4870 | 0,4861 | 0,5069 | 0,5050 | 0,5278 | 0,5268 | 0,5531 | 0,5488 |

**Table 4.49:** Radiation Protection Efficiency (RPE) 10 mm = 1 cm (FLUKA) results for the M series

| Energy (keV) | M-ABS-0 | M-ABS-Er5 | M-ABS-Gd5 | M-ABS-Er10 | M-ABS-Gd10 | M-ABS-Er10Gd5 | M-ABS-Er5Gd10 | M-ABS-Er20 | M-ABS-Gd20 |
|---|---|---|---|---|---|---|---|---|---|
| 59,5 | 17,1718 | 56,5893 | 52,5263 | 78,6204 | 74,1752 | 89,1742 | 88,0204 | 95,8648 | 93,6760 |
| 80,9 | 16,1330 | 37,3645 | 34,5188 | 54,5179 | 50,0488 | 66,3957 | 64,6887 | 78,3566 | 73,2783 |
| 276,3 | 11,6263 | 12,8666 | 12,6970 | 14,2074 | 13,8545 | 15,4760 | 15,2921 | 17,2377 | 16,4707 |
| 302,8 | 11,2832 | 12,3281 | 12,1918 | 13,4605 | 13,1760 | 14,5408 | 14,3921 | 16,0303 | 15,4063 |
| 356 | 10,6803 | 11,4738 | 11,3711 | 12,3356 | 12,1387 | 13,1714 | 13,0681 | 14,3036 | 13,8676 |
| 383,8 | 10,4004 | 11,1085 | 11,0291 | 11,8772 | 11,7098 | 12,6285 | 12,5399 | 13,6351 | 13,2639 |
| 511 | 9,3512 | 9,8386 | 9,7943 | 10,3701 | 10,2766 | 10,9021 | 10,8528 | 11,5907 | 11,3814 |
| 661,6 | 8,4225 | 8,7991 | 8,7712 | 9,2102 | 9,1512 | 9,6291 | 9,5979 | 10,1565 | 10,0230 |
| 1173,2 | 6,4746 | 6,7206 | 6,7082 | 6,9897 | 6,9632 | 7,2708 | 7,2789 | 7,6107 | 7,5495 |
| 1274,5 | 6,2117 | 6,4459 | 6,4345 | 6,7021 | 6,6776 | 6,9702 | 6,9571 | 7,2936 | 7,2372 |
| 1332,5 | 6,0728 | 6,3014 | 6,2905 | 6,5514 | 6,5280 | 6,8133 | 6,8006 | 7,1286 | 7,0745 |

**Table 4.50:** Radiation Protection Efficiency (RPE) 20 mm = 2 cm (FLUKA) results for the M series

| Energy (keV) | M-ABS-0 | M-ABS-Er5 | M-ABS-Gd5 | M-ABS-Er10 | M-ABS-Gd10 | M-ABS-Er10Gd5 | M-ABS-Er5Gd10 | M-ABS-Er20 | M-ABS-Gd20 |
|---|---|---|---|---|---|---|---|---|---|
| 59,5 | 31,3949 | 81,1551 | 77,4625 | 95,4291 | 93,3308 | 98,8280 | 98,5649 | 99,8290 | 99,6001 |
| 80,9 | 29,6633 | 60,7680 | 57,1222 | 79,3138 | 75,0487 | 88,7075 | 87,5311 | 95,3156 | 92,8595 |
| 276,3 | 21,9008 | 24,0777 | 23,7819 | 26,3963 | 25,7895 | 28,5570 | 28,2458 | 31,5040 | 30,2286 |
| 302,8 | 21,2933 | 23,1364 | 22,8972 | 25,1092 | 24,6159 | 26,9672 | 26,7128 | 29,4909 | 28,4390 |
| 356 | 20,2200 | 21,6311 | 21,4491 | 23,1495 | 22,8039 | 24,6079 | 24,4284 | 26,5612 | 25,8121 |
| 383,8 | 19,7191 | 20,9829 | 20,8418 | 22,3438 | 22,0484 | 23,6622 | 23,5074 | 25,4110 | 24,7685 |
| 511 | 17,8279 | 18,7091 | 18,6293 | 19,6648 | 19,4972 | 20,6157 | 20,5277 | 21,8379 | 21,4674 |
| 661,6 | 16,1356 | 16,8239 | 16,7730 | 17,5721 | 17,4649 | 18,3311 | 18,2746 | 19,2815 | 19,0414 |
| 1173,2 | 12,5301 | 12,9896 | 12,9663 | 13,4908 | 13,4415 | 14,0129 | 14,0279 | 14,6422 | 14,5291 |
| 1274,5 | 12,0375 | 12,4763 | 12,4550 | 12,9550 | 12,9093 | 13,4545 | 13,4302 | 14,0552 | 13,9506 |
| 1332,5 | 11,7768 | 12,2058 | 12,1852 | 12,6736 | 12,6298 | 13,1624 | 13,1387 | 13,7490 | 13,6485 |

**Table 4.51:** Radiation Protection Efficiency (RPE) 50mm = 5 cm (FLUKA) results for the M series

| Energy (keV) | M-ABS-0 | M-ABS-Er5 | M-ABS-Gd5 | M-ABS-Er10 | M-ABS-Gd10 | M-ABS-Er10Gd5 | M-ABS-Er5Gd10 | M-ABS-Er20 | M-ABS-Gd20 |
|---|---|---|---|---|---|---|---|---|---|
| 59,5 | 61,0156 | 98,4584 | 97,5886 | 99,9553 | 99,8851 | 99,9985 | 99,9975 | 100,0000 | 99,9999 |
| 80,9 | 58,5088 | 90,3595 | 87,9612 | 98,0537 | 96,8902 | 99,5715 | 99,4510 | 99,9525 | 99,8638 |
| 276,3 | 46,0966 | 49,7747 | 49,2840 | 53,5218 | 52,5579 | 56,8581 | 56,3867 | 61,1704 | 59,3376 |
| 302,8 | 45,0422 | 48,2034 | 47,7994 | 51,4632 | 50,6600 | 54,4178 | 54,0199 | 58,2542 | 56,6797 |
| 356 | 43,1493 | 45,6300 | 45,3138 | 48,2254 | 47,6414 | 50,6469 | 50,3526 | 53,7817 | 52,5941 |
| 383,8 | 42,2529 | 44,4988 | 44,2507 | 46,8577 | 46,3508 | 49,0846 | 48,8260 | 51,9508 | 50,9093 |
| 511 | 38,7916 | 40,4195 | 40,2730 | 42,1551 | 41,8529 | 43,8517 | 43,6960 | 45,9880 | 45,3457 |
| 661,6 | 35,5914 | 36,9047 | 36,8083 | 38,3141 | 38,1134 | 39,7243 | 39,6202 | 41,4627 | 41,0264 |
| 1173,2 | 28,4438 | 29,3800 | 29,3327 | 30,3926 | 30,2933 | 31,4380 | 31,4680 | 32,6855 | 32,4624 |
| 1274,5 | 27,4322 | 28,3338 | 28,2901 | 29,3097 | 29,2170 | 30,3196 | 30,2706 | 31,5223 | 31,3137 |
| 1332,5 | 26,8934 | 27,7787 | 27,7365 | 28,7370 | 28,6476 | 29,7300 | 29,6822 | 30,9108 | 30,7094 |

**Table 4.52:** Radiation Protection Efficiency (RPE) 100 mm = 10 cm (FLUKA) results for the M series

| Energy (keV) | M-ABS-0 | M-ABS-Er5 | M-ABS-Gd5 | M-ABS-Er10 | M-ABS-Gd10 | M-ABS-Er10Gd5 | M-ABS-Er5Gd10 | M-ABS-Er20 | M-ABS-Gd20 |
|---|---|---|---|---|---|---|---|---|---|
| 59,5 | 84,8021 | 99,9762 | 99,9419 | 100,0000 | 99,9999 | 100,0000 | 100,0000 | 100,0000 | 100,0000 |
| 80,9 | 82,7848 | 99,0706 | 98,5507 | 99,9621 | 99,9033 | 99,9982 | 99,9970 | 100,0000 | 99,9998 |
| 276,3 | 70,9443 | 74,7742 | 74,2789 | 78,3978 | 77,4925 | 81,3878 | 80,9788 | 84,9226 | 83,4657 |
| 302,8 | 69,7964 | 73,1711 | 72,7509 | 76,4418 | 75,6557 | 79,2227 | 78,8583 | 82,5729 | 81,2335 |
| 356 | 67,6800 | 70,4390 | 70,0942 | 73,1939 | 72,5858 | 75,6428 | 75,3514 | 78,6387 | 77,5268 |
| 383,8 | 66,6528 | 69,1962 | 68,9202 | 71,7589 | 71,2177 | 74,0762 | 73,8123 | 76,9127 | 75,9011 |
| 511 | 62,5353 | 64,5016 | 64,3269 | 66,5397 | 66,1892 | 68,4736 | 68,2986 | 70,8271 | 70,1291 |
| 661,6 | 58,5154 | 60,1899 | 60,0681 | 61,9485 | 61,7005 | 63,6684 | 63,5427 | 65,7338 | 65,2211 |
| 1173,2 | 48,7972 | 50,1281 | 50,0614 | 51,5480 | 51,4097 | 52,9925 | 53,0336 | 54,6876 | 54,3867 |
| 1274,5 | 47,3392 | 48,6395 | 48,5769 | 50,0288 | 49,8977 | 51,4464 | 51,3782 | 53,1081 | 52,8219 |
| 1332,5 | 46,5543 | 47,8409 | 47,7799 | 49,2158 | 49,0884 | 50,6213 | 50,5541 | 52,2668 | 51,9881 |

#### 4.1.1.7. Buildup factor (energy absorption) results for the M-series

The energy absorption buildup factor (also known as the energy absorption buildup factor) is similar to the exposure buildup factor but focuses on the amount of energy absorbed by the shielding material. This factor is particularly important when considering the effects of radiation on materials and biological tissues, as it accounts for the energy deposited by the radiation within the material. The energy absorption buildup factor considers how much energy is absorbed by the material as radiation passes through it. This factor is also influenced by the energy of the incident radiation, the properties of the shielding material, and the material's thickness. Increase in Energy Absorption: The buildup factor signifies that as the thickness of the material increases or as the energy of the radiation increases, the material absorbs more radiation energy. In other words, the material absorbs more energy and acts as a sink for it. Reduced Penetration into Deeper Regions: When the buildup factor increases, it means that radiation penetrates less into the material and reaches deeper regions less effectively. This implies that the radiation's effect is concentrated closer to the surface. Significant for Protective Purposes: In radiation shielding design, the buildup factor is considered to ensure that radiation's effect reaches the desired depth and absorbs more energy. This is important in designing shielding materials used to reduce the effects of a specific radiation source or protect workers, equipment, and the environment.

**Table 4.53:** Buildup Factor (Energy Absorption) - (1-MFP) results for the M series

| Energy (MeV) | M-ABS-0 | M-ABS-Er5 | M-ABS-Gd5 | M-ABS-Er10 | M-ABS-Gd10 | M-ABS-Er10Gd5 | M-ABS-Er5Gd10 | M-ABS-Er20 | M-ABS-Gd20 |
|---|---|---|---|---|---|---|---|---|---|
| 0,015 | 1,4694 | 1,0540 | 1,0684 | 1,0274 | 1,0323 | 1,0191 | 1,0201 | 1,0144 | 1,0169 |
| 0,02 | 2,0556 | 1,1087 | 1,1336 | 1,0557 | 1,0706 | 1,0407 | 1,0410 | 1,0301 | 1,0386 |
| 0,03 | 3,9189 | 1,2973 | 1,3592 | 1,1595 | 1,1914 | 1,1133 | 1,1202 | 1,0821 | 1,0988 |
| 0,04 | 5,1605 | 1,5834 | 1,6858 | 1,3183 | 1,3818 | 1,2369 | 1,2510 | 1,1673 | 1,2015 |
| 0,05 | 5,6192 | 1,9982 | 2,1850 | 1,5272 | 1,6128 | 1,3976 | 1,4206 | 1,2886 | 1,3430 |
| 0,06 | 5,4082 | 1,3498 | 1,3883 | 1,1778 | 1,2151 | 1,1243 | 1,1309 | 1,1777 | 1,1512 |
| 0,08 | 4,8073 | 1,6100 | 1,6815 | 1,3133 | 1,3673 | 1,2508 | 1,2484 | 1,2667 | 1,2593 |
| 0,1 | 4,2559 | 1,9361 | 2,0481 | 1,4804 | 1,5813 | 1,3510 | 1,3596 | 1,2964 | 1,3227 |
| 0,15 | 3,5456 | 2,7331 | 2,8946 | 2,1368 | 2,2834 | 1,9394 | 1,9717 | 1,7462 | 1,8451 |
| 0,2 | 3,1873 | 3,0445 | 3,1621 | 2,5857 | 2,6936 | 2,4957 | 2,5118 | 2,4039 | 2,4529 |
| 0,3 | 2,7839 | 3,0546 | 3,0836 | 2,8537 | 2,9325 | 2,7071 | 2,7347 | 2,5558 | 2,6400 |
| 0,4 | 2,6121 | 2,8248 | 2,8301 | 2,7738 | 2,7920 | 2,7426 | 2,7488 | 2,7102 | 2,7287 |
| 0,5 | 2,4514 | 2,6258 | 2,6233 | 2,6297 | 2,6165 | 2,6519 | 2,6474 | 2,6751 | 2,6616 |
| 0,6 | 2,3918 | 2,4859 | 2,4841 | 2,5189 | 2,4915 | 2,5642 | 2,5550 | 2,6118 | 2,5838 |
| 0,8 | 2,1959 | 2,2764 | 2,2735 | 2,3283 | 2,2911 | 2,3892 | 2,3765 | 2,4531 | 2,4154 |
| 1 | 2,0868 | 2,1299 | 2,1298 | 2,1905 | 2,1517 | 2,2527 | 2,2396 | 2,3185 | 2,2791 |
| 1,5 | 1,9371 | 1,9417 | 1,9395 | 1,9379 | 1,9372 | 1,9512 | 1,9520 | 1,9469 | 1,9492 |
| 2 | 1,8364 | 1,8438 | 1,8425 | 1,8373 | 1,8375 | 1,8350 | 1,8327 | 1,8294 | 1,8320 |
| 3 | 1,7150 | 1,7098 | 1,7098 | 1,7060 | 1,7066 | 1,6971 | 1,6958 | 1,6914 | 1,6916 |
| 4 | 1,6287 | 1,6233 | 1,6248 | 1,6158 | 1,6167 | 1,6062 | 1,6066 | 1,5953 | 1,5960 |
| 5 | 1,5687 | 1,5611 | 1,5629 | 1,5473 | 1,5487 | 1,5484 | 1,5472 | 1,5263 | 1,5292 |
| 6 | 1,5230 | 1,4997 | 1,4981 | 1,4910 | 1,4936 | 1,4759 | 1,4767 | 1,4560 | 1,4608 |
| 8 | 1,4440 | 1,4240 | 1,4266 | 1,3999 | 1,4019 | 1,3856 | 1,3867 | 1,3700 | 1,3738 |
| 10 | 1,3853 | 1,3619 | 1,3629 | 1,3416 | 1,3443 | 1,3218 | 1,3238 | 1,3043 | 1,3081 |
| 15 | 1,2910 | 1,2693 | 1,2708 | 1,2447 | 1,2474 | 1,2251 | 1,2259 | 1,2227 | 1,2288 |

**Table 4.54:** Buildup Factor (Energy Absorption) - (5-MFP) results for the M series

| Energy (MeV) | M-ABS-0 | M-ABS-Er5 | M-ABS-Gd5 | M-ABS-Er10 | M-ABS-Gd10 | M-ABS-Er10Gd5 | M-ABS-Er5Gd10 | M-ABS-Er20 | M-ABS-Gd20 |
|---|---|---|---|---|---|---|---|---|---|
| 0,015 | 2,2968 | 1,1159 | 1,1477 | 1,0569 | 1,0675 | 1,0410 | 1,0432 | 1,0288 | 1,0335 |
| 0,02 | 5,0519 | 1,2367 | 1,2922 | 1,1188 | 1,1406 | 1,0831 | 1,0876 | 1,0623 | 1,0715 |
| 0,03 | 21,1538 | 1,6905 | 1,8571 | 1,3391 | 1,4119 | 1,2364 | 1,2520 | 1,1629 | 1,2015 |
| 0,04 | 52,5299 | 2,5503 | 2,9408 | 1,7293 | 1,8976 | 1,5124 | 1,5449 | 1,3475 | 1,4316 |
| 0,05 | 77,9751 | 3,9427 | 4,6990 | 2,3485 | 2,6878 | 1,9321 | 2,0011 | 1,6261 | 1,7742 |
| 0,06 | 88,9573 | 1,8048 | 1,9126 | 1,3683 | 1,4562 | 1,2441 | 1,2590 | 1,3326 | 1,2915 |
| 0,08 | 89,2928 | 2,6228 | 2,8789 | 1,7071 | 1,8588 | 1,5251 | 1,5260 | 1,5016 | 1,5162 |
| 0,1 | 79,3780 | 3,7911 | 4,2992 | 2,2284 | 2,4549 | 1,8719 | 1,9061 | 1,6631 | 1,7618 |
| 0,15 | 57,2463 | 7,1696 | 8,2965 | 3,9376 | 4,5998 | 3,2508 | 3,3566 | 2,6582 | 2,9529 |
| 0,2 | 44,2853 | 10,2392 | 11,5365 | 6,3512 | 7,1589 | 5,4705 | 5,6283 | 4,5875 | 5,0542 |
| 0,3 | 29,9667 | 12,8592 | 13,7967 | 9,4243 | 10,3597 | 7,8558 | 8,1399 | 6,3996 | 7,1873 |
| 0,4 | 22,8108 | 12,9333 | 13,5356 | 10,5859 | 11,2664 | 9,4305 | 9,6565 | 8,2613 | 8,9226 |
| 0,5 | 18,3666 | 12,2100 | 12,6113 | 10,6625 | 11,1103 | 9,8834 | 10,0414 | 9,0423 | 9,5322 |
| 0,6 | 15,6210 | 11,3498 | 11,6380 | 10,3154 | 10,6124 | 9,7840 | 9,8961 | 9,1797 | 9,5404 |
| 0,8 | 12,1222 | 9,8372 | 10,0114 | 9,3521 | 9,4593 | 9,1339 | 9,1835 | 8,8525 | 9,0250 |
| 1 | 10,0895 | 8,7546 | 8,8547 | 8,4772 | 8,4955 | 8,4106 | 8,4284 | 8,2923 | 8,3688 |
| 1,5 | 7,4648 | 7,1636 | 7,1978 | 6,9752 | 7,0292 | 6,8217 | 6,8507 | 6,6658 | 6,7492 |
| 2 | 6,1463 | 6,0923 | 6,0998 | 6,0622 | 6,0719 | 6,0272 | 6,0320 | 5,9611 | 5,9889 |
| 3 | 4,8117 | 4,7959 | 4,7967 | 4,7849 | 4,7868 | 4,7650 | 4,7637 | 4,7542 | 4,7582 |
| 4 | 4,1004 | 4,0802 | 4,0825 | 4,0586 | 4,0616 | 4,0396 | 4,0416 | 4,0181 | 4,0229 |
| 5 | 3,6532 | 3,6229 | 3,6255 | 3,5922 | 3,5961 | 3,5636 | 3,5664 | 3,5323 | 3,5393 |
| 6 | 3,3345 | 3,2910 | 3,2926 | 3,2570 | 3,2619 | 3,2237 | 3,2262 | 3,1800 | 3,1892 |
| 8 | 2,8991 | 2,8474 | 2,8509 | 2,7963 | 2,8022 | 2,7557 | 2,7584 | 2,7073 | 2,7227 |
| 10 | 2,6212 | 2,5570 | 2,5609 | 2,5006 | 2,5071 | 2,4530 | 2,4562 | 2,4054 | 2,4164 |
| 15 | 2,1928 | 2,1226 | 2,1269 | 2,0621 | 2,0684 | 2,0130 | 2,0157 | 1,9724 | 1,9812 |

**Table 4.55:** Buildup Factor (Energy Absorption) - (10-MFP) results for the M series

| Energy (MeV) | M-ABS-0 | M-ABS-Er5 | M-ABS-Gd5 | M-ABS-Er10 | M-ABS-Gd10 | M-ABS-Er10Gd5 | M-ABS-Er5Gd10 | M-ABS-Er20 | M-ABS-Gd20 |
|---|---|---|---|---|---|---|---|---|---|
| 0,015 | 2,8777 | 1,1471 | 1,1884 | 1,0729 | 1,0870 | 1,0524 | 1,0550 | 1,0373 | 1,0430 |
| 0,02 | 8,0703 | 1,3042 | 1,3785 | 1,1502 | 1,1774 | 1,1042 | 1,1111 | 1,0780 | 1,0873 |
| 0,03 | 54,3564 | 1,9257 | 2,1650 | 1,4384 | 1,5349 | 1,3014 | 1,3221 | 1,2072 | 1,2570 |
| 0,04 | 211,7680 | 3,2146 | 3,8495 | 1,9726 | 2,2145 | 1,6675 | 1,7121 | 1,4461 | 1,5580 |
| 0,05 | 411,1990 | 5,5546 | 6,9400 | 2,8952 | 3,4398 | 2,2663 | 2,3683 | 1,8231 | 2,0360 |
| 0,06 | 549,6440 | 2,0780 | 2,2335 | 1,4725 | 1,5910 | 1,3082 | 1,3277 | 1,4737 | 1,3951 |
| 0,08 | 629,9960 | 3,3173 | 3,7281 | 1,9358 | 2,1526 | 1,6958 | 1,6906 | 1,6810 | 1,6992 |
| 0,1 | 578,5630 | 5,2909 | 6,2118 | 2,6938 | 3,0292 | 2,1935 | 2,2388 | 1,8989 | 2,0416 |
| 0,15 | 385,7890 | 12,0145 | 14,6551 | 5,4129 | 6,6144 | 4,2624 | 4,4359 | 3,3147 | 3,7806 |
| 0,2 | 265,0720 | 20,2527 | 24,1463 | 10,3257 | 12,1043 | 8,6132 | 8,9432 | 6,6759 | 7,7116 |
| 0,3 | 146,1800 | 29,6886 | 33,4494 | 18,4900 | 21,0153 | 14,3139 | 15,0689 | 10,5386 | 12,5551 |
| 0,4 | 94,1140 | 32,4006 | 35,1307 | 23,5294 | 25,7533 | 19,6364 | 20,4027 | 15,7138 | 17,9186 |
| 0,5 | 67,8529 | 31,3646 | 33,2733 | 24,9104 | 26,6714 | 21,7846 | 22,4201 | 18,4383 | 20,3763 |
| 0,6 | 51,8956 | 29,1120 | 30,4708 | 24,3943 | 25,7819 | 21,9192 | 22,4380 | 19,1827 | 20,8023 |
| 0,8 | 35,2702 | 24,6674 | 25,4744 | 22,0820 | 22,8542 | 20,6480 | 20,9617 | 18,9661 | 19,9784 |
| 1 | 26,8270 | 20,9847 | 21,3585 | 19,5262 | 19,9261 | 18,7347 | 18,9168 | 17,7196 | 18,3474 |
| 1,5 | 16,9917 | 15,9991 | 16,1296 | 15,3524 | 15,5515 | 14,9207 | 15,0139 | 14,4102 | 14,6849 |
| 2 | 12,7835 | 12,5862 | 12,6236 | 12,6182 | 12,6472 | 12,5766 | 12,5980 | 12,4379 | 12,4968 |
| 3 | 8,9539 | 8,9858 | 8,9815 | 9,0324 | 9,0252 | 9,0604 | 9,0538 | 9,1022 | 9,0956 |
| 4 | 7,1622 | 7,1833 | 7,1787 | 7,2119 | 7,2083 | 7,2080 | 7,2125 | 7,2800 | 7,2727 |
| 5 | 6,1068 | 6,1066 | 6,1051 | 6,1175 | 6,1163 | 6,1123 | 6,1147 | 6,1370 | 6,1272 |
| 6 | 5,4029 | 5,3983 | 5,4024 | 5,3885 | 5,3869 | 5,3903 | 5,3910 | 5,3949 | 5,3943 |
| 8 | 4,5098 | 4,4678 | 4,4681 | 4,4502 | 4,4524 | 4,4338 | 4,4350 | 4,4066 | 4,4076 |
| 10 | 3,9454 | 3,8941 | 3,8976 | 3,8583 | 3,8616 | 3,8324 | 3,8322 | 3,8172 | 3,8237 |
| 15 | 3,1396 | 3,0632 | 3,0669 | 3,0215 | 3,0251 | 2,9858 | 2,9883 | 2,9401 | 2,9347 |

**Table 4.56:** Buildup Factor (Energy Absorption) - (40-MFP) results for the M series

| Energy (MeV) | M-ABS-0 | M-ABS-Er5 | M-ABS-Gd5 | M-ABS-Er10 | M-ABS-Gd10 | M-ABS-Er10Gd5 | M-ABS-Er5Gd10 | M-ABS-Er20 | M-ABS-Gd20 |
|---|---|---|---|---|---|---|---|---|---|
| 0,015 | 4,9067 | 1,2247 | 1,2897 | 1,1066 | 1,1277 | 1,0777 | 1,0827 | 1,0599 | 1,0689 |
| 0,02 | 26,0081 | 1,4741 | 1,6029 | 1,2295 | 1,2767 | 1,1379 | 1,1644 | 1,1190 | 1,1304 |
| 0,03 | 680,4500 | 2,6267 | 3,1323 | 1,7037 | 1,8729 | 1,4654 | 1,5000 | 1,3164 | 1,3960 |
| 0,04 | 7497,0800 | 5,5289 | 7,2275 | 2,6795 | 3,1759 | 2,0902 | 2,1714 | 1,7020 | 1,8959 |
| 0,05 | 32346,2000 | 13,0684 | 19,7803 | 4,7312 | 6,1584 | 3,2898 | 3,5118 | 2,3856 | 2,8012 |
| 0,06 | 68351,9000 | 2,8819 | 3,2011 | 1,7404 | 1,9491 | 1,4684 | 1,5002 | 5,8749 | 2,1318 |
| 0,08 | 106904,0000 | 5,7361 | 6,8113 | 2,5812 | 3,0079 | 2,3183 | 2,2092 | 3,1435 | 2,7776 |
| 0,1 | 103185,0000 | 11,5110 | 14,4887 | 4,0849 | 4,8674 | 3,2842 | 3,3028 | 2,8869 | 3,1386 |
| 0,15 | 49187,1000 | 45,1702 | 64,7160 | 12,2190 | 16,2303 | 8,8779 | 9,3815 | 6,1438 | 7,4754 |
| 0,2 | 21729,4000 | 124,9450 | 179,1460 | 37,6143 | 45,1472 | 43,2524 | 43,7540 | 27,4935 | 38,0445 |
| 0,3 | 6123,9700 | 239,6580 | 316,4710 | 110,5100 | 118,9340 | 82,9634 | 89,6396 | 45,1423 | 65,6705 |
| 0,4 | 2555,3700 | 327,5890 | 442,3670 | 198,5870 | 204,1420 | 159,2920 | 169,4730 | 98,3663 | 133,6620 |
| 0,5 | 1364,2400 | 312,6250 | 367,9650 | 226,7510 | 235,7010 | 188,1230 | 197,7850 | 129,9250 | 164,6080 |
| 0,6 | 778,5140 | 279,1100 | 325,9170 | 214,4780 | 226,5620 | 178,8690 | 187,3640 | 130,4660 | 159,5240 |
| 0,8 | 352,6050 | 207,9140 | 225,9790 | 177,3180 | 186,2430 | 155,0740 | 160,3000 | 126,1520 | 143,6200 |
| 1 | 221,2090 | 159,5870 | 160,2310 | 136,8980 | 141,0290 | 125,5190 | 128,3110 | 109,8280 | 119,4910 |
| 1,5 | 100,8710 | 96,3485 | 97,1249 | 91,4883 | 93,1119 | 89,4640 | 89,9904 | 86,6239 | 88,1232 |
| 2 | 63,2822 | 62,3279 | 62,7617 | 65,7179 | 65,6722 | 66,8984 | 66,7852 | 67,6479 | 67,3549 |
| 3 | 35,7961 | 37,0425 | 36,8607 | 38,9468 | 38,6543 | 39,9653 | 39,6832 | 41,8797 | 41,3031 |
| 4 | 25,3249 | 26,5399 | 26,4152 | 27,9553 | 27,7435 | 28,5507 | 28,6045 | 30,8091 | 30,4252 |
| 5 | 20,0983 | 21,1371 | 21,0601 | 22,4423 | 22,2507 | 23,6248 | 23,5402 | 23,9395 | 23,6022 |
| 6 | 17,0895 | 17,2402 | 17,2070 | 17,8980 | 17,7663 | 18,7448 | 18,6839 | 20,2010 | 19,7985 |
| 8 | 13,7621 | 14,1728 | 14,1109 | 15,1645 | 15,0211 | 16,1986 | 16,1236 | 17,1663 | 16,3313 |
| 10 | 10,9551 | 11,6135 | 11,5741 | 12,4251 | 12,3126 | 13,2516 | 13,1695 | 14,9474 | 14,6492 |
| 15 | 7,8868 | 8,2704 | 8,2274 | 9,1592 | 9,0452 | 10,0066 | 9,9496 | 11,6308 | 11,0875 |

#### 4.1.1.8. Buildup factor (exposure) results for the M-series

Buildup factor (exposure)" is a term used in the field of radiation shielding or radiation protection. This factor represents the process of radiation penetrating into a material or substance, interacting inside, and losing energy during that interaction. Additionally, this term is a measure of the average unit exposure of radiation in a unit area within a material. Relevance in Radiation Shielding Design: This factor is used in radiation shielding design. To assess the effectiveness of a design, it's important to determine how deeply radiation penetrates into a material and how much it is absorbed by that material. This aids in the proper design of protective shields. Material and Energy Dependent: The buildup factor can vary depending on the type of radiation (e.g., gamma rays, X-rays, neutrons) and the energy level. Different types of radiation and energy levels have different buildup factors. Used in Exposure Calculations: This term is used in calculating radiation exposure or determining radiation protection requirements. Exposure is a measure used to assess radiation dose.

**Table 4.57:** Buildup Factor (Exposure) - (1-MFP) results for the M series

| Energy (MeV) | M-ABS-0 | M-ABS-Er5 | M-ABS-Gd5 | M-ABS-Er10 | M-ABS-Gd10 | M-ABS-Er10Gd5 | M-ABS-Er5Gd10 | M-ABS-Er20 | M-ABS-Gd20 |
|---|---|---|---|---|---|---|---|---|---|
| 0,015 | 1,4550 | 1,0549 | 1,0690 | 1,0277 | 1,0323 | 1,0194 | 1,0207 | 1,0152 | 1,0174 |
| 0,02 | 2,0244 | 1,1086 | 1,1342 | 1,0546 | 1,0659 | 1,0404 | 1,0410 | 1,0324 | 1,0381 |
| 0,03 | 3,7422 | 1,2911 | 1,3489 | 1,1590 | 1,1899 | 1,1133 | 1,1202 | 1,0821 | 1,0988 |
| 0,04 | 5,5764 | 1,5577 | 1,6500 | 1,3111 | 1,3679 | 1,2301 | 1,2427 | 1,1635 | 1,1982 |
| 0,05 | 6,9982 | 1,8401 | 2,0622 | 1,4891 | 1,5739 | 1,3684 | 1,3893 | 1,2686 | 1,3185 |
| 0,06 | 7,4662 | 1,3070 | 1,3402 | 1,1574 | 1,1898 | 1,1118 | 1,1174 | 1,4666 | 1,2997 |
| 0,08 | 7,0097 | 1,4670 | 1,5200 | 1,2449 | 1,2872 | 1,2311 | 1,2100 | 1,3700 | 1,3053 |
| 0,1 | 6,3242 | 1,5958 | 1,6647 | 1,3333 | 1,3803 | 1,2663 | 1,2722 | 1,2287 | 1,2468 |
| 0,15 | 4,6628 | 1,8120 | 1,8909 | 1,5259 | 1,5948 | 1,4437 | 1,4570 | 1,3642 | 1,4049 |
| 0,2 | 3,7816 | 1,9296 | 1,9973 | 1,6832 | 1,7409 | 1,6216 | 1,6326 | 1,5587 | 1,5923 |
| 0,3 | 3,1486 | 2,0060 | 2,0549 | 1,8280 | 1,8715 | 1,7531 | 1,7672 | 1,6758 | 1,7188 |
| 0,4 | 2,8464 | 2,0047 | 2,0433 | 1,8723 | 1,9030 | 1,8198 | 1,8302 | 1,7652 | 1,7964 |
| 0,5 | 2,6609 | 1,9706 | 2,0060 | 1,8803 | 1,9018 | 1,8445 | 1,8516 | 1,8069 | 1,8287 |
| 0,6 | 2,5437 | 1,9458 | 1,9707 | 1,8675 | 1,8823 | 1,8432 | 1,8481 | 1,8176 | 1,8327 |
| 0,8 | 2,3202 | 1,9008 | 1,9166 | 1,8363 | 1,8431 | 1,8251 | 1,8274 | 1,8134 | 1,8203 |
| 1 | 2,2036 | 1,8382 | 1,8523 | 1,8078 | 1,8130 | 1,7995 | 1,8013 | 1,7907 | 1,7960 |
| 1,5 | 2,0523 | 1,8107 | 1,8265 | 1,7527 | 1,7681 | 1,7251 | 1,7330 | 1,6829 | 1,7055 |
| 2 | 1,9355 | 1,8037 | 1,8126 | 1,7628 | 1,7728 | 1,7438 | 1,7468 | 1,7207 | 1,7299 |
| 3 | 1,7738 | 1,7096 | 1,7119 | 1,6840 | 1,6883 | 1,6705 | 1,6716 | 1,6588 | 1,6611 |
| 4 | 1,6736 | 1,6260 | 1,6273 | 1,6107 | 1,6129 | 1,6018 | 1,6000 | 1,5896 | 1,5868 |
| 5 | 1,5909 | 1,5572 | 1,5587 | 1,5424 | 1,5442 | 1,5378 | 1,5375 | 1,5216 | 1,5237 |
| 6 | 1,5356 | 1,5119 | 1,5137 | 1,4989 | 1,5000 | 1,4879 | 1,4894 | 1,4740 | 1,4782 |
| 8 | 1,4447 | 1,4211 | 1,4219 | 1,4117 | 1,4127 | 1,4057 | 1,4058 | 1,3920 | 1,3958 |
| 10 | 1,3796 | 1,3602 | 1,3606 | 1,3531 | 1,3540 | 1,3463 | 1,3469 | 1,3329 | 1,3351 |
| 15 | 1,2827 | 1,2697 | 1,2705 | 1,2642 | 1,2643 | 1,2628 | 1,2631 | 1,2424 | 1,2464 |

**Table 4.58:** Buildup Factor (Exposure) - (5-MFP) results for the M series

| Energy (MeV) | M-ABS-0 | M-ABS-Er5 | M-ABS-Gd5 | M-ABS-Er10 | M-ABS-Gd10 | M-ABS-Er10Gd5 | M-ABS-Er5Gd10 | M-ABS-Er20 | M-ABS-Gd20 |
|---|---|---|---|---|---|---|---|---|---|
| 0,015 | 2,2750 | 1,1141 | 1,1452 | 1,0577 | 1,0685 | 1,0410 | 1,0431 | 1,0310 | 1,0351 |
| 0,02 | 4,9152 | 1,2362 | 1,2899 | 1,1177 | 1,1383 | 1,0847 | 1,0894 | 1,0607 | 1,0722 |
| 0,03 | 20,0980 | 1,6805 | 1,8409 | 1,3385 | 1,4096 | 1,2364 | 1,2520 | 1,1629 | 1,2015 |
| 0,04 | 58,2591 | 2,4929 | 2,8599 | 1,7146 | 1,8723 | 1,5026 | 1,5341 | 1,3437 | 1,4252 |
| 0,05 | 105,9090 | 3,7099 | 4,3930 | 2,2583 | 2,5651 | 1,8785 | 1,9417 | 1,5936 | 1,7336 |
| 0,06 | 141,9580 | 1,7221 | 1,8150 | 1,3420 | 1,4197 | 1,2291 | 1,2427 | 2,0144 | 1,6398 |
| 0,08 | 162,4530 | 2,2728 | 2,4609 | 1,5858 | 1,7032 | 1,5356 | 1,4884 | 1,7886 | 1,6868 |
| 0,1 | 151,0840 | 2,8929 | 3,2028 | 1,8879 | 2,0495 | 1,6557 | 1,6788 | 1,5162 | 1,5819 |
| 0,15 | 106,0730 | 4,3300 | 4,8645 | 2,7500 | 3,0794 | 2,3726 | 2,4314 | 2,0425 | 2,2068 |
| 0,2 | 73,8728 | 5,6519 | 6,2755 | 3,7851 | 4,1889 | 3,2772 | 3,3649 | 2,8054 | 3,0511 |
| 0,3 | 45,7394 | 7,0699 | 7,6509 | 5,2053 | 5,6617 | 4,4621 | 4,5959 | 3,7779 | 4,1478 |
| 0,4 | 32,6625 | 7,6565 | 8,1192 | 6,0838 | 6,4984 | 5,4144 | 5,5423 | 4,7727 | 5,1318 |
| 0,5 | 25,2046 | 7,7446 | 8,1223 | 6,4693 | 6,8212 | 5,9067 | 6,0163 | 5,3545 | 5,6701 |
| 0,6 | 20,4726 | 7,6139 | 7,9265 | 6,5480 | 6,8452 | 6,0757 | 6,1700 | 5,6051 | 5,8788 |
| 0,8 | 14,9637 | 7,1818 | 7,3984 | 6,4396 | 6,6444 | 6,1118 | 6,1791 | 5,7792 | 5,9743 |
| 1 | 11,9777 | 6,7123 | 6,8729 | 6,1523 | 6,2998 | 5,9201 | 5,9687 | 5,6807 | 5,8232 |
| 1,5 | 8,7045 | 6,2592 | 6,3722 | 5,8096 | 5,9304 | 5,5694 | 5,6255 | 5,2695 | 5,4295 |
| 2 | 6,9047 | 5,8482 | 5,9142 | 5,6203 | 5,6749 | 5,4692 | 5,4924 | 5,3004 | 5,3826 |
| 3 | 5,1689 | 4,7958 | 4,8104 | 4,6864 | 4,7049 | 4,6365 | 4,6404 | 4,5881 | 4,6036 |
| 4 | 4,2951 | 4,1053 | 4,1107 | 4,0540 | 4,0613 | 4,0116 | 4,0153 | 4,0125 | 4,0107 |
| 5 | 3,7374 | 3,6216 | 3,6250 | 3,5909 | 3,5946 | 3,5720 | 3,5733 | 3,5677 | 3,5670 |
| 6 | 3,3935 | 3,3117 | 3,3135 | 3,2915 | 3,2938 | 3,2810 | 3,2811 | 3,2873 | 3,2807 |
| 8 | 2,9058 | 2,8539 | 2,8554 | 2,8432 | 2,8438 | 2,8398 | 2,8396 | 2,8348 | 2,8347 |
| 10 | 2,5923 | 2,5555 | 2,5565 | 2,5427 | 2,5441 | 2,5333 | 2,5331 | 2,5348 | 2,5360 |
| 15 | 2,1557 | 2,1241 | 2,1261 | 2,1073 | 2,1081 | 2,1014 | 2,1018 | 2,0836 | 2,0872 |

**Table 4.59:** Buildup Factor (Exposure) - (10-MFP) results for the M series

| Energy (MeV) | M-ABS-0 | M-ABS-Er5 | M-ABS-Gd5 | M-ABS-Er10 | M-ABS-Gd10 | M-ABS-Er10Gd5 | M-ABS-Er5Gd10 | M-ABS-Er20 | M-ABS-Gd20 |
|---|---|---|---|---|---|---|---|---|---|
| 0,015 | 2,8518 | 1,1454 | 1,1857 | 1,0736 | 1,0874 | 1,0529 | 1,0558 | 1,0414 | 1,0458 |
| 0,02 | 7,8317 | 1,3045 | 1,3756 | 1,1491 | 1,1771 | 1,1056 | 1,1126 | 1,0741 | 1,0877 |
| 0,03 | 51,9105 | 1,9144 | 2,1470 | 1,4369 | 1,5322 | 1,3014 | 1,3218 | 1,2072 | 1,2570 |
| 0,04 | 236,5460 | 3,1395 | 3,7483 | 1,9551 | 2,1869 | 1,6566 | 1,7000 | 1,4419 | 1,5509 |
| 0,05 | 576,5420 | 5,2701 | 6,4796 | 2,7827 | 3,2768 | 2,2026 | 2,2971 | 1,7897 | 1,9891 |
| 0,06 | 926,7310 | 1,9820 | 2,1200 | 1,4443 | 1,5505 | 1,2937 | 1,3117 | 2,9750 | 2,0069 |
| 0,08 | 1248,0000 | 2,8579 | 3,1699 | 1,7964 | 1,9665 | 1,7704 | 1,6793 | 2,3311 | 2,0971 |
| 0,1 | 1206,8200 | 3,9947 | 4,5736 | 2,2704 | 2,5269 | 1,9150 | 1,9498 | 1,7030 | 1,8031 |
| 0,15 | 827,7590 | 7,1498 | 8,4215 | 3,8079 | 4,4415 | 3,1312 | 3,2351 | 2,5592 | 2,8412 |
| 0,2 | 523,1620 | 10,9180 | 12,7483 | 6,1094 | 7,0433 | 5,0073 | 5,1998 | 3,9765 | 4,5108 |
| 0,3 | 259,0670 | 15,7931 | 17,8291 | 9,9596 | 11,2653 | 7,9075 | 8,2700 | 6,1220 | 7,0722 |
| 0,4 | 153,9230 | 18,4633 | 20,1539 | 13,0519 | 14,4212 | 10,8963 | 11,3017 | 8,9199 | 10,0131 |
| 0,5 | 103,8690 | 19,1546 | 20,5215 | 14,5721 | 15,8380 | 12,5944 | 12,9747 | 10,7237 | 11,7830 |
| 0,6 | 75,2377 | 18,8885 | 20,0447 | 14,9862 | 16,1145 | 13,2296 | 13,5765 | 11,5357 | 12,5133 |
| 0,8 | 46,5952 | 17,3862 | 18,1759 | 14,8196 | 15,6351 | 13,5146 | 13,7813 | 12,2149 | 12,9733 |
| 1 | 33,3707 | 15,6407 | 16,1165 | 13,8077 | 14,3823 | 12,9003 | 13,0899 | 11,9758 | 12,5244 |
| 1,5 | 20,4399 | 13,7635 | 14,0551 | 12,5677 | 12,8879 | 11,9261 | 12,0614 | 11,2022 | 11,5887 |
| 2 | 14,6235 | 12,0317 | 12,2024 | 11,6249 | 11,7320 | 11,2958 | 11,3465 | 10,9778 | 11,1431 |
| 3 | 9,7024 | 8,9868 | 9,0140 | 8,8297 | 8,8566 | 8,8049 | 8,8082 | 8,7926 | 8,7997 |
| 4 | 7,5166 | 7,2227 | 7,2306 | 7,2084 | 7,2094 | 7,1755 | 7,1872 | 7,2899 | 7,2712 |
| 5 | 6,2482 | 6,1103 | 6,1129 | 6,1299 | 6,1252 | 6,1952 | 6,1891 | 6,2719 | 6,2481 |
| 6 | 5,4976 | 5,4191 | 5,4168 | 5,4758 | 5,4673 | 5,5304 | 5,5263 | 5,6265 | 5,5991 |
| 8 | 4,4997 | 4,4851 | 4,4833 | 4,5357 | 4,5280 | 4,5879 | 4,5844 | 4,6693 | 4,6419 |
| 10 | 3,8918 | 3,8944 | 3,8925 | 3,9356 | 3,9298 | 3,9797 | 3,9741 | 4,0888 | 4,0783 |
| 15 | 3,0692 | 3,0634 | 3,0634 | 3,0863 | 3,0820 | 3,1183 | 3,1162 | 3,1726 | 3,1588 |

**Table 4.60:** Buildup Factor (Exposure) - (40-MFP) results for the M series

| Energy (MeV) | M-ABS-0 | M-ABS-Er5 | M-ABS-Gd5 | M-ABS-Er10 | M-ABS-Gd10 | M-ABS-Er10Gd5 | M-ABS-Er5Gd10 | M-ABS-Er20 | M-ABS-Gd20 |
|---|---|---|---|---|---|---|---|---|---|
| 0,015 | 4,8482 | 1,2247 | 1,2890 | 1,1067 | 1,1264 | 1,0783 | 1,0833 | 1,0619 | 1,0689 |
| 0,02 | 25,4163 | 1,4766 | 1,6006 | 1,2266 | 1,2765 | 1,1420 | 1,1658 | 1,1069 | 1,1269 |
| 0,03 | 670,6720 | 2,6031 | 3,1027 | 1,7026 | 1,8731 | 1,4654 | 1,4999 | 1,3164 | 1,3960 |
| 0,04 | 8515,6800 | 5,4035 | 7,1151 | 2,6502 | 3,1335 | 2,0808 | 2,1626 | 1,6972 | 1,8866 |
| 0,05 | 47772,6000 | 12,4225 | 18,6290 | 4,5702 | 5,8834 | 3,2136 | 3,4232 | 2,3575 | 2,7535 |
| 0,06 | 123289,0000 | 2,7632 | 3,0664 | 1,7152 | 1,9059 | 1,4607 | 1,4911 | 1302640,0000 | 73,7783 |
| 0,08 | 227412,0000 | 4,9954 | 5,8852 | 2,4218 | 2,7846 | 3,2841 | 2,4584 | 1482,5200 | 44,1921 |
| 0,1 | 228711,0000 | 8,6742 | 10,7812 | 3,4965 | 4,1258 | 2,7769 | 2,8319 | 2,3663 | 2,5747 |
| 0,15 | 117447,0000 | 24,8945 | 33,3599 | 8,1741 | 10,5606 | 6,2753 | 6,5709 | 4,6163 | 5,4361 |
| 0,2 | 51876,4000 | 58,0355 | 79,0550 | 20,0647 | 24,7588 | 16,7134 | 17,5462 | 11,1461 | 14,1983 |
| 0,3 | 12845,3000 | 117,6170 | 151,6740 | 50,7110 | 60,0293 | 35,0670 | 37,9412 | 21,2989 | 28,4673 |
| 0,4 | 4027,3700 | 167,7570 | 199,6130 | 91,0801 | 105,8180 | 66,3936 | 71,0755 | 44,3287 | 56,3090 |
| 0,5 | 2197,8100 | 179,6780 | 203,7980 | 112,9490 | 129,1800 | 86,8572 | 91,8661 | 62,9937 | 76,3025 |
| 0,6 | 1117,5600 | 172,3990 | 202,1090 | 115,1550 | 130,4600 | 91,0492 | 95,7722 | 68,8115 | 81,4445 |
| 0,8 | 482,5780 | 142,1410 | 158,3050 | 107,9370 | 118,8370 | 90,7492 | 94,2148 | 74,4144 | 83,8244 |
| 1 | 281,7520 | 116,9290 | 118,0170 | 90,6698 | 97,3351 | 80,2934 | 82,4416 | 70,0193 | 76,0741 |
| 1,5 | 124,1830 | 82,2057 | 84,0105 | 74,0857 | 76,2828 | 70,6572 | 70,6051 | 68,8001 | 70,3181 |
| 2 | 73,7220 | 59,4009 | 60,5513 | 60,2506 | 60,4691 | 59,9484 | 59,9473 | 61,0677 | 61,6827 |
| 3 | 38,9194 | 37,2532 | 37,2271 | 38,0279 | 37,9091 | 38,8313 | 38,7064 | 40,5194 | 39,9295 |
| 4 | 26,6029 | 26,5635 | 26,5020 | 27,9851 | 27,8043 | 28,7912 | 28,7774 | 29,8959 | 29,3390 |
| 5 | 20,4854 | 21,0703 | 20,9982 | 21,5046 | 21,4545 | 25,2131 | 24,3986 | 26,4077 | 26,0731 |
| 6 | 17,1650 | 17,5338 | 17,6507 | 19,1737 | 18,7932 | 21,3299 | 21,3126 | 22,4585 | 22,3302 |
| 8 | 12,4318 | 14,2706 | 14,2454 | 15,1543 | 15,0084 | 16,2478 | 16,1717 | 18,0154 | 17,5056 |
| 10 | 11,0784 | 11,5433 | 11,4751 | 12,8430 | 12,6664 | 14,2056 | 14,0895 | 16,7553 | 16,4561 |
| 15 | 7,7771 | 8,2624 | 8,2106 | 9,4275 | 9,2683 | 10,7157 | 10,6328 | 12,6519 | 12,1352 |

### 4.1.2. P-series (printed samples) gamma shielding results

#### 4.1.2.1. Linear attenuation coefficient (LAC) results for the P-series

**Table 4.61:** Linear attenuation coefficient (LAC) results for the P-ABS-0

| Energy (keV) | Experimental ($cm^{-1}$) | Uncertainty | EpiXS ($cm^{-1}$) | Xcom ($cm^{-1}$) | Geant4 ($cm^{-1}$) | FLUKA ($cm^{-1}$) |
|---|---|---|---|---|---|---|
| 59,5 | 0,1884 | 0,0185 | 0,1968 | 0,1968 | 0,1874 | 0,1964 |
| 80,9 | 0,1700 | 0,0153 | 0,1802 | 0,1803 | 0,1750 | 0,1801 |
| 276,3 | 0,1150 | 0,0103 | 0,1238 | 0,1239 | 0,1229 | 0,1239 |
| 302,8 | 0,1103 | 0,0163 | 0,1198 | 0,1198 | 0,1191 | 0,1198 |
| 356 | 0,1062 | 0,0086 | 0,1125 | 0,1127 | 0,1123 | 0,1125 |
| 383,8 | 0,1115 | 0,0088 | 0,1094 | 0,1094 | 0,1092 | 0,1093 |
| 511 | 0,0935 | 0,0123 | 0,0973 | 0,0974 | 0,0976 | 0,0976 |
| 661,6 | 0,0882 | 0,0176 | 0,0869 | 0,0870 | 0,0875 | 0,0872 |
| 1173,2 | 0,0612 | 0,0166 | 0,0662 | 0,0663 | 0,0666 | 0,0666 |
| 1274,5 | 0,0640 | 0,0078 | 0,0634 | 0,0635 | 0,0638 | 0,0634 |
| 1332,5 | 0,0606 | 0,0178 | 0,0620 | 0,0621 | 0,0623 | 0,0621 |

**Table 4.62:** Linear attenuation coefficient (LAC) results for the P-ABS-Er5

| Energy (keV) | Experimental ($cm^{-1}$) | Uncertainty | EpiXS ($cm^{-1}$) | Xcom ($cm^{-1}$) | Geant4 ($cm^{-1}$) | FLUKA ($cm^{-1}$) |
|---|---|---|---|---|---|---|
| 59,5 | 0,8353 | 0,0157 | 0,8420 | 0,8487 | 0,8182 | 0,8453 |
| 80,9 | 0,4736 | 0,0130 | 0,4743 | 0,4740 | 0,4587 | 0,4740 |
| 276,3 | 0,1329 | 0,0146 | 0,1371 | 0,1372 | 0,1350 | 0,1371 |
| 302,8 | 0,1252 | 0,0155 | 0,1307 | 0,1307 | 0,1290 | 0,1307 |
| 356 | 0,1189 | 0,0106 | 0,1204 | 0,1205 | 0,1195 | 0,1204 |
| 383,8 | 0,1236 | 0,0169 | 0,1162 | 0,1162 | 0,1155 | 0,1162 |
| 511 | 0,0942 | 0,0161 | 0,1015 | 0,1016 | 0,1015 | 0,1015 |
| 661,6 | 0,0882 | 0,0091 | 0,0899 | 0,0900 | 0,0903 | 0,0900 |
| 1173,2 | 0,0653 | 0,0088 | 0,0679 | 0,0680 | 0,0682 | 0,0679 |
| 1274,5 | 0,0640 | 0,0142 | 0,0650 | 0,0651 | 0,0653 | 0,0651 |
| 1332,5 | 0,0655 | 0,0189 | 0,0635 | 0,0636 | 0,0638 | 0,0635 |

**Table 4.63:** Linear attenuation coefficient (LAC) results for the P-ABS-Gd5

| Energy (keV) | Experimental ($cm^{-1}$) | Uncertainty | EpiXS ($cm^{-1}$) | Xcom ($cm^{-1}$) | Geant4 ($cm^{-1}$) | FLUKA ($cm^{-1}$) |
|---|---|---|---|---|---|---|
| 59,5 | 0,7240 | 0,0180 | 0,7547 | 0,7543 | 0,7304 | 0,7544 |
| 80,9 | 0,4289 | 0,0126 | 0,4308 | 0,4303 | 0,4151 | 0,4152 |
| 276,3 | 0,1257 | 0,0124 | 0,1351 | 0,1351 | 0,1331 | 0,1351 |
| 302,8 | 0,1197 | 0,0166 | 0,1290 | 0,1291 | 0,1275 | 0,1280 |
| 356 | 0,1198 | 0,0152 | 0,1193 | 0,1194 | 0,1184 | 0,1194 |
| 383,8 | 0,1075 | 0,0109 | 0,1153 | 0,1153 | 0,1146 | 0,1153 |
| 511 | 0,0935 | 0,0171 | 0,1010 | 0,1011 | 0,1011 | 0,1010 |
| 661,6 | 0,0864 | 0,0172 | 0,0896 | 0,0897 | 0,0900 | 0,0896 |
| 1173,2 | 0,0628 | 0,0080 | 0,0677 | 0,0678 | 0,0681 | 0,0677 |
| 1274,5 | 0,0624 | 0,0107 | 0,0649 | 0,0650 | 0,0652 | 0,0649 |
| 1332,5 | 0,0630 | 0,0157 | 0,0634 | 0,0635 | 0,0637 | 0,0635 |

**Table 4.64:** Linear attenuation coefficient (LAC) results for the P-ABS-Er10

| Energy (keV) | Experimental ($cm^{-1}$) | Uncertainty | EpiXS ($cm^{-1}$) | Xcom ($cm^{-1}$) | Geant4 ($cm^{-1}$) | FLUKA ($cm^{-1}$) |
|---|---|---|---|---|---|---|
| 1,4627 | 1,5356 | 0,0095 | 1,5527 | 1,5669 | 1,5129 | 1,5491 |
| 0,7411 | 0,7830 | 0,0158 | 0,7997 | 0,7990 | 0,7726 | 0,7904 |
| 0,1419 | 0,1506 | 0,0108 | 0,1536 | 0,1536 | 0,1503 | 0,1536 |
| 0,1347 | 0,1416 | 0,0107 | 0,1445 | 0,1445 | 0,1418 | 0,1439 |
| 0,1229 | 0,1283 | 0,0124 | 0,1308 | 0,1310 | 0,1291 | 0,1291 |
| 0,1216 | 0,1229 | 0,0114 | 0,1254 | 0,1254 | 0,1240 | 0,1254 |
| 0,1035 | 0,1056 | 0,0129 | 0,1077 | 0,1078 | 0,1074 | 0,1078 |
| 0,0873 | 0,0928 | 0,0150 | 0,0946 | 0,0947 | 0,0948 | 0,0948 |
| 0,0702 | 0,0695 | 0,0100 | 0,0707 | 0,0709 | 0,0711 | 0,0709 |

**Continuation of Table 4.64…**

| | | | | | | |
|---|---|---|---|---|---|---|
| 0,0732 | 0,0665 | 0,0162 | 0,0678 | 0,0679 | 0,0680 | 0,0679 |
| 0,0705 | 0,0650 | 0,0101 | 0,0662 | 0,0663 | 0,0664 | 0,0664 |

**Table 4.65:** Linear attenuation coefficient (LAC) results for the P-ABS-Gd10

| Energy (keV) | Experimental ($cm^{-1}$) | Uncertainty | EpiXS ($cm^{-1}$) | Xcom ($cm^{-1}$) | Geant4 ($cm^{-1}$) | FLUKA ($cm^{-1}$) |
|---|---|---|---|---|---|---|
| 59,5 | 1,5149 | 0,0131 | 1,3680 | 1,5517 | 1,3273 | 1,3568 |
| 80,9 | 0,7512 | 0,0149 | 0,7077 | 0,7922 | 0,6805 | 0,6781 |
| 276,3 | 0,1455 | 0,0138 | 0,1493 | 0,1531 | 0,1462 | 0,1493 |
| 302,8 | 0,1387 | 0,0185 | 0,1410 | 0,1440 | 0,1385 | 0,1440 |
| 356 | 0,1265 | 0,0090 | 0,1284 | 0,1305 | 0,1269 | 0,1273 |
| 383,8 | 0,1155 | 0,0101 | 0,1234 | 0,1250 | 0,1221 | 0,1234 |
| 511 | 0,1015 | 0,0159 | 0,1066 | 0,1075 | 0,1063 | 0,1066 |
| 661,6 | 0,0922 | 0,0145 | 0,0938 | 0,0944 | 0,0941 | 0,0944 |
| 1173,2 | 0,0686 | 0,0099 | 0,0704 | 0,0707 | 0,0708 | 0,0704 |
| 1274,5 | 0,0717 | 0,0083 | 0,0675 | 0,0677 | 0,0678 | 0,0678 |
| 1332,5 | 0,0680 | 0,0129 | 0,0659 | 0,0661 | 0,0662 | 0,0661 |

**Table 4.66:** Linear attenuation coefficient (LAC) results for the -ABS-Er10Gd5

| Energy (keV) | Experimental ($cm^{-1}$) | Uncertainty | EpiXS ($cm^{-1}$) | Xcom ($cm^{-1}$) | Geant4 ($cm^{-1}$) | FLUKA ($cm^{-1}$) |
|---|---|---|---|---|---|---|
| 59,5 | 2,1144 | 0,0121 | 2,2366 | 2,2513 | 2,1789 | 2,2359 |
| 80,9 | 1,0410 | 0,0109 | 1,1088 | 1,1074 | 1,0692 | 1,1079 |
| 276,3 | 0,1676 | 0,0105 | 0,1694 | 0,1695 | 0,1648 | 0,1694 |
| 302,8 | 0,1476 | 0,0106 | 0,1578 | 0,1579 | 0,1540 | 0,1540 |
| 356 | 0,1449 | 0,0165 | 0,1409 | 0,1410 | 0,1383 | 0,1409 |
| 383,8 | 0,1379 | 0,0187 | 0,1344 | 0,1344 | 0,1322 | 0,1344 |
| 511 | 0,1102 | 0,0095 | 0,1138 | 0,1139 | 0,1132 | 0,1139 |
| 661,6 | 0,0939 | 0,0200 | 0,0993 | 0,0994 | 0,0993 | 0,0993 |
| 1173,2 | 0,0719 | 0,0115 | 0,0737 | 0,0739 | 0,0740 | 0,0737 |
| 1274,5 | 0,0670 | 0,0176 | 0,0706 | 0,0707 | 0,0708 | 0,0706 |
| 1332,5 | 0,0713 | 0,0123 | 0,0689 | 0,0691 | 0,0692 | 0,0691 |

**Table 4.67:** Linear attenuation coefficient (LAC) results for the P-ABS-Er5Gd10

| Energy (keV) | Experimental ($cm^{-1}$) | Uncertainty | EpiXS ($cm^{-1}$) | Xcom ($cm^{-1}$) | Geant4 ($cm^{-1}$) | FLUKA ($cm^{-1}$) |
|---|---|---|---|---|---|---|
| 59,5 | 2,2081 | 0,0126 | 2,1391 | 2,1457 | 2,0808 | 2,1304 |
| 80,9 | 0,9787 | 0,0116 | 1,0602 | 1,0584 | 1,0205 | 1,0575 |
| 276,3 | 0,1658 | 0,0143 | 0,1672 | 0,1671 | 0,1627 | 0,1671 |
| 302,8 | 0,1581 | 0,0131 | 0,1560 | 0,1560 | 0,1525 | 0,1559 |
| 356 | 0,1464 | 0,0186 | 0,1396 | 0,1397 | 0,1373 | 0,1397 |
| 383,8 | 0,1358 | 0,0136 | 0,1333 | 0,1333 | 0,1314 | 0,1332 |
| 511 | 0,1055 | 0,0198 | 0,1133 | 0,1133 | 0,1126 | 0,1133 |
| 661,6 | 0,0926 | 0,0146 | 0,0989 | 0,0990 | 0,0989 | 0,0990 |
| 1173,2 | 0,0719 | 0,0154 | 0,0736 | 0,0737 | 0,0739 | 0,0739 |
| 1274,5 | 0,0748 | 0,0162 | 0,0705 | 0,0706 | 0,0707 | 0,0706 |
| 1332,5 | 0,0713 | 0,0100 | 0,0688 | 0,0689 | 0,0690 | 0,0690 |

**Table 4.68:** Linear attenuation coefficient (LAC) results for the -ABS-Er20

| Energy (keV) | Experimental ($cm^{-1}$) | Uncertainty | EpiXS ($cm^{-1}$) | Xcom ($cm^{-1}$) | Geant4 ($cm^{-1}$) | FLUKA ($cm^{-1}$) |
|---|---|---|---|---|---|---|
| 59,5 | 3,4301 | 0,0132 | 3,2004 | 3,2311 | 3,1235 | 3,2236 |
| 80,9 | 1,4221 | 0,0100 | 1,5538 | 1,5525 | 1,5004 | 1,5531 |
| 276,3 | 0,1845 | 0,0148 | 0,1918 | 0,1918 | 0,1855 | 0,1915 |
| 302,8 | 0,1779 | 0,0144 | 0,1765 | 0,1765 | 0,1713 | 0,1765 |
| 356 | 0,1655 | 0,0139 | 0,1547 | 0,1549 | 0,1513 | 0,1547 |
| 383,8 | 0,1544 | 0,0146 | 0,1466 | 0,1466 | 0,1437 | 0,1466 |
| 511 | 0,1142 | 0,0097 | 0,1219 | 0,1220 | 0,1208 | 0,1218 |
| 661,6 | 0,1060 | 0,0171 | 0,1053 | 0,1054 | 0,1048 | 0,1054 |
| 1173,2 | 0,0735 | 0,0157 | 0,0774 | 0,0775 | 0,0776 | 0,0775 |
| 1274,5 | 0,0794 | 0,0171 | 0,0741 | 0,0742 | 0,0743 | 0,0743 |
| 1332,5 | 0,0738 | 0,0122 | 0,0723 | 0,0725 | 0,0725 | 0,0725 |

**Table 4.69:** Linear attenuation coefficient (LAC) results for the P-ABS-Gd20

| Energy (keV) | Experimental ($cm^{-1}$) | Uncertainty | EpiXS ($cm^{-1}$) | Xcom ($cm^{-1}$) | Geant4 ($cm^{-1}$) | FLUKA ($cm^{-1}$) |
|---|---|---|---|---|---|---|
| 59,5 | 2,6361 | 0,0138 | 2,7856 | 2,7839 | 2,7069 | 2,7852 |
| 80,9 | 1,2516 | 0,0123 | 1,3476 | 1,3447 | 1,2939 | 1,3447 |
| 276,3 | 0,1732 | 0,0152 | 0,1822 | 0,1822 | 0,1765 | 0,1822 |
| 302,8 | 0,1671 | 0,0182 | 0,1687 | 0,1687 | 0,1640 | 0,1687 |
| 356 | 0,1486 | 0,0135 | 0,1494 | 0,1495 | 0,1464 | 0,1494 |
| 383,8 | 0,1441 | 0,0164 | 0,1421 | 0,1422 | 0,1395 | 0,1422 |
| 511 | 0,1109 | 0,0181 | 0,1194 | 0,1195 | 0,1185 | 0,1194 |
| 661,6 | 0,0971 | 0,0126 | 0,1037 | 0,1038 | 0,1036 | 0,1038 |
| 1173,2 | 0,0727 | 0,0135 | 0,0767 | 0,0769 | 0,0768 | 0,0769 |
| 1274,5 | 0,0748 | 0,0144 | 0,0735 | 0,0736 | 0,0737 | 0,0735 |
| 1332,5 | 0,0721 | 0,0136 | 0,0717 | 0,0719 | 0,0719 | 0,0719 |

**Table 4.70:** Linear attenuation coefficient (LAC) results for the Lead (Pb)

| Energy (keV) | EpiXS ($cm^{-1}$) | Xcom ($cm^{-1}$) | Geant4 ($cm^{-1}$) | FLUKA ($cm^{-1}$) |
|---|---|---|---|---|
| 59,5000 | 57,7042 | 58,1629 | 51,6140 | 56,8225 |
| 80,9000 | 25,9414 | 26,6830 | 22,9556 | 26,0775 |
| 276,3000 | 5,4382 | 5,4375 | 5,0634 | 5,4375 |
| 302,8000 | 4,4840 | 4,4861 | 4,1697 | 4,4852 |
| 356,0000 | 3,2545 | 3,2580 | 3,0253 | 3,2545 |
| 383,8000 | 2,8324 | 2,8350 | 2,6341 | 2,8361 |
| 511,0000 | 1,7701 | 1,7713 | 1,6581 | 1,7713 |
| 661,6000 | 1,2465 | 1,2497 | 1,1845 | 1,2474 |
| 1173,2000 | 0,6973 | 0,7002 | 0,6815 | 0,6985 |
| 1274,5000 | 0,6545 | 0,6568 | 0,6411 | 0,6545 |
| 1332,5000 | 0,6341 | 0,6366 | 0,6220 | 0,6355 |

### 4.1.2.2. Mass attenuation coefficient (MAC) results for the P-series

**Table 4.71:** Mass attenuation coefficient (MAC) results for the P-ABS-0

| Energy (keV) | Experimental ($cm^2/g$) | Uncertainty | EpiXS ($cm^2/g$) | Xcom ($cm^2/g$) | Geant4 ($cm^2/g$) | FLUKA ($cm^2/g$) |
|---|---|---|---|---|---|---|
| 59,5 | 0,1805 | 0,0177 | 0,1884 | 0,1885 | 0,1794 | 0,1880 |
| 80,9 | 0,1628 | 0,0147 | 0,1726 | 0,1727 | 0,1676 | 0,1725 |
| 276,3 | 0,1102 | 0,0099 | 0,1186 | 0,1187 | 0,1177 | 0,1187 |
| 302,8 | 0,1057 | 0,0156 | 0,1147 | 0,1147 | 0,1140 | 0,1147 |
| 356 | 0,1017 | 0,0082 | 0,1078 | 0,1079 | 0,1076 | 0,1078 |
| 383,8 | 0,1068 | 0,0084 | 0,1048 | 0,1048 | 0,1046 | 0,1047 |
| 511 | 0,0895 | 0,0118 | 0,0932 | 0,0932 | 0,0935 | 0,0935 |
| 661,6 | 0,0844 | 0,0169 | 0,0833 | 0,0833 | 0,0838 | 0,0835 |
| 1173,2 | 0,0586 | 0,0159 | 0,0634 | 0,0635 | 0,0638 | 0,0638 |
| 1274,5 | 0,0613 | 0,0075 | 0,0608 | 0,0608 | 0,0611 | 0,0608 |
| 1332,5 | 0,0580 | 0,0170 | 0,0593 | 0,0595 | 0,0597 | 0,0595 |

**Table 4.72:** Mass attenuation coefficient (MAC) results for the P-ABS-Er5

| Energy (keV) | Experimental ($cm^2/g$) | Uncertainty | EpiXS ($cm^2/g$) | Xcom ($cm^2/g$) | Geant4 ($cm^2/g$) | FLUKA ($cm^2/g$) |
|---|---|---|---|---|---|---|
| 59,5 | 0,7757 | 0,0146 | 0,7819 | 0,7882 | 0,7598 | 0,7850 |
| 80,9 | 0,4398 | 0,0121 | 0,4405 | 0,4402 | 0,4260 | 0,4402 |
| 276,3 | 0,1234 | 0,0136 | 0,1273 | 0,1274 | 0,1254 | 0,1273 |
| 302,8 | 0,1163 | 0,0144 | 0,1214 | 0,1214 | 0,1198 | 0,1214 |
| 356 | 0,1104 | 0,0098 | 0,1118 | 0,1119 | 0,1110 | 0,1118 |
| 383,8 | 0,1148 | 0,0157 | 0,1079 | 0,1079 | 0,1072 | 0,1079 |
| 511 | 0,0874 | 0,0150 | 0,0943 | 0,0944 | 0,0943 | 0,0943 |
| 661,6 | 0,0819 | 0,0085 | 0,0835 | 0,0836 | 0,0839 | 0,0836 |
| 1173,2 | 0,0606 | 0,0082 | 0,0630 | 0,0631 | 0,0633 | 0,0630 |
| 1274,5 | 0,0594 | 0,0132 | 0,0604 | 0,0605 | 0,0607 | 0,0605 |
| 1332,5 | 0,0608 | 0,0176 | 0,0590 | 0,0591 | 0,0593 | 0,0590 |

**Table 4.73:** Mass attenuation coefficient (MAC) results for the P-ABS-Gd5

| Energy (keV) | Experimental ($cm^2/g$) | Uncertainty | EpiXS ($cm^2/g$) | Xcom ($cm^2/g$) | Geant4 ($cm^2/g$) | FLUKA ($cm^2/g$) |
|---|---|---|---|---|---|---|
| 59,5 | 0,6731 | 0,0167 | 0,7017 | 0,7013 | 0,6791 | 0,7014 |
| 80,9 | 0,3987 | 0,0117 | 0,4005 | 0,4000 | 0,3859 | 0,3860 |
| 276,3 | 0,1169 | 0,0115 | 0,1256 | 0,1256 | 0,1238 | 0,1256 |
| 302,8 | 0,1113 | 0,0154 | 0,1200 | 0,1200 | 0,1185 | 0,1190 |
| 356 | 0,1114 | 0,0141 | 0,1109 | 0,1110 | 0,1101 | 0,1110 |
| 383,8 | 0,1000 | 0,0101 | 0,1072 | 0,1072 | 0,1065 | 0,1072 |
| 511 | 0,0869 | 0,0159 | 0,0939 | 0,0940 | 0,0940 | 0,0939 |
| 661,6 | 0,0803 | 0,0160 | 0,0833 | 0,0834 | 0,0837 | 0,0833 |
| 1173,2 | 0,0584 | 0,0074 | 0,0630 | 0,0631 | 0,0633 | 0,0630 |
| 1274,5 | 0,0580 | 0,0099 | 0,0603 | 0,0604 | 0,0606 | 0,0603 |
| 1332,5 | 0,0586 | 0,0146 | 0,0589 | 0,0591 | 0,0592 | 0,0591 |

**Table 4.74:** Mass attenuation coefficient (MAC) results for the P-ABS-Er10

| Energy (keV) | Experimental ($cm^2/g$) | Uncertainty | EpiXS ($cm^2/g$) | Xcom ($cm^2/g$) | Geant4 ($cm^2/g$) | FLUKA ($cm^2/g$) |
|---|---|---|---|---|---|---|
| 59,5 | 1,3602 | 0,0084 | 1,3754 | 1,3880 | 1,3402 | 1,3722 |
| 80,9 | 0,6936 | 0,0140 | 0,7084 | 0,7078 | 0,6844 | 0,7002 |
| 276,3 | 0,1334 | 0,0096 | 0,1361 | 0,1361 | 0,1331 | 0,1361 |
| 302,8 | 0,1254 | 0,0095 | 0,1280 | 0,1280 | 0,1256 | 0,1275 |
| 356 | 0,1137 | 0,0110 | 0,1158 | 0,1160 | 0,1144 | 0,1144 |
| 383,8 | 0,1089 | 0,0101 | 0,1111 | 0,1111 | 0,1098 | 0,1111 |
| 511 | 0,0936 | 0,0114 | 0,0954 | 0,0955 | 0,0951 | 0,0955 |
| 661,6 | 0,0822 | 0,0133 | 0,0838 | 0,0839 | 0,0839 | 0,0839 |
| 1173,2 | 0,0615 | 0,0089 | 0,0627 | 0,0628 | 0,0629 | 0,0628 |
| 1274,5 | 0,0589 | 0,0144 | 0,0600 | 0,0601 | 0,0603 | 0,0601 |
| 1332,5 | 0,0576 | 0,0089 | 0,0586 | 0,0587 | 0,0589 | 0,0589 |

**Table 4.75:** Mass attenuation coefficient (MAC) results for the P-ABS-Gd10

| Energy (keV) | Experimental ($cm^2/g$) | Uncertainty | EpiXS ($cm^2/g$) | Xcom ($cm^2/g$) | Geant4 ($cm^2/g$) | FLUKA ($cm^2/g$) |
|---|---|---|---|---|---|---|
| 59,5 | 1,3453 | 0,0116 | 1,2149 | 1,3780 | 1,1787 | 1,2049 |
| 80,9 | 0,6671 | 0,0132 | 0,6285 | 0,7035 | 0,6043 | 0,6022 |
| 276,3 | 0,1292 | 0,0123 | 0,1326 | 0,1360 | 0,1298 | 0,1326 |
| 302,8 | 0,1232 | 0,0164 | 0,1252 | 0,1279 | 0,1230 | 0,1279 |
| 356 | 0,1123 | 0,0080 | 0,1140 | 0,1159 | 0,1127 | 0,1131 |
| 383,8 | 0,1026 | 0,0090 | 0,1095 | 0,1110 | 0,1084 | 0,1095 |
| 511 | 0,0901 | 0,0141 | 0,0946 | 0,0955 | 0,0944 | 0,0946 |
| 661,6 | 0,0818 | 0,0129 | 0,0833 | 0,0839 | 0,0836 | 0,0839 |
| 1173,2 | 0,0609 | 0,0088 | 0,0625 | 0,0628 | 0,0628 | 0,0625 |
| 1274,5 | 0,0636 | 0,0074 | 0,0599 | 0,0601 | 0,0602 | 0,0602 |
| 1332,5 | 0,0604 | 0,0115 | 0,0585 | 0,0587 | 0,0588 | 0,0587 |

**Table 4.76:** Mass attenuation coefficient (MAC) results for the P-ABS-Er10Gd5

| Energy (keV) | Experimental ($cm^2/g$) | Uncertainty | EpiXS ($cm^2/g$) | Xcom ($cm^2/g$) | Geant4 ($cm^2/g$) | FLUKA ($cm^2/g$) |
|---|---|---|---|---|---|---|
| 59,5 | 1,7854 | 0,0102 | 1,8887 | 1,9010 | 1,8399 | 1,8880 |
| 80,9 | 0,8790 | 0,0092 | 0,9363 | 0,9351 | 0,9028 | 0,9355 |
| 276,3 | 0,1415 | 0,0089 | 0,1431 | 0,1431 | 0,1392 | 0,1431 |
| 302,8 | 0,1246 | 0,0090 | 0,1333 | 0,1333 | 0,1301 | 0,1301 |
| 356 | 0,1224 | 0,0139 | 0,1189 | 0,1191 | 0,1168 | 0,1189 |
| 383,8 | 0,1164 | 0,0158 | 0,1135 | 0,1135 | 0,1117 | 0,1135 |
| 511 | 0,0931 | 0,0080 | 0,0961 | 0,0962 | 0,0956 | 0,0962 |
| 661,6 | 0,0793 | 0,0169 | 0,0838 | 0,0839 | 0,0838 | 0,0838 |
| 1173,2 | 0,0607 | 0,0097 | 0,0623 | 0,0624 | 0,0625 | 0,0623 |
| 1274,5 | 0,0566 | 0,0149 | 0,0596 | 0,0597 | 0,0598 | 0,0596 |
| 1332,5 | 0,0602 | 0,0104 | 0,0582 | 0,0583 | 0,0584 | 0,0583 |

**Table 4.77:** Mass attenuation coefficient (MAC) results for the P-ABS-Er5Gd10

| Energy (keV) | Experimental ($cm^2/g$) | Uncertainty | EpiXS ($cm^2/g$) | Xcom ($cm^2/g$) | Geant4 ($cm^2/g$) | FLUKA ($cm^2/g$) |
|---|---|---|---|---|---|---|
| 59,5 | 1,8667 | 0,0107 | 1,8084 | 1,8140 | 1,7591 | 1,8011 |
| 80,9 | 0,8274 | 0,0098 | 0,8963 | 0,8948 | 0,8628 | 0,8940 |
| 276,3 | 0,1401 | 0,0121 | 0,1413 | 0,1413 | 0,1376 | 0,1413 |
| 302,8 | 0,1337 | 0,0111 | 0,1319 | 0,1319 | 0,1290 | 0,1318 |
| 356 | 0,1238 | 0,0157 | 0,1180 | 0,1181 | 0,1161 | 0,1181 |
| 383,8 | 0,1148 | 0,0115 | 0,1127 | 0,1127 | 0,1111 | 0,1126 |
| 511 | 0,0892 | 0,0167 | 0,0958 | 0,0958 | 0,0952 | 0,0958 |
| 661,6 | 0,0783 | 0,0123 | 0,0836 | 0,0837 | 0,0836 | 0,0837 |
| 1173,2 | 0,0607 | 0,0130 | 0,0622 | 0,0623 | 0,0624 | 0,0624 |
| 1274,5 | 0,0632 | 0,0137 | 0,0596 | 0,0597 | 0,0598 | 0,0597 |
| 1332,5 | 0,0603 | 0,0085 | 0,0582 | 0,0583 | 0,0584 | 0,0584 |

**Table 4.78:** Mass attenuation coefficient (MAC) results for the P-ABS-Er20

| Energy (keV) | Experimental ($cm^2/g$) | Uncertainty | EpiXS ($cm^2/g$) | Xcom ($cm^2/g$) | Geant4 ($cm^2/g$) | FLUKA ($cm^2/g$) |
|---|---|---|---|---|---|---|
| 59,5 | 2,1211 | 0,0111 | 2,2413 | 2,2400 | 2,1780 | 2,2410 |
| 80,9 | 1,0070 | 0,0099 | 1,0843 | 1,0820 | 1,0411 | 1,0820 |
| 276,3 | 0,1394 | 0,0122 | 0,1466 | 0,1466 | 0,1420 | 0,1466 |
| 302,8 | 0,1345 | 0,0146 | 0,1358 | 0,1357 | 0,1320 | 0,1357 |
| 356 | 0,1195 | 0,0109 | 0,1202 | 0,1203 | 0,1178 | 0,1202 |
| 383,8 | 0,1159 | 0,0132 | 0,1143 | 0,1144 | 0,1123 | 0,1144 |
| 511 | 0,0892 | 0,0146 | 0,0961 | 0,0962 | 0,0953 | 0,0961 |
| 661,6 | 0,0781 | 0,0101 | 0,0834 | 0,0835 | 0,0833 | 0,0835 |
| 1173,2 | 0,0585 | 0,0109 | 0,0617 | 0,0618 | 0,0618 | 0,0618 |
| 1274,5 | 0,0602 | 0,0116 | 0,0591 | 0,0592 | 0,0593 | 0,0591 |
| 1332,5 | 0,0581 | 0,0109 | 0,0577 | 0,0578 | 0,0579 | 0,0578 |

**Table 4.79:** Mass attenuation coefficient (MAC) results for the Lead (Pb)

| Energy (keV) | EpiXS ($cm^2/g$) | Xcom ($cm^2/g$) | Geant4 ($cm^2/g$) | FLUKA ($cm^2/g$) |
|---|---|---|---|---|
| 59,5 | 5,0886 | 5,1290 | 4,5515 | 5,0108 |
| 80,9 | 2,2876 | 2,3530 | 2,0243 | 2,2996 |
| 276,3 | 0,4796 | 0,4795 | 0,4465 | 0,4795 |
| 302,8 | 0,3954 | 0,3956 | 0,3677 | 0,3955 |
| 356 | 0,2870 | 0,2873 | 0,2668 | 0,2870 |
| 383,8 | 0,2498 | 0,2500 | 0,2323 | 0,2501 |
| 511 | 0,1561 | 0,1562 | 0,1462 | 0,1562 |
| 661,6 | 0,1099 | 0,1102 | 0,1045 | 0,1100 |
| 1173,2 | 0,0615 | 0,0618 | 0,0601 | 0,0616 |
| 1274,5 | 0,0577 | 0,0579 | 0,0565 | 0,0577 |
| 1332,5 | 0,0559 | 0,0561 | 0,0548 | 0,0560 |

### 4.1.2.3. Half value layer (HVL) results for the P-series

**Table 4.80:** Half value layer (HVL) results for the P-ABS-0

| Energy (keV) | Experimental (cm) | EpiXS (cm) | Xcom (cm) | Geant4 (cm) | FLUKA (cm) |
|---|---|---|---|---|---|
| 59,5 | 3,6786 | 3,5226 | 3,5216 | 3,6996 | 3,5301 |
| 80,9 | 4,0785 | 3,8455 | 3,8437 | 3,9609 | 3,8482 |
| 276,3 | 6,0257 | 5,5990 | 5,5924 | 5,6394 | 5,5924 |
| 302,8 | 6,2828 | 5,7874 | 5,7874 | 5,8219 | 5,7874 |
| 356 | 6,5254 | 6,1596 | 6,1521 | 6,1710 | 6,1596 |
| 383,8 | 6,2143 | 6,3369 | 6,3341 | 6,3462 | 6,3429 |
| 511 | 7,4131 | 7,1248 | 7,1194 | 7,0995 | 7,0995 |
| 661,6 | 7,8628 | 7,9733 | 7,9651 | 7,9219 | 7,9461 |
| 1173,2 | 11,3344 | 10,4765 | 10,4571 | 10,4128 | 10,4128 |
| 1274,5 | 10,8368 | 10,9255 | 10,9126 | 10,8687 | 10,9255 |
| 1332,5 | 11,4426 | 11,1858 | 11,1641 | 11,1253 | 11,1641 |

**Table 4.81:** Half value layer (HVL) results for the P-ABS-Er5

| Energy (keV) | Experimental (cm) | EpiXS (cm) | Xcom (cm) | Geant4 (cm) | FLUKA (cm) |
|---|---|---|---|---|---|
| 59,5 | 0,8299 | 0,8232 | 0,8167 | 0,8472 | 0,8200 |
| 80,9 | 1,4636 | 1,4613 | 1,4623 | 1,5111 | 1,4623 |
| 276,3 | 5,2173 | 5,0561 | 5,0526 | 5,1328 | 5,0561 |
| 302,8 | 5,5359 | 5,3044 | 5,3023 | 5,3731 | 5,3023 |
| 356 | 5,8305 | 5,7575 | 5,7525 | 5,8007 | 5,7575 |
| 383,8 | 5,6074 | 5,9649 | 5,9657 | 6,0035 | 5,9657 |
| 511 | 7,3610 | 6,8273 | 6,8217 | 6,8258 | 6,8258 |
| 661,6 | 7,8628 | 7,7080 | 7,6998 | 7,6753 | 7,6998 |
| 1173,2 | 10,6217 | 10,2152 | 10,1964 | 10,1613 | 10,2152 |
| 1274,5 | 10,8368 | 10,6577 | 10,6449 | 10,6098 | 10,6449 |
| 1332,5 | 10,5794 | 10,9132 | 10,8917 | 10,8614 | 10,9132 |

**Table 4.82:** Half value layer (HVL) results for the P-ABS-Gd5

| Energy (keV) | Experimental (cm) | EpiXS (cm) | Xcom (cm) | Geant4 (cm) | FLUKA (cm) |
|---|---|---|---|---|---|
| 59,5 | 0,957330713 | 0,9184 | 0,9189 | 0,9490 | 0,918751406 |
| 80,9 | 1,616133645 | 1,6089 | 1,6110 | 1,6697 | 1,669288769 |
| 276,3 | 5,514814413 | 5,1322 | 5,1307 | 5,2065 | 5,132223414 |
| 302,8 | 5,790707449 | 5,3716 | 5,3701 | 5,4376 | 5,415228877 |
| 356 | 5,784524149 | 5,8119 | 5,8055 | 5,8519 | 5,805515643 |
| 383,8 | 6,444921873 | 6,0141 | 6,0113 | 6,0497 | 6,011308175 |
| 511 | 7,413148079 | 6,8624 | 6,8569 | 6,8587 | 6,862421251 |
| 661,6 | 8,023965691 | 7,7363 | 7,7277 | 7,7013 | 7,736301297 |
| 1173,2 | 11,03847093 | 10,2364 | 10,2174 | 10,1814 | 10,23643486 |
| 1274,5 | 11,10325268 | 10,6789 | 10,6655 | 10,6298 | 10,67887162 |
| 1332,5 | 10,99458639 | 10,9345 | 10,9130 | 10,8815 | 10,912993 |

**Table 4.83:** Half value layer (HVL) results for the P-ABS-Er10

| Energy (keV) | Experimental (cm) | EpiXS (cm) | Xcom (cm) | Geant4 (cm) | FLUKA (cm) |
|---|---|---|---|---|---|
| 59,5 | 0,4514 | 0,4464 | 0,4424 | 0,4581 | 0,4475 |
| 80,9 | 0,8852 | 0,8668 | 0,8675 | 0,8971 | 0,8770 |
| 276,3 | 4,6035 | 4,5126 | 4,5115 | 4,6124 | 4,5126 |
| 302,8 | 4,8948 | 4,7969 | 4,7969 | 4,8890 | 4,8161 |
| 356 | 5,4012 | 5,3008 | 5,2932 | 5,3686 | 5,3686 |
| 383,8 | 5,6394 | 5,5278 | 5,5266 | 5,5900 | 5,5266 |
| 511 | 6,5620 | 6,4363 | 6,4308 | 6,4559 | 6,4308 |
| 661,6 | 7,4713 | 7,3299 | 7,3218 | 7,3150 | 7,3150 |
| 1173,2 | 9,9783 | 9,7981 | 9,7788 | 9,7544 | 9,7788 |
| 1274,5 | 10,4232 | 10,2272 | 10,2148 | 10,1885 | 10,2148 |
| 1332,5 | 10,6663 | 10,4740 | 10,4530 | 10,4312 | 10,4312 |

**Table 4.84:** Half value layer (HVL) results for the P-ABS-Gd10

| Energy (keV) | Experimental (cm) | EpiXS (cm) | Xcom (cm) | Geant4 (cm) | FLUKA (cm) |
|---|---|---|---|---|---|
| 59,5 | 0,4575 | 0,5067 | 0,4467 | 0,5222 | 0,5109 |
| 80,9 | 0,9227 | 0,9795 | 0,8750 | 1,0186 | 1,0221 |
| 276,3 | 4,7630 | 4,6434 | 4,5261 | 4,7409 | 4,6434 |
| 302,8 | 4,9968 | 4,9152 | 4,8128 | 5,0041 | 4,8128 |
| 356 | 5,4810 | 5,4003 | 5,3111 | 5,4634 | 5,4440 |
| 383,8 | 5,9987 | 5,6191 | 5,5456 | 5,6770 | 5,6191 |
| 511 | 6,8303 | 6,5042 | 6,4490 | 6,5200 | 6,5042 |
| 661,6 | 7,5219 | 7,3861 | 7,3403 | 7,3668 | 7,3403 |
| 1173,2 | 10,1112 | 9,8421 | 9,8034 | 9,7959 | 9,8421 |
| 1274,5 | 9,6710 | 10,2711 | 10,2388 | 10,2303 | 10,2303 |
| 1332,5 | 10,1935 | 10,5182 | 10,4793 | 10,4731 | 10,4793 |

**Table 4.85:** Half value layer (HVL) results for the P-ABS-Er10Gd5

| Energy (keV) | Experimental (cm) | EpiXS (cm) | Xcom (cm) | Geant4 (cm) | FLUKA (cm) |
|---|---|---|---|---|---|
| 59,5 | 0,3278 | 0,3099 | 0,3079 | 0,3181 | 0,3100 |
| 80,9 | 0,6659 | 0,6251 | 0,6259 | 0,6483 | 0,6257 |
| 276,3 | 4,1351 | 4,0911 | 4,0902 | 4,2051 | 4,0911 |
| 302,8 | 4,6975 | 4,3920 | 4,3909 | 4,4996 | 4,4996 |
| 356 | 4,7823 | 4,9210 | 4,9144 | 5,0125 | 4,9210 |
| 383,8 | 5,0270 | 5,1581 | 5,1569 | 5,2423 | 5,1581 |
| 511 | 6,2901 | 6,0885 | 6,0836 | 6,1249 | 6,0836 |
| 661,6 | 7,3793 | 6,9837 | 6,9754 | 6,9830 | 6,9837 |
| 1173,2 | 9,6460 | 9,4015 | 9,3844 | 9,3662 | 9,4015 |
| 1274,5 | 10,3394 | 9,8167 | 9,8041 | 9,7857 | 9,8167 |
| 1332,5 | 9,7194 | 10,0548 | 10,0344 | 10,0194 | 10,0344 |

**Table 4.86:** Half value layer (HVL) results for the P-ABS-Er5Gd10

| Energy (keV) | Experimental (cm) | EpiXS (cm) | Xcom (cm) | Geant4 (cm) | FLUKA (cm) |
|---|---|---|---|---|---|
| 59,5 | 0,3139 | 0,3240 | 0,3230 | 0,3331 | 0,3254 |
| 80,9 | 0,7082 | 0,6538 | 0,6549 | 0,6792 | 0,6555 |
| 276,3 | 4,1815 | 4,1466 | 4,1472 | 4,2602 | 4,1472 |
| 302,8 | 4,3841 | 4,4432 | 4,4427 | 4,5440 | 4,4461 |
| 356 | 4,7348 | 4,9653 | 4,9618 | 5,0486 | 4,9618 |
| 383,8 | 5,1029 | 5,1991 | 5,1996 | 5,2768 | 5,2042 |
| 511 | 6,5705 | 6,1198 | 6,1156 | 6,1545 | 6,1156 |
| 661,6 | 7,4857 | 7,0098 | 7,0011 | 7,0086 | 7,0011 |
| 1173,2 | 9,6460 | 9,4219 | 9,4045 | 9,3855 | 9,3855 |
| 1274,5 | 9,2700 | 9,8370 | 9,8238 | 9,8049 | 9,8238 |
| 1332,5 | 9,7194 | 10,0752 | 10,0548 | 10,0389 | 10,0389 |

**Table 4.87:** Half value layer (HVL) results for the P-ABS-Er20

| Energy (keV) | Experimental (cm) | EpiXS (cm) | Xcom (cm) | Geant4 (cm) | FLUKA (cm) |
|---|---|---|---|---|---|
| 59,5 | 0,2021 | 0,2166 | 0,2145 | 0,2219 | 0,2150 |
| 80,9 | 0,4874 | 0,4461 | 0,4465 | 0,4620 | 0,4463 |
| 276,3 | 3,7563 | 3,6139 | 3,6131 | 3,7365 | 3,6202 |
| 302,8 | 3,8968 | 3,9276 | 3,9277 | 4,0462 | 3,9277 |
| 356 | 4,1884 | 4,4794 | 4,4756 | 4,5798 | 4,4794 |
| 383,8 | 4,4879 | 4,7273 | 4,7272 | 4,8226 | 4,7272 |
| 511 | 6,0672 | 5,6848 | 5,6799 | 5,7384 | 5,6898 |
| 661,6 | 6,5369 | 6,5849 | 6,5764 | 6,6156 | 6,5764 |
| 1173,2 | 9,4286 | 8,9557 | 8,9383 | 8,9305 | 8,9383 |
| 1274,5 | 8,7251 | 9,3564 | 9,3431 | 9,3346 | 9,3346 |
| 1332,5 | 9,3909 | 9,5851 | 9,5653 | 9,5590 | 9,5653 |

**Table 4.88:** Half value layer (HVL) results for the P-ABS-Gd20

| Energy (keV) | Experimental (cm) | EpiXS (cm) | Xcom (cm) | Geant4 (cm) | FLUKA (cm) |
|---|---|---|---|---|---|
| 59,5 | 0,2629 | 0,2488 | 0,2490 | 0,2561 | 0,2489 |
| 80,9 | 0,5538 | 0,5144 | 0,5154 | 0,5357 | 0,5154 |
| 276,3 | 4,0013 | 3,8051 | 3,8043 | 3,9281 | 3,8051 |
| 302,8 | 4,1477 | 4,1079 | 4,1099 | 4,2254 | 4,1099 |
| 356 | 4,6652 | 4,6399 | 4,6360 | 4,7356 | 4,6399 |
| 383,8 | 4,8114 | 4,8776 | 4,8751 | 4,9681 | 4,8751 |
| 511 | 6,2518 | 5,8029 | 5,7993 | 5,8509 | 5,8029 |
| 661,6 | 7,1417 | 6,6852 | 6,6768 | 6,6937 | 6,6768 |
| 1173,2 | 9,5361 | 9,0356 | 9,0187 | 9,0206 | 9,0187 |
| 1274,5 | 9,2700 | 9,4363 | 9,4241 | 9,4105 | 9,4363 |
| 1332,5 | 9,6075 | 9,6655 | 9,6457 | 9,6352 | 9,6457 |

**Table 4.89:** Half value layer (HVL) results for the Lead (Pb)

| Energy (keV) | EpiXS (cm) | Xcom (cm) | Geant4 (cm) | FLUKA (cm) |
|---|---|---|---|---|
| 59,5 | 0,0120 | 0,0119 | 0,0134 | 0,0122 |
| 80,9 | 0,0267 | 0,0260 | 0,0302 | 0,0266 |
| 276,3 | 0,1275 | 0,1275 | 0,1369 | 0,1275 |
| 302,8 | 0,1546 | 0,1545 | 0,1662 | 0,1545 |
| 356 | 0,2130 | 0,2128 | 0,2291 | 0,2130 |
| 383,8 | 0,2447 | 0,2445 | 0,2631 | 0,2444 |
| 511 | 0,3916 | 0,3913 | 0,4180 | 0,3913 |
| 661,6 | 0,5561 | 0,5547 | 0,5852 | 0,5557 |
| 1173,2 | 0,9940 | 0,9899 | 1,0171 | 0,9923 |
| 1274,5 | 1,0591 | 1,0553 | 1,0812 | 1,0591 |
| 1332,5 | 1,0931 | 1,0888 | 1,1144 | 1,0907 |

### 4.1.2.4. Tenth value layer (TVL) results for the P-series

**Table 4.90:** Tenth value layer (TVL) results for the P-ABS-0

| Energy (keV) | Experimental (cm) | EpiXS (cm) | Xcom (cm) | Geant4 (cm) | FLUKA (cm) |
|---|---|---|---|---|---|
| 59,5 | 12,2202 | 11,7017 | 11,6984 | 12,2897 | 11,7266 |
| 80,9 | 13,5484 | 12,7744 | 12,7686 | 13,1580 | 12,7835 |
| 276,3 | 20,0171 | 18,5996 | 18,5775 | 18,7337 | 18,5775 |
| 302,8 | 20,8710 | 19,2252 | 19,2253 | 19,3400 | 19,2253 |
| 356 | 21,6771 | 20,4616 | 20,4369 | 20,4996 | 20,4616 |
| 383,8 | 20,6433 | 21,0507 | 21,0415 | 21,0817 | 21,0708 |
| 511 | 24,6259 | 23,6681 | 23,6502 | 23,5839 | 23,5839 |
| 661,6 | 26,1196 | 26,4868 | 26,4596 | 26,3160 | 26,3963 |
| 1173,2 | 37,6520 | 34,8021 | 34,7376 | 34,5905 | 34,5905 |
| 1274,5 | 35,9991 | 36,2936 | 36,2510 | 36,1049 | 36,2936 |
| 1332,5 | 38,0113 | 37,1584 | 37,0862 | 36,9575 | 37,0862 |

**Table 4.91:** Tenth value layer (TVL) results for the P-ABS-Er5

| Energy (keV) | Experimental (cm) | EpiXS (cm) | Xcom (cm) | Geant4 (cm) | FLUKA (cm) |
|---|---|---|---|---|---|
| 59,5 | 2,7567 | 2,7346 | 2,7129 | 2,8143 | 2,7240 |
| 80,9 | 4,8621 | 4,8544 | 4,8576 | 5,0197 | 4,8577 |
| 276,3 | 17,3313 | 16,7961 | 16,7843 | 17,0507 | 16,7961 |
| 302,8 | 18,3898 | 17,6210 | 17,6139 | 17,8491 | 17,6139 |
| 356 | 19,3684 | 19,1262 | 19,1092 | 19,2694 | 19,1262 |
| 383,8 | 18,6272 | 19,8149 | 19,8176 | 19,9433 | 19,8176 |
| 511 | 24,4527 | 22,6797 | 22,6613 | 22,6748 | 22,6748 |
| 661,6 | 26,1196 | 25,6053 | 25,5780 | 25,4969 | 25,5780 |
| 1173,2 | 35,2844 | 33,9341 | 33,8718 | 33,7552 | 33,9341 |
| 1274,5 | 35,9991 | 35,4040 | 35,3617 | 35,2452 | 35,3617 |
| 1332,5 | 35,1440 | 36,2530 | 36,1815 | 36,0807 | 36,2530 |

**Table 4.92:** Tenth value layer (TVL) results for the P-ABS-Gd5

| Energy (keV) | Experimental (cm) | EpiXS (cm) | Xcom (cm) | Geant4 (cm) | FLUKA (cm) |
|---|---|---|---|---|---|
| 59,5 | 3,1802 | 3,0508 | 3,0525 | 3,1524 | 3,0520 |
| 80,9 | 5,3687 | 5,3445 | 5,3517 | 5,5467 | 5,5453 |
| 276,3 | 18,3198 | 17,0489 | 17,0437 | 17,2957 | 17,0489 |
| 302,8 | 19,2363 | 17,8440 | 17,8391 | 18,0634 | 17,9890 |
| 356 | 19,2158 | 19,3067 | 19,2855 | 19,4396 | 19,2855 |
| 383,8 | 21,4096 | 19,9783 | 19,9691 | 20,0966 | 19,9691 |
| 511 | 24,6259 | 22,7965 | 22,7782 | 22,7840 | 22,7965 |
| 661,6 | 26,6550 | 25,6994 | 25,6708 | 25,5831 | 25,6994 |
| 1173,2 | 36,6690 | 34,0047 | 33,9415 | 33,8219 | 34,0047 |
| 1274,5 | 36,8842 | 35,4744 | 35,4302 | 35,3115 | 35,4744 |
| 1332,5 | 36,5232 | 36,3237 | 36,2522 | 36,1475 | 36,2522 |

**Table 4.93:** Tenth value layer (TVL) results for the P-ABS-Er10

| Energy (keV) | Experimental (cm) | EpiXS (cm) | Xcom (cm) | Geant4 (cm) | FLUKA (cm) |
|---|---|---|---|---|---|
| 59,5 | 1,4995 | 1,4829 | 1,4695 | 1,5219 | 1,4864 |
| 80,9 | 2,9405 | 2,8795 | 2,8817 | 2,9802 | 2,9132 |
| 276,3 | 15,2926 | 14,9907 | 14,9867 | 15,3222 | 14,9907 |
| 302,8 | 16,2603 | 15,9350 | 15,9351 | 16,2409 | 15,9989 |
| 356 | 17,9424 | 17,6089 | 17,5836 | 17,8342 | 17,8342 |
| 383,8 | 18,7338 | 18,3630 | 18,3591 | 18,5697 | 18,3591 |
| 511 | 21,7985 | 21,3811 | 21,3625 | 21,4461 | 21,3625 |
| 661,6 | 24,8190 | 24,3495 | 24,3226 | 24,3000 | 24,3000 |
| 1173,2 | 33,1473 | 32,5487 | 32,4844 | 32,4033 | 32,4844 |
| 1274,5 | 34,6252 | 33,9739 | 33,9327 | 33,8454 | 33,9327 |
| 1332,5 | 35,4328 | 34,7938 | 34,7241 | 34,6515 | 34,6515 |

**Table 4.94:** Tenth value layer (TVL) results for the P-ABS-Gd10

| Energy (keV) | Experimental (cm) | EpiXS (cm) | Xcom (cm) | Geant4 (cm) | FLUKA (cm) |
|---|---|---|---|---|---|
| 59,5 | 1,5199 | 1,6831 | 1,4839 | 1,7348 | 1,6971 |
| 80,9 | 3,0650 | 3,2537 | 2,9067 | 3,3836 | 3,3954 |
| 276,3 | 15,8224 | 15,4251 | 15,0355 | 15,7489 | 15,4251 |
| 302,8 | 16,5990 | 16,3281 | 15,9877 | 16,6233 | 15,9877 |
| 356 | 18,2076 | 17,9393 | 17,6431 | 18,1489 | 18,0847 |
| 383,8 | 19,9273 | 18,6661 | 18,4219 | 18,8586 | 18,6661 |
| 511 | 22,6898 | 21,6065 | 21,4231 | 21,6588 | 21,6065 |
| 661,6 | 24,9871 | 24,5361 | 24,3839 | 24,4720 | 24,3839 |
| 1173,2 | 33,5885 | 32,6947 | 32,5662 | 32,5413 | 32,6947 |
| 1274,5 | 32,1265 | 34,1200 | 34,0125 | 33,9843 | 33,9843 |
| 1332,5 | 33,8620 | 34,9406 | 34,8116 | 34,7909 | 34,8116 |

**Table 4.95:** Tenth value layer (TVL) results for the P-ABS-Er10Gd5

| Energy (keV) | Experimental (cm) | EpiXS (cm) | Xcom (cm) | Geant4 (cm) | FLUKA (cm) |
|---|---|---|---|---|---|
| 59,5 | 1,0890 | 1,0295 | 1,0228 | 1,0568 | 1,0298 |
| 80,9 | 2,2120 | 2,0767 | 2,0793 | 2,1537 | 2,0784 |
| 276,3 | 13,7364 | 13,5904 | 13,5873 | 13,9690 | 13,5904 |
| 302,8 | 15,6047 | 14,5898 | 14,5862 | 14,9473 | 14,9473 |
| 356 | 15,8865 | 16,3472 | 16,3253 | 16,6510 | 16,3472 |
| 383,8 | 16,6993 | 17,1347 | 17,1307 | 17,4146 | 17,1347 |
| 511 | 20,8951 | 20,2257 | 20,2093 | 20,3464 | 20,2093 |
| 661,6 | 24,5134 | 23,1994 | 23,1717 | 23,1972 | 23,1994 |
| 1173,2 | 32,0433 | 31,2312 | 31,1743 | 31,1139 | 31,2312 |
| 1274,5 | 34,3468 | 32,6105 | 32,5685 | 32,5075 | 32,6105 |
| 1332,5 | 32,2872 | 33,4012 | 33,3334 | 33,2838 | 33,3334 |

**Table 4.96:** Tenth value layer (TVL) results for the P-ABS-Er5Gd10

| Energy (keV) | Experimental (cm) | EpiXS (cm) | Xcom (cm) | Geant4 (cm) | FLUKA (cm) |
|---|---|---|---|---|---|
| 59,5 | 1,0428 | 1,0764 | 1,0731 | 1,1066 | 1,0808 |
| 80,9 | 2,3526 | 2,1718 | 2,1755 | 2,2563 | 2,1774 |
| 276,3 | 13,8905 | 13,7748 | 13,7765 | 14,1521 | 13,7765 |
| 302,8 | 14,5637 | 14,7601 | 14,7583 | 15,0948 | 14,7695 |
| 356 | 15,7287 | 16,4944 | 16,4829 | 16,7711 | 16,4829 |
| 383,8 | 16,9515 | 17,2711 | 17,2726 | 17,5293 | 17,2880 |
| 511 | 21,8266 | 20,3296 | 20,3154 | 20,4447 | 20,3154 |
| 661,6 | 24,8671 | 23,2860 | 23,2572 | 23,2822 | 23,2572 |
| 1173,2 | 32,0433 | 31,2987 | 31,2410 | 31,1779 | 31,1779 |
| 1274,5 | 30,7942 | 32,6779 | 32,6341 | 32,5713 | 32,6341 |
| 1332,5 | 32,2872 | 33,4690 | 33,4012 | 33,3486 | 33,3486 |

**Table 4.97:** Tenth value layer (TVL) results for the P-ABS-Er20

| Energy (keV) | Experimental (cm) | EpiXS (cm) | Xcom (cm) | Geant4 (cm) | FLUKA (cm) |
|---|---|---|---|---|---|
| 59,5 | 0,6713 | 0,7195 | 0,7126 | 0,7372 | 0,7143 |
| 80,9 | 1,6191 | 1,4819 | 1,4832 | 1,5347 | 1,4826 |
| 276,3 | 12,4782 | 12,0050 | 12,0026 | 12,4123 | 12,0261 |
| 302,8 | 12,9450 | 13,0473 | 13,0474 | 13,4412 | 13,0474 |
| 356 | 13,9134 | 14,8803 | 14,8677 | 15,2137 | 14,8803 |
| 383,8 | 14,9084 | 15,7037 | 15,7036 | 16,0202 | 15,7036 |
| 511 | 20,1546 | 18,8846 | 18,8681 | 19,0626 | 18,9010 |
| 661,6 | 21,7149 | 21,8746 | 21,8462 | 21,9767 | 21,8462 |
| 1173,2 | 31,3211 | 29,7501 | 29,6924 | 29,6666 | 29,6924 |
| 1274,5 | 28,9843 | 31,0812 | 31,0370 | 31,0089 | 31,0089 |
| 1332,5 | 31,1959 | 31,8410 | 31,7753 | 31,7545 | 31,7753 |

**Table 4.98:** Tenth value layer (TVL) results for the P-ABS-Gd20

| Energy (keV) | Experimental (cm) | EpiXS (cm) | Xcom (cm) | Geant4 (cm) | FLUKA (cm) |
|---|---|---|---|---|---|
| 59,5 | 0,8735 | 0,8266 | 0,8271 | 0,8506 | 0,8267 |
| 80,9 | 1,8398 | 1,7087 | 1,7123 | 1,7796 | 1,7123 |
| 276,3 | 13,2921 | 12,6402 | 12,6377 | 13,0490 | 12,6402 |
| 302,8 | 13,7782 | 13,6461 | 13,6528 | 14,0366 | 13,6528 |
| 356 | 15,4974 | 15,4133 | 15,4006 | 15,7314 | 15,4133 |
| 383,8 | 15,9830 | 16,2029 | 16,1948 | 16,5036 | 16,1948 |
| 511 | 20,7682 | 19,2769 | 19,2647 | 19,4363 | 19,2769 |
| 661,6 | 23,7243 | 22,2078 | 22,1799 | 22,2358 | 22,1799 |
| 1173,2 | 31,6782 | 30,0156 | 29,9594 | 29,9657 | 29,9594 |
| 1274,5 | 30,7942 | 31,3469 | 31,3060 | 31,2611 | 31,3469 |
| 1332,5 | 31,9153 | 32,1081 | 32,0424 | 32,0075 | 32,0424 |

**Table 4.99:** Tenth value layer (TVL) results for the Lead (Pb)

| Energy (keV) | EpiXS (cm) | Xcom (cm) | Geant4 (cm) | FLUKA (cm) |
|---|---|---|---|---|
| 59,5 | 0,0399 | 0,0396 | 0,0446 | 0,0405 |
| 80,9 | 0,0888 | 0,0863 | 0,1003 | 0,0883 |
| 276,3 | 0,4234 | 0,4235 | 0,4547 | 0,4235 |
| 302,8 | 0,5135 | 0,5133 | 0,5522 | 0,5134 |
| 356 | 0,7075 | 0,7068 | 0,7611 | 0,7075 |
| 383,8 | 0,8129 | 0,8122 | 0,8742 | 0,8119 |
| 511 | 1,3009 | 1,2999 | 1,3887 | 1,2999 |
| 661,6 | 1,8473 | 1,8426 | 1,9440 | 1,8459 |
| 1173,2 | 3,3019 | 3,2883 | 3,3788 | 3,2963 |
| 1274,5 | 3,5181 | 3,5057 | 3,5918 | 3,5181 |
| 1332,5 | 3,6311 | 3,6168 | 3,7020 | 3,6233 |

### 4.1.2.5. Mean free path (MFP) results for the P-series

**Table 4.100:** Mean free path (MFP) results for the P-ABS-0

| Energy (keV) | Experimental (cm) | EpiXS (cm) | Xcom (cm) | Geant4 (cm) | FLUKA (cm) |
|---|---|---|---|---|---|
| 59,5 | 5,3072 | 5,0820 | 5,0805 | 5,3374 | 5,0928 |
| 80,9 | 5,8840 | 5,5479 | 5,5454 | 5,7144 | 5,5518 |
| 276,3 | 8,6933 | 8,0777 | 8,0681 | 8,1359 | 8,0681 |
| 302,8 | 9,0641 | 8,3494 | 8,3495 | 8,3993 | 8,3495 |
| 356 | 9,4142 | 8,8864 | 8,8756 | 8,9029 | 8,8864 |
| 383,8 | 8,9653 | 9,1422 | 9,1382 | 9,1557 | 9,1509 |
| 511 | 10,6949 | 10,2789 | 10,2712 | 10,2424 | 10,2424 |
| 661,6 | 11,3436 | 11,5031 | 11,4913 | 11,4289 | 11,4638 |
| 1173,2 | 16,3520 | 15,1144 | 15,0864 | 15,0225 | 15,0225 |
| 1274,5 | 15,6342 | 15,7621 | 15,7436 | 15,6802 | 15,7621 |
| 1332,5 | 16,5081 | 16,1377 | 16,1063 | 16,0505 | 16,1063 |

**Table 4.101:** Mean free path (MFP) results for the P-ABS-Er5

| Energy (keV) | Experimental (cm) | EpiXS (cm) | Xcom (cm) | Geant4 (cm) | FLUKA (cm) |
|---|---|---|---|---|---|
| 59,5 | 1,1972 | 1,1876 | 1,1782 | 1,2222 | 1,1830 |
| 80,9 | 2,1116 | 2,1082 | 2,1096 | 2,1800 | 2,1097 |
| 276,3 | 7,5269 | 7,2944 | 7,2893 | 7,4050 | 7,2944 |
| 302,8 | 7,9866 | 7,6527 | 7,6496 | 7,7518 | 7,6496 |
| 356 | 8,4116 | 8,3064 | 8,2990 | 8,3686 | 8,3064 |
| 383,8 | 8,0897 | 8,6055 | 8,6067 | 8,6613 | 8,6067 |
| 511 | 10,6197 | 9,8497 | 9,8417 | 9,8475 | 9,8475 |
| 661,6 | 11,3436 | 11,1203 | 11,1084 | 11,0732 | 11,1084 |
| 1173,2 | 15,3238 | 14,7374 | 14,7103 | 14,6597 | 14,7374 |
| 1274,5 | 15,6342 | 15,3758 | 15,3574 | 15,3068 | 15,3574 |
| 1332,5 | 15,2628 | 15,7445 | 15,7134 | 15,6697 | 15,7445 |

**Table 4.102:** Mean free path (MFP) results for the P-ABS-Gd5

| Energy (keV) | Experimental (cm) | EpiXS (cm) | Xcom (cm) | Geant4 (cm) | FLUKA (cm) |
|---|---|---|---|---|---|
| 59,5 | 1,3811 | 1,3250 | 1,3257 | 1,3691 | 1,3255 |
| 80,9 | 2,3316 | 2,3211 | 2,3242 | 2,4089 | 2,4083 |
| 276,3 | 7,9562 | 7,4042 | 7,4020 | 7,5114 | 7,4042 |
| 302,8 | 8,3542 | 7,7496 | 7,7474 | 7,8448 | 7,8125 |
| 356 | 8,3453 | 8,3848 | 8,3756 | 8,4425 | 8,3756 |
| 383,8 | 9,2981 | 8,6765 | 8,6725 | 8,7278 | 8,6725 |
| 511 | 10,6949 | 9,9004 | 9,8924 | 9,8950 | 9,9004 |
| 661,6 | 11,5761 | 11,1611 | 11,1487 | 11,1106 | 11,1611 |
| 1173,2 | 15,9251 | 14,7681 | 14,7406 | 14,6887 | 14,7681 |
| 1274,5 | 16,0186 | 15,4064 | 15,3871 | 15,3356 | 15,4064 |
| 1332,5 | 15,8618 | 15,7752 | 15,7441 | 15,6987 | 15,7441 |

**Table 4.103:** Mean free path (MFP) results for the P-ABS-Er10

| Energy (keV) | Experimental (cm) | EpiXS (cm) | Xcom (cm) | Geant4 (cm) | FLUKA (cm) |
|---|---|---|---|---|---|
| 59,5 | 0,6512 | 0,6440 | 0,6382 | 0,6610 | 0,6456 |
| 80,9 | 1,2771 | 1,2505 | 1,2515 | 1,2943 | 1,2652 |
| 276,3 | 6,6415 | 6,5104 | 6,5087 | 6,6544 | 6,5104 |
| 302,8 | 7,0618 | 6,9205 | 6,9205 | 7,0533 | 6,9482 |
| 356 | 7,7923 | 7,6475 | 7,6364 | 7,7453 | 7,7453 |
| 383,8 | 8,1360 | 7,9750 | 7,9732 | 8,0647 | 7,9732 |
| 511 | 9,4670 | 9,2857 | 9,2776 | 9,3139 | 9,2776 |
| 661,6 | 10,7787 | 10,5748 | 10,5632 | 10,5534 | 10,5534 |
| 1173,2 | 14,3957 | 14,1357 | 14,1078 | 14,0726 | 14,1078 |
| 1274,5 | 15,0375 | 14,7547 | 14,7368 | 14,6989 | 14,7368 |
| 1332,5 | 15,3882 | 15,1108 | 15,0805 | 15,0490 | 15,0490 |

**Table 4.104:** Mean free path (MFP) results for the P-ABS-Gd10

| Energy (keV) | Experimental (cm) | EpiXS (cm) | Xcom (cm) | Geant4 (cm) | FLUKA (cm) |
|---|---|---|---|---|---|
| 59,5 | 0,6601 | 0,7310 | 0,6445 | 0,7534 | 0,7370 |
| 80,9 | 1,3311 | 1,4131 | 1,2623 | 1,4695 | 1,4746 |
| 276,3 | 6,8716 | 6,6991 | 6,5299 | 6,8396 | 6,6991 |
| 302,8 | 7,2089 | 7,0912 | 6,9434 | 7,2194 | 6,9434 |
| 356 | 7,9075 | 7,7910 | 7,6623 | 7,8820 | 7,8541 |
| 383,8 | 8,6543 | 8,1066 | 8,0005 | 8,1902 | 8,1066 |
| 511 | 9,8540 | 9,3836 | 9,3039 | 9,4063 | 9,3836 |
| 661,6 | 10,8518 | 10,6559 | 10,5898 | 10,6281 | 10,5898 |
| 1173,2 | 14,5873 | 14,1991 | 14,1433 | 14,1325 | 14,1991 |
| 1274,5 | 13,9524 | 14,8181 | 14,7715 | 14,7592 | 14,7592 |
| 1332,5 | 14,7061 | 15,1745 | 15,1185 | 15,1095 | 15,1185 |

**Table 4.105:** Mean free path (MFP) results for the P-ABS-Er10Gd5

| Energy (keV) | Experimental (cm) | EpiXS (cm) | Xcom (cm) | Geant4 (cm) | FLUKA (cm) |
|---|---|---|---|---|---|
| 59,5 | 0,4729 | 0,4471 | 0,4442 | 0,4589 | 0,4473 |
| 80,9 | 0,9606 | 0,9019 | 0,9030 | 0,9353 | 0,9026 |
| 276,3 | 5,9656 | 5,9022 | 5,9009 | 6,0666 | 5,9022 |
| 302,8 | 6,7770 | 6,3363 | 6,3347 | 6,4915 | 6,4915 |
| 356 | 6,8994 | 7,0995 | 7,0900 | 7,2314 | 7,0995 |
| 383,8 | 7,2524 | 7,4415 | 7,4398 | 7,5631 | 7,4415 |
| 511 | 9,0746 | 8,7839 | 8,7768 | 8,8363 | 8,7768 |
| 661,6 | 10,6460 | 10,0754 | 10,0634 | 10,0744 | 10,0754 |
| 1173,2 | 13,9162 | 13,5635 | 13,5388 | 13,5126 | 13,5635 |
| 1274,5 | 14,9166 | 14,1626 | 14,1443 | 14,1178 | 14,1626 |
| 1332,5 | 14,0221 | 14,5060 | 14,4765 | 14,4550 | 14,4765 |

**Table 4.106:** Mean free path (MFP) results for the P-ABS-Er5Gd10

| Energy (keV) | Experimental (cm) | EpiXS (cm) | Xcom (cm) | Geant4 (cm) | FLUKA (cm) |
|---|---|---|---|---|---|
| 59,5 | 0,4529 | 0,4675 | 0,4660 | 0,4806 | 0,4694 |
| 80,9 | 1,0217 | 0,9432 | 0,9448 | 0,9799 | 0,9456 |
| 276,3 | 6,0326 | 5,9823 | 5,9831 | 6,1462 | 5,9831 |
| 302,8 | 6,3249 | 6,4102 | 6,4095 | 6,5556 | 6,4143 |
| 356 | 6,8309 | 7,1634 | 7,1584 | 7,2836 | 7,1584 |
| 383,8 | 7,3619 | 7,5007 | 7,5014 | 7,6129 | 7,5081 |
| 511 | 9,4792 | 8,8290 | 8,8229 | 8,8790 | 8,8229 |
| 661,6 | 10,7996 | 10,1130 | 10,1005 | 10,1113 | 10,1005 |
| 1173,2 | 13,9162 | 13,5929 | 13,5678 | 13,5404 | 13,5404 |
| 1274,5 | 13,3738 | 14,1918 | 14,1728 | 14,1455 | 14,1728 |
| 1332,5 | 14,0221 | 14,5354 | 14,5060 | 14,4831 | 14,4831 |

**Table 4.107:** Mean free path (MFP) results for the P-ABS-Er20

| Energy (keV) | Experimental (cm) | EpiXS (cm) | Xcom (cm) | Geant4 (cm) | FLUKA (cm) |
|---|---|---|---|---|---|
| 59,5 | 0,2915 | 0,3125 | 0,3095 | 0,3202 | 0,3102 |
| 80,9 | 0,7032 | 0,6436 | 0,6441 | 0,6665 | 0,6439 |
| 276,3 | 5,4192 | 5,2137 | 5,2127 | 5,3906 | 5,2229 |
| 302,8 | 5,6219 | 5,6664 | 5,6664 | 5,8375 | 5,6664 |
| 356 | 6,0425 | 6,4625 | 6,4570 | 6,6072 | 6,4625 |
| 383,8 | 6,4746 | 6,8200 | 6,8200 | 6,9575 | 6,8200 |
| 511 | 8,7531 | 8,2015 | 8,1943 | 8,2788 | 8,2086 |
| 661,6 | 9,4307 | 9,5000 | 9,4877 | 9,5443 | 9,4877 |
| 1173,2 | 13,6026 | 12,9203 | 12,8952 | 12,8840 | 12,8952 |
| 1274,5 | 12,5877 | 13,4984 | 13,4792 | 13,4670 | 13,4670 |
| 1332,5 | 13,5482 | 13,8284 | 13,7998 | 13,7908 | 13,7998 |

**Table 4.108:** Mean free path (MFP) results for the P-ABS-Gd20

| Energy (keV) | Experimental (cm) | EpiXS (cm) | Xcom (cm) | Geant4 (cm) | FLUKA (cm) |
|---|---|---|---|---|---|
| 59,5 | 0,3793 | 0,3590 | 0,3592 | 0,3694 | 0,3590 |
| 80,9 | 0,7990 | 0,7421 | 0,7436 | 0,7728 | 0,7436 |
| 276,3 | 5,7727 | 5,4896 | 5,4885 | 5,6671 | 5,4896 |
| 302,8 | 5,9838 | 5,9264 | 5,9294 | 6,0960 | 5,9294 |
| 356 | 6,7304 | 6,6939 | 6,6884 | 6,8321 | 6,6939 |
| 383,8 | 6,9413 | 7,0368 | 7,0333 | 7,1674 | 7,0333 |
| 511 | 9,0195 | 8,3718 | 8,3666 | 8,4411 | 8,3718 |
| 661,6 | 10,3033 | 9,6447 | 9,6326 | 9,6569 | 9,6326 |
| 1173,2 | 13,7577 | 13,0356 | 13,0112 | 13,0139 | 13,0112 |
| 1274,5 | 13,3738 | 13,6138 | 13,5960 | 13,5765 | 13,6138 |
| 1332,5 | 13,8607 | 13,9444 | 13,9158 | 13,9007 | 13,9158 |

**Table 4.109:** Mean free path (MFP) results for the Lead (Pb)

| Energy (keV) | EpiXS (cm) | Xcom (cm) | Geant4 (cm) | FLUKA (cm) |
|---|---|---|---|---|
| 59,5 | 0,0173 | 0,0172 | 0,0194 | 0,0176 |
| 80,9 | 0,0385 | 0,0375 | 0,0436 | 0,0383 |
| 276,3 | 0,1839 | 0,1839 | 0,1975 | 0,1839 |
| 302,8 | 0,2230 | 0,2229 | 0,2398 | 0,2230 |
| 356 | 0,3073 | 0,3069 | 0,3305 | 0,3073 |
| 383,8 | 0,3531 | 0,3527 | 0,3796 | 0,3526 |
| 511 | 0,5650 | 0,5646 | 0,6031 | 0,5646 |
| 661,6 | 0,8023 | 0,8002 | 0,8443 | 0,8017 |
| 1173,2 | 1,4340 | 1,4281 | 1,4674 | 1,4315 |
| 1274,5 | 1,5279 | 1,5225 | 1,5599 | 1,5279 |
| 1332,5 | 1,5770 | 1,5708 | 1,6078 | 1,5736 |

#### 4.1.2.6. Radiation protection efficiency (RPE) results for the P-series

Radiation protection efficiency (RPE) is a parameter that measures how effective a shielding material or protective measure is in reducing exposure levels to radiation. This value is important for assessing the effectiveness of protective measures used to limit the adverse effects of radiation on humans or the environment. A high RPE value indicates that radiation is effectively blocked, reducing exposure levels and thus mitigating health risks. Radiation protection efficiency can be influenced by various factors, including the properties of the material used, its thickness, energy levels, and usage conditions. Therefore, RPE assessments and measurements play a critical role in the design and implementation of radiation safety and protection measures. There are several strategies and methods to increase Radiation Protection Efficiency (RPE) against gamma radiation. Here are some measures that can be taken to enhance RPE: Use High-Density Materials: Denser materials tend to absorb gamma radiation more effectively. Therefore, materials with higher density should be preferred. Increase Material Thickness: To enhance the ability to absorb gamma radiation, you can increase the thickness of the material. A thicker material layer provides greater protection. Utilize High Atomic Number Materials: Materials with a high atomic number absorb gamma radiation more effectively. For example, materials like lead with a high atomic number can be preferred. Use Composite Materials: Some composite materials, formed by the combination of different elements, can provide better RPE. For instance, incorporating lead granules into concrete can result in more effective shielding. Apply Surface Coatings: Adding special coatings or coating materials to the surface of the material can increase RPE. These coatings can absorb gamma radiation emitted from the surface.Optimized Design: The design of radiation protection equipment should aim to effectively absorb gamma radiation. Considerations such as material placement, shape, and thickness design are crucial. Incorporate Radiation-Absorbing Materials: Certain specialized radiation-absorbing materials can enhance RPE. For example, materials like boron carbide or lead-impregnated plastics can effectively absorb gamma radiation. Regular Maintenance and Inspection: Radiation protection equipment should undergo regular maintenance and inspection. Damage or weakening of materials can reduce RPE.Simulation and Testing: It's essential to evaluate different material and design options through specialized simulations and tests before attempting to increase RPE.

**Table 4.110:** Radiation Protection Efficiency (RPE) 0,50 mm = 0,05 cm (FLUKA) results for the P series

| Energy (keV) | P-ABS-0 | P-ABS-Er5 | P-ABS-Gd5 | P-ABS-Er10 | P-ABS-Gd10 | P-ABS-Er10Gd5 | P-ABS-Er5Gd10 | P-ABS-Er20 | P-ABS-Gd20 |
|---|---|---|---|---|---|---|---|---|---|
| 59,5 | 0,9324 | 4,0084 | 3,5862 | 7,2856 | 6,4210 | 10,3220 | 9,8809 | 14,4592 | 12,6585 |
| 80,9 | 0,8712 | 2,2675 | 2,0542 | 3,7895 | 3,3453 | 5,2054 | 4,9746 | 7,2274 | 6,2647 |
| 276,3 | 0,6127 | 0,6729 | 0,6634 | 0,7486 | 0,7284 | 0,8208 | 0,8102 | 0,9233 | 0,8784 |
| 302,8 | 0,5935 | 0,6429 | 0,6353 | 0,7064 | 0,6902 | 0,7673 | 0,7598 | 0,8529 | 0,8169 |
| 356 | 0,5600 | 0,5957 | 0,5905 | 0,6435 | 0,6324 | 0,6890 | 0,6841 | 0,7539 | 0,7292 |
| 383,8 | 0,5446 | 0,5756 | 0,5712 | 0,6181 | 0,6086 | 0,6589 | 0,6546 | 0,7161 | 0,6952 |
| 511 | 0,4870 | 0,5065 | 0,5040 | 0,5354 | 0,5301 | 0,5642 | 0,5615 | 0,6021 | 0,5906 |
| 661,6 | 0,4365 | 0,4505 | 0,4490 | 0,4727 | 0,4693 | 0,4951 | 0,4933 | 0,5225 | 0,5164 |
| 1173,2 | 0,3323 | 0,3405 | 0,3398 | 0,3547 | 0,3532 | 0,3693 | 0,3686 | 0,3873 | 0,3835 |
| 1274,5 | 0,3184 | 0,3261 | 0,3255 | 0,3396 | 0,3382 | 0,3535 | 0,3528 | 0,3706 | 0,3676 |
| 1332,5 | 0,3110 | 0,3186 | 0,3180 | 0,3317 | 0,3304 | 0,3453 | 0,3446 | 0,3619 | 0,3590 |

**Table 4.111:** Radiation Protection Efficiency (RPE) 0,75 mm = 0,075 cm (FLUKA) results for the P series

| Energy (keV) | P-ABS-0 | P-ABS-Er5 | P-ABS-Gd5 | P-ABS-Er10 | P-ABS-Gd10 | P-ABS-Er10Gd5 | P-ABS-Er5Gd10 | P-ABS-Er20 | P-ABS-Gd20 |
|---|---|---|---|---|---|---|---|---|---|
| 59,5 | 1,3954 | 5,9519 | 5,3308 | 10,7269 | 9,4751 | 15,0764 | 14,4490 | 20,8847 | 18,3735 |
| 80,9 | 1,3039 | 3,3818 | 3,0655 | 5,6301 | 4,9757 | 7,7056 | 7,3684 | 10,6428 | 9,2483 |
| 276,3 | 0,9176 | 1,0077 | 0,9935 | 1,1208 | 1,0906 | 1,2287 | 1,2129 | 1,3817 | 1,3147 |
| 302,8 | 0,8890 | 0,9629 | 0,9515 | 1,0577 | 1,0335 | 1,1487 | 1,1375 | 1,2766 | 1,2228 |
| 356 | 0,8389 | 0,8922 | 0,8844 | 0,9637 | 0,9470 | 1,0318 | 1,0244 | 1,1287 | 1,0918 |
| 383,8 | 0,8158 | 0,8622 | 0,8556 | 0,9257 | 0,9116 | 0,9868 | 0,9803 | 1,0722 | 1,0409 |
| 511 | 0,7296 | 0,7587 | 0,7551 | 0,8020 | 0,7942 | 0,8452 | 0,8411 | 0,9018 | 0,8846 |
| 661,6 | 0,6541 | 0,6750 | 0,6728 | 0,7082 | 0,7032 | 0,7417 | 0,7390 | 0,7827 | 0,7736 |
| 1173,2 | 0,4980 | 0,5103 | 0,5093 | 0,5315 | 0,5293 | 0,5535 | 0,5524 | 0,5804 | 0,5746 |
| 1274,5 | 0,4772 | 0,4888 | 0,4879 | 0,5089 | 0,5069 | 0,5298 | 0,5288 | 0,5554 | 0,5509 |
| 1332,5 | 0,4662 | 0,4775 | 0,4766 | 0,4971 | 0,4951 | 0,5175 | 0,5165 | 0,5424 | 0,5381 |

**Table 4.112:** Radiation Protection Efficiency (RPE) 10 mm = 1 cm (FLUKA) results for the P series

| Energy (keV) | P-ABS-0 | P-ABS-Er5 | P-ABS-Gd5 | P-ABS-Er10 | P-ABS-Gd10 | P-ABS-Er10Gd5 | P-ABS-Er5Gd10 | P-ABS-Er20 | P-ABS-Gd20 |
|---|---|---|---|---|---|---|---|---|---|
| 59,5 | 17,0854 | 55,8769 | 51,8296 | 77,9738 | 73,4801 | 88,6834 | 87,5166 | 95,5998 | 93,3256 |
| 80,9 | 16,0539 | 36,7904 | 33,9744 | 53,8205 | 49,3639 | 65,6701 | 63,9594 | 77,6954 | 72,5804 |
| 276,3 | 11,5658 | 12,6322 | 12,4649 | 13,9531 | 13,6021 | 15,1967 | 15,0156 | 16,9318 | 16,1766 |
| 302,8 | 11,2244 | 12,1028 | 11,9682 | 13,2185 | 12,9350 | 14,2769 | 14,1477 | 15,7438 | 15,1293 |
| 356 | 10,6245 | 11,2631 | 11,1702 | 12,1124 | 11,9154 | 12,9149 | 12,8287 | 14,0452 | 13,6161 |
| 383,8 | 10,3469 | 10,9041 | 10,8256 | 11,6618 | 11,4938 | 12,3853 | 12,3095 | 13,3879 | 13,0225 |
| 511 | 9,3019 | 9,6562 | 9,6123 | 10,1803 | 10,0856 | 10,7001 | 10,6514 | 11,3781 | 11,1720 |
| 661,6 | 8,3779 | 8,6351 | 8,6073 | 9,0406 | 8,9800 | 9,4494 | 9,4166 | 9,9472 | 9,8372 |
| 1173,2 | 6,4400 | 6,5940 | 6,5814 | 6,8594 | 6,8313 | 7,1333 | 7,1192 | 7,4680 | 7,3963 |
| 1274,5 | 6,1784 | 6,3242 | 6,3127 | 6,5770 | 6,5510 | 6,8382 | 6,8253 | 7,1566 | 7,1009 |
| 1332,5 | 6,0402 | 6,1824 | 6,1713 | 6,4290 | 6,4041 | 6,6842 | 6,6716 | 6,9946 | 6,9412 |

**Table 4.113:** Radiation Protection Efficiency (RPE) 20 mm = 2 cm (FLUKA) results for the P series

| Energy (keV) | P-ABS-0 | P-ABS-Er5 | P-ABS-Gd5 | P-ABS-Er10 | P-ABS-Gd10 | P-ABS-Er10Gd5 | P-ABS-Er5Gd10 | P-ABS-Er20 | P-ABS-Gd20 |
|---|---|---|---|---|---|---|---|---|---|
| 59,5 | 31,2516 | 80,5316 | 76,7962 | 95,1484 | 92,9670 | 98,7194 | 98,4416 | 99,8064 | 99,5545 |
| 80,9 | 29,5305 | 60,0454 | 56,4062 | 78,6745 | 74,3599 | 88,2146 | 87,0108 | 95,0250 | 92,4817 |
| 276,3 | 21,7939 | 23,6687 | 23,3761 | 25,9593 | 25,3540 | 28,0840 | 27,7765 | 30,9967 | 29,7363 |
| 302,8 | 21,1889 | 22,7409 | 22,5041 | 24,6898 | 24,1969 | 26,5154 | 26,2938 | 29,0088 | 27,9697 |
| 356 | 20,1201 | 21,2576 | 21,0927 | 22,7576 | 22,4110 | 24,1619 | 24,0116 | 26,1178 | 25,3782 |
| 383,8 | 19,6232 | 20,6191 | 20,4792 | 21,9635 | 21,6665 | 23,2367 | 23,1038 | 24,9834 | 24,3491 |
| 511 | 17,7385 | 18,3800 | 18,3006 | 19,3243 | 19,1539 | 20,2552 | 20,1683 | 21,4615 | 21,0958 |
| 661,6 | 16,0539 | 16,5245 | 16,4737 | 17,2638 | 17,1535 | 18,0059 | 17,9464 | 18,9049 | 18,7066 |
| 1173,2 | 12,4652 | 12,7531 | 12,7296 | 13,2483 | 13,1960 | 13,7577 | 13,7315 | 14,3783 | 14,2455 |
| 1274,5 | 11,9750 | 12,2485 | 12,2269 | 12,7214 | 12,6729 | 13,2088 | 13,1847 | 13,8010 | 13,6976 |
| 1332,5 | 11,7156 | 11,9826 | 11,9618 | 12,4447 | 12,3981 | 12,9215 | 12,8981 | 13,4999 | 13,4006 |

**Table 4.114**: Radiation Protection Efficiency (RPE) 50 mm = 5 cm (FLUKA) results for the P series

| Energy (keV) | P-ABS-0 | P-ABS-Er5 | P-ABS-Gd5 | P-ABS-Er10 | P-ABS-Gd10 | P-ABS-Er10Gd5 | P-ABS-Er5Gd10 | P-ABS-Er20 | P-ABS-Gd20 |
|---|---|---|---|---|---|---|---|---|---|
| 59,5 | 60,8117 | 98,3276 | 97,4064 | 99,9482 | 99,8688 | 99,9981 | 99,9970 | 100,0000 | 99,9999 |
| 80,9 | 58,3128 | 89,9094 | 87,4524 | 97,8999 | 96,6711 | 99,5232 | 99,3919 | 99,9448 | 99,8450 |
| 276,3 | 45,9119 | 49,0955 | 48,6062 | 52,8289 | 51,8588 | 56,1405 | 55,6702 | 60,4475 | 58,6165 |
| 302,8 | 44,8598 | 47,5345 | 47,1315 | 50,7807 | 49,9715 | 53,7096 | 53,3598 | 57,5370 | 55,9660 |
| 356 | 42,9713 | 44,9799 | 44,6913 | 47,5628 | 46,9726 | 49,9138 | 49,6652 | 53,0809 | 51,8978 |
| 383,8 | 42,0801 | 43,8578 | 43,6100 | 46,2048 | 45,6914 | 48,3721 | 48,1483 | 51,2591 | 50,2223 |
| 511 | 38,6250 | 39,8146 | 39,6680 | 41,5402 | 41,2311 | 43,2121 | 43,0573 | 45,3354 | 44,6969 |
| 661,6 | 35,4344 | 36,3354 | 36,2385 | 37,7358 | 37,5281 | 39,1226 | 39,0121 | 40,7776 | 40,4149 |
| 1173,2 | 28,3111 | 28,8992 | 28,8513 | 29,9037 | 29,7980 | 30,9283 | 30,8758 | 32,1640 | 31,9007 |
| 1274,5 | 27,3033 | 27,8666 | 27,8223 | 28,8345 | 28,7355 | 29,8239 | 29,7752 | 31,0148 | 30,8078 |
| 1332,5 | 26,7665 | 27,3188 | 27,2760 | 28,2691 | 28,1736 | 29,2418 | 29,1942 | 30,4108 | 30,2111 |

**Table 4.115:** Radiation Protection Efficiency (RPE) 100 mm = 10 cm (FLUKA) results for the P series

| Energy (keV) | P-ABS-0 | P-ABS-Er5 | P-ABS-Gd5 | P-ABS-Er10 | P-ABS-Gd10 | P-ABS-Er10Gd5 | P-ABS-Er5Gd10 | P-ABS-Er20 | P-ABS-Gd20 |
|---|---|---|---|---|---|---|---|---|---|
| 59,5 | 84,6428 | 99,9720 | 99,9327 | 100,0000 | 99,9998 | 100,0000 | 100,0000 | 100,0000 | 100,0000 |
| 80,9 | 82,6218 | 98,9818 | 98,4256 | 99,9559 | 99,8892 | 99,9977 | 99,9963 | 100,0000 | 99,9998 |
| 276,3 | 70,7448 | 74,0873 | 73,5867 | 77,7488 | 76,8243 | 80,7634 | 80,3487 | 84,3560 | 82,8740 |
| 302,8 | 69,5956 | 72,4737 | 72,0492 | 75,7746 | 74,9715 | 78,5720 | 78,2470 | 81,9689 | 80,6101 |
| 356 | 67,4773 | 69,7279 | 69,4095 | 72,5034 | 71,8809 | 74,9137 | 74,6641 | 77,9860 | 76,8618 |
| 383,8 | 66,4529 | 68,4805 | 68,2017 | 71,0607 | 70,5058 | 73,3456 | 73,1140 | 76,2433 | 75,2218 |
| 511 | 62,3311 | 63,7772 | 63,6005 | 65,8246 | 65,4622 | 67,7513 | 67,5753 | 70,1178 | 69,4156 |
| 661,6 | 58,3128 | 59,4682 | 59,3447 | 61,2316 | 60,9726 | 62,9394 | 62,8048 | 64,9271 | 64,4961 |
| 1173,2 | 48,6071 | 49,4467 | 49,3786 | 50,8651 | 50,7168 | 52,2910 | 52,2185 | 53,9828 | 53,6248 |
| 1274,5 | 47,1519 | 47,9677 | 47,9038 | 49,3547 | 49,2138 | 50,7531 | 50,6847 | 52,4105 | 52,1244 |
| 1332,5 | 46,3686 | 47,1745 | 47,1122 | 48,5468 | 48,4097 | 49,9328 | 49,8654 | 51,5734 | 51,2950 |

#### 4.1.1.7. Buildup factor (energy absorption) results for the P-series

The energy absorption buildup factor (also known as the energy absorption buildup factor) is similar to the exposure buildup factor but focuses on the amount of energy absorbed by the shielding material. This factor is particularly important when considering the effects of radiation on materials and biological tissues, as it accounts for the energy deposited by the radiation within the material. The energy absorption buildup factor considers how much energy is absorbed by the material as radiation passes through it. This factor is also influenced by the energy of the incident radiation, the properties of the shielding material, and the material's thickness.

**Table 4.116:** Buildup Factor (Energy Absorption) - (1-MFP) results for the P series

| Energy (MeV) | P-ABS-0 | P-ABS-Er5 | P-ABS-Gd5 | P-ABS-Er10 | P-ABS-Gd10 | P-ABS-Er10Gd5 | P-ABS-Er5Gd10 | P-ABS-Er20 | P-ABS-Gd20 |
|---|---|---|---|---|---|---|---|---|---|
| 0,015 | 1,4694 | 1,0540 | 1,0684 | 1,0274 | 1,0323 | 1,0191 | 1,0201 | 1,0144 | 1,0169 |
| 0,02 | 2,0556 | 1,1087 | 1,1336 | 1,0557 | 1,0706 | 1,0407 | 1,0410 | 1,0301 | 1,0386 |
| 0,03 | 3,9189 | 1,2973 | 1,3592 | 1,1595 | 1,1914 | 1,1133 | 1,1202 | 1,0821 | 1,0988 |
| 0,04 | 5,1605 | 1,5834 | 1,6858 | 1,3183 | 1,3818 | 1,2369 | 1,2510 | 1,1673 | 1,2015 |
| 0,05 | 5,6192 | 1,9982 | 2,1850 | 1,5272 | 1,6128 | 1,3976 | 1,4206 | 1,2886 | 1,3430 |
| 0,06 | 5,4082 | 1,3498 | 1,3883 | 1,1778 | 1,2151 | 1,1243 | 1,1309 | 1,1777 | 1,1512 |
| 0,08 | 4,8073 | 1,6100 | 1,6815 | 1,3133 | 1,3673 | 1,2508 | 1,2484 | 1,2667 | 1,2593 |
| 0,1 | 4,2559 | 1,9361 | 2,0481 | 1,4804 | 1,5813 | 1,3510 | 1,3596 | 1,2964 | 1,3227 |
| 0,15 | 3,5456 | 2,7331 | 2,8946 | 2,1368 | 2,2834 | 1,9394 | 1,9717 | 1,7462 | 1,8451 |
| 0,2 | 3,1873 | 3,0445 | 3,1621 | 2,5857 | 2,6936 | 2,4957 | 2,5118 | 2,4039 | 2,4529 |
| 0,3 | 2,7839 | 3,0546 | 3,0836 | 2,8537 | 2,9325 | 2,7071 | 2,7347 | 2,5558 | 2,6400 |
| 0,4 | 2,6121 | 2,8248 | 2,8301 | 2,7738 | 2,7920 | 2,7426 | 2,7488 | 2,7102 | 2,7287 |
| 0,5 | 2,4514 | 2,6258 | 2,6233 | 2,6297 | 2,6165 | 2,6519 | 2,6474 | 2,6751 | 2,6616 |
| 0,6 | 2,3918 | 2,4859 | 2,4841 | 2,5189 | 2,4915 | 2,5642 | 2,5550 | 2,6118 | 2,5838 |
| 0,8 | 2,1959 | 2,2764 | 2,2735 | 2,3283 | 2,2911 | 2,3892 | 2,3765 | 2,4531 | 2,4154 |
| 1 | 2,0868 | 2,1299 | 2,1298 | 2,1905 | 2,1517 | 2,2527 | 2,2396 | 2,3185 | 2,2791 |
| 1,5 | 1,9371 | 1,9417 | 1,9395 | 1,9379 | 1,9372 | 1,9512 | 1,9520 | 1,9469 | 1,9492 |
| 2 | 1,8364 | 1,8438 | 1,8425 | 1,8373 | 1,8375 | 1,8350 | 1,8327 | 1,8294 | 1,8320 |
| 3 | 1,7150 | 1,7098 | 1,7098 | 1,7060 | 1,7066 | 1,6971 | 1,6958 | 1,6914 | 1,6916 |
| 4 | 1,6287 | 1,6233 | 1,6248 | 1,6158 | 1,6167 | 1,6062 | 1,6066 | 1,5953 | 1,5960 |
| 5 | 1,5687 | 1,5611 | 1,5629 | 1,5473 | 1,5487 | 1,5484 | 1,5472 | 1,5263 | 1,5292 |
| 6 | 1,5230 | 1,4997 | 1,4981 | 1,4910 | 1,4936 | 1,4759 | 1,4767 | 1,4560 | 1,4608 |
| 8 | 1,4440 | 1,4240 | 1,4266 | 1,3999 | 1,4019 | 1,3856 | 1,3867 | 1,3700 | 1,3738 |
| 10 | 1,3853 | 1,3619 | 1,3629 | 1,3416 | 1,3443 | 1,3218 | 1,3238 | 1,3043 | 1,3081 |
| 15 | 1,2910 | 1,2693 | 1,2708 | 1,2447 | 1,2474 | 1,2251 | 1,2259 | 1,2227 | 1,2288 |

**Table 4.117:** Buildup Factor (Energy Absorption) - (5-MFP) results for the P series

| Energy (MeV) | P-ABS-0 | P-ABS-Er5 | P-ABS-Gd5 | P-ABS-Er10 | P-ABS-Gd10 | P-ABS-Er10Gd5 | P-ABS-Er5Gd10 | P-ABS-Er20 | P-ABS-Gd20 |
|---|---|---|---|---|---|---|---|---|---|
| 0,015 | 2,2969 | 1,1159 | 1,1477 | 1,0569 | 1,0675 | 1,0410 | 1,0432 | 1,0288 | 1,0335 |
| 0,02 | 5,0519 | 1,2367 | 1,2922 | 1,1188 | 1,1406 | 1,0831 | 1,0876 | 1,0623 | 1,0715 |
| 0,03 | 21,1539 | 1,6905 | 1,8571 | 1,3391 | 1,4119 | 1,2364 | 1,2520 | 1,1629 | 1,2015 |
| 0,04 | 52,5301 | 2,5503 | 2,9408 | 1,7293 | 1,8976 | 1,5124 | 1,5449 | 1,3475 | 1,4316 |
| 0,05 | 77,9753 | 3,9427 | 4,6990 | 2,3485 | 2,6878 | 1,9321 | 2,0011 | 1,6261 | 1,7742 |
| 0,06 | 88,9575 | 1,8048 | 1,9126 | 1,3683 | 1,4562 | 1,2441 | 1,2590 | 1,3326 | 1,2915 |
| 0,08 | 89,2929 | 2,6228 | 2,8789 | 1,7071 | 1,8588 | 1,5251 | 1,5260 | 1,5016 | 1,5162 |
| 0,1 | 79,3781 | 3,7911 | 4,2992 | 2,2284 | 2,4549 | 1,8719 | 1,9061 | 1,6631 | 1,7618 |
| 0,15 | 57,2463 | 7,1696 | 8,2965 | 3,9376 | 4,5998 | 3,2508 | 3,3566 | 2,6582 | 2,9529 |
| 0,2 | 44,2854 | 10,2392 | 11,5365 | 6,3512 | 7,1589 | 5,4705 | 5,6283 | 4,5875 | 5,0542 |
| 0,3 | 29,9667 | 12,8592 | 13,7967 | 9,4243 | 10,3597 | 7,8558 | 8,1399 | 6,3996 | 7,1873 |
| 0,4 | 22,8108 | 12,9333 | 13,5356 | 10,5859 | 11,2664 | 9,4305 | 9,6565 | 8,2613 | 8,9226 |
| 0,5 | 18,3666 | 12,2100 | 12,6113 | 10,6625 | 11,1103 | 9,8834 | 10,0414 | 9,0423 | 9,5322 |
| 0,6 | 15,6210 | 11,3498 | 11,6380 | 10,3154 | 10,6124 | 9,7840 | 9,8961 | 9,1797 | 9,5404 |
| 0,8 | 12,1222 | 9,8372 | 10,0114 | 9,3521 | 9,4593 | 9,1339 | 9,1835 | 8,8525 | 9,0250 |
| 1 | 10,0895 | 8,7546 | 8,8547 | 8,4772 | 8,4955 | 8,4106 | 8,4284 | 8,2923 | 8,3688 |
| 1,5 | 7,4648 | 7,1636 | 7,1978 | 6,9752 | 7,0292 | 6,8217 | 6,8507 | 6,6658 | 6,7492 |
| 2 | 6,1463 | 6,0923 | 6,0998 | 6,0622 | 6,0719 | 6,0272 | 6,0320 | 5,9611 | 5,9889 |
| 3 | 4,8117 | 4,7959 | 4,7967 | 4,7849 | 4,7868 | 4,7650 | 4,7637 | 4,7542 | 4,7582 |
| 4 | 4,1004 | 4,0802 | 4,0825 | 4,0586 | 4,0616 | 4,0396 | 4,0416 | 4,0181 | 4,0229 |
| 5 | 3,6532 | 3,6229 | 3,6255 | 3,5922 | 3,5961 | 3,5636 | 3,5664 | 3,5323 | 3,5393 |
| 6 | 3,3345 | 3,2910 | 3,2926 | 3,2570 | 3,2619 | 3,2237 | 3,2262 | 3,1800 | 3,1892 |
| 8 | 2,8991 | 2,8474 | 2,8509 | 2,7963 | 2,8022 | 2,7557 | 2,7584 | 2,7073 | 2,7227 |
| 10 | 2,6212 | 2,5570 | 2,5609 | 2,5006 | 2,5071 | 2,4530 | 2,4562 | 2,4054 | 2,4164 |
| 15 | 2,1928 | 2,1226 | 2,1269 | 2,0621 | 2,0684 | 2,0130 | 2,0157 | 1,9724 | 1,9812 |

**Table 4.118:** Buildup Factor (Energy Absorption) - (10-MFP) results for the P series

| Energy (MeV) | P-ABS-0 | P-ABS-Er5 | P-ABS-Gd5 | P-ABS-Er10 | P-ABS-Gd10 | P-ABS-Er10Gd5 | P-ABS-Er5Gd10 | P-ABS-Er20 | P-ABS-Gd20 |
|---|---|---|---|---|---|---|---|---|---|
| 0,015 | 2,8778 | 1,1471 | 1,1884 | 1,0729 | 1,0870 | 1,0524 | 1,0550 | 1,0373 | 1,0430 |
| 0,02 | 8,0704 | 1,3042 | 1,3785 | 1,1502 | 1,1774 | 1,1042 | 1,1111 | 1,0780 | 1,0873 |
| 0,03 | 54,3568 | 1,9257 | 2,1650 | 1,4384 | 1,5349 | 1,3014 | 1,3221 | 1,2072 | 1,2570 |
| 0,04 | 211,7690 | 3,2146 | 3,8495 | 1,9726 | 2,2145 | 1,6675 | 1,7121 | 1,4461 | 1,5580 |
| 0,05 | 411,2010 | 5,5546 | 6,9400 | 2,8952 | 3,4398 | 2,2663 | 2,3683 | 1,8231 | 2,0360 |
| 0,06 | 549,6460 | 2,0780 | 2,2335 | 1,4725 | 1,5910 | 1,3082 | 1,3277 | 1,4737 | 1,3951 |
| 0,08 | 629,9980 | 3,3173 | 3,7281 | 1,9358 | 2,1526 | 1,6958 | 1,6906 | 1,6810 | 1,6992 |
| 0,1 | 578,5640 | 5,2909 | 6,2118 | 2,6938 | 3,0292 | 2,1935 | 2,2388 | 1,8989 | 2,0416 |
| 0,15 | 385,7890 | 12,0145 | 14,6551 | 5,4129 | 6,6144 | 4,2624 | 4,4359 | 3,3147 | 3,7806 |
| 0,2 | 265,0720 | 20,2527 | 24,1463 | 10,3257 | 12,1043 | 8,6132 | 8,9432 | 6,6759 | 7,7116 |
| 0,3 | 146,1800 | 29,6886 | 33,4494 | 18,4900 | 21,0153 | 14,3139 | 15,0689 | 10,5386 | 12,5551 |
| 0,4 | 94,1140 | 32,4006 | 35,1307 | 23,5294 | 25,7533 | 19,6364 | 20,4027 | 15,7138 | 17,9186 |
| 0,5 | 67,8529 | 31,3646 | 33,2733 | 24,9104 | 26,6714 | 21,7846 | 22,4201 | 18,4383 | 20,3763 |
| 0,6 | 51,8956 | 29,1120 | 30,4708 | 24,3943 | 25,7819 | 21,9192 | 22,4380 | 19,1827 | 20,8023 |
| 0,8 | 35,2702 | 24,6674 | 25,4744 | 22,0820 | 22,8542 | 20,6480 | 20,9617 | 18,9661 | 19,9784 |
| 1 | 26,8270 | 20,9847 | 21,3585 | 19,5262 | 19,9261 | 18,7347 | 18,9168 | 17,7196 | 18,3474 |
| 1,5 | 16,9917 | 15,9991 | 16,1296 | 15,3524 | 15,5515 | 14,9207 | 15,0139 | 14,4102 | 14,6849 |
| 2 | 12,7835 | 12,5862 | 12,6236 | 12,6182 | 12,6472 | 12,5766 | 12,5980 | 12,4379 | 12,4968 |
| 3 | 8,9539 | 8,9858 | 8,9815 | 9,0324 | 9,0252 | 9,0604 | 9,0538 | 9,1022 | 9,0956 |
| 4 | 7,1622 | 7,1833 | 7,1787 | 7,2119 | 7,2083 | 7,2080 | 7,2125 | 7,2800 | 7,2727 |
| 5 | 6,1068 | 6,1066 | 6,1051 | 6,1175 | 6,1163 | 6,1123 | 6,1147 | 6,1370 | 6,1272 |
| 6 | 5,4029 | 5,3983 | 5,4024 | 5,3885 | 5,3869 | 5,3903 | 5,3910 | 5,3949 | 5,3943 |
| 8 | 4,5098 | 4,4678 | 4,4681 | 4,4502 | 4,4524 | 4,4338 | 4,4350 | 4,4066 | 4,4076 |
| 10 | 3,9454 | 3,8941 | 3,8976 | 3,8583 | 3,8616 | 3,8324 | 3,8322 | 3,8172 | 3,8237 |
| 15 | 3,1396 | 3,0632 | 3,0669 | 3,0215 | 3,0251 | 2,9858 | 2,9883 | 2,9401 | 2,9347 |

**Table 4.119:** Buildup Factor (Energy Absorption) - (40-MFP) results for the P series

| Energy (MeV) | P-ABS-0 | P-ABS-Er5 | P-ABS-Gd5 | P-ABS-Er10 | P-ABS-Gd10 | P-ABS-Er10Gd5 | P-ABS-Er5Gd10 | P-ABS-Er20 | P-ABS-Gd20 |
|---|---|---|---|---|---|---|---|---|---|
| 0,015 | 4,9068 | 1,2247 | 1,2897 | 1,1066 | 1,1277 | 1,0777 | 1,0827 | 1,0599 | 1,0689 |
| 0,02 | 26,0084 | 1,4741 | 1,6029 | 1,2295 | 1,2767 | 1,1379 | 1,1644 | 1,1190 | 1,1304 |
| 0,03 | 680,4630 | 2,6267 | 3,1323 | 1,7037 | 1,8729 | 1,4654 | 1,5000 | 1,3164 | 1,3960 |
| 0,04 | 7497,1900 | 5,5289 | 7,2275 | 2,6795 | 3,1759 | 2,0902 | 2,1714 | 1,7020 | 1,8959 |
| 0,05 | 32346,6000 | 13,0684 | 19,7803 | 4,7312 | 6,1584 | 3,2898 | 3,5118 | 2,3856 | 2,8012 |
| 0,06 | 68352,6000 | 2,8819 | 3,2011 | 1,7404 | 1,9491 | 1,4684 | 1,5002 | 5,8749 | 2,1318 |
| 0,08 | 106905,0000 | 5,7361 | 6,8113 | 2,5812 | 3,0079 | 2,3183 | 2,2092 | 3,1435 | 2,7776 |
| 0,1 | 103185,0000 | 11,5110 | 14,4887 | 4,0849 | 4,8674 | 3,2842 | 3,3028 | 2,8869 | 3,1386 |
| 0,15 | 49187,2000 | 45,1702 | 64,7160 | 12,2190 | 16,2303 | 8,8779 | 9,3815 | 6,1438 | 7,4754 |
| 0,2 | 21729,4000 | 124,9450 | 179,1460 | 37,6143 | 45,1472 | 43,2524 | 43,7540 | 27,4935 | 38,0445 |
| 0,3 | 6123,9800 | 239,6580 | 316,4710 | 110,5100 | 118,9340 | 82,9634 | 89,6396 | 45,1423 | 65,6705 |
| 0,4 | 2555,3700 | 327,5890 | 442,3670 | 198,5870 | 204,1420 | 159,2920 | 169,4730 | 98,3663 | 133,6620 |
| 0,5 | 1364,2400 | 312,6250 | 367,9650 | 226,7510 | 235,7010 | 188,1230 | 197,7850 | 129,9250 | 164,6080 |
| 0,6 | 778,5140 | 279,1100 | 325,9170 | 214,4780 | 226,5620 | 178,8690 | 187,3640 | 130,4660 | 159,5240 |
| 0,8 | 352,6050 | 207,9140 | 225,9790 | 177,3180 | 186,2430 | 155,0740 | 160,3000 | 126,1520 | 143,6200 |
| 1 | 221,2090 | 159,5870 | 160,2310 | 136,8980 | 141,0290 | 125,5190 | 128,3110 | 109,8280 | 119,4910 |
| 1,5 | 100,8710 | 96,3485 | 97,1249 | 91,4883 | 93,1119 | 89,4640 | 89,9904 | 86,6239 | 88,1232 |
| 2 | 63,2822 | 62,3279 | 62,7617 | 65,7179 | 65,6722 | 66,8984 | 66,7852 | 67,6479 | 67,3549 |
| 3 | 35,7961 | 37,0425 | 36,8607 | 38,9468 | 38,6543 | 39,9653 | 39,6832 | 41,8797 | 41,3031 |
| 4 | 25,3249 | 26,5399 | 26,4152 | 27,9553 | 27,7435 | 28,5507 | 28,6045 | 30,8091 | 30,4252 |
| 5 | 20,0983 | 21,1371 | 21,0601 | 22,4423 | 22,2507 | 23,6248 | 23,5402 | 23,9395 | 23,6022 |
| 6 | 17,0895 | 17,2402 | 17,2070 | 17,8980 | 17,7663 | 18,7448 | 18,6839 | 20,2010 | 19,7985 |
| 8 | 13,7621 | 14,1728 | 14,1109 | 15,1645 | 15,0211 | 16,1986 | 16,1236 | 17,1663 | 16,3313 |
| 10 | 10,9551 | 11,6135 | 11,5741 | 12,4251 | 12,3126 | 13,2516 | 13,1695 | 14,9474 | 14,6492 |
| 15 | 7,8868 | 8,2704 | 8,2274 | 9,1592 | 9,0452 | 10,0066 | 9,9496 | 11,6308 | 11,0875 |

**Table 4.120 :** Buildup Factor (Energy Absorption) results for the Lead

| Energy (keV) | Pb (Lead) (1-MFP) | Pb (Lead) (5-MFP) | Pb (Lead) (10-MFP) | Pb (Lead) (40-MFP) |
|---|---|---|---|---|
| 0,015 | 0,0000 | 0,0000 | 0,0000 | 0,0000 |
| 0,02 | 0,0000 | 0,0000 | 0,0000 | 0,0000 |
| 0,03 | 1,0070 | 1,0129 | 1,0159 | 1,0241 |
| 0,04 | 1,0140 | 1,0255 | 1,0310 | 1,0491 |
| 0,05 | 1,0240 | 1,0428 | 1,0518 | 1,0791 |
| 0,06 | 1,0360 | 1,0656 | 1,0806 | 1,1251 |
| 0,08 | 1,0760 | 1,1343 | 1,1652 | 1,2584 |
| 0,1 | 1,9340 | 14,6864 | 226,6150 | 44628300000,0000 |
| 0,15 | 1,7280 | 2,3897 | 2,8255 | 9,1101 |
| 0,2 | 1,5890 | 1,7094 | 1,7715 | 1,9914 |
| 0,3 | 1,5300 | 1,7604 | 1,9073 | 2,3637 |
| 0,4 | 1,5940 | 2,0667 | 2,3773 | 3,4364 |
| 0,5 | 1,6740 | 2,4113 | 2,9234 | 4,7951 |
| 0,6 | 1,5550 | 2,4323 | 3,0697 | 5,3242 |
| 0,8 | 1,6850 | 2,9832 | 4,0355 | 8,2021 |
| 1 | 1,7410 | 3,3664 | 4,8222 | 11,1452 |
| 1,5 | 1,7190 | 3,8570 | 6,3113 | 22,3463 |
| 2 | 1,7300 | 3,9654 | 6,7761 | 29,8153 |
| 3 | 1,6420 | 3,6344 | 6,4798 | 42,1453 |
| 4 | 1,5240 | 3,2004 | 5,8351 | 63,4333 |
| 5 | 1,5210 | 3,1045 | 5,7605 | 113,3620 |
| 6 | 1,4750 | 3,0146 | 5,8564 | 224,2610 |
| 8 | 1,4800 | 3,2856 | 7,4538 | 1263,6500 |
| 10 | 1,4280 | 3,6339 | 10,5000 | 7841,1500 |
| 15 | 1,4370 | 4,7366 | 21,9220 | 309422,0000 |

#### 4.1.2.8. Buildup factor (exposure) results for the P-series

The exposure buildup factor is a parameter used to quantify how much a shielding material reduces the exposure (or dose) of radiation to a certain level. It takes into account the scattering and secondary radiation that occurs within the shielding material. Exposure is a measure of the ionization produced in air by the incident radiation. The buildup factor for exposure helps determine the radiation intensity at a certain point behind a shielding material. It is influenced by factors such as the energy of the incident radiation, the atomic number and density of the shielding material, and the thickness of the material. The exposure buildup factor is a parameter used to measure how effective a shielding material is against radiation. Whether this factor is high or low indicates the effectiveness of the shielding material in reducing radiation. High Exposure Buildup Factor: A material having a high buildup factor means that it effectively reduces radiation. A high buildup factor indicates that radiation scatters more within the shielding material and loses energy. This leads to more effective neutralization of radiation and lower exposure levels. In other words, a high buildup factor provides better radiation protection. Low Exposure Buildup Factor: A material with a low buildup factor means that it reduces radiation less effectively. A low buildup factor indicates that radiation scatters less within the shielding material and loses less energy. This results in less effective neutralization of radiation and higher exposure levels. In other words, a low buildup factor signifies less effective radiation protection. In conclusion, the exposure buildup factor of a material is a critical parameter that reveals how effectively the material reduces radiation. A high buildup factor represents better radiation protection, while a low buildup factor signifies weaker protection.

**Table 4.121:** Buildup Factor (Exposure) - (1-MFP) results for the P series

| Energy (MeV) | P-ABS-0 | P-ABS-Er5 | P-ABS-Gd5 | P-ABS-Er10 | P-ABS-Gd10 | P-ABS-Er10Gd5 | P-ABS-Er5Gd10 | P-ABS-Er20 | P-ABS-Gd20 |
|---|---|---|---|---|---|---|---|---|---|
| 0,015 | 1,4550 | 1,0549 | 1,0690 | 1,0277 | 1,0323 | 1,0194 | 1,02067 | 1,0152 | 1,0174 |
| 0,02 | 2,0244 | 1,1086 | 1,1342 | 1,0546 | 1,0659 | 1,0404 | 1,04095 | 1,0324 | 1,0381 |
| 0,03 | 3,7422 | 1,2911 | 1,3489 | 1,1590 | 1,1899 | 1,1133 | 1,12015 | 1,0821 | 1,0988 |
| 0,04 | 5,5764 | 1,5577 | 1,6500 | 1,3111 | 1,3679 | 1,2301 | 1,24269 | 1,1635 | 1,1982 |
| 0,05 | 6,9982 | 1,8401 | 2,0622 | 1,4891 | 1,5739 | 1,3684 | 1,38934 | 1,2686 | 1,3185 |
| 0,06 | 7,4662 | 1,3070 | 1,3402 | 1,1574 | 1,1898 | 1,1118 | 1,11740 | 1,4666 | 1,2997 |
| 0,08 | 7,0098 | 1,4670 | 1,5200 | 1,2449 | 1,2872 | 1,2311 | 1,21002 | 1,3700 | 1,3053 |
| 0,1 | 6,3242 | 1,5958 | 1,6647 | 1,3333 | 1,3803 | 1,2663 | 1,27221 | 1,2287 | 1,2468 |
| 0,15 | 4,6628 | 1,8120 | 1,8909 | 1,5259 | 1,5948 | 1,4437 | 1,45698 | 1,3642 | 1,4049 |
| 0,2 | 3,7816 | 1,9296 | 1,9973 | 1,6832 | 1,7409 | 1,6216 | 1,63259 | 1,5587 | 1,5923 |
| 0,3 | 3,1486 | 2,0060 | 2,0549 | 1,8280 | 1,8715 | 1,7531 | 1,76721 | 1,6758 | 1,7188 |
| 0,4 | 2,8464 | 2,0047 | 2,0433 | 1,8723 | 1,9030 | 1,8198 | 1,83018 | 1,7652 | 1,7964 |
| 0,5 | 2,6609 | 1,9706 | 2,0060 | 1,8803 | 1,9018 | 1,8445 | 1,85163 | 1,8069 | 1,8287 |
| 0,6 | 2,5437 | 1,9458 | 1,9707 | 1,8675 | 1,8823 | 1,8432 | 1,84814 | 1,8176 | 1,8327 |
| 0,8 | 2,3202 | 1,9008 | 1,9166 | 1,8363 | 1,8431 | 1,8251 | 1,82742 | 1,8134 | 1,8203 |
| 1 | 2,2036 | 1,8382 | 1,8523 | 1,8078 | 1,8130 | 1,7995 | 1,80126 | 1,7907 | 1,7960 |
| 1,5 | 2,0523 | 1,8107 | 1,8265 | 1,7527 | 1,7681 | 1,7251 | 1,73299 | 1,6829 | 1,7055 |
| 2 | 1,9355 | 1,8037 | 1,8126 | 1,7628 | 1,7728 | 1,7438 | 1,74683 | 1,7207 | 1,7299 |
| 3 | 1,7738 | 1,7096 | 1,7119 | 1,6840 | 1,6883 | 1,6705 | 1,67158 | 1,6588 | 1,6611 |
| 4 | 1,6736 | 1,6260 | 1,6273 | 1,6107 | 1,6129 | 1,6018 | 1,60002 | 1,5896 | 1,5868 |
| 5 | 1,5909 | 1,5572 | 1,5587 | 1,5424 | 1,5442 | 1,5378 | 1,53749 | 1,5216 | 1,5237 |
| 6 | 1,5356 | 1,5119 | 1,5137 | 1,4989 | 1,5000 | 1,4879 | 1,48936 | 1,4740 | 1,4782 |
| 8 | 1,4447 | 1,4211 | 1,4219 | 1,4117 | 1,4127 | 1,4057 | 1,40584 | 1,3920 | 1,3958 |
| 10 | 1,3796 | 1,3602 | 1,3606 | 1,3531 | 1,3540 | 1,3463 | 1,34693 | 1,3329 | 1,3351 |
| 15 | 1,2827 | 1,2697 | 1,2705 | 1,2642 | 1,2643 | 1,2628 | 1,26305 | 1,2424 | 1,2464 |

**Table 4.122 :** Buildup Factor (Exposure) - (5-MFP) results for the P series

| Energy (MeV) | P-ABS-0 | P-ABS-Er5 | P-ABS-Gd5 | P-ABS-Er10 | P-ABS-Gd10 | P-ABS-Er10Gd5 | P-ABS-Er5Gd10 | P-ABS-Er20 | P-ABS-Gd20 |
|---|---|---|---|---|---|---|---|---|---|
| 0,015 | 2,2751 | 1,1141 | 1,1452 | 1,0577 | 1,0685 | 1,0410 | 1,04306 | 1,0310 | 1,0351 |
| 0,02 | 4,9152 | 1,2362 | 1,2899 | 1,1177 | 1,1383 | 1,0847 | 1,08939 | 1,0607 | 1,0722 |
| 0,03 | 20,0981 | 1,6805 | 1,8409 | 1,3385 | 1,4096 | 1,2364 | 1,25201 | 1,1629 | 1,2015 |
| 0,04 | 58,2594 | 2,4929 | 2,8599 | 1,7146 | 1,8723 | 1,5026 | 1,53408 | 1,3437 | 1,4252 |
| 0,05 | 105,9090 | 3,7099 | 4,3930 | 2,2583 | 2,5651 | 1,8785 | 1,94166 | 1,5936 | 1,7336 |
| 0,06 | 141,9580 | 1,7221 | 1,8150 | 1,3420 | 1,4197 | 1,2291 | 1,24266 | 2,0144 | 1,6398 |
| 0,08 | 162,4540 | 2,2728 | 2,4609 | 1,5858 | 1,7032 | 1,5356 | 1,48843 | 1,7886 | 1,6868 |
| 0,1 | 151,0840 | 2,8929 | 3,2028 | 1,8879 | 2,0495 | 1,6557 | 1,67883 | 1,5162 | 1,5819 |
| 0,15 | 106,0730 | 4,3300 | 4,8645 | 2,7500 | 3,0794 | 2,3726 | 2,43136 | 2,0425 | 2,2068 |
| 0,2 | 73,8730 | 5,6519 | 6,2755 | 3,7851 | 4,1889 | 3,2772 | 3,36494 | 2,8054 | 3,0511 |
| 0,3 | 45,7395 | 7,0699 | 7,6509 | 5,2053 | 5,6617 | 4,4621 | 4,59590 | 3,7779 | 4,1478 |
| 0,4 | 32,6625 | 7,6565 | 8,1192 | 6,0838 | 6,4984 | 5,4144 | 5,54227 | 4,7727 | 5,1318 |
| 0,5 | 25,2047 | 7,7446 | 8,1223 | 6,4693 | 6,8212 | 5,9067 | 6,01633 | 5,3545 | 5,6701 |
| 0,6 | 20,4726 | 7,6139 | 7,9265 | 6,5480 | 6,8452 | 6,0757 | 6,17001 | 5,6051 | 5,8788 |
| 0,8 | 14,9637 | 7,1818 | 7,3984 | 6,4396 | 6,6444 | 6,1118 | 6,17909 | 5,7792 | 5,9743 |
| 1 | 11,9777 | 6,7123 | 6,8729 | 6,1523 | 6,2998 | 5,9201 | 5,96872 | 5,6807 | 5,8232 |
| 1,5 | 8,7045 | 6,2592 | 6,3722 | 5,8096 | 5,9304 | 5,5694 | 5,62548 | 5,2695 | 5,4295 |
| 2 | 6,9047 | 5,8482 | 5,9142 | 5,6203 | 5,6749 | 5,4692 | 5,49235 | 5,3004 | 5,3826 |
| 3 | 5,1689 | 4,7958 | 4,8104 | 4,6864 | 4,7049 | 4,6365 | 4,64042 | 4,5881 | 4,6036 |
| 4 | 4,2951 | 4,1053 | 4,1107 | 4,0540 | 4,0613 | 4,0116 | 4,01527 | 4,0125 | 4,0107 |
| 5 | 3,7374 | 3,6216 | 3,6250 | 3,5909 | 3,5946 | 3,5720 | 3,57328 | 3,5677 | 3,5670 |
| 6 | 3,3935 | 3,3117 | 3,3135 | 3,2915 | 3,2938 | 3,2810 | 3,28108 | 3,2873 | 3,2807 |
| 8 | 2,9058 | 2,8539 | 2,8554 | 2,8432 | 2,8438 | 2,8398 | 2,83962 | 2,8348 | 2,8347 |
| 10 | 2,5923 | 2,5555 | 2,5565 | 2,5427 | 2,5441 | 2,5333 | 2,53312 | 2,5348 | 2,5360 |
| 15 | 2,1557 | 2,1241 | 2,1261 | 2,1073 | 2,1081 | 2,1014 | 2,10177 | 2,0836 | 2,0872 |

**Table 4.123:** Buildup Factor (Exposure) - (10-MFP) results for the P series

| Energy (MeV) | P-ABS-0 | P-ABS-Er5 | P-ABS-Gd5 | P-ABS-Er10 | P-ABS-Gd10 | P-ABS-Er10Gd5 | P-ABS-Er5Gd10 | P-ABS-Er20 | P-ABS-Gd20 |
|---|---|---|---|---|---|---|---|---|---|
| 0,015 | 2,8519 | 1,1454 | 1,1857 | 1,0736 | 1,0874 | 1,0529 | 1,05577 | 1,0414 | 1,0458 |
| 0,02 | 7,8318 | 1,3045 | 1,3756 | 1,1491 | 1,1771 | 1,1056 | 1,11260 | 1,0741 | 1,0877 |
| 0,03 | 51,9109 | 1,9144 | 2,1470 | 1,4369 | 1,5322 | 1,3014 | 1,32182 | 1,2072 | 1,2570 |
| 0,04 | 236,5480 | 3,1395 | 3,7483 | 1,9551 | 2,1869 | 1,6566 | 1,69996 | 1,4419 | 1,5509 |
| 0,05 | 576,5460 | 5,2701 | 6,4796 | 2,7827 | 3,2768 | 2,2026 | 2,29709 | 1,7897 | 1,9891 |
| 0,06 | 926,7370 | 1,9820 | 2,1200 | 1,4443 | 1,5505 | 1,2937 | 1,31171 | 2,9750 | 2,0069 |
| 0,08 | 1248,0100 | 2,8579 | 3,1699 | 1,7964 | 1,9665 | 1,7704 | 1,67928 | 2,3311 | 2,0971 |
| 0,1 | 1206,8300 | 3,9947 | 4,5736 | 2,2704 | 2,5269 | 1,9150 | 1,94977 | 1,7030 | 1,8031 |
| 0,15 | 827,7640 | 7,1498 | 8,4215 | 3,8079 | 4,4415 | 3,1312 | 3,23508 | 2,5592 | 2,8412 |
| 0,2 | 523,1650 | 10,9180 | 12,7483 | 6,1094 | 7,0433 | 5,0073 | 5,19984 | 3,9765 | 4,5108 |
| 0,3 | 259,0680 | 15,7931 | 17,8291 | 9,9596 | 11,2653 | 7,9075 | 8,27001 | 6,1220 | 7,0722 |
| 0,4 | 153,9240 | 18,4633 | 20,1539 | 13,0519 | 14,4212 | 10,8963 | 11,30170 | 8,9199 | 10,0131 |
| 0,5 | 103,8700 | 19,1546 | 20,5215 | 14,5721 | 15,8380 | 12,5944 | 12,97470 | 10,7237 | 11,7830 |
| 0,6 | 75,2379 | 18,8885 | 20,0447 | 14,9862 | 16,1145 | 13,2296 | 13,57650 | 11,5357 | 12,5133 |
| 0,8 | 46,5953 | 17,3862 | 18,1759 | 14,8196 | 15,6351 | 13,5146 | 13,78130 | 12,2149 | 12,9733 |
| 1 | 33,3707 | 15,6407 | 16,1165 | 13,8077 | 14,3823 | 12,9003 | 13,08990 | 11,9758 | 12,5244 |
| 1,5 | 20,4400 | 13,7635 | 14,0551 | 12,5677 | 12,8879 | 11,9261 | 12,06140 | 11,2022 | 11,5887 |
| 2 | 14,6235 | 12,0317 | 12,2024 | 11,6249 | 11,7320 | 11,2958 | 11,34650 | 10,9778 | 11,1431 |
| 3 | 9,7024 | 8,9868 | 9,0140 | 8,8297 | 8,8566 | 8,8049 | 8,80819 | 8,7926 | 8,7997 |
| 4 | 7,5166 | 7,2227 | 7,2306 | 7,2084 | 7,2094 | 7,1755 | 7,18722 | 7,2899 | 7,2712 |
| 5 | 6,2482 | 6,1103 | 6,1129 | 6,1299 | 6,1252 | 6,1952 | 6,18914 | 6,2719 | 6,2481 |
| 6 | 5,4976 | 5,4191 | 5,4168 | 5,4758 | 5,4673 | 5,5304 | 5,52626 | 5,6265 | 5,5991 |
| 8 | 4,4997 | 4,4851 | 4,4833 | 4,5357 | 4,5280 | 4,5879 | 4,58442 | 4,6693 | 4,6419 |
| 10 | 3,8918 | 3,8944 | 3,8925 | 3,9356 | 3,9298 | 3,9797 | 3,97413 | 4,0888 | 4,0783 |
| 15 | 3,0692 | 3,0634 | 3,0634 | 3,0863 | 3,0820 | 3,1183 | 3,11619 | 3,1726 | 3,1588 |

**Table 4.124:** Buildup Factor (Exposure) - (40-MFP) results for the P series

| Energy (MeV) | P-ABS-0 | P-ABS-Er5 | P-ABS-Gd5 | P-ABS-Er10 | P-ABS-Gd10 | P-ABS-Er10Gd5 | P-ABS-Er5Gd10 | P-ABS-Er20 | P-ABS-Gd20 |
|---|---|---|---|---|---|---|---|---|---|
| 0,015 | 4,8482 | 1,2247 | 1,2890 | 1,1067 | 1,1264 | 1,0783 | 1,08334 | 1,0619 | 1,0689 |
| 0,02 | 25,4166 | 1,4766 | 1,6006 | 1,2266 | 1,2765 | 1,1420 | 1,16580 | 1,1069 | 1,1269 |
| 0,03 | 670,6860 | 2,6031 | 3,1027 | 1,7026 | 1,8731 | 1,4654 | 1,49992 | 1,3164 | 1,3960 |
| 0,04 | 8515,8300 | 5,4035 | 7,1151 | 2,6502 | 3,1335 | 2,0808 | 2,16263 | 1,6972 | 1,8866 |
| 0,05 | 47773,3000 | 12,4225 | 18,6290 | 4,5702 | 5,8834 | 3,2136 | 3,42324 | 2,3575 | 2,7535 |
| 0,06 | 123290,0000 | 2,7632 | 3,0664 | 1,7152 | 1,9059 | 1,4607 | 1,49112 | 1302640,0000 | 73,7783 |
| 0,08 | 227414,0000 | 4,9954 | 5,8852 | 2,4218 | 2,7846 | 3,2841 | 2,45841 | 1482,5200 | 44,1921 |
| 0,1 | 228713,0000 | 8,6742 | 10,7812 | 3,4965 | 4,1258 | 2,7769 | 2,83191 | 2,3663 | 2,5747 |
| 0,15 | 117448,0000 | 24,8945 | 33,3599 | 8,1741 | 10,5606 | 6,2753 | 6,57088 | 4,6163 | 5,4361 |
| 0,2 | 51876,8000 | 58,0355 | 79,0550 | 20,0647 | 24,7588 | 16,7134 | 17,54620 | 11,1461 | 14,1983 |
| 0,3 | 12845,4000 | 117,6170 | 151,6740 | 50,7110 | 60,0293 | 35,0670 | 37,94120 | 21,2989 | 28,4673 |
| 0,4 | 4027,3900 | 167,7570 | 199,6130 | 91,0801 | 105,8180 | 66,3936 | 71,07550 | 44,3287 | 56,3090 |
| 0,5 | 2197,8200 | 179,6780 | 203,7980 | 112,9490 | 129,1800 | 86,8572 | 91,86610 | 62,9937 | 76,3025 |
| 0,6 | 1117,5600 | 172,3990 | 202,1090 | 115,1550 | 130,4600 | 91,0492 | 95,77220 | 68,8115 | 81,4445 |
| 0,8 | 482,5800 | 142,1410 | 158,3050 | 107,9370 | 118,8370 | 90,7492 | 94,21480 | 74,4144 | 83,8244 |
| 1 | 281,7530 | 116,9290 | 118,0170 | 90,6698 | 97,3351 | 80,2934 | 82,44160 | 70,0193 | 76,0741 |
| 1,5 | 124,1830 | 82,2057 | 84,0105 | 74,0857 | 76,2828 | 70,6572 | 70,60510 | 68,8001 | 70,3181 |
| 2 | 73,7220 | 59,4009 | 60,5513 | 60,2506 | 60,4691 | 59,9484 | 59,94730 | 61,0677 | 61,6827 |
| 3 | 38,9194 | 37,2532 | 37,2271 | 38,0279 | 37,9091 | 38,8313 | 38,70640 | 40,5194 | 39,9295 |
| 4 | 26,6029 | 26,5635 | 26,5020 | 27,9851 | 27,8043 | 28,7912 | 28,77740 | 29,8959 | 29,3390 |
| 5 | 20,4854 | 21,0703 | 20,9982 | 21,5046 | 21,4545 | 25,2131 | 24,39860 | 26,4077 | 26,0731 |
| 6 | 17,1650 | 17,5338 | 17,6507 | 19,1737 | 18,7932 | 21,3299 | 21,31260 | 22,4585 | 22,3302 |
| 8 | 12,4318 | 14,2706 | 14,2454 | 15,1543 | 15,0084 | 16,2478 | 16,17170 | 18,0154 | 17,5056 |
| 10 | 11,0784 | 11,5433 | 11,4751 | 12,8430 | 12,6664 | 14,2056 | 14,08950 | 16,7553 | 16,4561 |
| 15 | 7,7771 | 8,2624 | 8,2106 | 9,4275 | 9,2683 | 10,7157 | 10,63280 | 12,6519 | 12,1352 |

**Table 4.125:** Buildup Factor (Exposure) results for the Lead

| Energy (keV) | Pb (Lead) (1-MFP) | Pb (Lead) (5-MFP) | Pb (Lead) (10-MFP) | Pb (Lead) (40-MFP) |
|---|---|---|---|---|
| 0,015 | 0,0000 | 0,0000 | 0,0000 | 0,0000 |
| 0,02 | 0,0000 | 0,0000 | 0,0000 | 0,0000 |
| 0,03 | 1,0070 | 1,0130 | 1,0159 | 1,0241 |
| 0,04 | 1,0140 | 1,0258 | 1,0312 | 1,0490 |
| 0,05 | 1,0230 | 1,0421 | 1,0512 | 1,0784 |
| 0,06 | 1,0330 | 1,0623 | 1,0775 | 1,1227 |
| 0,08 | 1,0580 | 1,1172 | 1,1487 | 1,2410 |
| 0,1 | 1,9300 | 17,1467 | 296,4250 | 57844700000,0000 |
| 0,15 | 1,4020 | 1,8372 | 2,1422 | 6,6429 |
| 0,2 | 1,2010 | 1,2906 | 1,3414 | 1,5071 |
| 0,3 | 1,1480 | 1,3311 | 1,4374 | 1,7554 |
| 0,4 | 1,1870 | 1,5180 | 1,7453 | 2,4624 |
| 0,5 | 1,2330 | 1,7171 | 2,0847 | 3,3268 |
| 0,6 | 1,2690 | 1,8862 | 2,3787 | 4,0274 |
| 0,8 | 1,3290 | 2,2013 | 2,9762 | 5,8580 |
| 1 | 1,3670 | 2,4439 | 3,4945 | 7,8118 |
| 1,5 | 1,3690 | 2,7461 | 4,4562 | 15,0349 |
| 2 | 1,3840 | 2,9274 | 5,0333 | 21,0426 |
| 3 | 1,3670 | 2,9608 | 5,4875 | 34,2562 |
| 4 | 1,3370 | 2,8544 | 5,5245 | 59,2099 |
| 5 | 1,3600 | 2,9277 | 5,9187 | 119,6270 |
| 6 | 1,3630 | 3,0111 | 6,4888 | 264,8420 |
| 8 | 1,4410 | 3,6662 | 9,5142 | 1738,1900 |
| 10 | 1,4640 | 4,5053 | 15,1691 | 12234,3000 |
| 15 | 1,5730 | 6,9365 | 38,0783 | 564310,0000 |

### 4.1.3. Common gamma shielding results of the M and P series

#### 4.1.3.1. Effective atomic number ($Z_{eff}$) results for the M and P Series

The Effective Atomic Number ($Z_{eff}$) is a value calculated based on the interaction between an atom's nuclear charge and the surrounding electron cloud. It can be thought of as the difference between an element's actual atomic number (Z) and the effective charge caused by electron interactions. The $Z_{eff}$ value is important for understanding the chemical behavior and electron distribution of an element. The effectiveness of materials used in radiation shielding is determined by the energy transfer of radiation within these materials. The effective atomic number ($Z_{eff}$) of atoms within a material is a factor that determines their interaction with radiation. Materials with low $Z_{eff}$ values absorb less radiation and transfer less energy, which can reduce the effects of radiation. On the other hand, materials with high Zeff values can facilitate more energy transfer and effectively detect or absorb radiation. Therefore, the $Z_{eff}$ value of materials used in radiation shielding is crucial for determining their effectiveness. By selecting appropriate materials, it's possible to mitigate or control the undesired effects of radiation. This plays a critical role in protecting individuals exposed to radiation, such as personnel working in nuclear power plants, radiotherapy patients, and industrial workers.

**Table 4.126 :** Effective Atomic Number (Zeff) results for the M and P Series

| Energy (keV) | ABS-0 | ABS-Er5 | ABS-Gd5 | ABS-Er10 | ABS-Gd10 | ABS-Er10Gd5 | ABS-Er5Gd10 | ABS-Er20 | ABS-Gd20 |
|---|---|---|---|---|---|---|---|---|---|
| 59,5 | 3,6305 | 10,9811 | 10,3800 | 14,3165 | 13,6436 | 16,3148 | 16,0752 | 18,3176 | 17,5566 |
| 80,9 | 3,5571 | 8,6789 | 8,0349 | 12,4294 | 11,5529 | 14,8258 | 14,5100 | 17,2416 | 16,2570 |
| 276,3 | 3,4952 | 3,9052 | 3,8564 | 4,3956 | 4,2767 | 4,8507 | 4,7944 | 5,5028 | 5,2426 |
| 302,8 | 3,4943 | 3,8528 | 3,8122 | 4,2695 | 4,1693 | 4,6808 | 4,6328 | 5,2295 | 5,0056 |
| 356 | 3,4932 | 3,7836 | 3,7540 | 4,1001 | 4,0257 | 4,4495 | 4,4134 | 4,8783 | 4,7376 |
| 383,8 | 3,4928 | 3,7590 | 3,7335 | 4,0390 | 3,9803 | 4,3655 | 4,3340 | 4,7638 | 4,6405 |
| 511 | 3,4917 | 3,6960 | 3,6811 | 3,9077 | 3,8783 | 4,1463 | 4,1274 | 4,4615 | 4,3862 |
| 661,6 | 3,4911 | 3,6648 | 3,6550 | 3,8465 | 3,8269 | 4,0351 | 4,0224 | 4,3063 | 4,2555 |
| 1173,2 | 3,4905 | 3,6343 | 3,6301 | 3,7861 | 3,7776 | 3,9423 | 3,9380 | 4,1510 | 4,1281 |
| 1274,5 | 3,4906 | 3,6329 | 3,6290 | 3,7832 | 3,7752 | 3,9381 | 3,9341 | 4,1430 | 4,1218 |
| 1332,5 | 3,4909 | 3,6326 | 3,6289 | 3,7823 | 3,7747 | 3,9368 | 3,9329 | 4,1405 | 4,1200 |

### 4.1.3.2. Electron density ($N_E x10^{23}$) results for the M and P Series

Electron density ($N_e x10^{23}$), often represented in units of electrons per cubic centimeter ($cm^{-3}$), refers to the concentration of electrons within a given volume of material. In the context of radiation shielding, electron density plays a crucial role due to its influence on the attenuation (reduction) of ionizing radiation such as X-rays and gamma rays. When ionizing radiation passes through a material, interactions occur between the radiation and the atomic particles within the material. These interactions include scattering and absorption processes involving electrons. The higher the electron density of a material, the more likely it is to interact with and attenuate the incoming radiation. This is due to the fact that the interactions between the radiation and electrons lead to the conversion of the radiation's energy into other forms, ultimately reducing its intensity.

**Table 4.127 :** Electron density ($N_E$ $x10^{23}$) results for the M and P series

| Energy (keV) | ABS-0 | ABS-Er5 | ABS-Gd5 | ABS-Er10 | ABS-Gd10 | ABS-Er10Gd5 | ABS-Er5Gd10 | ABS-Er20 | ABS-Gd20 |
|---|---|---|---|---|---|---|---|---|---|
| 59,5 | 3,4145 | 9,8545 | 9,3173 | 12,2308 | 11,6619 | 13,2386 | 13,0476 | 14,0705 | 13,5012 |
| 80,9 | 3,3454 | 7,7885 | 7,2123 | 10,6187 | 9,8748 | 12,0303 | 11,7773 | 13,2440 | 12,5018 |
| 276,3 | 3,2872 | 3,5046 | 3,4616 | 3,7552 | 3,6556 | 3,9361 | 3,8914 | 4,2269 | 4,0316 |
| 302,8 | 3,2864 | 3,4575 | 3,4219 | 3,6475 | 3,5637 | 3,7982 | 3,7603 | 4,0170 | 3,8494 |
| 356 | 3,2853 | 3,3954 | 3,3697 | 3,5028 | 3,4410 | 3,6105 | 3,5822 | 3,7472 | 3,6432 |
| 383,8 | 3,2850 | 3,3733 | 3,3512 | 3,4506 | 3,4022 | 3,5424 | 3,5178 | 3,6593 | 3,5686 |
| 511 | 3,2840 | 3,3168 | 3,3043 | 3,3384 | 3,3150 | 3,3645 | 3,3500 | 3,4271 | 3,3731 |
| 661,6 | 3,2834 | 3,2888 | 3,2808 | 3,2861 | 3,2711 | 3,2743 | 3,2649 | 3,3079 | 3,2725 |
| 1173,2 | 3,2828 | 3,2615 | 3,2585 | 3,2346 | 3,2289 | 3,1990 | 3,1963 | 3,1886 | 3,1746 |
| 1274,5 | 3,2829 | 3,2602 | 3,2575 | 3,2320 | 3,2269 | 3,1955 | 3,1931 | 3,1824 | 3,1697 |
| 1332,5 | 3,2831 | 3,2600 | 3,2574 | 3,2313 | 3,2264 | 3,1945 | 3,1922 | 3,1805 | 3,1683 |

## 4.2. Neutron Radiation Shielding Analysis Results

Another aspect considered after gamma shielding is the evaluation of the samples produced in terms of their neutron shielding capabilities. This analysis consists of two stages: theoretical calculations and simulations. The value to be theoretically calculated is referred to in the literature as the effective neutron removal cross-section, and the calculated value is a parameter for 4.5 MeV neutrons. It has been calculated for all ABS samples, and the findings for ABS are presented in Tables 4.128 and 4.129. In addition, for the purpose of making a better comparison, the neutron removal cross-section for ordinary concrete and paraffin is also provided in Table 4.130. It should be noted that the larger the effective neutron removal cross-section parameter, the better the neutron shielding capability. As can be seen from the tables, adding nano-powders does not have a significant effect on the neutron shielding capability of both samples for 4.5 MeV

neutrons. The discussion section will provide insights into the preference for using these samples for specific neutron types. No significant differences have been found between the similar P series and M series. Both production techniques have yielded very close values.

### 4.2.1. Effective neutron removal cross section results for the M and P series

The effective neutron removal cross-section is a fundamental concept in nuclear physics, representing the probability of a neutron being captured or scattered by a specific nucleus. This cross-section is a critical parameter for examining various aspects of nuclear reactions. When calculated, it takes into account factors such as the properties of the target nucleus, the energy of the neutron, and the interaction mechanisms. Neutron Energy: First, the energy level of the neutrons to be used for the calculation is determined. Neutrons can have different energy levels, and the cross-section can vary depending on the neutron's energy level, so the calculation must consider the energy dependence within the cross-section. Properties of the Target Nucleus: The type of the target nucleus, its isotopic composition, energy levels, and spin values are crucial in calculating the cross-section. These properties indicate which energy levels or spin values neutrons must have to interact with a specific target nucleus. Interaction Mechanisms: Neutrons can interact with the target nucleus through various mechanisms, including neutron capture, scattering, or other nuclear reactions.

The calculation should include the probabilities of these interaction mechanisms. Nuclear Data: Nuclear data used for the calculation describe the interactions between the target nucleus and neutrons. These data particularly encompass the probabilities of neutron capture and scattering reactions. The value to be theoretically calculated is referred to in the literature as the effective neutron removal cross-section, and the calculated value is a parameter for 4.5 MeV neutrons. It has been calculated for all ABS samples, and the findings for ABS are presented in Tables 4.128 and 4.129. In addition, for the purpose of making a better comparison, the neutron removal cross-section for ordinary concrete and paraffin is also provided in Table 4.130. It should be noted that the larger the effective neutron removal cross-section parameter, the better the neutron shielding capability. As can be seen from the tables, adding nano-powders does not have a significant effect on the neutron shielding capability of both samples for 4.5 MeV neutrons.

**Table 4.128:** The effective neutron removal cross-section values for the ABS-M series

| Element | M-ABS-0 | | M-ABS-Er5 | | M-ABS-Gd5 | | M-ABS-Er10 | | M-ABS-Gd10 | | M-ABS-Er10Gd5 | | M-ABS-Er5Gd10 | | M-ABS-Er20 | | M-ABS-Gd20 | |
|---|---|---|---|---|---|---|---|---|---|---|---|---|---|---|---|---|---|---|
| | Partial density ($g/cm^3$) | Removal cross section ($cm^{-1}$) | Partial density ($g/cm^3$) | Removal cross section ($cm^{-1}$) | Partial density ($g/cm^3$) | Removal cross section ($cm^{-1}$) | Partial density ($g/cm^3$) | Removal cross section ($cm^{-1}$) | Partial density ($g/cm^3$) | Removal cross section ($cm^{-1}$) | Partial density ($g/cm^3$) | Removal cross section ($cm^{-1}$) | Partial density ($g/cm^3$) | Removal cross section ($cm^{-1}$) | Partial density ($g/cm^3$) | Removal cross section ($cm^{-1}$) | Partial density ($g/cm^3$) | Removal cross section ($cm^{-1}$) |
| **C** | 0,8953 | 0,0449 | 0,8896 | 0,0447 | 0,8886 | 0,0446 | 0,8833 | 0,0443 | 0,8814 | 0,0442 | 0,8754 | 0,0439 | 0,8744 | 0,0439 | 0,8689 | 0,0436 | 0,8646 | 0,0434 |
| **H** | 0,0851 | 0,0509 | 0,0846 | 0,0506 | 0,0845 | 0,0505 | 0,0840 | 0,0502 | 0,0838 | 0,0501 | 0,0833 | 0,0498 | 0,0832 | 0,0497 | 0,0826 | 0,0494 | 0,0822 | 0,0492 |
| **O** | 0,0000 | 0,0000 | 0,0069 | 0,0003 | 0,0073 | 0,0003 | 0,0144 | 0,0006 | 0,0152 | 0,0006 | 0,0232 | 0,0009 | 0,0235 | 0,0010 | 0,0320 | 0,0013 | 0,0336 | 0,0014 |
| **N** | 0,0696 | 0,0031 | 0,0692 | 0,0031 | 0,0691 | 0,0031 | 0,0687 | 0,0031 | 0,0685 | 0,0031 | 0,0681 | 0,0030 | 0,0680 | 0,0030 | 0,0675 | 0,0030 | 0,0672 | 0,0030 |
| **Er** | 0,0000 | 0,0000 | 0,0480 | 0,0006 | 0,0000 | 0,0000 | 0,1007 | 0,0012 | 0,0000 | 0,0000 | 0,1056 | 0,0012 | 0,0528 | 0,0006 | 0,2228 | 0,0026 | 0,0000 | 0,0000 |
| **Gd** | 0,0000 | 0,0000 | 0,0000 | 0,0000 | 0,0476 | 0,0006 | 0,0000 | 0,0000 | 0,0996 | 0,0012 | 0,0524 | 0,0006 | 0,1047 | 0,0012 | 0,0000 | 0,0000 | 0,2200 | 0,0026 |
| **Total** | 1,0500 | 0,0990 | 1,0982 | 0,0992 | 1,0971 | 0,0991 | 1,1511 | 0,0994 | 1,1486 | 0,0992 | 1,2080 | 0,0996 | 1,2066 | 0,0995 | 1,2738 | 0,0999 | 1,2676 | 0,0996 |

**Table 4.129:** The effective neutron removal cross-section values for the ABS-P series

| Element | P-ABS-0 | | P-ABS-Er5 | | P-ABS-Gd5 | | P-ABS-Er10 | | P-ABS-Gd10 | | P-ABS-Er10Gd5 | | P-ABS-Er5Gd10 | | P-ABS-Er20 | | P-ABS-Gd20 | |
|---|---|---|---|---|---|---|---|---|---|---|---|---|---|---|---|---|---|---|
| | Partial density ($g/cm^3$) | Removal cross section ($cm^{-1}$) | Partial density ($g/cm^3$) | Removal cross section ($cm^{-1}$) | Partial density ($g/cm^3$) | Removal cross section ($cm^{-1}$) | Partial density ($g/cm^3$) | Removal cross section ($cm^{-1}$) | Partial density ($g/cm^3$) | Removal cross section ($cm^{-1}$) | Partial density ($g/cm^3$) | Removal cross section ($cm^{-1}$) | Partial density ($g/cm^3$) | Removal cross section ($cm^{-1}$) | Partial density ($g/cm^3$) | Removal cross section ($cm^{-1}$) | Partial density ($g/cm^3$) | Removal cross section ($cm^{-1}$) |
| **C** | 0,8903 | 0,0447 | 0,8722 | 0,0438 | 0,8712 | 0,0437 | 0,8663 | 0,0435 | 0,8641 | 0,0434 | 0,8583 | 0,0431 | 0,8573 | 0,0430 | 0,8519 | 0,0428 | 0,8477 | 0,0426 |
| **H** | 0,0847 | 0,0506 | 0,0830 | 0,0496 | 0,0829 | 0,0496 | 0,0824 | 0,0493 | 0,0822 | 0,0491 | 0,0816 | 0,0488 | 0,0815 | 0,0488 | 0,0810 | 0,0485 | 0,0806 | 0,0482 |
| **O** | 0,0000 | 0,0000 | 0,0068 | 0,0003 | 0,0071 | 0,0003 | 0,0142 | 0,0006 | 0,0149 | 0,0006 | 0,0227 | 0,0009 | 0,0231 | 0,0009 | 0,0313 | 0,0013 | 0,0329 | 0,0013 |
| **N** | 0,0692 | 0,0031 | 0,0678 | 0,0030 | 0,0677 | 0,0030 | 0,0673 | 0,0030 | 0,0672 | 0,0030 | 0,0667 | 0,0030 | 0,0666 | 0,0030 | 0,0662 | 0,0030 | 0,0659 | 0,0030 |
| **Er** | 0,0000 | 0,0000 | 0,0471 | 0,0005 | 0,0000 | 0,0000 | 0,0987 | 0,0011 | 0,0000 | 0,0000 | 0,1036 | 0,0012 | 0,0517 | 0,0006 | 0,2184 | 0,0025 | 0,0000 | 0,0000 |
| **Gd** | 0,0000 | 0,0000 | 0,0000 | 0,0000 | 0,0467 | 0,0006 | 0,0000 | 0,0000 | 0,0977 | 0,0012 | 0,0514 | 0,0006 | 0,1026 | 0,0012 | 0,0000 | 0,0000 | 0,2157 | 0,0026 |
| **Total** | 1,0442 | 0,0984 | 1,0768 | 0,0972 | 1,0756 | 0,0972 | 1,1289 | 0,0975 | 1,1261 | 0,0973 | 1,1843 | 0,0976 | 1,1829 | 0,0975 | 1,2490 | 0,0980 | 1,2428 | 0,0976 |

**Table 4.130 :** The effective neutron removal cross-section values for paraffin and ordinary concrete

| Element | Paraffin | | Ordinary Concrete | |
|---|---|---|---|---|
| | **Partial density ($g/cm^3$)** | **Removal cross section ($cm^{-1}$)** | **Partial density ($g/cm^3$)** | **Removal cross section ($cm^{-1}$)** |
| **C** | 0,7918 | 0,0397 | 0,0000 | 0,0000 |
| **H** | 0,1382 | 0,0826 | 0,0074 | 0,0044 |
| **O** | 0,0000 | 0,0000 | 1,1160 | 0,0452 |
| **Na** | 0,0000 | 0,0000 | 0,0333 | 0,0011 |
| **Mg** | 0,0000 | 0,0000 | 0,0137 | 0,0005 |
| **Al** | 0,0000 | 0,0000 | 0,1029 | 0,0030 |
| **Si** | 0,0000 | 0,0000 | 0,7552 | 0,0223 |
| **P** | 0,0000 | 0,0000 | 0,0007 | 0,0000 |
| **S** | 0,0000 | 0,0000 | 0,0034 | 0,0001 |
| **Cl** | 0,0000 | 0,0000 | 0,0002 | 0,0000 |
| **K** | 0,0000 | 0,0000 | 0,0425 | 0,0011 |
| **Ca** | 0,0000 | 0,0000 | 0,1434 | 0,0035 |
| **Ti** | 0,0000 | 0,0000 | 0,0020 | 0,0000 |
| **Mn** | 0,0000 | 0,0000 | 0,0005 | 0,0000 |
| **Fe** | 0,0000 | 0,0000 | 0,0295 | 0,0006 |
| **Total** | 0,9300 | 0,1224 | 2,2510 | 0,0542 |

### 4.2.2. M-series (molded samples) neutron shielding results

**Table 4.131:** The results of 4.5 MeV neutron irradiation on ABS-M series samples with a thickness of 1 cm

| Sample | Total macroscopic cross section ($cm^{-1}$) | MFP (cm) | GEANT4 Number of Transmitted neutrons | FLUKA Number of Transmitted neutrons |
|---|---|---|---|---|
| **M-ABS-0** | 2,0585 | 0,4858 | 8439752 | 8452412 |
| **M-ABS-Er5** | 2,0579 | 0,4859 | 8440244 | 8452904 |
| **M-ABS-Gd5** | 2,0581 | 0,4859 | 8440080 | 8452740 |
| **M-ABS-Er10** | 2,0587 | 0,4858 | 8437003 | 8449659 |
| **M-ABS-Gd10** | 2,0582 | 0,4859 | 8439699 | 8452359 |
| **M-ABS-Er10Gd5** | 2,0593 | 0,4856 | 8434964 | 8447616 |
| **M-ABS-Er5Gd10** | 2,0588 | 0,4857 | 8439138 | 8451797 |
| **M-ABS-Er20** | 2,0565 | 0,4863 | 8429842 | 8442487 |
| **M-ABS-Gd20** | 2,0585 | 0,4858 | 8437936 | 8450593 |
| **Paraffin** | 2,0743 | 0,4820 | 8093556 | 8105696 |
| **Ordinary Concrete** | 2,0403 | 0,4901 | 8846700 | 8859970 |

**Table 4.132:** The types of interactions between 4.5 MeV neutrons and ABS-M series samples with a thickness of 1 cm

| Sample | Inelastic interaction | Elastic interaction | Capture interaction | Transmitted particle |
|---|---|---|---|---|
| **M-ABS-0** | 11537 | 1548682 | 29 | 8439752 |
| **M-ABS-Er5** | 16205 | 1543516 | 35 | 8440244 |
| **M-ABS-Gd5** | 14912 | 1544917 | 91 | 8440080 |
| **M-ABS-Er10** | 21489 | 1541464 | 44 | 8437003 |
| **M-ABS-Gd10** | 18751 | 1541444 | 106 | 8439699 |
| **M-ABS-Er10Gd5** | 25643 | 1539292 | 101 | 8434964 |
| **M-ABS-Er5Gd10** | 24456 | 1536248 | 158 | 8439138 |
| **M-ABS-Er20** | 33994 | 1536105 | 59 | 8429842 |
| **M-ABS-Gd20** | 27965 | 1533819 | 280 | 8437936 |
| **Paraffin** | 32 | 1906380 | 32 | 8093556 |
| **Ordinary Concrete** | 153604 | 999517 | 179 | 8846700 |

**Table 4.133:** The number of neutrons that pass through ABS-M series samples at different sample thicknesses with a neutron energy of 4.5 MeV

| Number of Transmitted neutrons | | | | | | | | | | | | | | | | | | | | |
|---|---|---|---|---|---|---|---|---|---|---|---|---|---|---|---|---|---|---|---|---|
| **Sample** | **1mm** | | **3mm** | | **5mm** | | **7mm** | | **9 mm** | | **11mm** | | **13 mm** | | **15 mm** | | **17mm** | | **19 mm** | |
| | **GEANT** | **FLUKA** | **GEANT** | **FLUKA** | **GEANT** | **FLUKA** | **GEANT** | **FLUKA** | **GEANT** | **FLUKA** | **GEANT** | **FLUKA** | **GEANT** | **FLUKA** | **GEANT** | **FLUKA** | **GEANT** | **FLUKA** | **GEANT** | **FLUKA** |
| **M-ABS-0** | 9832255 | 9847003 | 9504206 | 9518462 | 9186538 | 9200318 | 8881002 | 8894324 | 8584582 | 8597459 | 8300098 | 8312548 | 8022198 | 8034231 | 7758119 | 7769756 | 7497347 | 7508593 | 7244716 | 7255583 |
| **M-ABS-Er5** | 9830887 | 9845633 | 9502813 | 9517067 | 9186943 | 9200723 | 8878406 | 8891724 | 8584317 | 8597193 | 8297831 | 8310278 | 8018652 | 8030680 | 7749715 | 7761340 | 7491983 | 7503221 | 7243484 | 7254349 |
| **M-ABS-Gd5** | 9831912 | 9846660 | 9504851 | 9519108 | 9186770 | 9200550 | 8878526 | 8891844 | 8585489 | 8598367 | 8299774 | 8312224 | 8021897 | 8033930 | 7756775 | 7768410 | 7495069 | 7506312 | 7245826 | 7256695 |
| **M-ABS-Er10** | 9831847 | 9846595 | 9502532 | 9516786 | 9185008 | 9198786 | 8879684 | 8893004 | 8579903 | 8592773 | 8293474 | 8305914 | 8020163 | 8032193 | 7749617 | 7761241 | 7489846 | 7501081 | 7241967 | 7252830 |
| **M-ABS-Gd10** | 9830751 | 9845497 | 9503132 | 9517387 | 9187342 | 9201123 | 8879414 | 8892733 | 8583514 | 8596389 | 8297712 | 8310159 | 8020758 | 8032789 | 7752386 | 7764015 | 7493648 | 7504888 | 7244364 | 7255231 |
| **M-ABS-Er10Gd5** | 9831516 | 9846263 | 9502737 | 9516991 | 9185806 | 9199585 | 8878579 | 8891897 | 8580976 | 8593847 | 8293810 | 8306251 | 8016012 | 8028036 | 7749695 | 7761320 | 7486849 | 7498079 | 7239302 | 7250161 |
| **M-ABS-Er5Gd10** | 9831208 | 9845955 | 9503151 | 9517406 | 9185293 | 9199071 | 8878419 | 8891737 | 8580648 | 8593519 | 8296788 | 8309233 | 8019928 | 8031958 | 7750816 | 7762442 | 7489697 | 7500932 | 7240127 | 7250987 |
| **M-ABS-Er20** | 9830941 | 9845687 | 9500331 | 9514581 | 9183122 | 9196897 | 8871841 | 8885149 | 8576147 | 8589011 | 8288295 | 8300727 | 8011439 | 8023456 | 7744450 | 7756067 | 7481594 | 7492816 | 7229620 | 7240464 |
| **M-ABS-Gd20** | 9831656 | 9846403 | 9502599 | 9516853 | 9185040 | 9198818 | 8878492 | 8891810 | 8580521 | 8593392 | 8296348 | 8308793 | 8018216 | 8030243 | 7753244 | 7764874 | 7493065 | 7504305 | 7241340 | 7252202 |
| **Paraffin** | 9791391 | 9806078 | 9385900 | 9399979 | 8996233 | 9009727 | 8624320 | 8637256 | 8267346 | 8279747 | 7924886 | 7936773 | 7594858 | 7606250 | 7283353 | 7294278 | 6979815 | 6990285 | 6691799 | 6701837 |
| **Ordinary Concrete** | 9878358 | 9893176 | 9639290 | 9653749 | 9405386 | 9419494 | 9176951 | 9190716 | 8955286 | 8968719 | 8738694 | 8751802 | 8526836 | 8539626 | 8321561 | 8334043 | 8119958 | 8132138 | 7922947 | 7934831 |

**Table 4.134:** The number of neutrons that pass through 1 cm thickness ABS-M series samples at different neutron energies

| Number of Transmitted neutrons | | | | | | | | | | | | | | | | |
|---|---|---|---|---|---|---|---|---|---|---|---|---|---|---|---|---|
| **Sample** | 0,1 MeV | | 0,5 MeV | | 1 MeV | | 3 MeV | | 4,5 MeV | | 6 MeV | | 10 MeV | | 14,5 MeV | |
| | **GEANT** | **FLUKA** | **GEANT** | **FLUKA** | **GEANT** | **FLUKA** | **GEANT** | **FLUKA** | **GEANT** | **FLUKA** | **GEANT** | **FLUKA** | **GEANT** | **FLUKA** | **GEANT** | **FLUKA** |
| **M-ABS-0** | 4223609 | 4229944 | 6198627 | 6207925 | 7097255 | 7107901 | 8397214 | 8409810 | 8439752 | 8452412 | 8803821 | 8817027 | 9005168 | 9018676 | 9059108 | 9072697 |
| **M-ABS-Er5** | 4233567 | 4239917 | 6200676 | 6209977 | 7084550 | 7095177 | 8396053 | 8408647 | 8440244 | 8452904 | 8801666 | 8814868 | 9000231 | 9013731 | 9051543 | 9065120 |
| **M-ABS-Gd5** | 4234188 | 4240539 | 6205410 | 6214718 | 7087916 | 7098548 | 8396655 | 8409250 | 8440080 | 8452740 | 8802189 | 8815392 | 9000740 | 9014241 | 9052207 | 9065785 |
| **M-ABS-Er10** | 4245448 | 4251816 | 6204423 | 6213730 | 7074347 | 7084959 | 8392475 | 8405064 | 8437003 | 8449659 | 8794451 | 8807643 | 8992857 | 9006346 | 9045376 | 9058944 |
| **M-ABS-Gd10** | 4255030 | 4261413 | 6211087 | 6220404 | 7079897 | 7090517 | 8394383 | 8406975 | 8439699 | 8452359 | 8796439 | 8809634 | 8996566 | 9010061 | 9045929 | 9059498 |
| **M-ABS-Er10Gd5** | 4265656 | 4272054 | 6211897 | 6221215 | 7063862 | 7074458 | 8391080 | 8403667 | 8434964 | 8447616 | 8791484 | 8804671 | 8990988 | 9004474 | 9038774 | 9052332 |
| **M-ABS-Er5Gd10** | 4270824 | 4277230 | 6214181 | 6223502 | 7070758 | 7081364 | 8392993 | 8405582 | 8439138 | 8451797 | 8792050 | 8805238 | 8990874 | 9004360 | 9037690 | 9051247 |
| **M-ABS-Er20** | 4277650 | 4284066 | 6214311 | 6223632 | 7055463 | 7066046 | 8388625 | 8401208 | 8429842 | 8442487 | 8785086 | 8798264 | 8982965 | 8996439 | 9029278 | 9042822 |
| **M-ABS-Gd20** | 4297963 | 4304410 | 6229616 | 6238960 | 7062509 | 7073103 | 8388829 | 8401412 | 8437936 | 8450593 | 8788977 | 8802160 | 8987959 | 9001441 | 9032666 | 9046215 |
| **Paraffin** | 2924584 | 2928971 | 5217768 | 5225595 | 6318041 | 6327518 | 7897362 | 7909208 | 8093556 | 8105696 | 8496209 | 8508953 | 8825384 | 8838622 | 8971278 | 8984735 |
| **Ordinary Concrete** | 7762235 | 7773878 | 7523260 | 7534545 | 6388106 | 6397688 | 8919847 | 8933227 | 8846700 | 8859970 | 8847340 | 8860611 | 9018053 | 9031580 | 8911395 | 8924762 |

**Table 4.135:** The number of neutrons that pass through 5 cm thickness ABS-M series samples at different neutron energies

| Number of Transmitted neutrons | | | | | | | | | | | | | | | | |
|---|---|---|---|---|---|---|---|---|---|---|---|---|---|---|---|---|
| **Sample** | 0,1 MeV | | 0,5 MeV | | 1 MeV | | 3 MeV | | 4,5 MeV | | 6 MeV | | 10 MeV | | 14,5 MeV | |
| | **GEANT** | **FLUKA** | **GEANT** | **FLUKA** | **GEANT** | **FLUKA** | **GEANT** | **FLUKA** | **GEANT** | **FLUKA** | **GEANT** | **FLUKA** | **GEANT** | **FLUKA** | **GEANT** | **FLUKA** |
| **M-ABS-0** | 136016 | 137376 | 916205 | 925367 | 1792652 | 1810579 | 4156923 | 4198492 | 4263686 | 4306323 | 5257890 | 5310469 | 5935452 | 5994807 | 6118769 | 6179957 |
| **M-ABS-Er5** | 147005 | 148475 | 951721 | 961238 | 1828121 | 1846402 | 4200299 | 4242302 | 4307293 | 4350366 | 5289730 | 5342628 | 5935452 | 5994807 | 6118769 | 6179957 |
| **M-ABS-Gd5** | 147539 | 149014 | 953900 | 963439 | 1831406 | 1849720 | 4203750 | 4245787 | 4309611 | 4352707 | 5291307 | 5344221 | 5935452 | 5994807 | 6118769 | 6179957 |
| **M-ABS-Er10** | 148879 | 150368 | 957380 | 966953 | 1827122 | 1845393 | 4201169 | 4243181 | 4301338 | 4344352 | 5275790 | 5328548 | 5935452 | 5994807 | 6118769 | 6179957 |
| **M-ABS-Gd10** | 150305 | 151808 | 959096 | 968687 | 1822903 | 1841132 | 4199288 | 4241281 | 4308995 | 4352085 | 5283458 | 5336292 | 5935452 | 5994807 | 6118769 | 6179957 |
| **M-ABS-Er10Gd5** | 152030 | 153551 | 959358 | 968951 | 1802164 | 1820186 | 4188953 | 4230843 | 4298824 | 4341812 | 5262816 | 5315444 | 5935452 | 5994807 | 6118769 | 6179957 |
| **M-ABS-Er5Gd10** | 152934 | 154464 | 962151 | 971773 | 1807582 | 1825657 | 4191568 | 4233484 | 4304689 | 4347736 | 5263741 | 5316378 | 5935452 | 5994807 | 6118769 | 6179957 |
| **M-ABS-Er20** | 153539 | 155074 | 958957 | 968546 | 1788797 | 1806685 | 4178074 | 4219855 | 4288043 | 4330924 | 5243256 | 5295688 | 5935452 | 5994807 | 6118769 | 6179957 |
| **M-ABS-Gd20** | 157847 | 159425 | 972194 | 981916 | 1801061 | 1819072 | 4190827 | 4232736 | 4304607 | 4347653 | 5260156 | 5312758 | 5935452 | 5994807 | 6118769 | 6179957 |
| **Paraffin** | 21450 | 4320427 | 387383 | 6276454 | 1006451 | 7126018 | 3072470 | 8472511 | 3475695 | 8514140 | 4423951 | 8872937 | 5360814 | 9072795 | 5802685 | 9119571 |
| **Ordinary Concrete** | 2819811 | 4340943 | 2410180 | 6291912 | 1063648 | 7133134 | 5645994 | 8472717 | 5420266 | 8522315 | 5420539 | 8876867 | 5959369 | 9077839 | 5618299 | 9122993 |

### 4.2.3. P-series (printed samples) neutron shielding results

**Table 4.136.:** The results of 4.5 MeV neutron irradiation on ABS-P series samples with a thickness of 1 cm

| Sample | Total macroscopic cross section ($cm^{-1}$) | MFP (cm) | GEANT4 Number of Transmitted neutrons | FLUKA Number of Transmitted neutrons |
|---|---|---|---|---|
| **P-ABS-0** | 2,0577 | 0,4860 | 8449600 | 8462274 |
| **P-ABS-Er5** | 2,0560 | 0,4864 | 8469190 | 8481894 |
| **P-ABS-Gd5** | 2,0574 | 0,4861 | 8467981 | 8480683 |
| **P-ABS-Er10** | 2,0576 | 0,4860 | 8463815 | 8476511 |
| **P-ABS-Gd10** | 2,0566 | 0,4863 | 8467871 | 8480573 |
| **P-ABS-Er10Gd5** | 2,0576 | 0,4860 | 8464175 | 8476871 |
| **P-ABS-Er5Gd10** | 2,0570 | 0,4861 | 8467098 | 8479799 |
| **P-ABS-Er20** | 2,0565 | 0,4863 | 8459399 | 8472088 |
| **P-ABS-Gd20** | 2,0560 | 0,4864 | 8464469 | 8477166 |
| **Paraffin** | 2,0743 | 0,4820 | 8093556 | 8105696 |
| **Ordinary Concrete** | 2,0403 | 0,4901 | 8846700 | 8859970 |

**Table 4.137.:** The types of interactions between 4.5 MeV neutrons and ABS-P series samples with a thickness of 1 cm

| Sample | Inelastic interaction | Elastic interaction | Capture interaction | Transmitted particle |
|---|---|---|---|---|
| **P-ABS-0** | 11381 | 1538990 | 29 | 8449600 |
| **P-ABS-Er5** | 15923 | 1514867 | 20 | 8469190 |
| **P-ABS-Gd5** | 14812 | 1517141 | 66 | 8467981 |
| **P-ABS-Er10** | 21252 | 1514896 | 37 | 8463815 |
| **P-ABS-Gd10** | 18395 | 1513612 | 122 | 8467871 |
| **P-ABS-Er10Gd5** | 25305 | 1510432 | 88 | 8464175 |
| **P-ABS-Er5Gd10** | 24147 | 1508612 | 143 | 8467098 |
| **P-ABS-Er20** | 33394 | 1507161 | 46 | 8459399 |
| **P-ABS-Gd20** | 27370 | 1507899 | 262 | 8464469 |
| **Paraffin** | 32 | 1906380 | 32 | 8093556 |
| **Ordinary Concrete** | 153604 | 999517 | 179 | 8846700 |

**Table 4.138:** The number of neutrons that pass through ABS-P series samples at different sample thicknesses with a neutron energy of 4.5 MeV

| Number of Transmitted neutrons | | | | | | | | | | | | | | | | | | | | |
|---|---|---|---|---|---|---|---|---|---|---|---|---|---|---|---|---|---|---|---|---|
| **Sample** | **1mm** | | **3mm** | | **5mm** | | **7mm** | | **9 mm** | | **11mm** | | **13 mm** | | **15 mm** | | **17mm** | | **19 mm** | |
| | **GEANT** | **FLUKA** | **GEANT** | **FLUKA** | **GEANT** | **FLUKA** | **GEANT** | **FLUKA** | **GEANT** | **FLUKA** | **GEANT** | **FLUKA** | **GEANT** | **FLUKA** | **GEANT** | **FLUKA** | **GEANT** | **FLUKA** | **GEANT** | **FLUKA** |
| **P-ABS-0** | 9833171 | 9847921 | 9506669 | 9520929 | 9192780 | 9206569 | 8886883 | 8900213 | 8592085 | 8604973 | 8307106 | 8319567 | 8032183 | 8044231 | 7765932 | 7777581 | 7507225 | 7518486 | 7261021 | 7271913 |
| **P-ABS-Er5** | 9834437 | 9849189 | 9513912 | 9528183 | 9202722 | 9216526 | 8901305 | 8914657 | 8609758 | 8622673 | 8325399 | 8337887 | 8056896 | 8068981 | 7792316 | 7804004 | 7536192 | 7547496 | 7291932 | 7302870 |
| **P-ABS-Gd5** | 9835275 | 9850028 | 9513340 | 9527610 | 9201690 | 9215493 | 8901292 | 8914644 | 8609771 | 8622686 | 8329485 | 8341979 | 8056761 | 8068846 | 7794233 | 7805924 | 7537588 | 7548894 | 7294209 | 7305150 |
| **P-ABS-Er10** | 9834243 | 9848994 | 9513127 | 9527397 | 9199741 | 9213541 | 8897917 | 8911264 | 8607836 | 8620748 | 8325223 | 8337711 | 8054215 | 8066296 | 7788792 | 7800475 | 7533463 | 7544763 | 7286081 | 7297010 |
| **P-ABS-Gd10** | 9834974 | 9849726 | 9513270 | 9527540 | 9202132 | 9215935 | 8900947 | 8914298 | 8610790 | 8623706 | 8327693 | 8340185 | 8055967 | 8068051 | 7792009 | 7803697 | 7536662 | 7547967 | 7291565 | 7302502 |
| **P-ABS-Er10Gd5** | 9834701 | 9849453 | 9511795 | 9526063 | 9200488 | 9214289 | 8897453 | 8910799 | 8605237 | 8618145 | 8323136 | 8335621 | 8049141 | 8061215 | 7786159 | 7797838 | 7530729 | 7542025 | 7283874 | 7294800 |
| **P-ABS-Er5Gd10** | 9835024 | 9849777 | 9513628 | 9527898 | 9199052 | 9212851 | 8898116 | 8911463 | 8607639 | 8620550 | 8324861 | 8337348 | 8053439 | 8065519 | 7789473 | 7801157 | 7533189 | 7544489 | 7287288 | 7298219 |
| **P-ABS-Er20** | 9834413 | 9849165 | 9510438 | 9524704 | 9197852 | 9211649 | 8895254 | 8908597 | 8601327 | 8614229 | 8319280 | 8331759 | 8045077 | 8057145 | 7781306 | 7792978 | 7525100 | 7536388 | 7276711 | 7287626 |
| **P-ABS-Gd20** | 9835077 | 9849830 | 9512989 | 9527258 | 9200148 | 9213948 | 8900880 | 8914231 | 8609297 | 8622211 | 8328680 | 8341173 | 8053926 | 8066007 | 7788353 | 7800036 | 7533646 | 7544946 | 7287917 | 7298849 |
| **Paraffin** | 9791391 | 9806078 | 9385900 | 9399979 | 8996233 | 9009727 | 8624320 | 8637256 | 8267346 | 8279747 | 7924886 | 7936773 | 7594858 | 7606250 | 7283353 | 7294278 | 6979815 | 6990285 | 6691799 | 6701837 |
| **Ordinary Concrete** | 9878358 | 9893176 | 9639290 | 9653749 | 9405386 | 9419494 | 9176951 | 9190716 | 8955286 | 8968719 | 8738694 | 8751802 | 8526836 | 8539626 | 8321561 | 8334043 | 8119958 | 8132138 | 7922947 | 7934831 |

**Table 4.139:** The number of neutrons that pass through 1 cm thickness ABS-P series samples at different neutron energies

| Number of Transmitted neutrons | | | | | | | | | | | | | | | | |
|---|---|---|---|---|---|---|---|---|---|---|---|---|---|---|---|---|
| **Sample** | 0,1 MeV | | 0,5 MeV | | 1 MeV | | 3 MeV | | 4,5 MeV | | 6 MeV | | 10 MeV | | 14,5 MeV | |
| | **GEANT** | **FLUKA** | **GEANT** | **FLUKA** | **GEANT** | **FLUKA** | **GEANT** | **FLUKA** | **GEANT** | **FLUKA** | **GEANT** | **FLUKA** | **GEANT** | **FLUKA** | **GEANT** | **FLUKA** |
| **P-ABS-0** | 4241380 | 4247742 | 6214281 | 6223602 | 7106925 | 7117585 | 8405322 | 8417930 | 8449600 | 8462274 | 8811217 | 8824434 | 9009218 | 9022732 | 9063919 | 9077515 |
| **P-ABS-Er5** | 4305628 | 4312086 | 6257623 | 6267009 | 7134221 | 7144922 | 8423484 | 8436119 | 8469190 | 8481894 | 8822362 | 8835596 | 9018026 | 9031553 | 9069156 | 9082760 |
| **P-ABS-Gd5** | 4311479 | 4317946 | 6263505 | 6272900 | 7137568 | 7148274 | 8424625 | 8437262 | 8467981 | 8480683 | 8823855 | 8837091 | 9020899 | 9034430 | 9069425 | 9083029 |
| **P-ABS-Er10** | 4316403 | 4322878 | 6263501 | 6272896 | 7120405 | 7131086 | 8421666 | 8434298 | 8463815 | 8476511 | 8817891 | 8831118 | 9012072 | 9025590 | 9063039 | 9076634 |
| **P-ABS-Gd10** | 4326325 | 4332814 | 6270411 | 6279817 | 7127595 | 7138286 | 8424370 | 8437007 | 8467871 | 8480573 | 8819860 | 8833090 | 9014612 | 9028134 | 9062672 | 9076266 |
| **P-ABS-Er10Gd5** | 4338066 | 4344573 | 6274083 | 6283494 | 7114089 | 7124760 | 8418827 | 8431455 | 8464175 | 8476871 | 8814605 | 8827827 | 9007806 | 9021318 | 9055711 | 9069295 |
| **P-ABS-Er5Gd10** | 4339714 | 4346224 | 6275463 | 6284876 | 7118803 | 7129481 | 8421310 | 8433942 | 8467098 | 8479799 | 8813844 | 8827065 | 9010141 | 9023656 | 9056836 | 9070421 |
| **P-ABS-Er20** | 4344930 | 4351447 | 6272704 | 6282113 | 7100690 | 7111341 | 8414244 | 8426865 | 8459399 | 8472088 | 8806181 | 8819390 | 8999552 | 9013051 | 9047241 | 9060812 |
| **P-ABS-Gd20** | 4370215 | 4376770 | 6286218 | 6295647 | 7111231 | 7121898 | 8420375 | 8433006 | 8464469 | 8477166 | 8811804 | 8825022 | 9005191 | 9018699 | 9050510 | 9064086 |
| **Paraffin** | 2924584 | 2928971 | 5217768 | 5225595 | 6318041 | 6327518 | 7897362 | 7909208 | 8093556 | 8105696 | 8496209 | 8508953 | 8825384 | 8838622 | 8971278 | 8984735 |
| **Ordinary Concrete** | 7762235 | 7773878 | 7523260 | 7534545 | 6388106 | 6397688 | 8919847 | 8933227 | 8846700 | 8859970 | 8847340 | 8860611 | 9018053 | 9031580 | 8911395 | 8924762 |

**Table 4.140:** The number of neutrons that pass through 5 cm thickness ABS-P series samples at different neutron energies

| Number of Transmitted neutrons | | | | | | | | | | | | | | | | |
|---|---|---|---|---|---|---|---|---|---|---|---|---|---|---|---|---|
| **Sample** | 0,1 MeV | | 0,5 MeV | | 1 MeV | | 3 MeV | | 4,5 MeV | | 6 MeV | | 10 MeV | | 14,5 MeV | |
| | **GEANT** | **FLUKA** | **GEANT** | **FLUKA** | **GEANT** | **FLUKA** | **GEANT** | **FLUKA** | **GEANT** | **FLUKA** | **GEANT** | **FLUKA** | **GEANT** | **FLUKA** | **GEANT** | **FLUKA** |
| **P-ABS-0** | 137390 | 138764 | 925460 | 934715 | 1810760 | 1828868 | 4198912 | 4240901 | 4306754 | 4349822 | 5311000 | 5364110 | 5935452 | 5994807 | 6118769 | 6179957 |
| **P-ABS-Er5** | 148490 | 149975 | 961334 | 970947 | 1846587 | 1865053 | 4242726 | 4285153 | 4350801 | 4394309 | 5343162 | 5396594 | 5962345 | 6021968 | 6135568 | 6196924 |
| **P-ABS-Gd5** | 149029 | 150519 | 963535 | 973170 | 1849905 | 1868404 | 4246212 | 4288674 | 4353142 | 4396673 | 5344755 | 5398203 | 5965791 | 6025449 | 6139990 | 6201390 |
| **P-ABS-Er10** | 150383 | 151887 | 967050 | 976721 | 1845578 | 1864034 | 4243605 | 4286041 | 4344786 | 4388234 | 5329081 | 5382372 | 5945579 | 6005035 | 6111650 | 6172767 |
| **P-ABS-Gd10** | 151823 | 153341 | 968784 | 978472 | 1841316 | 1859729 | 4241705 | 4284122 | 4352520 | 4396045 | 5336826 | 5390194 | 5953873 | 6013412 | 6116976 | 6178146 |
| **P-ABS-Er10Gd5** | 153566 | 155102 | 969048 | 978738 | 1820368 | 1838572 | 4231266 | 4273579 | 4342246 | 4385668 | 5315976 | 5369136 | 5930925 | 5990234 | 6089118 | 6150009 |
| **P-ABS-Er5Gd10** | 154479 | 156024 | 971870 | 981589 | 1825840 | 1844098 | 4233907 | 4276246 | 4348171 | 4391653 | 5316910 | 5370079 | 5933674 | 5993011 | 6093066 | 6153997 |
| **P-ABS-Er20** | 155090 | 156641 | 968643 | 978329 | 1806866 | 1824935 | 4220277 | 4262480 | 4331357 | 4374671 | 5296218 | 5349180 | 5905796 | 5964854 | 6059868 | 6120467 |
| **P-ABS-Gd20** | 159441 | 161035 | 982014 | 991834 | 1819254 | 1837447 | 4233159 | 4275491 | 4348088 | 4391569 | 5313289 | 5366422 | 5919642 | 5978838 | 6070746 | 6131453 |
| **Paraffin** | 21450 | 21665 | 387383 | 391257 | 1006451 | 1016516 | 3072470 | 3103195 | 3475695 | 3510452 | 4423951 | 4468191 | 5360814 | 5414422 | 5802685 | 5860712 |
| **Ordinary Concrete** | 2819811 | 2848009 | 2410180 | 2434282 | 1063648 | 1074284 | 5645994 | 5702454 | 5420266 | 5474469 | 5420539 | 5474744 | 5959369 | 6018963 | 5618299 | 5674482 |

**Table 4.141:** GEANT4 simulation results for thermal and fast neutrons for 1 cm thick ABS-P series samples

| **Sample** | **Number of transmitted neutrons** | **Thermal Neutron (0,025 eV)** | **Fast Neutron (4,5 MeV)** |
|---|---|---|---|
| | | **Number of sent neutrons** | **Number of transmitted neutrons** |
| **P-ABS-0** | 10000000 | 1540437 | 8462274 |
| **P-ABS-Er5** | 10000000 | 1444614 | 8481894 |
| **P-ABS-Gd5** | 10000000 | 202 | 8480683 |
| **P-ABS-Er10** | 10000000 | 1744266 | 8476511 |
| **P-ABS-Gd10** | 10000000 | 0 | 8480573 |
| **P-ABS-Er10Gd5** | 10000000 | 91 | 8476871 |
| **P-ABS-Er5Gd10** | 10000000 | 0 | 8479799 |
| **P-ABS-Er20** | 10000000 | 1391195 | 8472088 |
| **P-ABS-Gd20** | 10000000 | 0 | 8477166 |
| **Paraffin** | 10000000 | 446207 | 8105696 |
| **Ordinary Concrete** | 10000000 | 6935829 | 8859970 |

### 4.3. Structural Analysis Results

#### 4.3.1. SEM (scanning electron microscopy) analysis results

##### 4.3.1.1. M-series (molded samples) SEM analysis results

After radiation shielding analyses, when SEM (Scanning Electron Microscopy) analysis was conducted, the SEM image of a manually produced pure ABS sample (M-ABS) is presented in Figure x0. Upon examining the image, it is noticeable that there are long, line-shaped scratches and distinct pits with widths reaching up to 100 µm on the surface of the sample. It is speculated that these scratches and pits are associated with the production method. During the production process, due to factors such as the temperature degree and stability, applied pressure levels, and irregularities in the pressing process, air gaps have formed on the surface, and these air gaps correspond to the pits observed in the SEM images.

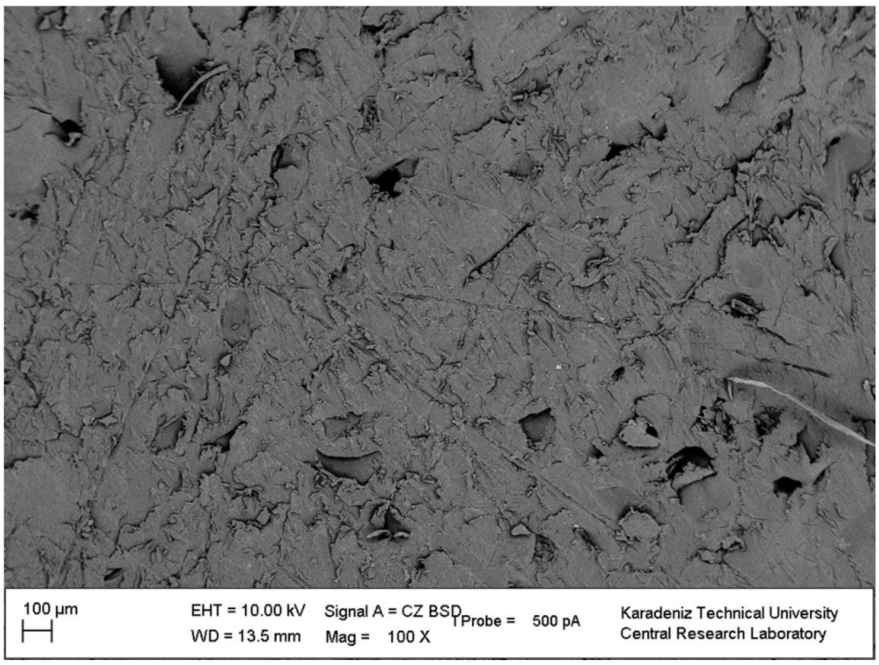
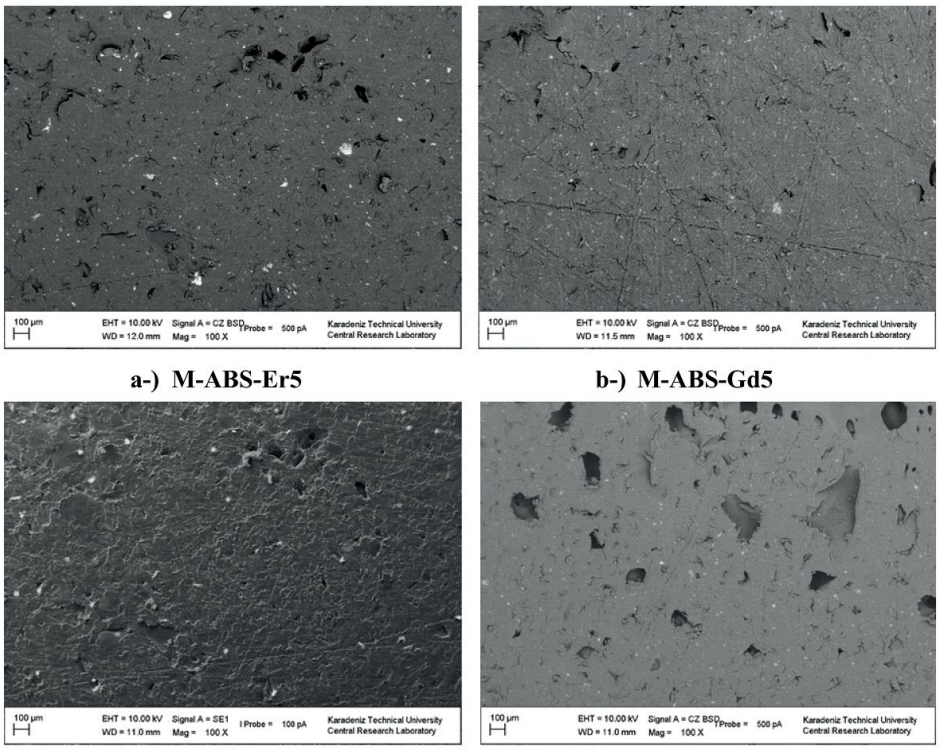


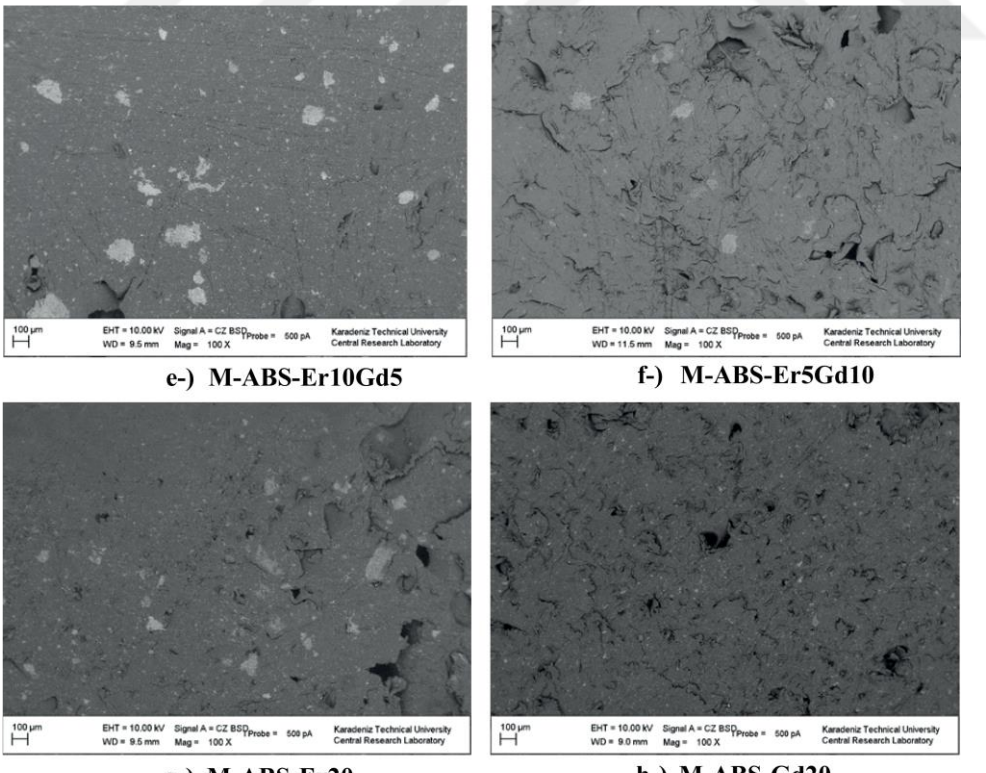

**Figure 4.1:** SEM image of the ABS sample produced by mold production without additives (M-ABS-0)




**a-) M-ABS-Er5** **b-) M-ABS-Gd5**

**c-) M-ABS-Er10** **d-) M-ABS-Gd10**

**Figure 4.2:** SEM images of ABS samples with additives produced by the mold production method; a) %5Er, b) %5Gd, c) %10Er, d) %10Gd




**e-) M-ABS-Er10Gd5** **f-) M-ABS-Er5Gd10**

**g-) M-ABS-Er20** **h-) M-ABS-Gd20**

**Figure 4.3:** SEM images of ABS samples with additives produced by the mold production method; e) %10Er, %5Gd, f) %5Er, %10Gd, g) %20Er ve h) %20Gd

In Figure 4.2, the SEM image of an ABS sample with 5 wt% Erbium addition (M-ABS-Er5) shows surface pits and lines similar to those seen in Figure 4.1 for the pure ABS sample with 0 wt% Erbium, 0 wt% Gadolinium (M-ABS-0), which are thought to be due to the production method. Additionally, clusters appearing in light color on the surface are noticeable. These clusters were identified as the additive element (Erbium) through EDS mapping, and it is observed that the particles are homogeneously distributed on the surface. Figure 4.3 presents the surface image of an ABS sample with 10 wt% Erbium addition (M-ABS-Er10), and it is noticeable that there are fewer pits on the surface of this sample. Similar to the sample with 5 wt% Erbium (M-ABS-Er5), light-colored spots on the surface indicate the presence of Erbium, and surface scratches are noticeable. In the sample with the highest 20 wt% Erbium addition (M-ABS-Er20), clustering is more intense, indicating that the additive element is not distributed homogeneously enough on the surface. Figure 4.3 reveals that as the proportion of the additive increases, the homogenization of production through the manual method is negatively affected, and this has been noted as a weakness of the mold production method. The surface morphologies of Gadolinium-doped samples are observed to exhibit similar characteristics to those of Erbium-doped samples. The air gaps and scratches on the surface of the sample with 5 wt% Gadolinium addition (M-ABS-Gd5) are noticeably visible, while the distribution of light-colored spots representing the additive element can also be distinguished in the same figure. The sample with 10 wt% Gadolinium addition, which appears to be the densest in terms of air gaps, clearly shows the distribution of the additive element on the surface, while there is a decrease in production-related scratches. The air gaps have decreased in samples with 20 wt% Gadolinium (M-ABS-Gd20) addition and 5 wt% Erbium, 10 wt% Gadolinium (M-ABS-Er5Gd10) addition. The additive distribution on the surface of the sample with 20 wt% Gadolinium addition is more homogeneous compared to the ABS sample with 10 wt% Erbium, 5 wt% Gadolinium (M-ABS-10Er5Gd) addition. The sample with 10% Gadolinium & 5% Er exhibits an unexpected appearance similar to that with 10 wt% Er & 5 wt% Gd.

#### 4.3.1.2. P-series (printed samples) SEM analysis results

In the SEM images of ABS samples produced using the 3D printer method, there are noticeable differences compared to the mold production method. The surface morpho-

logy of the undoped ABS sample is quite smooth and free of pits, and the lines formed by the layers made during the printing process can be seen in Figure 4.4. The absence of gaps between the layers is due to the high fill ratio preferred during the printing of the samples.

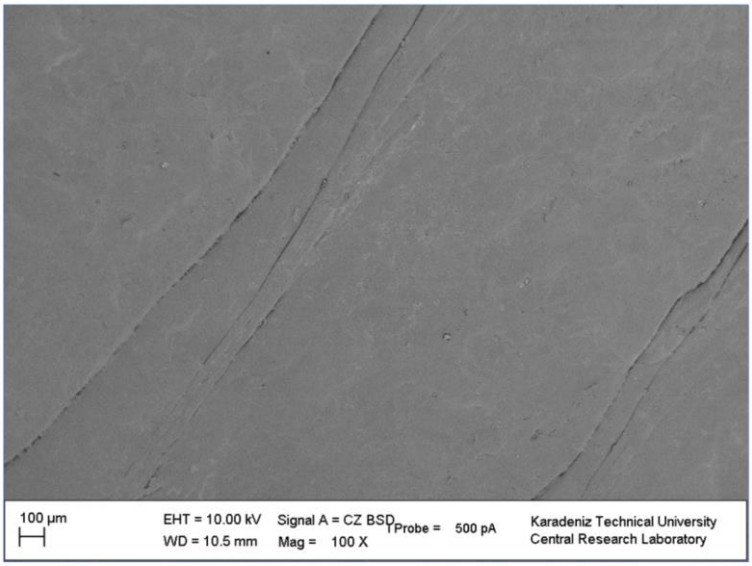



**Figure 4.4:** SEM image of the ABS sample produced with a 3D printer without additives (P-ABS-0)

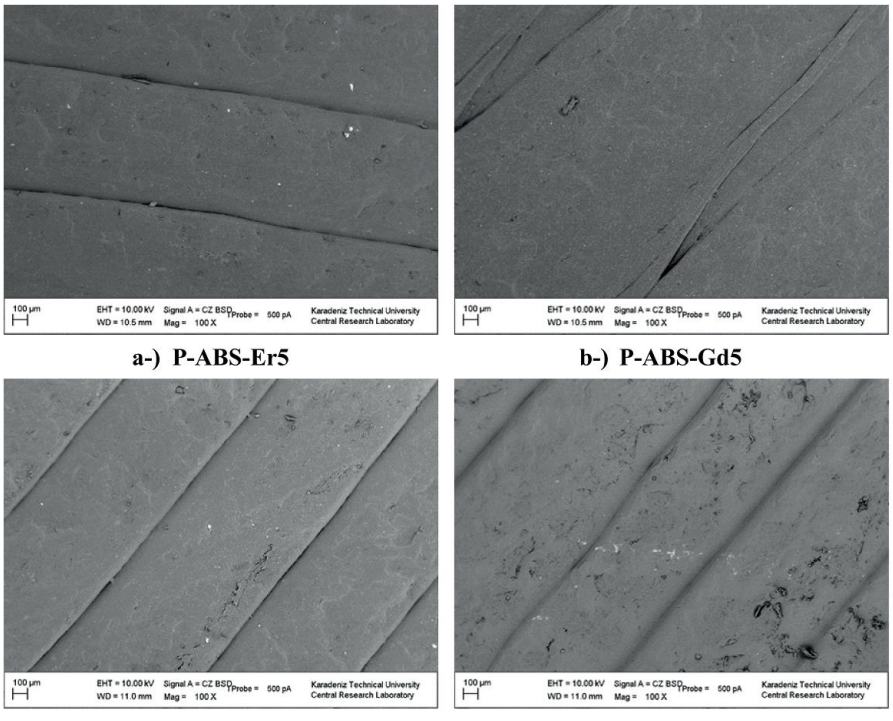



**Figure 4.5:** SEM images of ABS samples with additives produced by the 3D printer method; a) %5Er, b) %5Gd, c) %10Er, d) %10Gd

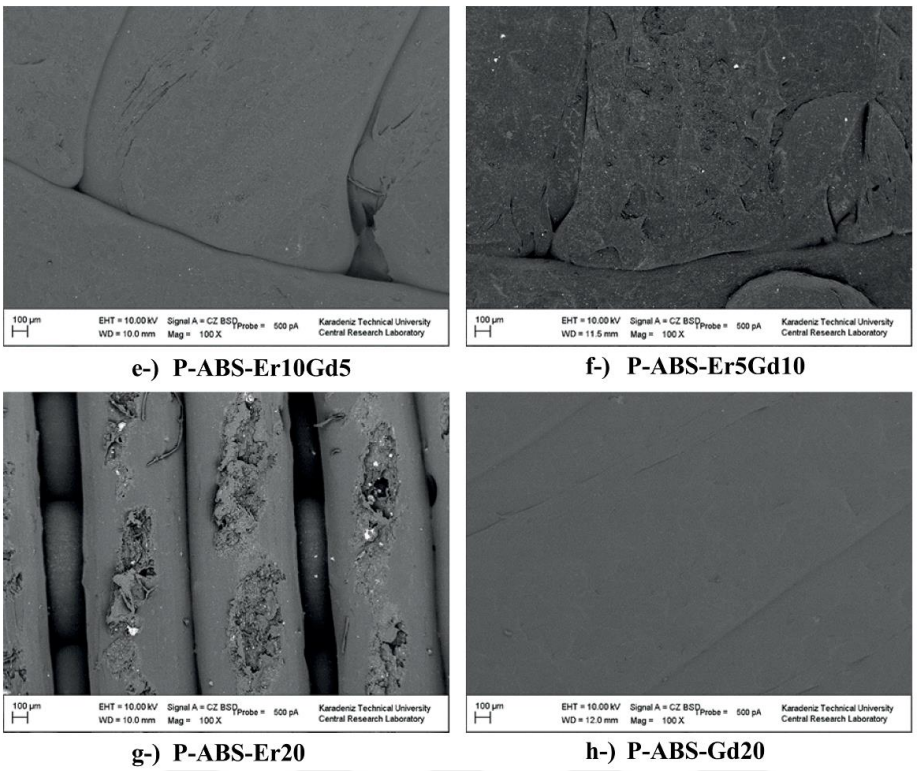



**Figure 4.6:** SEM images of ABS samples with additives produced by the 3D printer method; ; e) %10Er, %5Gd, f) %5Er, %10Gd, g) %20Er ve h) %20Gd

In Figure x2, the surface of the P-ABS sample with 5% Erbium addition (P-ABS-Er5) shows the presence of the additive element, as is the case in all doped samples. In contrast to the sample with 5% Erbium addition (P-ABS-Er5), where the additive process was carried out without surface damage and a print was taken, noticeable surface deteriorations are observed in P-ABS samples doped with ABS at rates of 10% (P-ABS-Er10) and 20% Erbium (P-ABS-Er20). It is evident that there are significant surface deteriorations with the increase in the doping ratio, and this deterioration increases with the increase in the additive. In this sense, it can be said that Erbium deteriorates the surface morphology in 3D Printed ABS samples. In samples produced by 3D printing, there is less surface deterioration in the morphology of Gadolinium-doped samples compared to Erbium-doped samples. In the sample with the lowest Gadolinium doping ratio of 5% Gadolinium (P-ABS-Gd5), no surface deformation is observed, whereas with a 10% Gadolinium (P-ABS-Gd10) doping ratio, faint pits are noticeable. However, this is not observed in samples with 20% Gadolinium (P-ABS-Gd20) addition, unlike Erbium-doped samples. When examining the samples with dual doping, it is observed that the surface fractures caused by Erbium doping alone are not formed. In all samples,

the distribution of the additive element on the surface is evident from the light-colored spots. It is clear that a more homogeneous distribution is achieved in these samples, where agglomeration/clustering is almost not encountered, compared to the manual method.

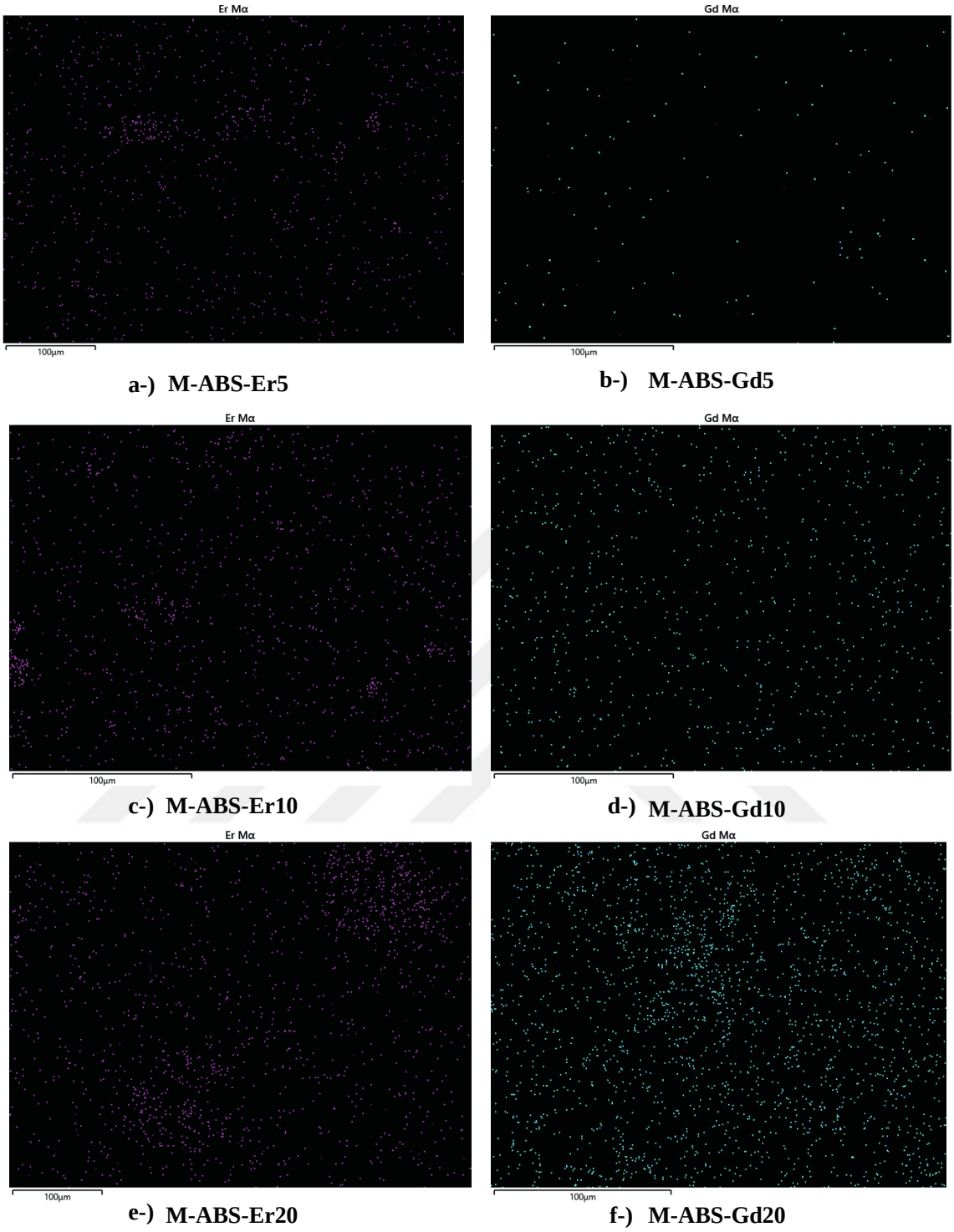
### 4.3.1. EDS (energy dispersive x-ray spectroscopy) analysis results

After SEM (scanning electron microscopy) analyses, when EDS (energy dispersive x-ray spectroscopy) analysis was conducted, the probabilities or energies of distinctive X-rays emitted by various elements vary. EDS can objectively and quantitatively evaluate the components of test materials quickly by examining photon energy. The EDS results of the samples produced with the mold production method are given in Table x1. When we examine the EDS maps, we observe that the M-ABS-0 sample, which are pure, contain the elements C and O. The occurrence of a zero value for the element N is common; the literature points to the extremely low reactivity of nitrogen atoms as the reason for this. The low reactivity of nitrogen atoms can lead to insufficient scattering of X-rays, and therefore they may not be detected.

**Table 4.142 :** The elemental mass percentages of the produced ABS samples can be determined through Energy Dispersive Spectroscopy (EDS) maping analysis.

| Sample | C (%wt) | O (%wt) | Er (%wt) | Gd (%wt) | Total Additives |
|---|---|---|---|---|---|
| M-ABS-0 | 92,0000 | 8,0000 | 0,0000 | 0,0000 | Additive-free |
| M-ABS-Er5 | 93,5000 | 5,2000 | 1,2000 | 0,0000 | % 5Er |
| M-ABS-Gd5 | 91,8000 | 5,1000 | 0,0000 | 3,0000 | % 5Gd |
| M-ABS-Er10 | 92,7000 | 3,2000 | 4,1000 | 0,0000 | % 10Er |
| M-ABS-Gd10 | 89,9000 | 3,4000 | 0,0000 | 6,7000 | % 10Gd |
| M-ABS-Er10Gd5 | 87,1000 | 5,2000 | 5,8000 | 2,0000 | % 10Er-%5Gd |
| M-ABS-Er5Gd10 | 80,4000 | 5,8000 | 3,9000 | 9,8000 | % 5Er-%10Gd |
| M-ABS-Er20 | 87,7000 | 5,2000 | 7,2000 | 0,0000 | % 20Er |
| M-ABS-Gd20 | 89,6000 | 3,5000 | 0,0000 | 6,9000 | % 20Gd |

Since EDS analysis is an analysis where a specific region of the sample is examined, it does not provide the general distribution within the sample but allows for gaining an understanding of the content. According to the data obtained with this analysis, a general increase in Er and Gd additives is observed as planned in the production stage. In samples with Er and Gd additives at different ratios (%5Er, %5Gd, %10Er, %10Gd, %20Er, %20Gd), it is observed that the values obtained in the EDS results are generally consistent. When Figure 1 is examined, it is observed that the additive element is distributed homogeneously on the surface to a certain extent, but there are accumulations in places.




**a-) M-ABS-Er5** **b-) M-ABS-Gd5**

**c-) M-ABS-Er10** **d-) M-ABS-Gd10**

**e-) M-ABS-Er20** **f-) M-ABS-Gd20**

**Figure 4.7:** a) Er element distribution for M-ABS-Er5, b) Gd element distribution for M-ABS-Gd5, c) Er element distribution for M-ABS-Er10, d) Gd element distribution for M-ABS-Gd10, e) Er element distribution for M-ABS-Er20, f) Gd element distribution for M-ABS-Gd20

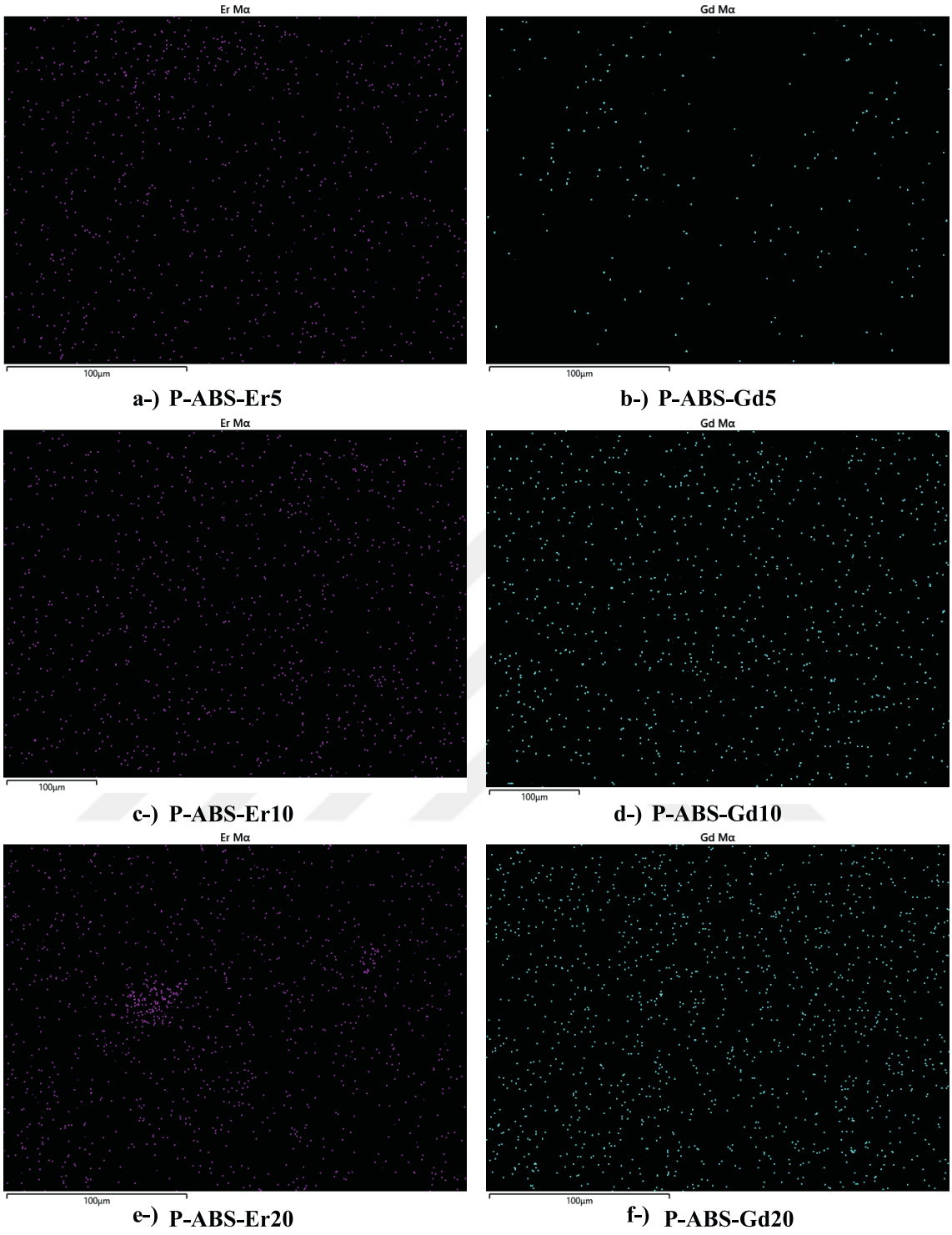



**Figure 4.8:** a) Er element distribution for P-ABS-Er5, b) Gd element distribution for P-ABS-Gd5, c) Er element distribution for P-ABS-Er10, d) Gd element distribution for P-ABS-Gd10, e) Er element distribution for P-ABS-Er20, f) Gd element distribution for P-ABS-Gd20

### 4.4. Thermal Analysis Results

After structural analyses, another analysis conducted is the determination of the temperature-dependent changes in the prepared samples. Initially, mass changes occurring as a function of temperature for each nanooxide-modified polymer sample produced via the M series and P series production routes were analyzed using a drying oven and a precision balance. These analyses were conducted by subjecting the samples to constant temperatures of 120°C, 140°C, 160°C, 180°C, 200°C, and 220°C, with each temperature level being maintained for 10 minutes. The masses of the samples not exposed to these temperature levels were examined by comparing them to the mass changes of the samples held at the respective temperature levels. Figure 5.26 presents the graph obtained for ABS.

#### 4.4.1. M-series (molded samples) thermal analysis results

**Table 4.143:** Percentage mass loss in temperature-dependent ABS-M series samples using a thermostatic drying oven

| Samples | 120 ºC | 140 ºC | 160 ºC | 200 ºC | 220 ºC |
|---|---|---|---|---|---|
| M-ABS-0 (%) | 0,0048 | 0,0073 | 0,0102 | 0,0111 | 0,0112 |
| M-ABS-Er5 (%) | 0,0050 | 0,0057 | 0,0081 | 0,0088 | 0,0089 |
| M-ABS-Gd5 (%) | 0,0048 | 0,0054 | 0,0072 | 0,0083 | 0,0085 |
| M-ABS-Er10 (%) | 0,0054 | 0,0109 | 0,0170 | 0,0194 | 0,0192 |
| M-ABS-Gd10 (%) | 0,0046 | 0,0055 | 0,0071 | 0,0079 | 0,0075 |
| M-ABS-Er10Gd5 (%) | 0,0050 | 0,0057 | 0,0066 | 0,0075 | 0,0069 |
| M-ABS-Er5Gd10 (%) | 0,0041 | 0,0042 | 0,0048 | 0,0054 | 0,0045 |
| M-ABS-Er20 (%) | 0,0046 | 0,0058 | 0,0075 | 0,0088 | 0,0079 |
| M-ABS-Gd20 (%) | 0,0052 | 0,0064 | 0,0083 | 0,0096 | 0,0085 |

#### 4.4.2. P-series (printed samples) thermal analysis results

**Table 4.144:** Percentage mass loss in temperature-dependent ABS-P series samples using a thermostatic drying oven

| Samples | 120 ºC | 140 ºC | 160 ºC | 200 ºC | 220 ºC |
|---|---|---|---|---|---|
| P-ABS-0 (%) | 0,0009 | 0,0018 | 0,0024 | 0,0023 | 0,0030 |
| P-ABS-Er5 (%) | 0,0009 | 0,0019 | 0,0026 | 0,0030 | 0,0040 |
| P-ABS-Gd5 (%) | 0,0012 | 0,0018 | 0,0024 | 0,0021 | 0,0029 |
| P-ABS-Er10 (%) | 0,0003 | 0,0012 | 0,0016 | 0,0021 | 0,0038 |
| P-ABS-Gd10 (%) | 0,0013 | 0,0019 | 0,0022 | 0,0017 | 0,0026 |
| P-ABS-Er10Gd5 (%) | 0,0010 | 0,0016 | 0,0019 | 0,0023 | 0,0033 |
| P-ABS-Er5Gd10 (%) | 0,0007 | 0,0015 | 0,0011 | 0,0004 | 0,0016 |
| P-ABS-Er20 (%) | 0,0003 | 0,0015 | 0,0018 | 0,0023 | 0,0040 |
| P-ABS-Gd20 (%) | 0,0004 | 0,0015 | 0,0019 | 0,0024 | 0,0037 |

**Table 4.145:** Percentage mass change in temperature-dependent P-ABS-Er20, P-ABS-Gd20, P-ABS-0 samples using a Thermogravimetric Analyzer.

| **Samples** | **100 ºC** | **200 ºC** | **300 ºC** | **400 ºC** | **500 ºC** | **600 ºC** |
|---|---|---|---|---|---|---|
| P-ABS-0 (%) | 100 | 99,9528 | 99,9964 | 77,7926 | 12,9078 | 5,3203 |
| P-ABS-Er20 (%) | 99,98 | 99,9211 | 99,1402 | 71,1963 | 22,9652 | 23,5746 |
| P-ABS-Gd20 (%) | 99,98 | 98,7784 | 97,8548 | 76,4308 | 22,1236 | 15,0373 |

## 5. CONCLUSION AND DISCUSSION

In conclusion, while time, distance, and shielding are fundamental principles of radiation protection, in certain situations, the weightage of shielding can be observed to be more substantial. These situations illustrate the critical role that shielding plays in protecting from radiation, and it can sometimes be more important than other protection strategies. In this thesis work, it is aimed to investigate the gamma and neutron shielding charac-teristics of ABS thermoplastics, known as 3D printer polymers with $Er_2O_3$ and Gd2O3 additives, using experimental, theoretical, and simulation methods at different material thicknesses and different radiation energies. To maintain integrity, the microstructures of the produced materials have also been examined. In the production of ABS polymer samples, two different production options have been compared by utilizing both cas-ting type and 3D printing technology. These produced samples, fortified with nano-oxide compounds, were tested with vari-ous radioactive point sources ($^{241}$Am (59,5 keV), $^{133}$Ba (80,9, 276,3, 302,8, 356,0 and 383,8 keV), $^{22}$Na (511,0 and 1274,5 keV), $^{137}$Cs (661,6 keV), ve $^{60}$Co (1173,2 and 1332,5 keV)) using experimental (HPGe detector system), theoretical (XCOM, EpiXS), and simulation (FLUKA, GEANT4) methods to determine their gamma radiation atte-nuation capabilities. The compatibility of each method with the experimental results was determined. Also, within the scope of the thesis work, the neutron attenuation characteristics of all samples to be produced were evaluated with theoretical and simulation calculations. The SEM / EDS analyses of the produced samples were conducted. And the best performing shielding material was determined for each sample. When analyzing the Scanning Electron Microscopy (SEM) and Energy-Dispersive Spectroscopy (EDS) images, it is evident that all of the filaments produced are of printable quality. Moreover, a comparative analysis between the P series and the M series reveals that the P series is characterized by a more homogeneous and structured arrangement. This characteristic enables the end-users to fabricate radiation shielding materials in bespoke shapes and intricate designs. This study, therefore, serves as a vanguard, especially for companies engaged in the production domain, thereby underlining the extensive implications of this research. In the context of gamma shielding, the research observed that the inclusion of two selected nanomaterials in the ABS (Acrylonitrile Butadiene Styrene) polymer matrix led to an enhancement in its gamma shielding efficiency. This enhancement was extensively inves-

tigated over a broad spectrum of energy bands utilizing an amalgam of experimental, theoretical, and simulation methodologies. When the P series was juxtaposed with the M series concerning their gamma shielding efficiencies, the M series demonstrated a marginally superior performance, approximately by 2%. The plausible reason attributed to this variation is the higher density inherent in the M series compared to the P series. Consequently, it can be articulated that the P series can potentially be used as a substitute for the M series. Considering that the integrated nanomaterials possess excellent absorption cross-section attributes for thermal neutrons, additional computations were executed for fast neutrons using the GEANT4 simulation package. According to the findings, an approximate thermal neutron shielding efficiency of 90% was discerned, whereas for fast neutrons it was 20%. To delve into the fast neutron shielding capability in more detail, simulations were carried out across various neutron energy levels and sample thicknesses, bolstered by effective neutron removal cross-section analyses. The insights garnered indicate that the nanoparticle additives do not contribute significantly to fast neutron shielding and could even potentially weaken the material's neutron shielding efficiency. However, in the case of thermal neutrons, it appears that the nanoparticle-enhanced samples generated in this research outperform conventional materials like paraffin and concrete. It should be noted, though, that this does not apply to neutrons with an energy of 4.5 MeV.

If we first examine the results of radiation shielding, figures 5.1 and 5.2 display the LAC (Linear Attenuation Coefficient) results as a function of gamma energy for the ABS M series. Similarly, Figures 5.3 and 5.4 show the LAC results as a function of gamma energy for the ABS P series. It can be observed that the experimental, theoretical, and simulation results are in good agreement with each other, with a maximum discrepancy of around 7-8 percent. As gamma energy increases, an exponential decrease in the LAC value is also observed. Since a larger LAC value indicates better gamma radiation shielding capability, an increase in energy leads to an improvement in radiation shielding capability. It has been determined that both Erbium (Er) and Gadolinium (Gd) contribute to an increase in the LAC value as the additive material content is increased. Further details on this will be discussed in the discussion section. A comparison of the two production techniques will also be addressed in the discussion section.

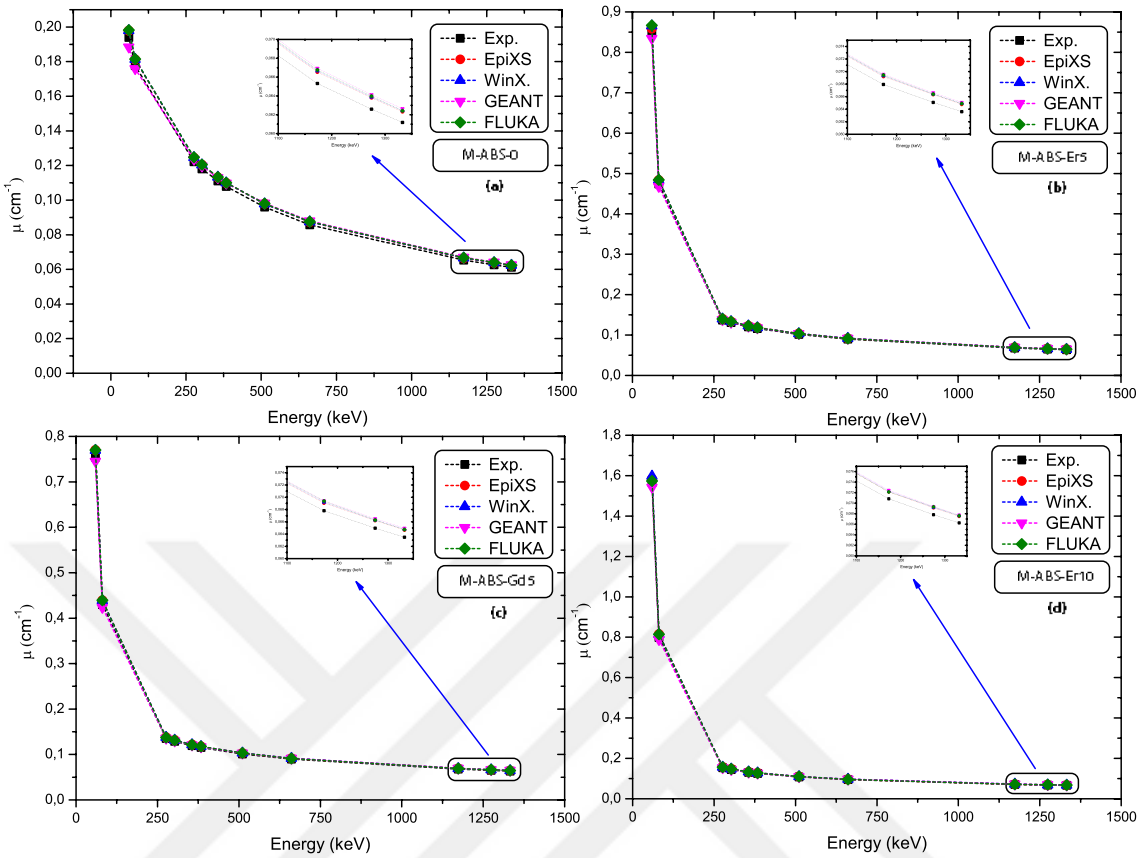



**Figure 5.1:** Linear attenuation coefficient graphs for M-ABS-0, M-ABS-Er5, M-ABS-Gd5, and M-ABS-Er10

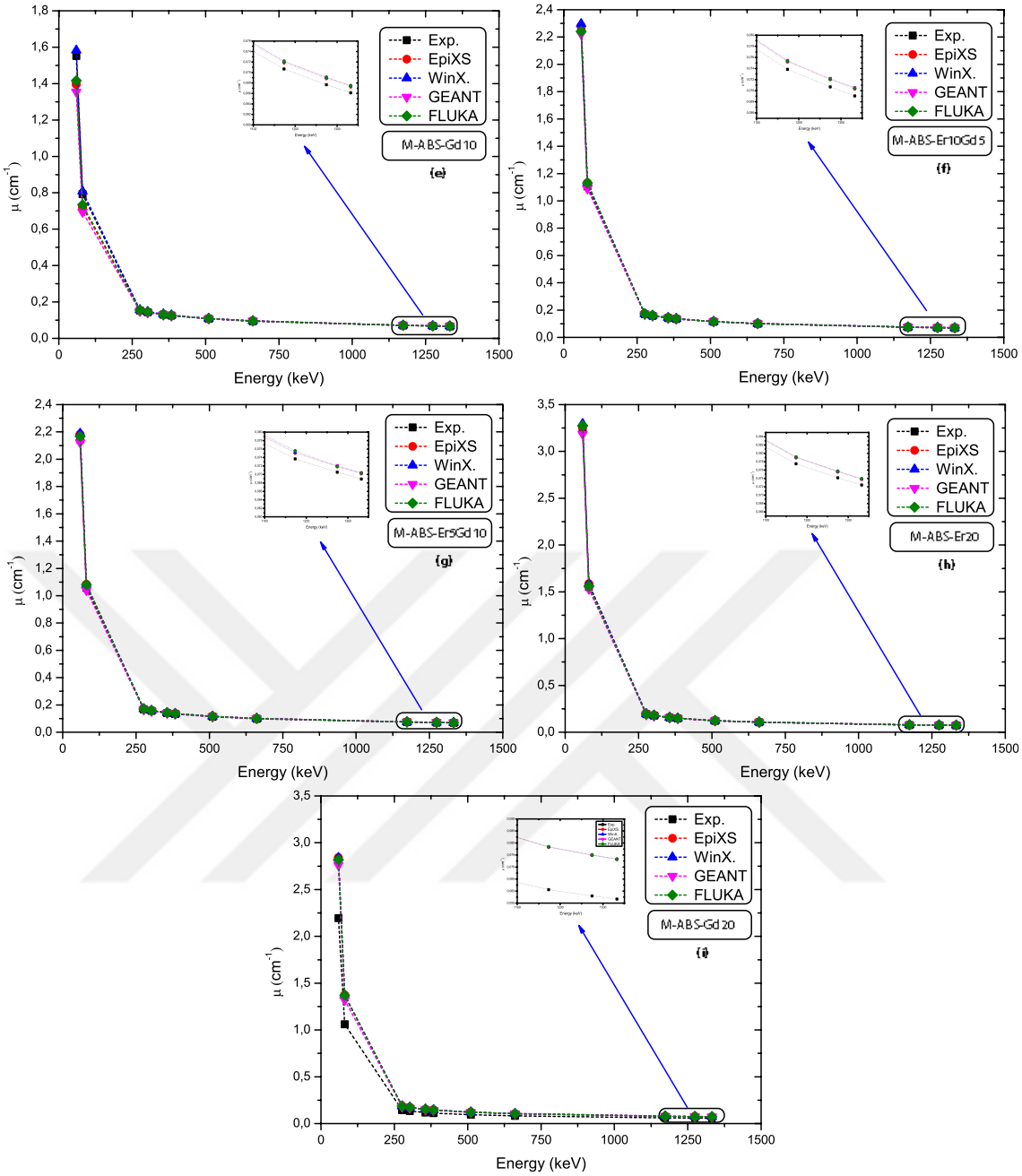



**Figure 5.2:** Linear attenuation coefficient graphs for M-ABS-Gd10, M-ABS-Er10Gd5, M-ABS-Er5Gd10, M-ABS-Er20, and M-ABS-Gd20

Figures 5.1 and 5.2 display the MAC (Mass Attenuation Coefficient) results as a function of gamma energy for the ABS M series. Similarly, Figures 5.3 and 5.4show the MAC results as a function of gamma energy for the ABS P series. It can be observed that the experimental, theoretical, and simulation results are in good agreement with each other, with a maximum discrepancy of around 7-8 percent. As gamma energy increases, an exponential decrease in the MAC value is also observed. Since a larger MAC value indicates better gamma radiation shielding capability, an increase in energy

leads to an improvement in radiation shielding capability. It has been determined that both Erbium (Er) and Gadolinium (Gd) contribute to an increase in the MAC value as the additive material content is increased. Further details on this will be discussed in the discussion section. A comparison of the two production techniques will also be addressed in the discussion section.

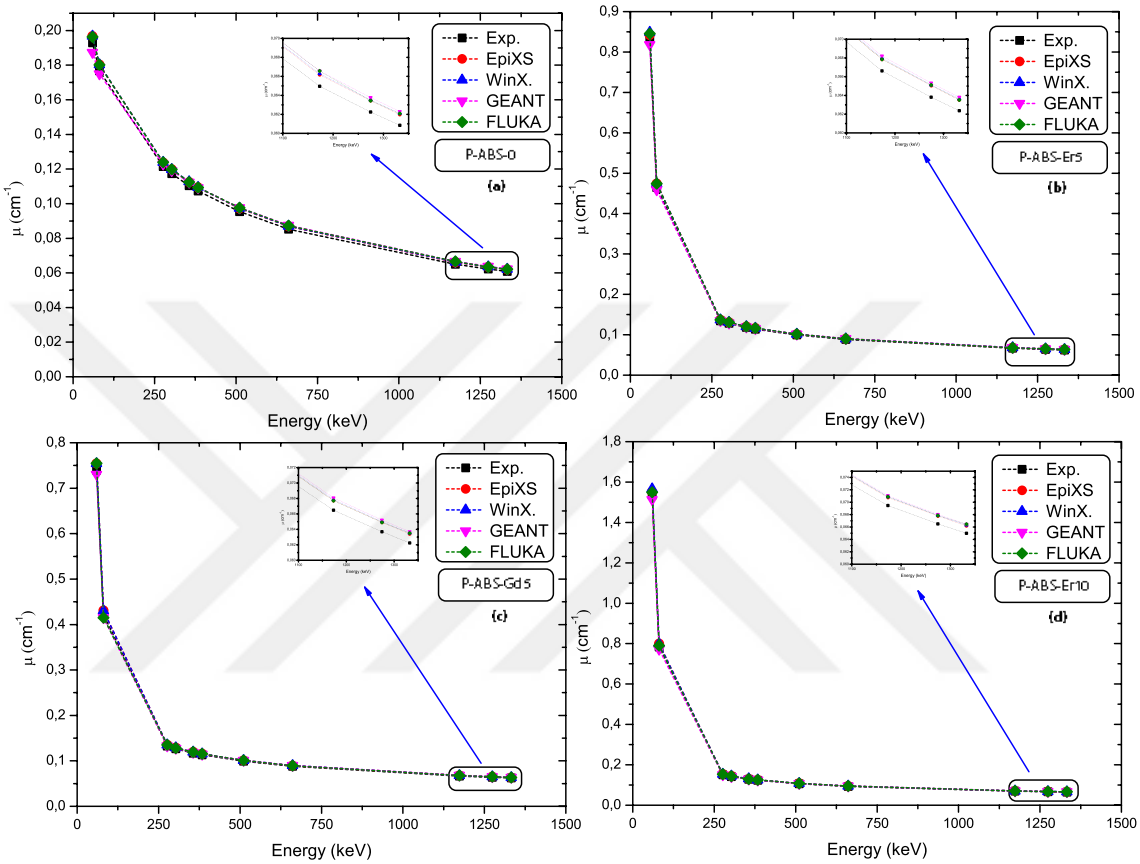



**Figure 5.3 :** Mass attenuation coefficient graphs for P-ABS-0, P-ABS-Er5, P-ABS-Gd5, and P-ABS-Er10

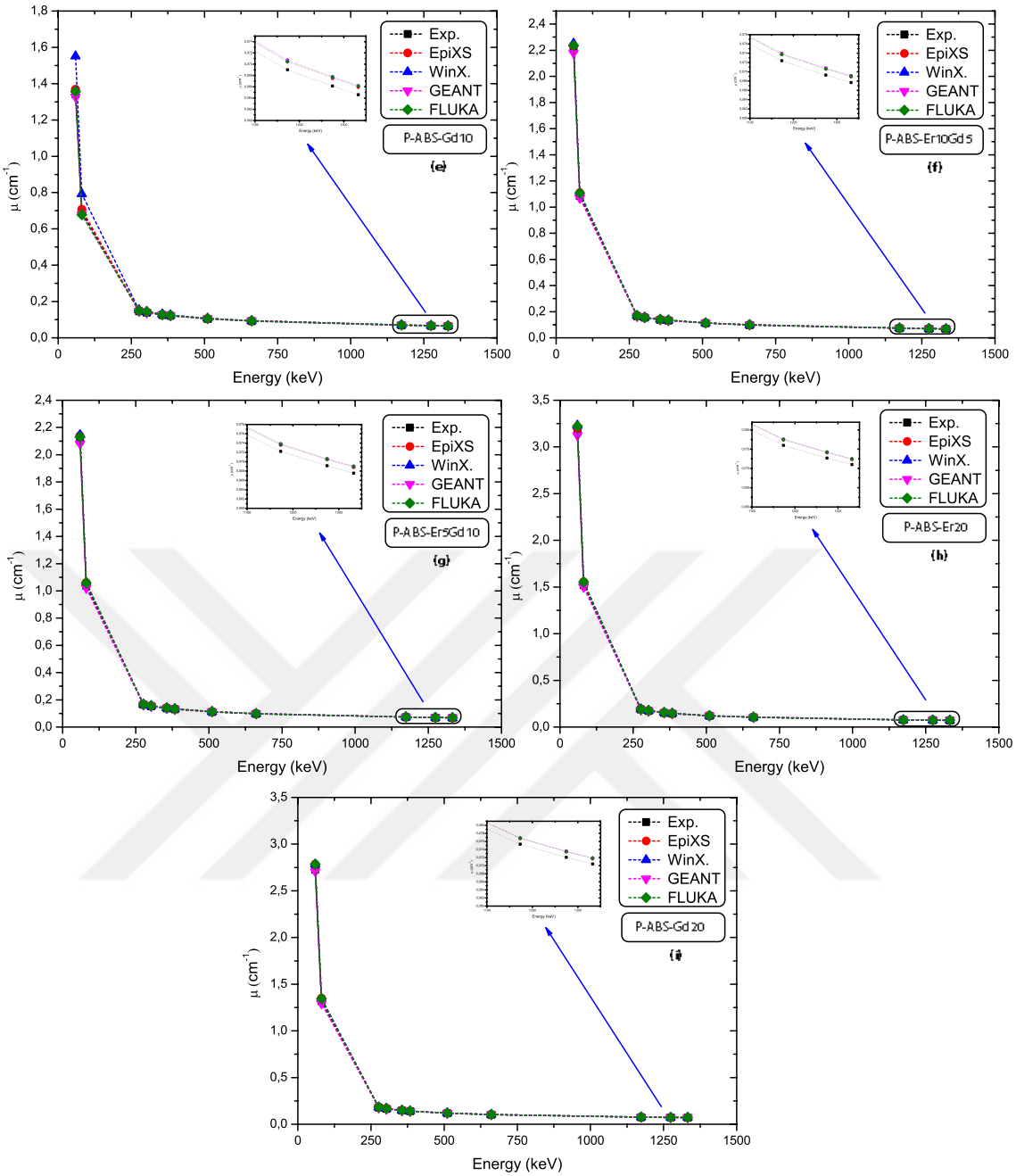



**Figure 5.4:** Mass attenuation coefficient graphs for P-ABS-Gd10, P-ABS-Er10Gd5, P-ABS-Er5Gd10, P-ABS-Er20, and P-ABS-Gd20

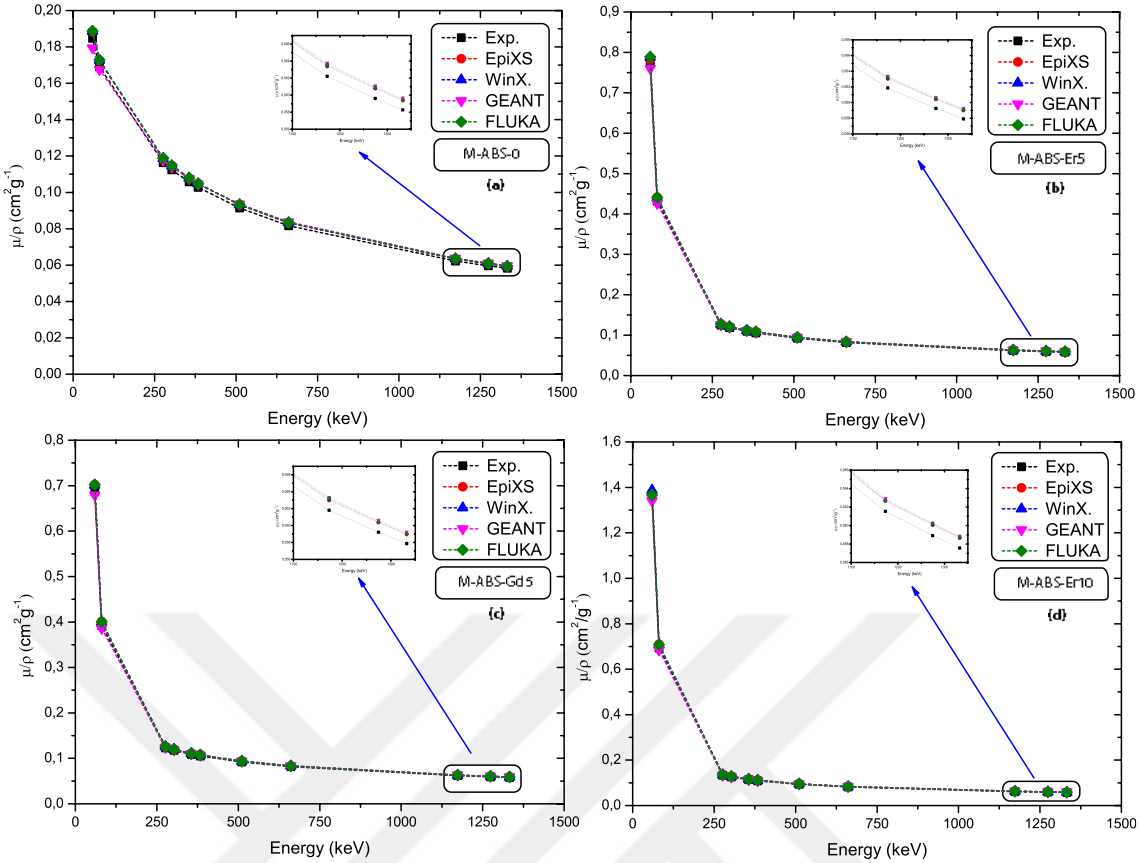



**Figure 5.5.:** Mass attenuation coefficient graphs for M-ABS-0, M-ABS-Er5, M-ABS-Gd5, and M-ABS-Er10

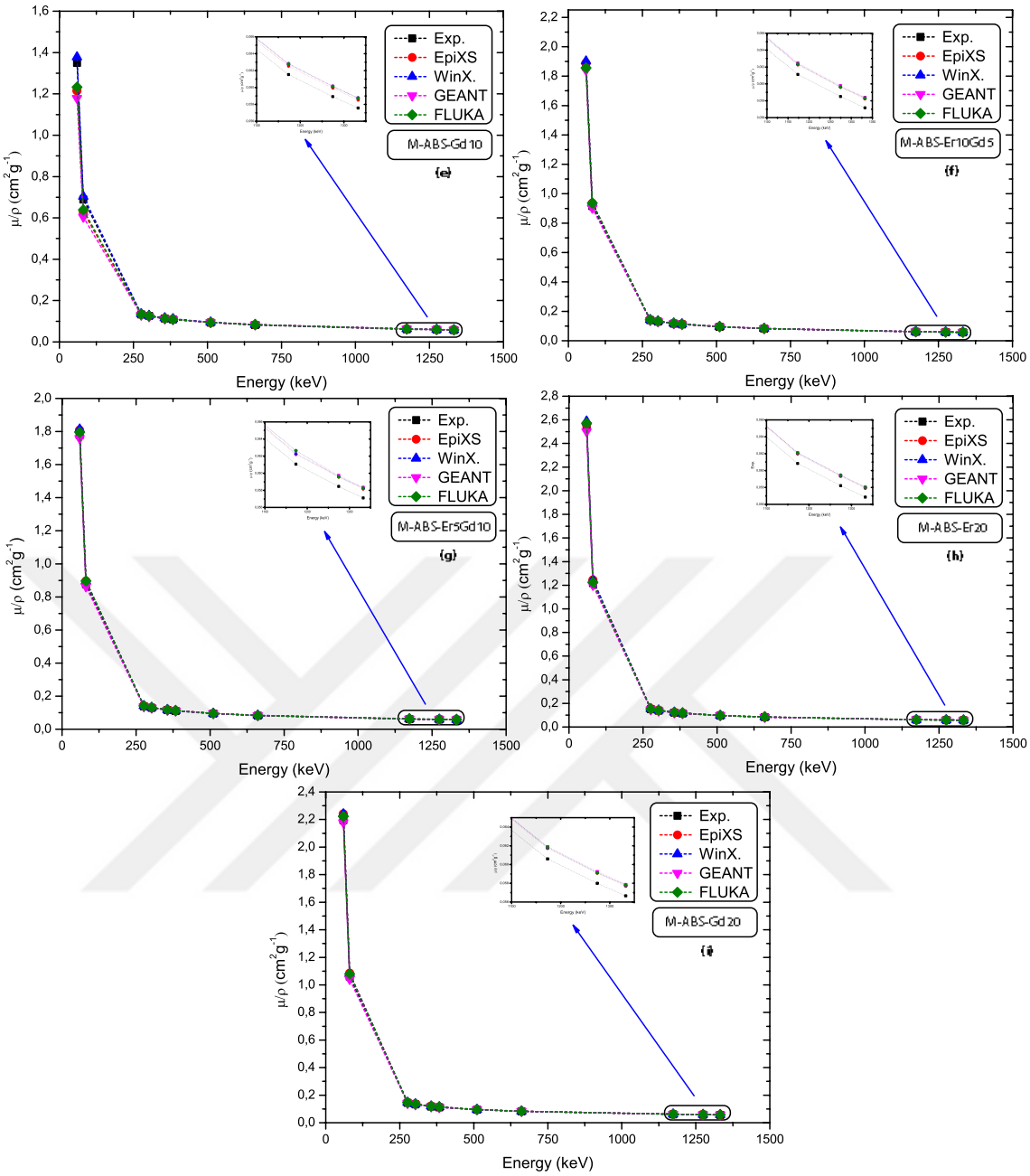



**Figure 5.6**: Mass attenuation coefficient graphs for M-ABS-Gd10, M-ABS-Er10Gd5, M-ABS-Er5Gd10, M-ABS-Er20, and M-ABS-Gd20

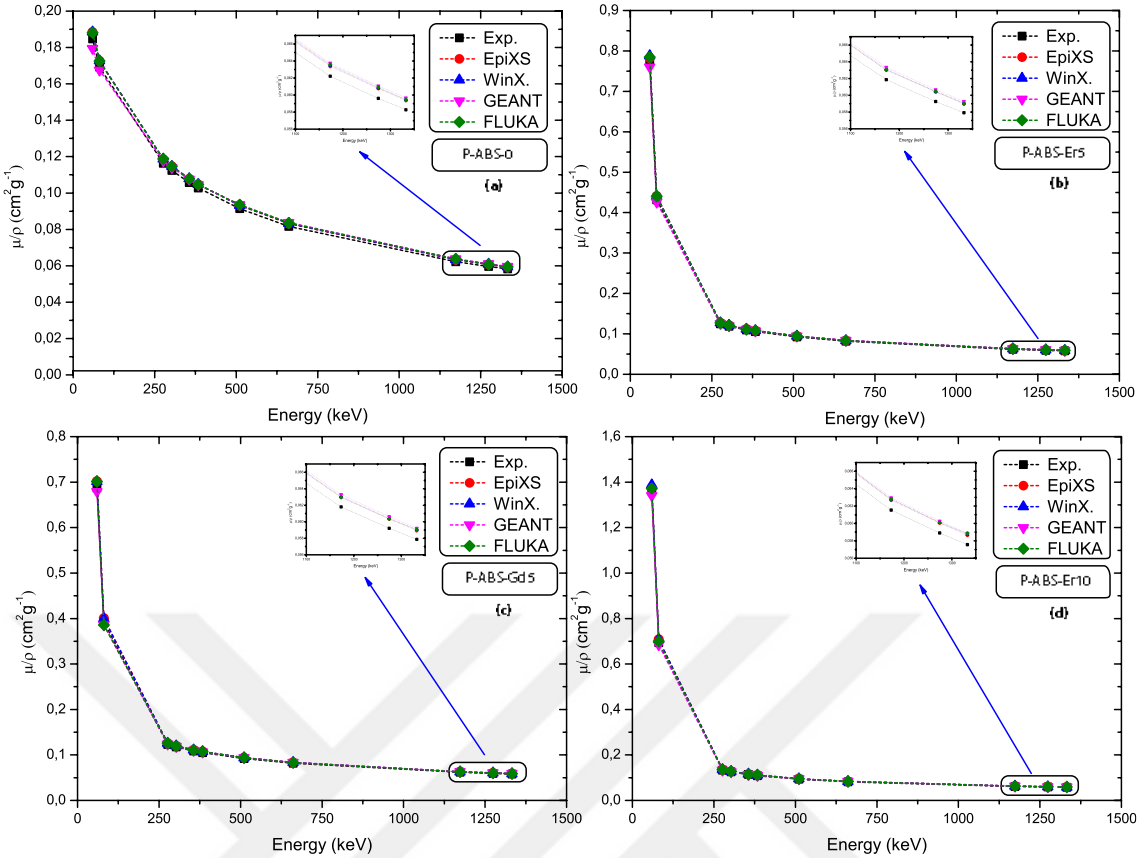



**Figure 5.7.:** Mass attenuation coefficient graphs for P-ABS-0, P-ABS-Er5, P-ABS-Gd5, and P-ABS-Er10

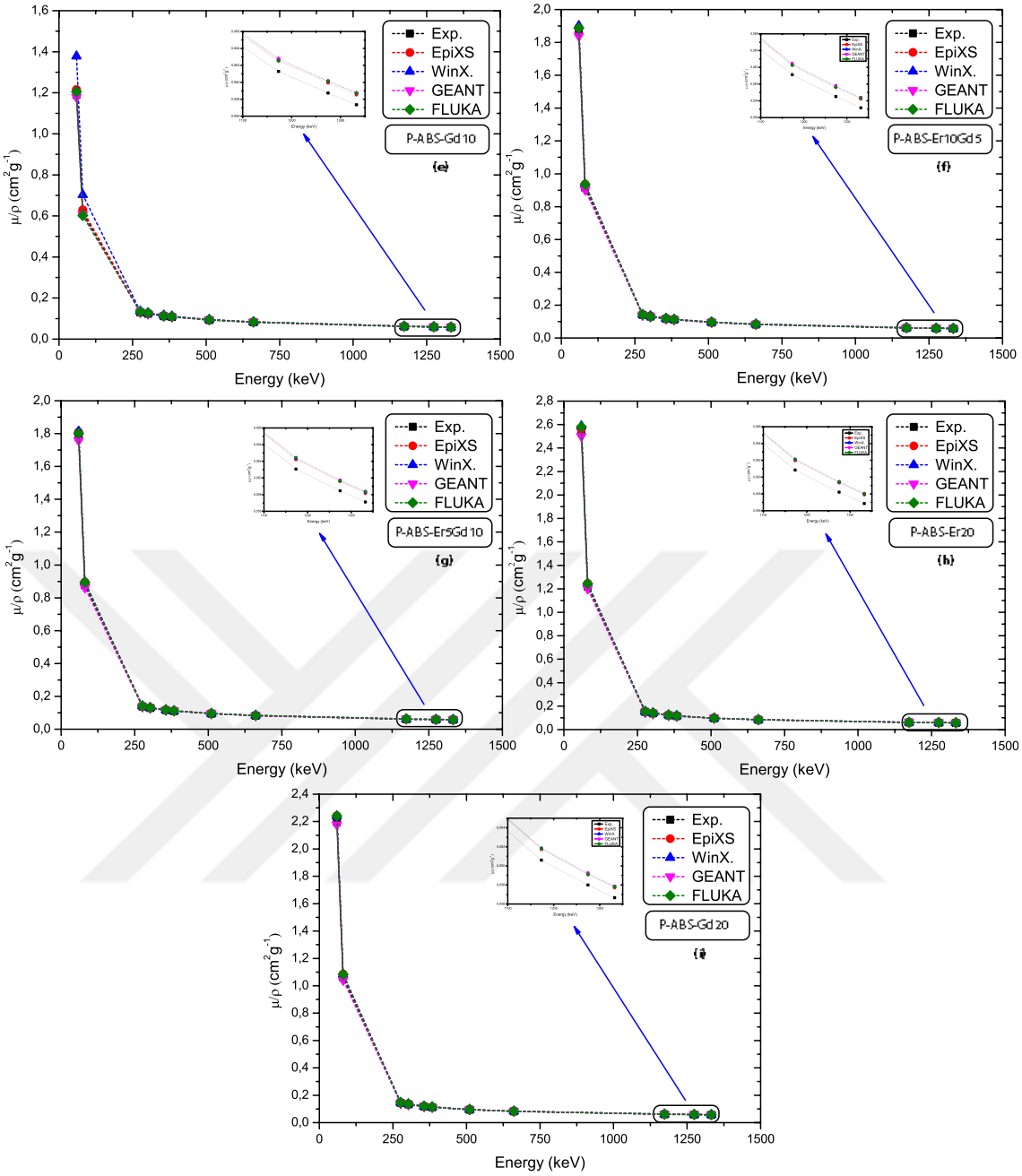



**Figure 5.8.:** Mass attenuation coefficient graphs for P-ABS-Gd10, P-ABS-Er10Gd5, P-ABS-Er5Gd10, P-ABS-Er20, and P-ABS-Gd20

After the MAC (Mass Attenuation Coefficient) values, the next set of results presented are the half-value layer (HVL) measurements of the samples. The half-value layer can be expressed as the thickness of the sample required to reduce the radiation intensity incident on the sample to half. The smaller this value, the better the gamma radiation shielding capability of the material. In Figures 5.5 and 5.6, HVL values for the ABS M series are visualized, while the results for the P series are presented in Figures 5.7 and 5.8. As the gamma energy increases, it is observed that the HVL value also increases.

There is good agreement between experimental, theoretical, and simulation results, with a maximum discrepancy of approximately 6-7 percent.

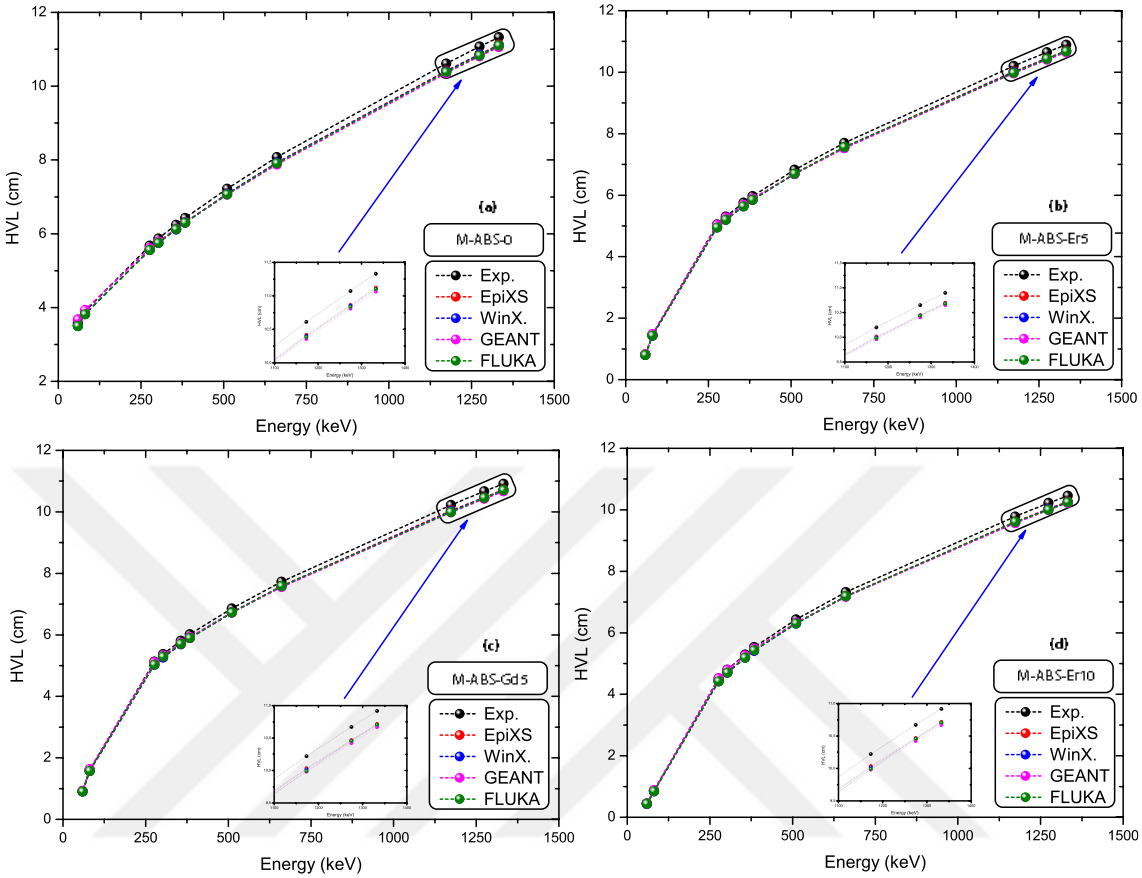



**Figure 5.9:** HVL (Half-Value Layer) graphs for M-ABS-0, M-ABS-Er5, M-ABS-Gd5, and M-ABS-Er10

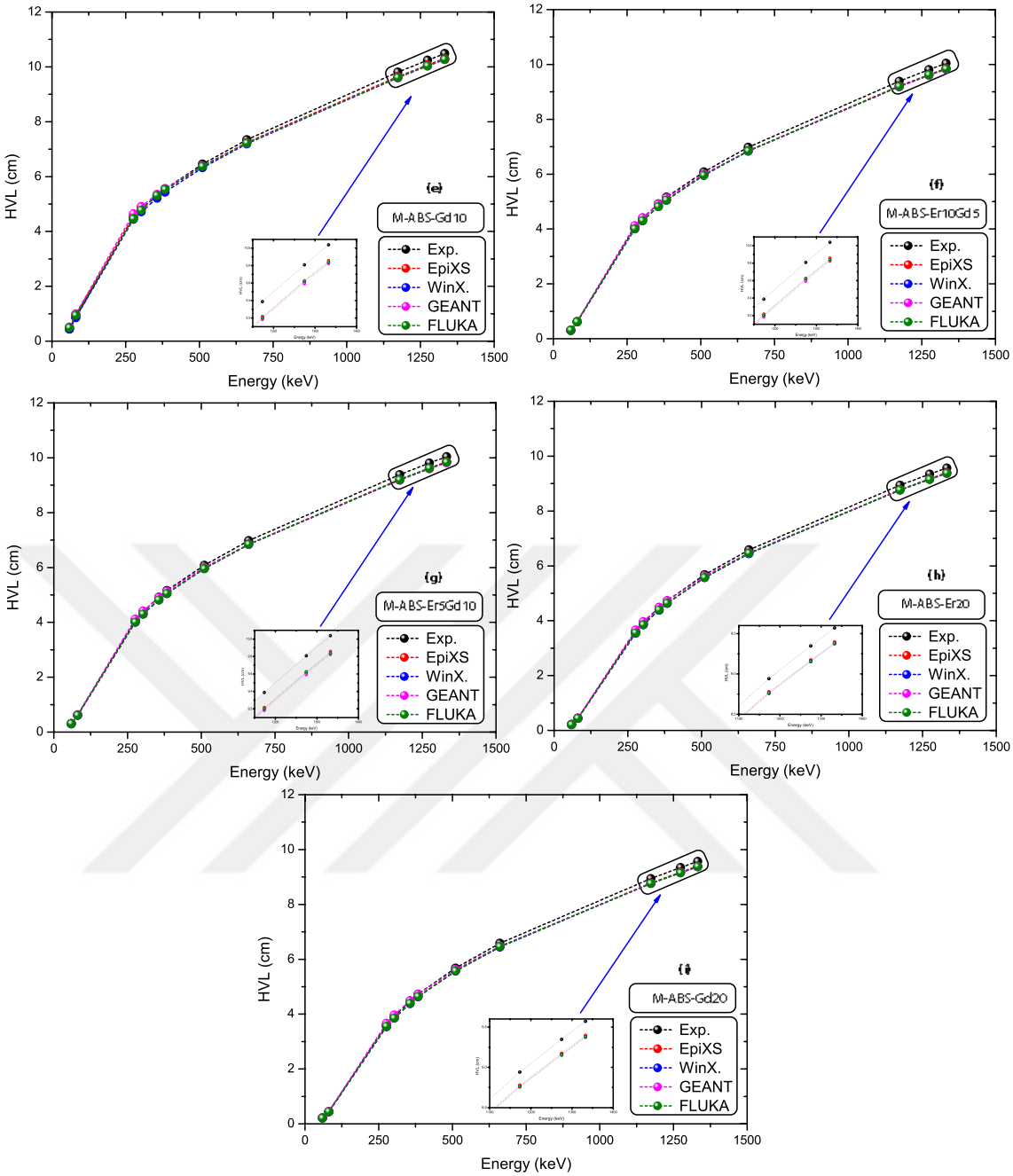



**Figure 5.10.:** HVL (Half-Value Layer) graphs for M-ABS-Gd10, M-ABS-Er10Gd5, M-ABS-Er5Gd10, M-ABS-Er20, and M-ABS-Gd20

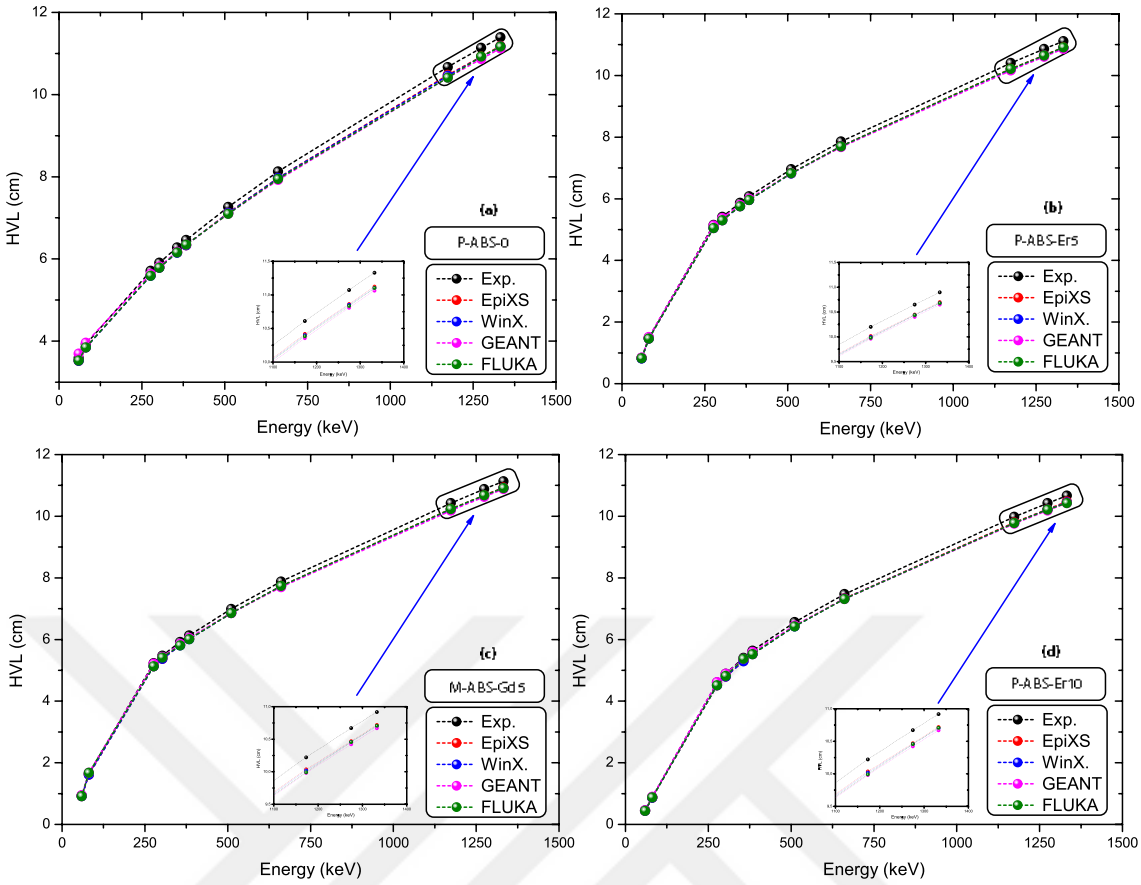



**Figure 5.11 :** HVL (Half-Value Layer) graphs for P-ABS-0, P-ABS-Er5, P-ABS-Gd5, and P-ABS-Er10

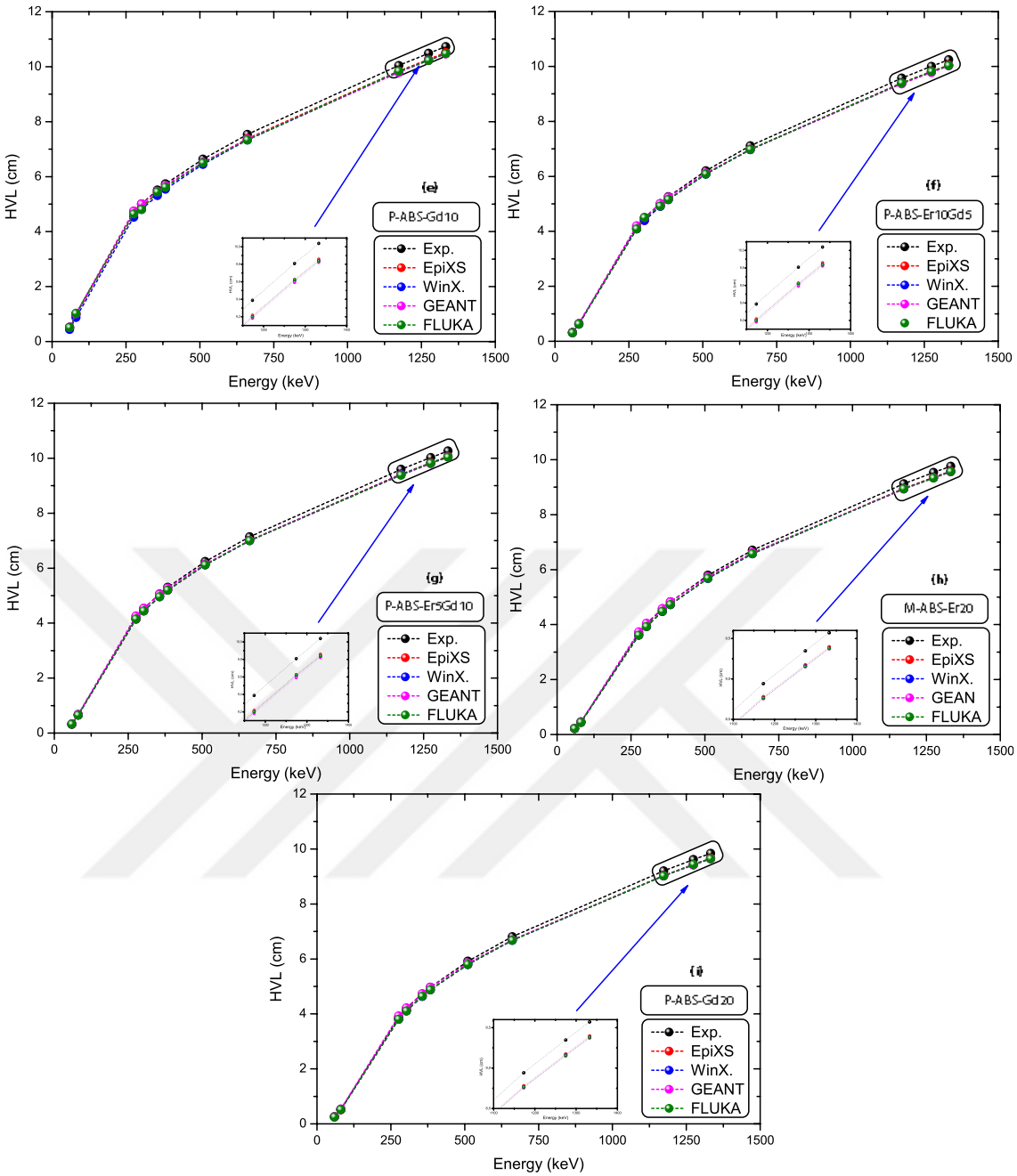



**Figure 5.12.:** HVL (Half-Value Layer) graphs for P-ABS-Gd10, P-ABS-Er10Gd5, P-ABS-Er5Gd10, P-ABS-Er20, and P-ABS-Gd20

Another parameter considered in radiation shielding is the Radiation Protection Efficiency (RPE), which is also known as RKV (Radiation Kinematic Viscosity) in some contexts. This parameter has been calculated for both ABS and PLA samples at all energy levels. Some of the results have been visualized for certain energies and are presented in this section. It should be noted that the higher the efficiency, the better the shielding capability. In the discussion section, all results will be examined, with specific examples and applications mentioned. Figures 5.13 and 5.14 present RPE graphs for

ABS samples as a function of sample thickness. As the sample thickness increases, RPE also increases. Additionally, an increase in both Gd and Er additive amounts also contributes to an increase in the RPE value.

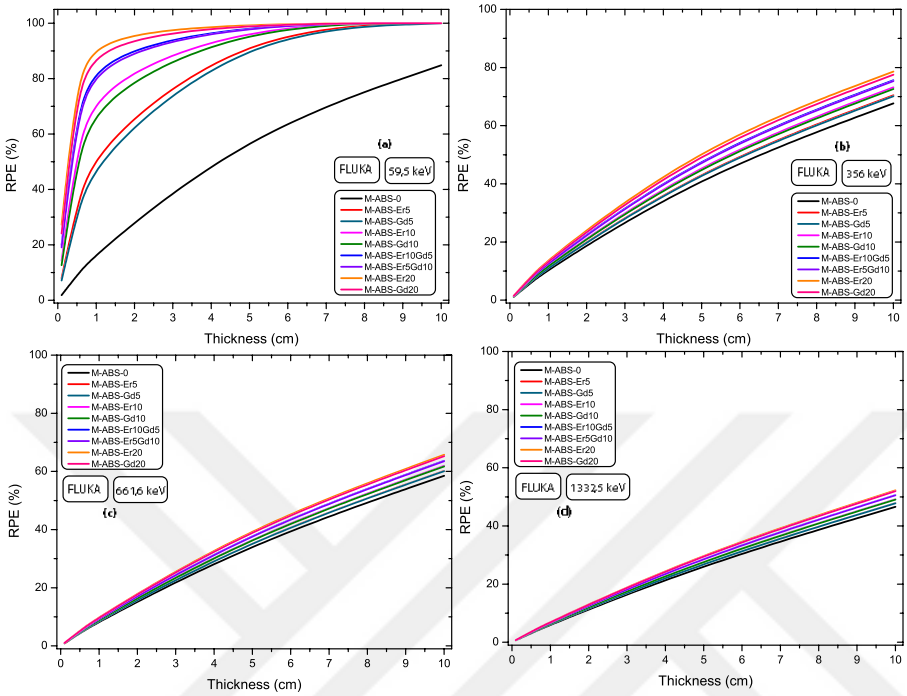



**Figure 5.13.:** RPE (Radiation Protection Efficiency) graphs dependent on sample thickness for ABS-M series

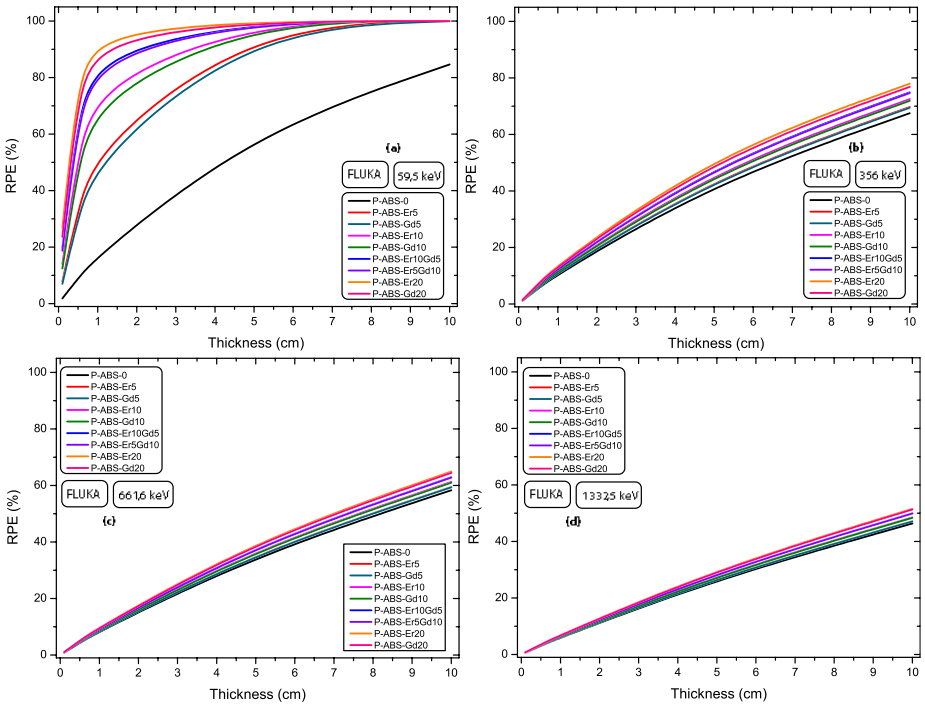



**Figure 5.14.:** RPE (Radiation Protection Efficiency) graphs dependent on sample thickness for ABS-P series

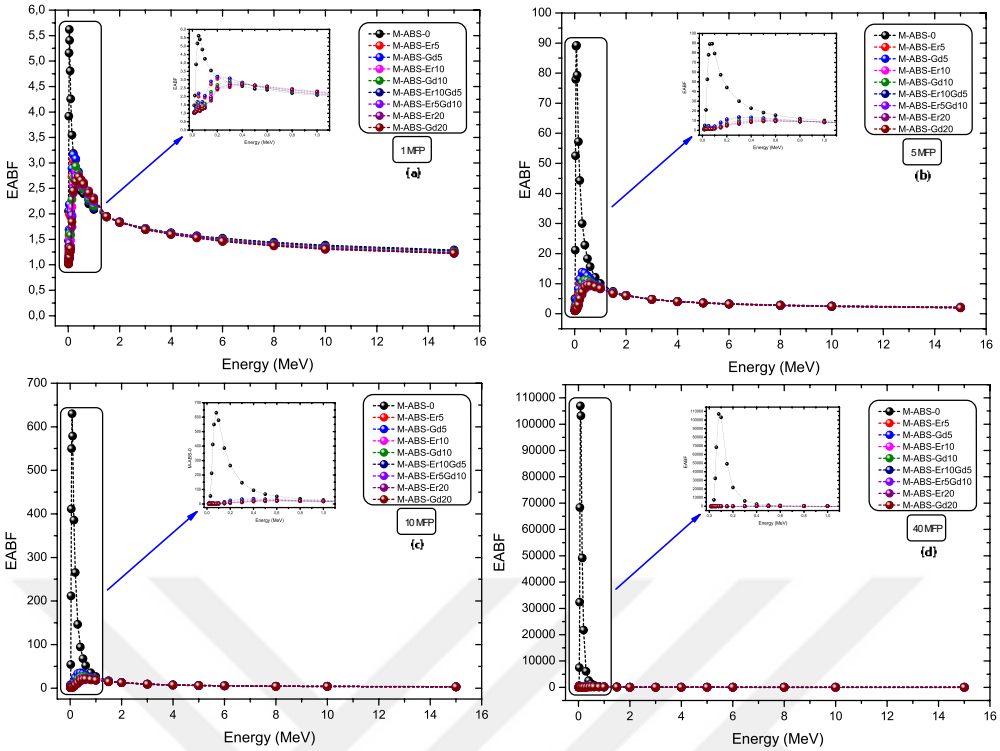



**Figure 5.15.:** Buildup factor (energy absorption) graphs: graphs dependent on Mean Free Path (MFP) and energy for ABS-M series

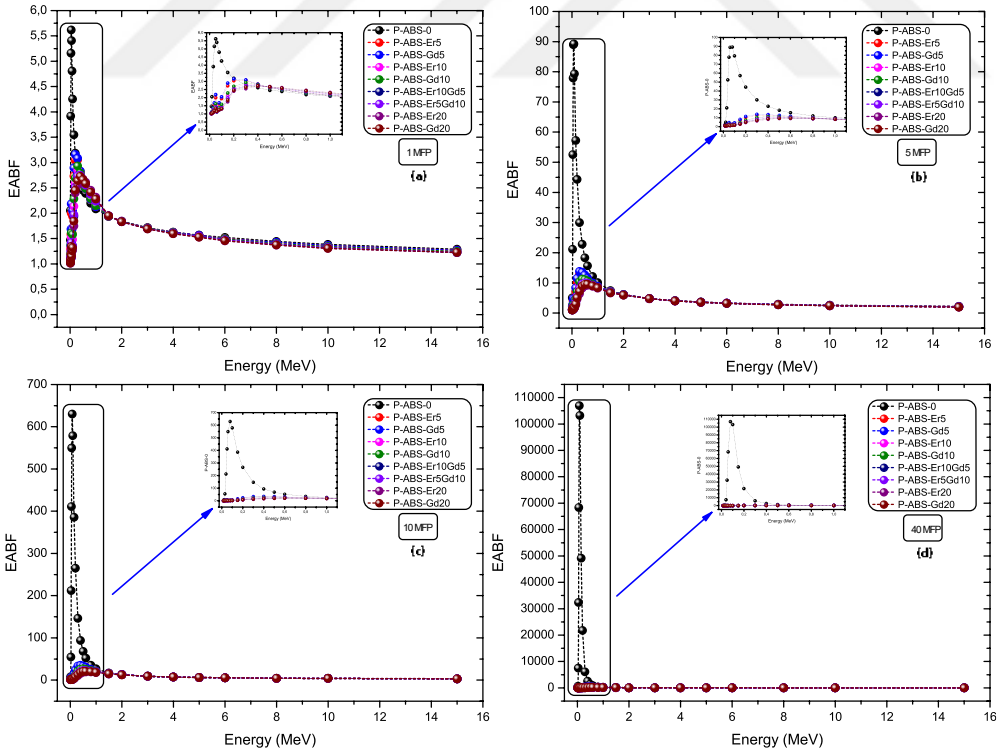



**Figure 5.16.:** Buildup factor (energy absorption) graphs: graphs dependent on Mean Free Path (MFP) and energy for ABS-P series

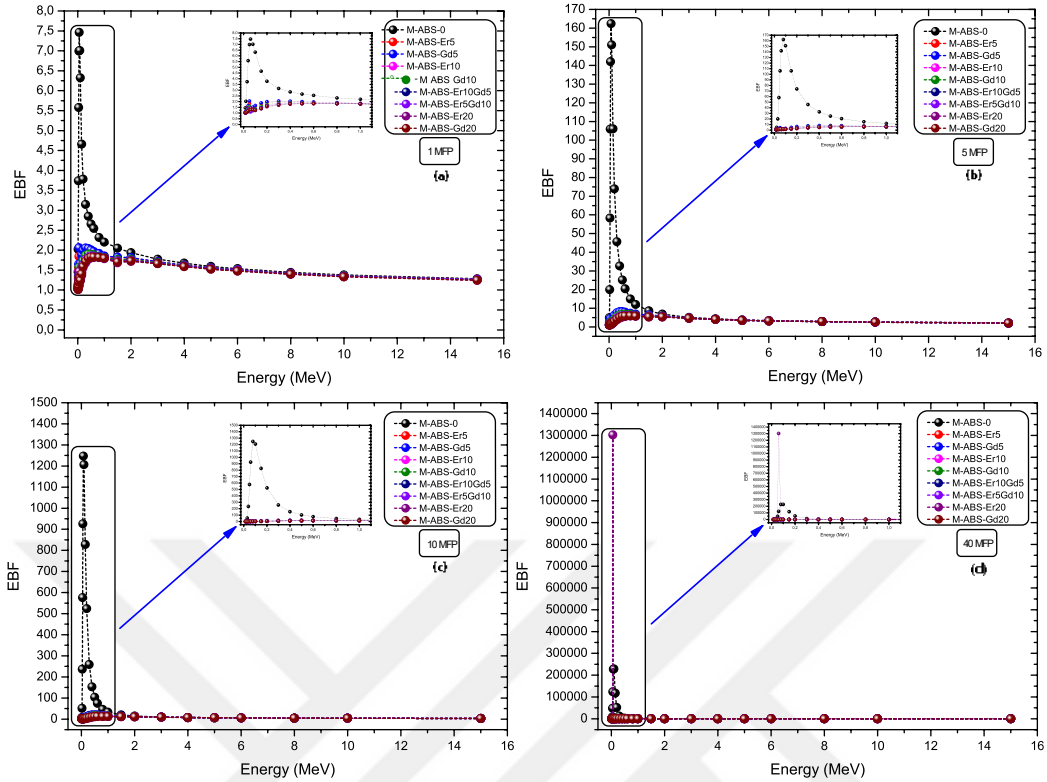



**Figure 5.17.:** Buildup factor (Exposure) graphs: graphs dependent on Mean Free Path (MFP) and energy for ABS-M series

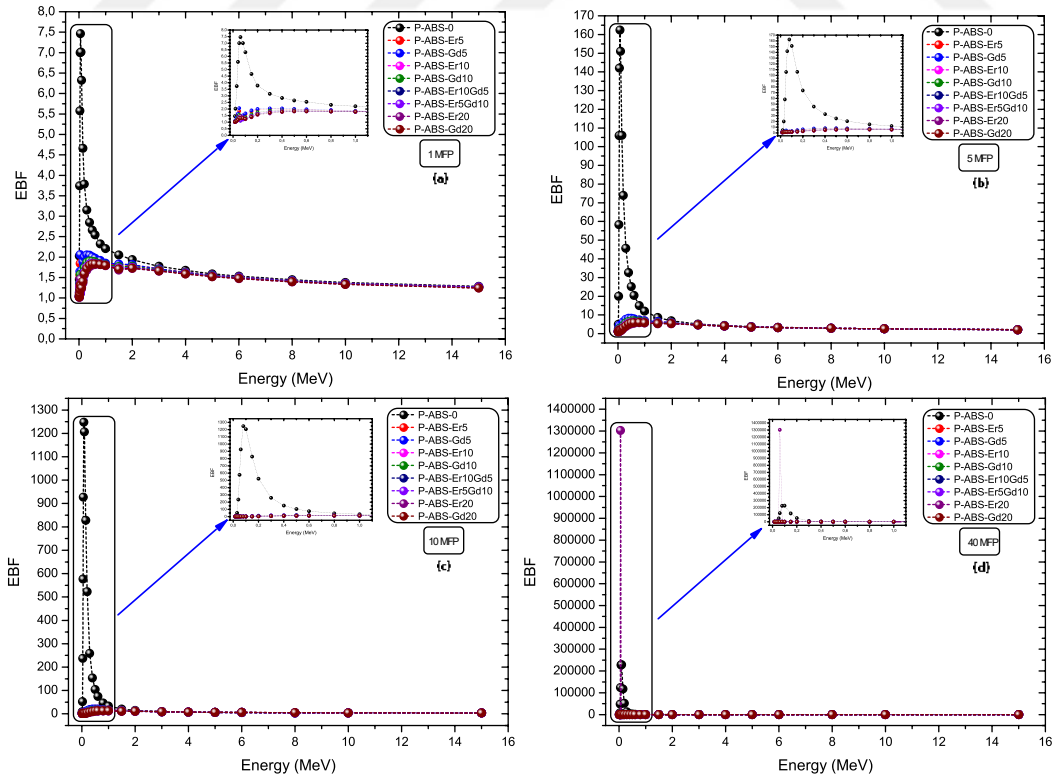



**Figure 5.18.:** Buildup factor (Exposure) graphs: graphs dependent on Mean Free Path (MFP) and energy for ABS-M series

The energy absorption buildup factor (also known as the energy absorption buildup factor) is similar to the exposure buildup factor but focuses on the amount of energy absorbed by the shielding material. This factor is particularly important when considering the effects of radiation on materials and biological tissues, as it accounts for the energy deposited by the radiation within the material. The energy absorption buildup factor considers how much energy is absorbed by the material as radiation passes through it. This factor is also influenced by the energy of the incident radiation, the properties of the shielding material, and the material's thickness.

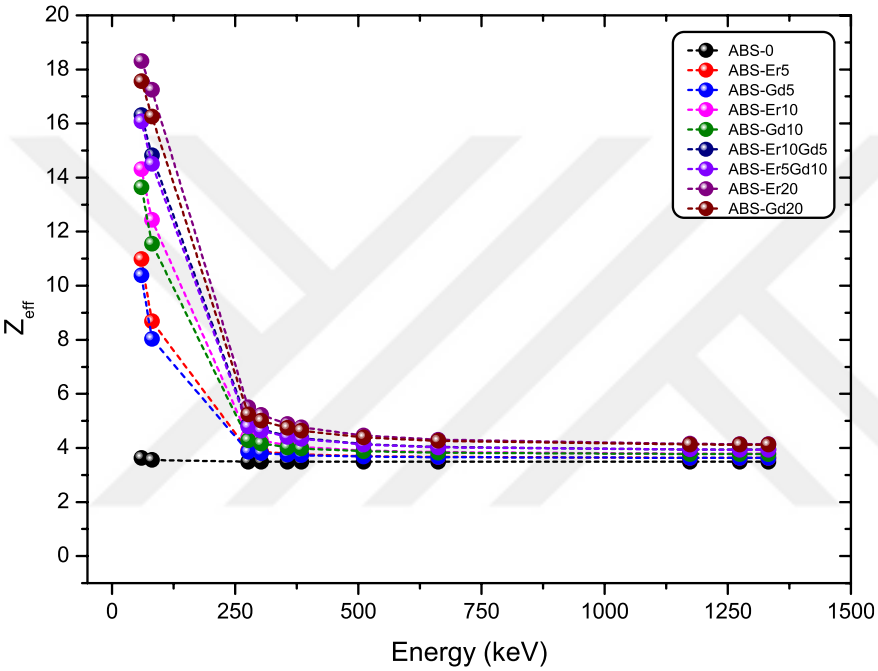



**Figure 5.19 :** Zeff graph of the prepared M and P series samples as a function of gamma energy

$Z_{Eff}$ is a parameter that represents the chemical composition of a material and the elements it contains. Each element has an atomic number, and Z-Eff calculates the effective atomic number of a material by taking into account the contributions of different elements present in the material. This is used in radiation shielding design to determine how radiation interacts with and loses energy within the material. $N_E$ the nuclear (atomic) number density within a material. It represents the number and density of atoms present within a material. The interaction of radiation within the material and the loss of energy are closely related to this nuclear number density. It has been provided in Figure 5.19 and Figure 20

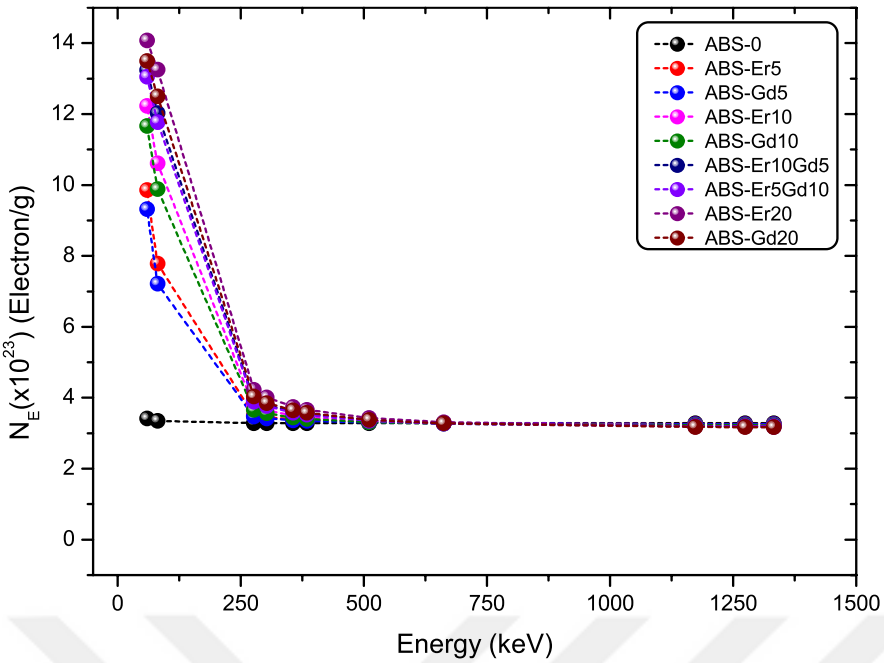



**Figure 5.20 :** NE graph of the prepared M and P series samples as a function of gamma energy

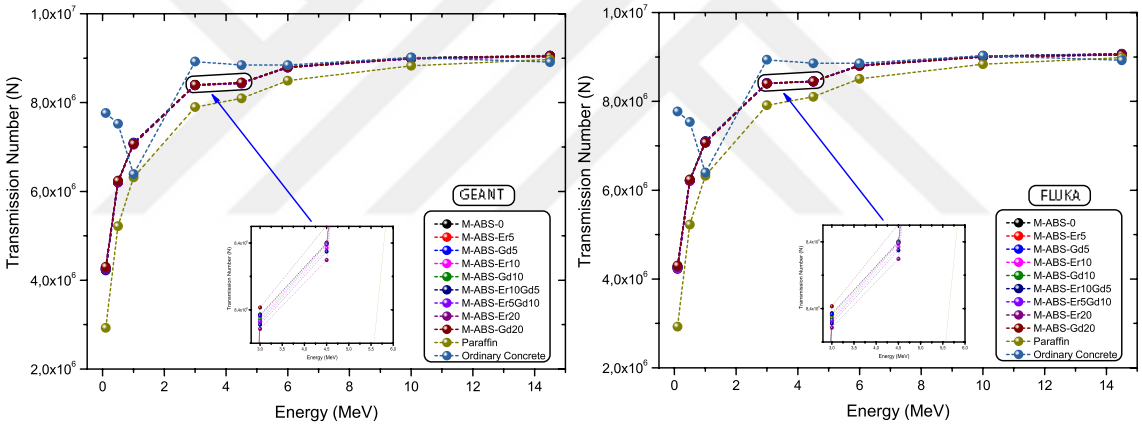



**Figure 5.21 :** The number of 10 million neutrons in the energy range of 0.1 to 14.5 MeV transmitted through the M series samples with a thickness of 1 cm

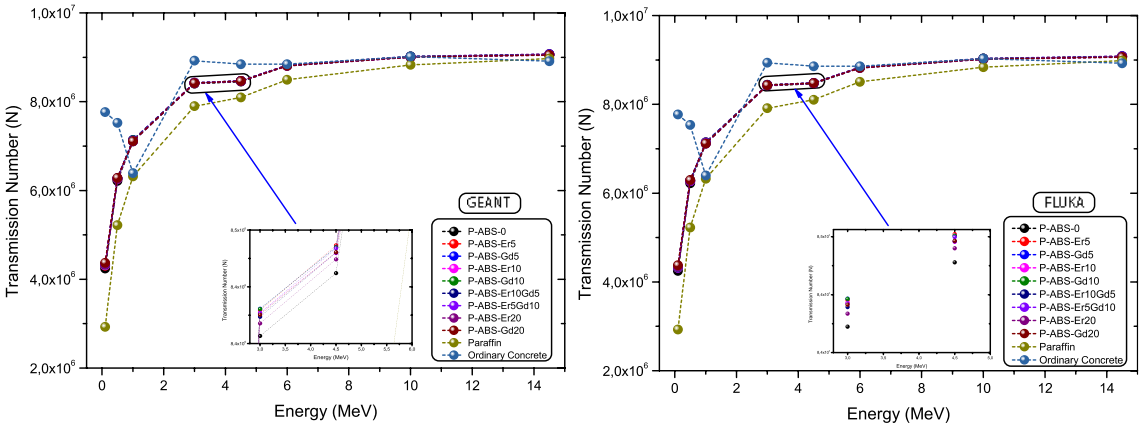



**Figure 5.22 :** The number of 10 million neutrons in the energy range of 0.1 to 14.5 MeV transmitted through the P series samples with a thickness of 1 cm.

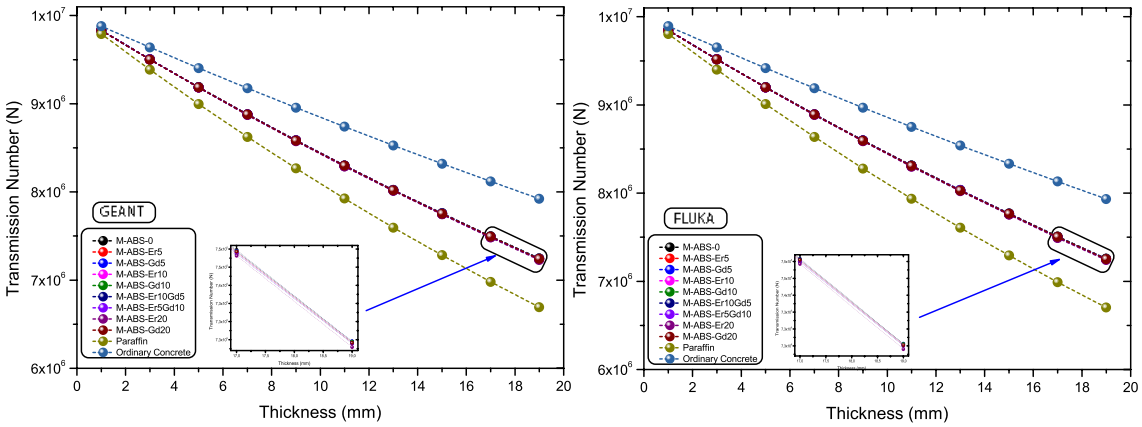



**Figure 5.23.:** The number of 10 million neutrons with an energy of 4.5 MeV that passed through different thicknesses of M series samples

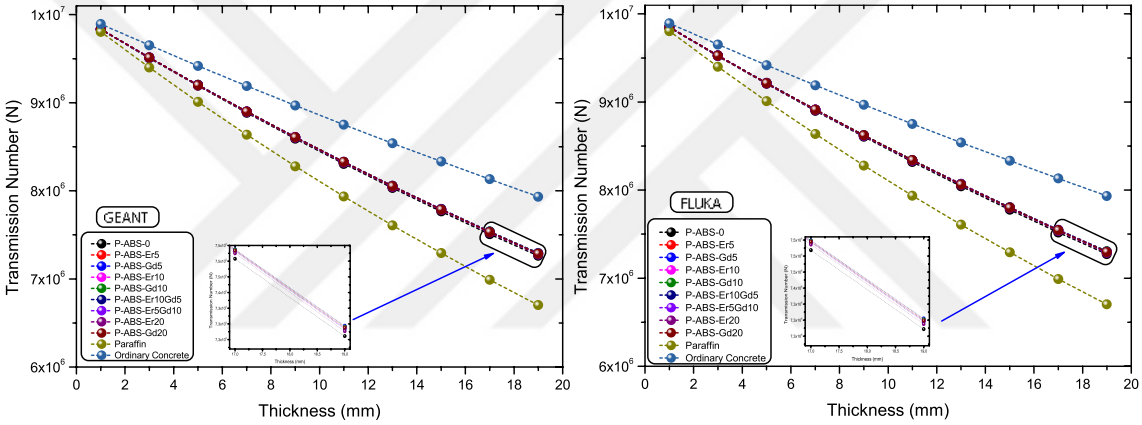



**Figure 5.24.:** The number of 10 million neutrons with an energy of 4.5 MeV that passed through different thicknesses of P series samples

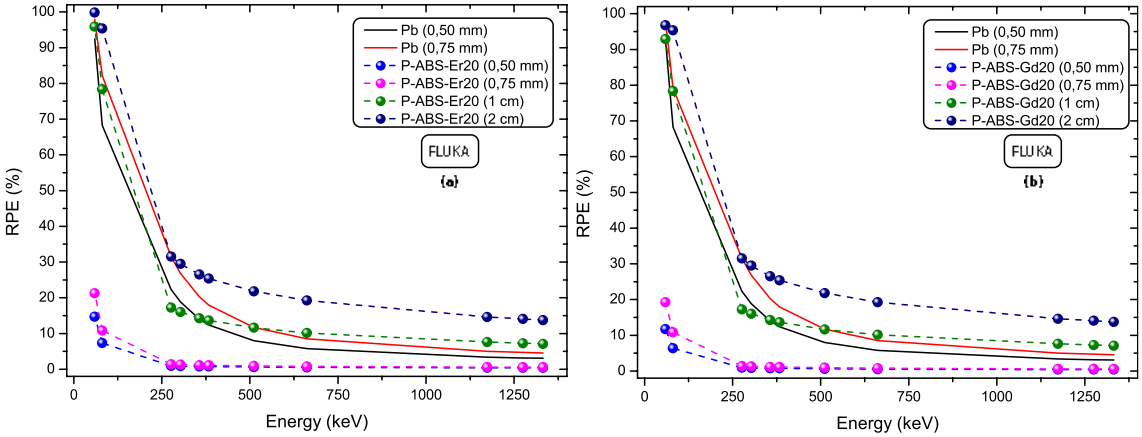



**Figure 5.25.:** Radiation protection efficiency graphs obtained through FLUKA: a-) ABS-Er20 and b-) ABS-Gd20

While Figure 3.13 provide photos of samples produced using the casting method, Figure 3.17 show samples produced using the 3D printing method. Even in the comparison of photos, it can be observed that samples produced using the 3D printing method are visually smoother and better structured. To delve deeper into these images, SEM images were taken at 100X magnification, and EDS mapping was preferred to obtain data from the entire sample surface. SEM and EDS analyses of the produced samples were carried out through outsourcing. Based on the SEM images provided in Figures 4.1-8, it is evident that structurally, samples produced with the 3D printing method are superior in the ABS samples. Only printing lines are present on the surface, which is quite normal in 3D printing technology. It is noteworthy that ABS samples are printable at all additive levels. The SEM images presented in the figures demonstrate excellent print quality and well-structured samples. In addition to SEM images for each sample, EDS mapping results are also included. The additive element (both Er and Gd) is presented in color and is evenly distributed on the surface. It was observed that additive clustering was more significant in the casting method. Since there is no clumping of the additive on the sample surfaces, it can be concluded that the production of additive samples was successful. In light of all these results, it can be stated that samples obtained from the 3D printing method are structurally better than those produced by the casting method. On the other hand, in addition to structural analysis, the mass percentages of the produced P-type and M-type samples were examined between 120 °C and 220 °C concerning temperature. According to the obtained graphs, it was found that with the increase in temperature, P-type samples had less mass loss. 3D printing allows the material to completely melt and then cool and harden again. This process can lead to small changes in the chemical structure of ABS, including variations in the arrangement of polymer chains and chemical bonds. These changes can enhance the thermal stability of ABS, resulting in less mass loss. Therefore, within the scope of this project, it was found that 3D printing is advantageous compared to the casting method regarding the structural and thermal analysis.

From this point on, if we focus on the P-series, when examining ABS samples from a gamma shielding perspective, it can be seen that the best sample in the ABS series is P-ABS-Er20, followed by P-ABS-Gd20 with a slight difference. Although a wide range of gamma ray energies was considered in this study, the focus here is on the possible use of 3D-printed materials. Radiation protection aprons are considered in this context.

Most existing commercial aprons are made of lead, which has disadvantages such as being expensive, heavy, and ineffective against secondary radiation (Crane and Abbott, 2016). Therefore, significant efforts have been made to find lead-free aprons. Commercial lead aprons are produced in two different thicknesses of lead: 0.50 mm and 0.75 mm. To compare our samples with existing commercial aprons, Figure 5.1 was prepared using the FLUKA simulation program. The sample thickness was changed to determine at which polymer thickness identical performance could be achieved with lead aprons, keeping the lead apron and polymer apron at the same thickness. It is observed that when the lead apron and polymer apron are the same thickness, the lead apron is much more effective. However, polymer aprons produced with a thickness of 2 cm, such as ABS-Er20 or ABS-Gd20, provide similar gamma radiation protection in the low gamma ray energy range, which is the relevant energy range for medical applications and X-ray laboratories. This 2 cm apron thickness exceeds that of lead aprons because lead is layered around it many times to avoid harming the living body. Comparing the weights of polymer and lead aprons, we can take another step. Commercial aprons are produced in two sizes: medium (M) and large (L) (INFAB, 2023). The surface area of the large apron is approximately 5999.4680 $cm^2$, while the medium apron's surface area is 5218.4856 $cm^2$ (INFAB, 2023). The weights of the 0.50 mm and 0.75 mm large aprons are 6.803 kg and 10.205 kg, respectively, while the weights of the medium aprons are 5.917 kg and 8.876 kg (INFAB, 2023). ABS-Er20 or ABS-Gd20 samples with a thickness of 2 cm provide the same level of protection as large aprons, with weights of 2.951 kg and 1.778 kg, respectively. For medium size, the weights are calculated as 2.280 kg and 1.456 kg. The newly produced protective materials are quite lightweight compared to commercial lead aprons. This is a significant advantage as it provides ease to healthcare personnel who would otherwise carry heavy lead aprons for hours. In other words, healthcare personnel will tire less, which can lead to improved performance. In this regard, it is anticipated that the ABS-based filaments and samples produced in the scope of the project have the potential for commercialization.

With all these results in mind, the next step is to evaluate the project's primary motivation, which is radiation shielding. Although a wide range of gamma ray energies was considered in this study, the focus here is on the possible use of 3D-printed materials. Radiation protection aprons are considered in this context. Most existing commercial aprons are made of lead, which has disadvantages such as being expensive, heavy, and

ineffective against secondary radiation (Crane and Abbott, 2016). Therefore, significant efforts have been made to find lead-free aprons. Commercial lead aprons are produced in two different thicknesses of lead: 0.50 mm and 0.75 mm. To compare our samples with existing commercial aprons, Figure 5.1 was prepared using the FLUKA simulation program. The sample thickness was changed to determine at which polymer thickness identical performance could be achieved with lead aprons, keeping the lead apron and polymer apron at the same thickness. It is observed that when the lead apron and polymer apron are the same thickness, the lead apron is much more effective. However, polymer aprons produced with a thickness of 2 cm, such as ABS-Er20 or ABS-Gd20, provide similar gamma radiation protection in the low gamma ray energy range, which is the relevant energy range for medical applications and X-ray laboratories. This 2 cm apron thickness exceeds that of lead aprons because lead is layered around it many times to avoid harming the living body. Comparing the weights of polymer and lead aprons, we can take another step. Commercial aprons are produced in two sizes: medium (M) and large (L) (INFAB, 2023). The surface area of the large apron is approximately 5999.4680 $cm^2$, while the medium apron's surface area is 5218.4856 $cm^2$ (INFAB, 2023). The weights of the 0.50 mm and 0.75 mm large aprons are 6.803 kg and 10.205 kg, respectively, while the weights of the medium aprons are 5.917 kg and 8.876 kg (INFAB, 2023). ABS-Er20 or ABS-Gd20 samples with a thickness of 2 cm provide the same level of protection as large aprons, with weights of 2.951 kg and 1.778 kg, respectively. For medium size, the weights are calculated as 2.280 kg and 1.456 kg. The newly produced protective materials are quite lightweight compared to commercial lead aprons. This is a significant advantage as it provides ease to healthcare personnel who would otherwise carry heavy lead aprons for hours. In other words, healthcare personnel will tire less, which can lead to improved performance. In this regard, it is anticipated that the ABS-based filaments and samples produced in the scope of the project have the potential for commercialization.

With all these results in mind, the next step is to evaluate the project's primary motivation, which is radiation shielding. Although a wide range of gamma ray energies was considered in this study, the focus here is on the possible use of 3D-printed materials. Radiation protection aprons are considered in this context. Most existing commercial aprons are made of lead, which has disadvantages such as being expensive, heavy, and ineffective against secondary radiation (Crane and Abbott, 2016). Therefore, significant

efforts have been made to find lead-free aprons. Commercial lead aprons are produced in two different thicknesses of lead: 0.50 mm and 0.75 mm. To compare our samples with existing commercial aprons, Figure 5.1 was prepared using the FLUKA simulation program. The sample thickness was changed to determine at which polymer thickness identical performance could be achieved with lead aprons, keeping the lead apron and polymer apron at the same thickness. It is observed that when the lead apron and polymer apron are the same thickness, the lead apron is much more effective. However, polymer aprons produced with a thickness of 2 cm, such as ABS-Er20 or ABS-Gd20, provide similar gamma radiation protection in the low gamma ray energy range, which is the relevant energy range for medical applications and X-ray laboratories. This 2 cm apron thickness exceeds that of lead aprons because lead is layered around it many times to avoid harming the living body. Comparing the weights of polymer and lead aprons, we can take another step. Commercial aprons are produced in two sizes: medium (M) and large (L) (INFAB, 2023). The surface area of the large apron is approximately 5999.4680 $cm^2$, while the medium apron's surface area is 5218.4856 $cm^2$ (INFAB, 2023). The weights of the 0.50 mm and 0.75 mm large aprons are 6.803 kg and 10.205 kg, respectively, while the weights of the medium aprons are 5.917 kg and 8.876 kg (INFAB, 2023). ABS-Er20 or ABS-Gd20 samples with a thickness of 2 cm provide the same level of protection as large aprons, with weights of 2.951 kg and 1.778 kg, respectively. For medium size, the weights are calculated as 2.280 kg and 1.456 kg. The newly produced protective materials are quite lightweight compared to commercial lead aprons. This is a significant advantage as it provides ease to healthcare personnel who would otherwise carry heavy lead aprons for hours. In other words, healthcare personnel will tire less, which can lead to improved performance. In this regard, it is anticipated that the ABS-based filaments and samples produced in the scope of the project have the potential for commercialization.

In conclusion, the structural and thermal analyses have shown that the 3D printing technique is advantageous. The main focus of the project, radiation shielding, will be evaluated from this point onwards. Although a wide range of gamma ray energies was considered in this study, the focus here is on the possible use of 3D-printed materials. Radiation protection aprons are considered in this context. Most existing commercial aprons are made of lead, which has disadvantages such as being expensive, heavy, and ineffective against secondary radiation (Crane and Abbott, 2016). Therefore, significant efforts

have been made to find lead-free aprons. Commercial lead aprons are produced in two different thicknesses of lead: 0.50 mm and 0.75 mm. To compare our samples with existing commercial aprons, Figure 5.1 was prepared using the FLUKA simulation program. The sample thickness was changed to determine at which polymer thickness identical performance could be achieved with lead aprons, keeping the lead apron and polymer apron at the same thickness. It is observed that when the lead apron and polymer apron are the same thickness, the lead apron is much more effective. However, polymer aprons produced with a thickness of 2 cm, such as ABS-Er20 or ABS-Gd20, provide similar gamma radiation protection in the low gamma ray energy range, which is the relevant energy range for medical applications and X-ray laboratories. This 2 cm apron thickness exceeds that of lead aprons because lead is layered around it many times to avoid harming the living body. Comparing the weights of polymer and lead aprons, we can take another step. Commercial aprons are produced in two sizes: medium (M) and large (L) (INFAB, 2023). The surface area of the large apron is approximately 5999.4680 $cm^2$, while the medium apron's surface area is 5218.4856 $cm^2$ (INFAB, 2023). The weights of the 0.50 mm and 0.75 mm large aprons are 6.803 kg and 10.205 kg, respectively, while the weights of the medium aprons are 5.917 kg and 8.876 kg (INFAB, 2023). ABS-Er20 or ABS-Gd20 samples with a thickness of 2 cm provide the same level of protection as large aprons, with weights of 2.951 kg and 1.778 kg, respectively. For medium size, the weights are calculated as 2.280 kg and 1.456 kg. The newly produced protective materials are quite lightweight compared to commercial lead aprons. This is a significant advantage as it provides ease to healthcare personnel who would otherwise carry heavy lead aprons for hours. In other words, healthcare personnel will tire less, which can lead to improved performance. In this regard, it is anticipated that the ABS-based filaments and samples produced in the scope of the project have the potential for commercialization.

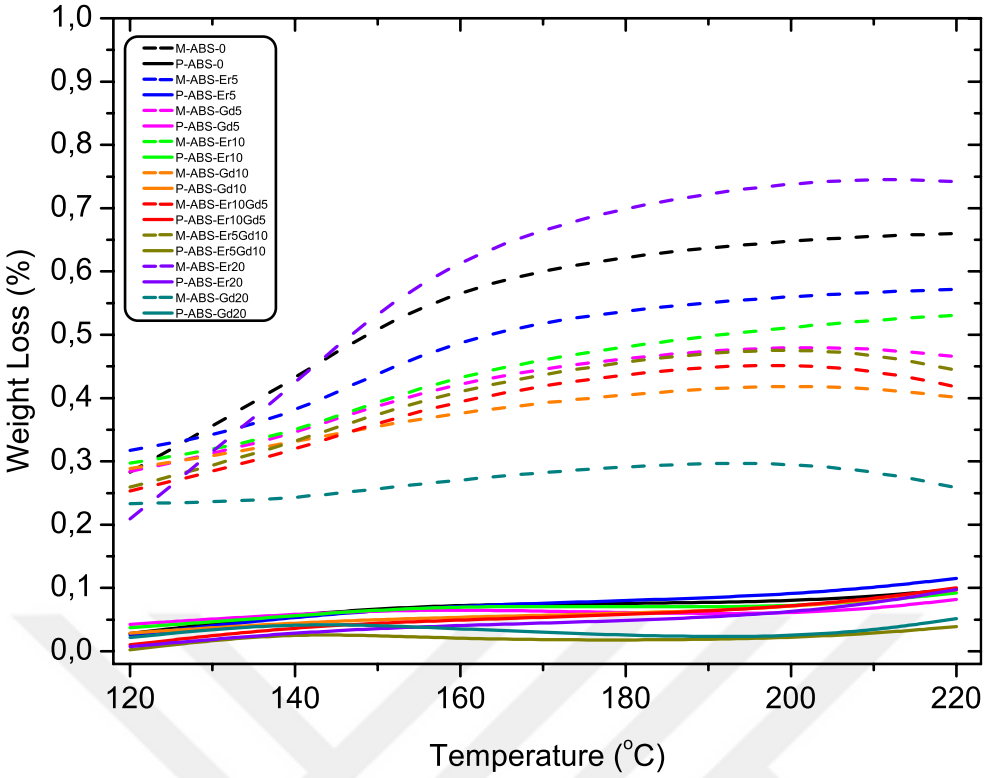



**Figure 5.26 :** Percentage mass loss in temperature-dependent ABS samples using a thermostatic drying oven

As seen in Figure 5.25 the percentage mass loss of samples produced with 3D printers is generally lower compared to the casting-type samples. It can be stated that the samples produced with 3D printers have better thermal stability within the specified temperature range. On the other hand, a comparison was made between ABS-Er20 and ABS-Gd20 samples, which are expected to be the best gamma shielding materials among the prepared samples, and the pristine samples. The obtained graph is presented in Figure 5.26 Erbium (Er) and Gadolinium (Gd) oxides belong to the lanthanide series and are rare earth elements known for their high thermal stability and resistance. When erbium oxide ($Er_2O_3$) and gadolinium oxide ($Gd_2O_3$) are added, it can generally be said that thermal stability improves, as observed in both Figure 5.25 and Figure 5.6 Only the Er20 doped sample from the casting-type series contradicts this statement, which is considered to be a result of measurement errors conducted by scholarship students.

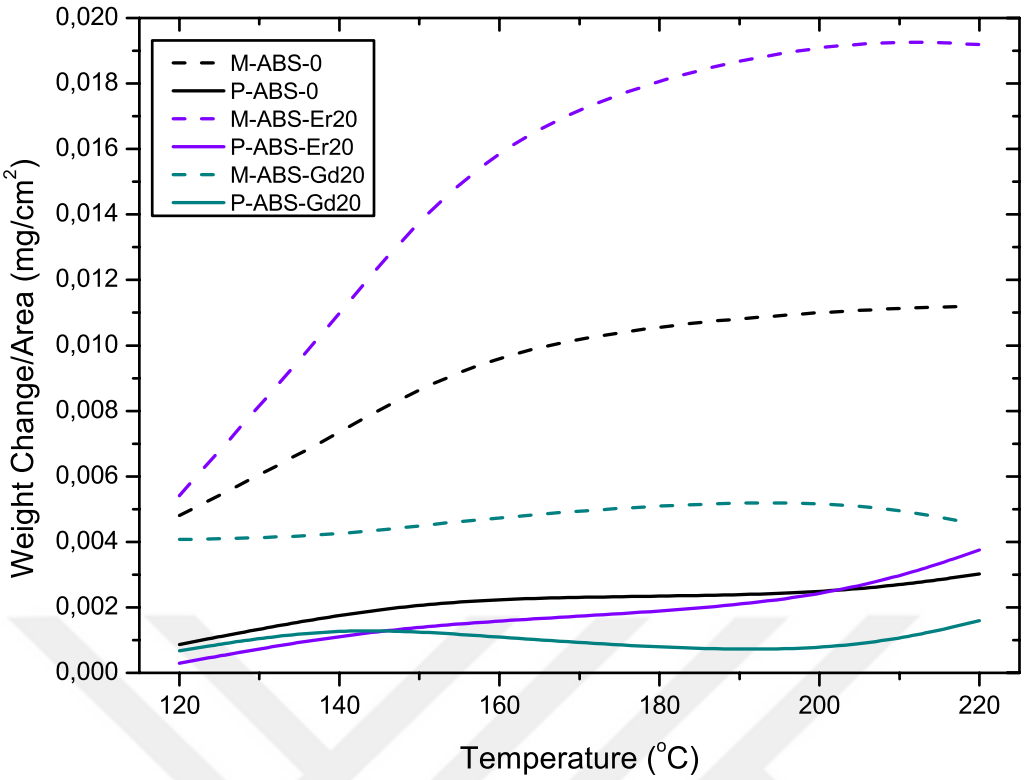



**Figure 5.27 :** The percentage mass loss at varying temperatures of ABS-Er20 and ABS-Gd20 samples was compared with ABS-0 samples using a thermostatic drying oven

In addition to using the thermostatic drying oven, to access a wider temperature range, Thermogravimetric (TGA) Analysis was performed as a service by selecting samples from the P series, including P-ABS-0, P-ABS-Er20, and P-ABS-Gd20.

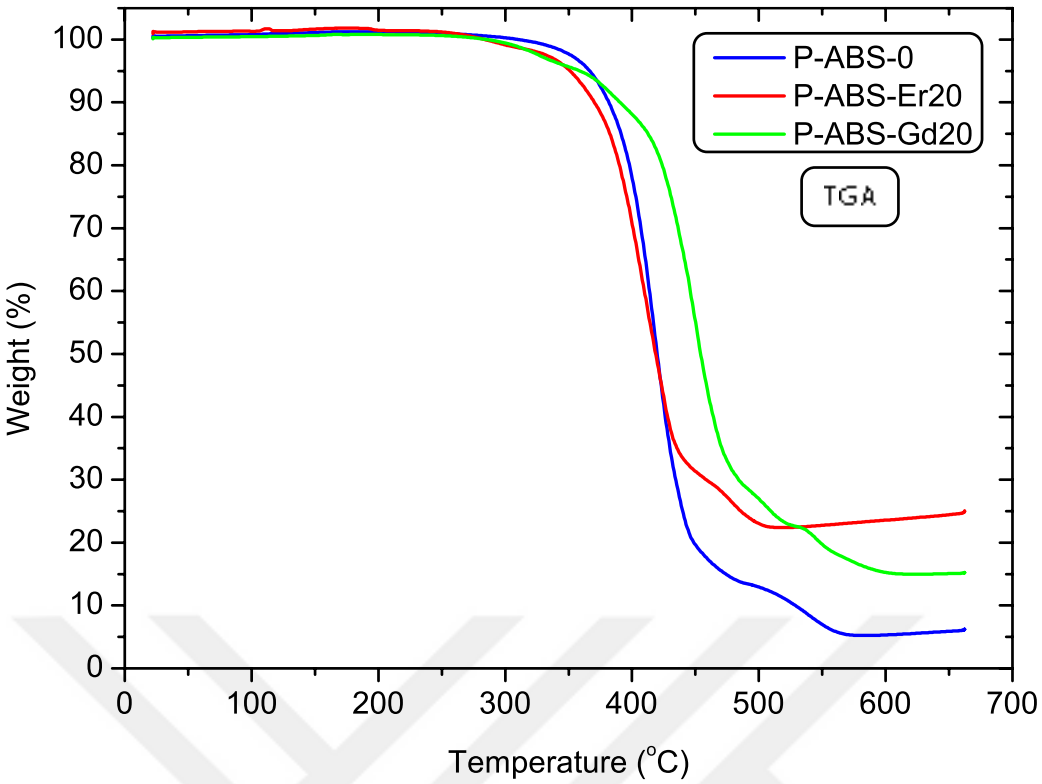



**Figure 5.28 :** ABS-Er20 and ABS-Gd20 samples' percentage mass change at different temperatures was compared with ABS-0 samples using a Thermogravimetric Analyzer.

ABS (Acrylonitrile Butadiene Styrene) is generally known for its excellent impact resistance and good thermal stability. However, as indicated in your data, pure ABS samples experienced a significant mass loss of 80% when exposed to temperatures up to 450 degrees Celsius, and this rate increased to 95% at 600 degrees Celsius. This suggests that ABS can undergo thermal degradation at high temperatures. On the other hand, when Erbium (Er) and Gadolinium (Gd) oxides are added to ABS to improve its thermal properties, the situation changes. These elements belong to the lanthanide series of elements and are known for their high thermal stability and resistance. When Erbium oxide (Er2O3) and Gadolinium oxide (Gd2O3) are added to ABS, thermal stability significantly increases. The ABS sample with erbium oxide added showed a mass retention of 70% at 450 degrees Celsius and 75% at 600 degrees Celsius. The ABS sample with gadolinium oxide added, on the other hand, experienced a mass loss of 15% at 450 degrees Celsius and 90% at 600 degrees Celsius. These data indicate that erbium and gadolinium oxides substantially enhance the thermal stability of ABS. This aligns with the tendency of these oxides to exhibit thermal resistance at high temperatures. However, we can also observe a difference in thermal stability between erbium and gadolinium

oxides. The ABS with erbium oxide demonstrated higher thermal stability compared to the ABS with gadolinium oxide. This suggests that erbium oxide may integrate more effectively with the ABS matrix and distribute thermal energy more efficiently. In the TGA analysis, you observed the first mass loss occurring after 300 degrees Celsius in erbium and gadolinium-added samples. This may indicate the initiation of the material's thermal degradation process at a specific temperature, in this case, 300 degrees Celsius. This temperature range is typically where organic components begin to degrade, and the earlier onset of thermal degradation in erbium and gadolinium-added samples might suggest that these additives have influenced the thermal degradation in ABS. However, the pure ABS sample showed less mass loss at this temperature. This indicates that the absence of additives may have slightly delayed the thermal degradation of ABS. The two additive-containing samples begin to degrade more rapidly after 300 degrees Celsius, possibly because erbium and gadolinium interact with the ABS matrix, triggering thermal degradation. If pure ABS still shows less mass loss at 350 degrees Celsius, it is generally related to ABS's unique thermal degradation profile. However, when evaluating the overall mass losses up to 450 degrees Celsius, we see that the additive-containing samples experience less mass loss than pure ABS. This indicates that erbium and gadolinium additives have improved ABS's thermal stability at this temperature. In conclusion, while it may seem initially that the additives accelerate thermal degradation, they generally enhance the thermal stability of ABS and result in less mass loss at high temperatures. Therefore, these additives may potentially be more suitable for high-temperature applications.

In the presented thesis, ABS material was modified by adding rare earth element nanoparticles. In this context, two important production techniques were used: casting and 3D printing. SEM and EDS analyses revealed that samples produced with 3D printing exhibited a more homogeneous and well-structured appearance. It was observed that all filaments based on ABS were suitable for printing at the desired additive ratios. Considering the lower mass loss in thermal tests, it was concluded that production with 3D printing is better. From a gamma shielding perspective, experimental, theoretical, and simulation results showed a significant correlation, indicating that increasing the additive amount in polymer composites enhances gamma ray shielding efficiency. RPE calculations demonstrated that printed ABS-Er20 aprons could serve as excellent alternatives

to commercial aprons in medical applications and X-ray laboratories. Essentially, 3D printers offer a valuable tool to the manufacturing industry for producing lightweight protective materials with lower material costs and desired properties, whether in complex or simple shapes. Furthermore, gadolinium-doped samples for thermal neutrons demonstrate excellent thermal neutron shielding capabilities, positioning them as a viable alternative to paraffin in the literature. The obtained results are promising for future applications.

## REFERENCES


Al-Buriahi, M. S., Alrowaili, Z. A., Canel Eke, Alzahrani, J. S., Olarinoye, I. O., Sriwunkum, C. (2022). Optical and radiation shielding studies on tellurite glass system containing ZnO and Na2O. Optik, 257, 168821. https://doi.org/10.1016/j.ijleo.2022.168821

Aktas, B., Acikgoz, A., Yilmaz, D., Yalcin, S., Dogru, K., Yorulmaz, N. (2022). The role of TeO2 insertion on the radiation shielding, structural and physical properties of borosilicate glasses. Journal of Nuclear Materials, 563, 153619. https://doi.org/10.1016/j.jnucmat.2022.153619

Esawii, H. A., Salama, E., El-ahll, L. S., Moustafa, M., Saleh, H. M. (2022). High impact tungsten-doped borosilicate glass composite for gamma and neutron transparent radiation shielding. Progress in Nuclear Energy, 150, 104321. https://doi.org/10.1016/j.pnucene.2022.104321

Turhan, M. F., Akman, F., Taşer, A., Dilsiz, K., Oğul, H., Kaçal, M. R., Agar, O. (2022). Gamma radiation shielding performance of CuxAg(1-x)-alloys: Experimental, theoretical and simulation results. Progress in Nuclear Energy, 143, 104036. https://doi.org/10.1016/j.pnucene.2021.104036

Yaykaşlı, H., Eskalen, H., Kavun, Y., et al. (2022). Microstructural, thermal, and radiation shielding properties of Al50B25Mg25 alloy prepared by mechanical alloying. Journal of Materials Science: Materials in Electronics, 33, 2350–2359. https://doi.org/10.1007/s10854-021-07434-9

Bagheri, R., Forati Rad, H., Ranjbar, H. (2023). Radiation shielding studies of low melting point MCP alloys in the photon energy range of 10 keV–10 MeV. Annals of Nuclear Energy, 181, 109525. https://doi.org/10.1016/j.anucene.2022.109525

Ardiansyah, A., Tahir, D., Heryanto, H., Armynah, B., Salah, H., Sulieman, A., Bradley, D. A. (2023). Science mapping for concrete composites as radiation shielding: A review. Radiation Physics and Chemistry, 207, 110835. https://doi.org/10.1016/j.radphyschem.2023.110835

Daungwilailuk, T., Yenchai, C., Rungjaroenkiti, W., Pheinsusom, P., Panwisawas, C., Pansuk, W. (2022). Use of barite concrete for radiation shielding against gamma-rays and neutrons. Construction and Building Materials, 326, 126838. https://doi.org/10.1016/j.conbuildmat.2022.126838

Öz, A., Bayrak, B., Kavaz, E., Kaplan, G., Çelebi, O., Alcan, H. G., Aydın, A. C. (2022). The radiation shielding and microstructure properties of quartzic and metakaolin based geopolymer concrete. Construction and Building Materials, 342(Part B), 127923. https://doi.org/10.1016/j.conbuildmat.2022.127923

Oğul, H., Agar, O., Bulut, F., Kaçal, M. R., Dilsiz, K., Polat, H., Akman, F. (2023). A comparative neutron and gamma-ray radiation shielding investigation of molybdenum and boron filled polymer composites. Applied Radiation and Isotopes, 194, 110731. https://doi.org/10.1016/j.apradiso.2023.110731

Sayyed, M. I., Yasmin, S., Almousa, N., Elsafi, M. (2022). The Radiation Shielding Performance of Polyester with TeO2 and B2O3. Processes, 10(9), 1725. https://doi.org/10.3390/pr10091725

Abbas, M. I., Alahmadi, A. H., Elsafi, M., Alqahtani, S. A., Yasmin, S., Sayyed, M. I., Gouda, M. M., El-Khatib, A. M. (2022). Effect of Kaolin Clay and ZnO-Nanoparticles on the Radiation Shielding Properties of Epoxy Resin Composites. Polymers, 14(22), 4801. https://doi.org/10.3390/polym14224801

Kilicoglu, O., More, C. V., Akman, F., Dilsiz, K., Oğul, H., Kaçal, M. R., Polat, H., Agar, O. (2022). Micro Pb filled polymer composites: Theoretical, experimental and simulation results for γ-ray shielding performance. Radiation Physics and Chemistry, 194, 110039. https://doi.org/10.1016/j.radphyschem.2022.110039

Oğul, H., Polat, H., Akman, F., Kaçal, M. R., Dilsiz, K., Bulut, F., Agar, O. (2022). Gamma and Neutron Shielding Parameters of Polyester-based composites reinforced with boron and

tin nanopowders. Radiation Physics and Chemistry, 201, 110474. https://doi.org/10.1016/j.radphyschem.2022.110474

Gong, P., Ni, M., Chai, H., Chen, F., Tang, X. (2018). Preparation and characteristics of a flexible neutron and γ-ray shielding and radiation-resistant material reinforced by benzophenone. Nuclear Engineering and Technology, 50(3), 470-477. https://doi.org/10.1016/j.net.2018.01.005

Elsafi, M., El-Nahal, M. A., Sayyed, M. I., Saleh, H., Abbas, M. I. (2022). Novel 3-D printed radiation shielding materials embedded with bulk and nanoparticles of bismuth. Scientific Reports, 12, 12467. https://doi.org/10.1038/s41598-022-16317-w

Jreije, A., Mutyala, S. K., Urbonavičius, B. G., Šablinskaitė, A., Keršienė, N., Puišo, J., Rutkūnienė, Ž., Adlienė, D. (2023). Modification of 3D Printable Polymer Filaments for Radiation Shielding Applications. Polymers, 15(7), 1700. https://doi.org/10.3390/polym15071700

Viskadourakis, Z., Vasiolopoulos, K. C., Economou, E. N., Soukoulis, C. M., Kenanakis, G. (2017). Electromagnetic Shielding Effectiveness of 3D Printed Polymer Composites. Applied Physics A, 123, 736. https://doi.org/10.1007/s00339-017-1231-9

Gultekin, B., Ogul, H. (2023). Evaluation of Acrylonitrile Butadiene Styrene (ABS) polymer reinforced with Bi and TiO2 nanopowders for gamma and neutron shielding. Radiochimica Acta, 111(2), 137-145. https://doi.org/10.1515/ract-2022-0081

Alssabbagh, M., Tajuddina, A. A., Abdulmanap, M., Zainon, R. (2017). Evaluation of 3D Printing Materials for Fabrication of a Novel Multi-Functional 3D Thyroid Phantom for Medical Dosimetry and Image Quality. Radiation Physics and Chemistry, 135, 106-112. https://doi.org/10.1016/j.radphyschem.2017.02.023

Woosley, S., Galehdari, N. A., Kelkar, A., Aravamudhan, S. (2018). Fused Deposition Modeling 3D Printing of Boron Nitride Composites for Neutron Radiation Shielding. Journal of Materials Research, 33, 3657-3664. https://doi.org/10.1557/jmr.2018.359

Ogul, H. (2022). Radiation attenuation properties of polymer composites mixed with tantalum carbide. Radiation Effects and Defects in Solids, 177(5-6), 493-504. https://doi.org/10.1080/10420150.2022.2033247

Sarkar, S., Vinokur, Z., Xu, C., Soloviova, T., Shahbaz, A., Gjoni, A. (2020). Mapping gadolinium contrast in a complex ionic and photosynthesis environment of pineapple by near-infrared and X-ray imaging. Spectroscopy Letters, 53(7), 505-511. https://doi.org/10.1080/00387010.2020.1786405

Lamarsh, J. R., & Baratta, A. J. (2001). Introduction to Nuclear Engineering. Upper Saddle River, NJ: Prentice Hall.

Mann, K. S., Rani, A., Heer, M. S. (2015). Shielding behaviors of some polymer and plastic materials for gamma-rays. Radiation Physics and Chemistry, 106, 247-254. https://doi.org/10.1016/j.radphyschem.2014.08.005

Obregón, S., Kubacka, A., Fernández-García, M., & Colón, G. (2013). High-performance Er3+–TiO2 system: dual up-conversion and electronic role of the lanthanide. Journal of Catalysis, 299, 298-306. https://doi.org/10.1016/j.jcat.2012.12.021

Effendy, N., Wahab, Z. A., Abdul Aziz, S. H., Matori, K. A., Zaid, M. H. M., & Rashid, S. S. A. (2017). Characterization and optical properties of erbium oxide doped ZnO–SLS glass for potential optical and optoelectronic materials. Materials Express, 7(1), 59-65. https://doi.org/10.1166/mex.2017.1328

Olsson, A., Hellsing, M. S., Rennie, A. R. (2017). New Possibilities Using Additive Manufacturing with Materials That Are Difficult to Process and with Complex Structures. Physica Scripta, 92(5), 053002. https://doi.org/10.1088/1402-4896/aa694e

Mahmoud, M. E., El-Khatib, A. M., Badawi, M. S., Rashad, A. R., El-Sharkawy, R. M., Thabet, A. A. (2018). Fabrication, characterization and gamma rays shielding properties of nano and micro lead oxide-dispersed-high density polyethylene composites. Radiation Physics and Chemistry, 145, 160-173. https://doi.org/10.1016/j.radphyschem.2017.10.017

Gerward, L., Guilbert, N., Jensen, K., Levring, H. (2004). WinXCom - A program for calculating X-ray attenuation coefficients. Radiation Physics and Chemistry, 71, 653-654. https://doi.org/10.1016/j.radphyschem.2004.04.040

Agostinelli, S., Allison, J., Amako, K., Apostolakis, J., Araujo, H., Arce, P., Asai, M., Axen, D., Banerjee, S., Barrand, G., Behner, F., Bellagamba, L., Boudreau, J., Broglia, L., Brunengo, A., Burkhardt, H., Chauvie, S., Chuma, J., Chytracek, R., Cooperman, G., et al. (2003). Geant4 - a Simulation Toolkit. Nuclear Instruments and Methods in Physics Research Section A: Accelerators, Spectrometers, Detectors and Associated Equipment, 506(3), 250-303. https://doi.org/10.1016/S0168-9002(03)01368-8

Böhlen, T. T., Cerutti, F., Chin, M. P. W., Fassò, A., Ferrari, A., Ortega, P. G., Mairani, A., Sala, P. R., Smirnov, G., Vlachoudis, V. (2014). The FLUKA Code: Developments and Challenges for High Energy and Medical Applications. Nuclear Data Sheets, 120, 211-214. https://doi.org/10.1016/j.nds.2014.07.049

## CURRICULUM VITAE

**Name Surname** **:** Batuhan GÜLTEKİN

❖ **Education Information**

- **High School :** Istanbul Büyükçekmece Recep Güngör Anatolian High School, 2015

- **Bachelor's Degree (Erasmus) :** University of Castilla-La Mancha (UCLM-Spain) – Faculty of Architecture and Engineering – Mechanical Engineering, 2017

- **Bachelor's Degree :** Sinop University – Faculty of Architecture and Engineering – Nuclear Engineering, 2019

❖ **Internship Experience**

- **Power Plant Engineering Trainee** : EUAS Ambarlı Natural Gas Combined Cycle Power Plant (A) 1350,9 MW – internship, 2017

- **Nuclear Engineering Trainee :** TENMAK (Turkish Energy, Nuclear, and Mining Research Institution): Istanbul Çekmece Nuclear Research and Training Center, – internship, 2018

❖ **Work Experience**

- **Research Scholar:** AKTURK Research Group (ARG)- Aydın Adnan Menderes University - TUBITAK- (1003 Project) - Project No:118F508 – (2020-2021)

✓ **Project Title:** Investigation of Interactions of Some Graphene-Like Two- Dimensional MXene Materials with Neurotransmitter Molecules and Amino Acids

- ✓ **Study Area:** Analysis of the quantum chemical properties of semiconductors, formation of atomic crystal configurations of materials and investigation of the stability of these structures.

- ❖ **Research Scholar:** Radiation Applications Research&Development Group (SUR R&D) Sinop University - TUBITAK- (1002-A) Project - Project No:122M736 – (2021-2023)

- ✓ **Project Title:** Investigation of the Use of 3D Printers in the Production of Radiation Shielding Materials and Comparison with the Traditional Moulding Technique

- ✓ **Study Area:** It is aimed to investigate the gamma and neutron shielding characteristics of ABS and PLA thermoplastics, known as $Er_2O_3$ and $Gd_2O_3$ doped 3D printer polymers, with experimental, theoretical and simulation methods at different material thicknesses and different radiation energies. In order to ensure integrity, the microstructures of the produced materials will also be examined. In ABS and PLA polymersample production, 2 different production options will be compared by using moulding type and 3D printer technology.

- ❖ **Scholarship holder:** TUBITAK 2210-C Domestic Priority Fields Graduate Scholarship Program (This scholarship has been awarded to only 80 individuals in Turkey in the year 2022.)

- ✓ **Priority Field:** Advanced Functional Materials Technologies